Stochastic Spatial-Temporal Models for Rainfall Processes

Nanda Ram Aryal

ORCID Identifier: orcid.org/0000-0003-3118-2006

Submitted in total fulfilment of the requirements of the degree of *Doctor of Philosophy*

November 2018

The School of Mathematics and Statistics
The University of Melbourne
Australia

Abstract

Currently clustered rainfall models have been fitted using Generalized Method of Moments (GMM), because typically they have intractable likelihood functions. GMM fitting matches theoretical and observed moments of the process and thus is restricted to models for which analytic expressions are available for the moments. We show that Approximate Bayesian Computation (ABC) can also be used to fit clustered rainfall models. We also validate that ABC readily adapts to more general, and thus more realistic, variants of spatial-temporal rainfall models.

ABC fitting compares the observed process with simulations and hence places no restrictions on the statistics used for the comparison. This opens up the possibility of fitting much more realistic stochastic rainfall models. The penalty we pay for this increased flexibility is an increase in computational time. Simulated Method of Moments (SMM) is used to initialize the ABC. This can also be used to estimate the weights of the distance measure in the ABC-MCMC setting. We found that our method requires much smaller computation time in comparison with what previous authors have suggested using a separate ABC step to estimate initialization.

A spatial-temporal rainfall model based on a cluster process is constructed by taking a primary process, called the storm arrival process, and attaching to each storm centre a finite secondary process, called a cell process. The total intensity at a point in $\mathbb{R}^2 \times [0, \infty)$ is the sum of the intensities of all cells active at that point. Typically, the model parameters are interdependent.This dependency produces complexity in model fitting procedures, and has also restricted further extension of the model, particularly finding theoretical expressions for the moments. Fortunately, ABC can be applied without having analytical expressions for the moments. We reparameterized the models and the parameters were log transformed to reduce dependence and skewness, also simplifies the chain proposal in MCMC steps.

We also present two new stochastic spatial-temporal rainfall models that yield with better representation of observed rainfall processes, and also capture the dependence between size and intensity for rain cells.

Keywords: *Poisson cluster process, Bartlett-Lewis process, spatial-temporal, spatiotemporal; rainfall, simulation, Generalized Method of Moments, Simulated Method of Moments, Approximate Bayesian Computation, Markov Chain Monte Carlo.*

Declaration

This is to certify that:

1. the thesis comprises only my original work towards the PhD except where indicated in the Preface,
2. due acknowledgment has been made in the text to all other material used,
3. the thesis is fewer than 100 000 words in length, exclusive of tables, maps, bibliographies and appendices.

Signed,

Nanda Ram Aryal

Preface

The major contribution of this research is in Chapters two, three, and four. The publications based on Chapter two are as follows:

1. Aryal, Nanda R. and Jones, Owen D."Fitting the Bartlett-Lewis rainfall model using Approximate Bayesian Computation." *22nd International Congress on Modelling and Simulation*, Hobart, Australia, December 2017.

2. Aryal, Nanda R. and Jones, Owen D."Fitting the Bartlett-Lewis rainfall model using Approximate Bayesian Computation". *Journal of Mathematics and Computers in Simulation*, 2018. Accepted.

Based on Chapter three, a poster and 6-page abstract paper were presented at the following:

3. Aryal, Nanda R. and Jones, Owen D."Fitting a spatial-temporal rainfall model using Approximate Bayesian Computation". *International Workshop on Statistical Modelling 2018*; University of Bristol, UK, July 2018.

Acknowledgments

I would like to express my serious appreciation to all people who provide supports duration my PhD. First, to my principal supervisor Prof. Owen Jones for his supervision, motivation and continuous support throughout the study. Second to my co-supervisor Prof. Peter Taylor for his consistent encouragement and help, and to my PhD committee member Prof. Ian Golden for his support and valuable suggestions.

Similarly, I would like to thank University of Melbourne colleagues Kate, Peter, Nicholas, Shrupa, Joanne and others.

This thesis wouldn't be completed without unconditional support from my wife Jharana, son Arjav, and my parents. I appreciate your understanding and support.

I acknowledge with thanks the support received from an Australian Government Research Training Program Scholarship, a Melbourne Research Scholarship, and a Studentship (Stipend) Scholarship.

Contents

Chapter 1

Introduction

1.1 Objectives

Currently Poisson cluster rainfall models have been fitted using Generalized Method of Moments (GMM). GMM fitting matches theoretical and observed moments of the process and thus is restricted to moments for which we have analytic expressions. However, we investigated whether Approximate Bayesian Computation (ABC) could also be used to fit the Poisson clustered rainfall models. ABC fitting compares the observed process with simulations and hence places no restrictions on the statistics used for the comparison. This opens up the possibility of fitting much more realistic stochastic rainfall models.

We present two new stochastic spatial-temporal rainfall models. These lead to better representations of observed rainfall processes and allow us to study relationships between the cell intensity and the cell area.

These models may be used in conjunction with urban flood models to determine and assess the flood risks, as we require rainfall data as input to flood models.

1.2 Motivation

There is concern about how much rainfall can occur in a particular region over time. Rainfall processes have high variability. Uncertainty and variability of rainfall processes can be obtained through simulation using stochastic rainfall

models.

Since technology has evolved over time, we have the privilege of obtaining more accurate observed processes via radar. Radar provides high-resolution rainfalls (for instance the rainfall processes may be recorded every 6 minutes in time and 1×1 km square in space). Our goal has been to present high resolution spatial-temporal models that capture some of the intense localized patches of rainfall that are not uncommon in many storms. We fit the models using likelihood-free simulation-based techniques such as Approximate Bayesian Computation, and ideally fitting these models require high resolution data.

Poisson cluster processes are used to model both temporal and spatial-temporal rainfall processes. A Poisson cluster rainfall model generates a continuous rainfall process, which can easily be digitized in both time and space. These model properties appealed us to focus on Poisson cluster rainfall models, and facilitated the use of Approximate Bayesian Computation fitting.

A Poisson cluster process is constructed by taking a primary process, called the storm arrival process, and then attaching to each storm centre a finite secondary process, called a cell process. The total intensity at a point in $\mathbb{R}^2 \times [0, \infty)$ is the sum of the intensities of all active cells at that point. Typically, the model parameters are interdependent. The dependency produces complexity in model fitting procedures, and also restricts further development of theoretical frameworks. Fortunately, ABC can be applied without needing analytical expressions for the moments.

The existence of supercomputers, however, can allow us to simulate data using these complex models relatively quickly. In simulations we can relax those restricted conditions which do not allow us to develop realistic stochastic rainfall processes. This opens up a new region of model fitting for Poisson cluster rainfall models, and allows us to modify or develop better models.

1.3 Research Contribution

1.3.1 Previous Work

1. Temporal rainfall models

Rodriguez-Iturbe et al., 1987 [39] introduced two Poisson cluster process models: Bartlett-Lewis (BL) and Neyman-Scott (NS) rainfall models. They also provide the some theoretical expectations particularly first and second order moments. Rodriguez-Iturbe et al., 1987 [41] applied the orig-

inal Bartlett-Lewis rectangular pulse model to rainfall data from Denver, Colorado, US.

Acreman, 1990 [1] and Onof & Wheather, 1994 [35] also fitted the BL model at Farnborough and Elmdon, Birmingham to UK data sets respectively. Onof & Wheather, 1994 [35] further studied the relationship between cell arrival rate and cell durations.

Many modifications have been presented. One is a Generalized Point Process Model, endorsed by Cowpertwait, 1994 [8]. The model allows different types of rain cells to exist within the same storm. In particular, the two types of cells are considered the short duration convective and long-duration stratiform cells. The refinement was applied in the Neyman-Scott rectangular pulse model.

The second is the Bartlett-Lewis instantaneous pulse model, introduced by Cowpertwait et al., 2007 [9]. The model has three Poisson processes, generally, storm origins arrive in a Poisson process, each storm initiates a number of cells in another Poisson process, and cell origins generate a number of pulses in a Poisson process. Each pulse has intensity but no duration. The observations of the model comprise a point process of pulses with marks as intensity. This model has one parameter more than the original Bartlett-Lewis rectangular pulse model.

A third modification is of the original Bartlett-Lewis model. The model keeps the same structure as before, but randomizes the cell duration parameter, which follows an exponential distribution. The Modified Bartlett-Lewis rectangular pulse model allows the cell duration parameter to vary randomly between storms and also the cell arrival rate may vary. This model was introduced by Rodriguez-Iturbe et al., 1988 [40]. The parameter of the cell duration was randomized in the cell process in the Bartlett-Lewis models studied by Rodriguez-Iturbe et al., 1988 [40] and in Neyman-Scott models studied by Entelhabi et al., 1989 [15].

An other refinement is made by Kaczmarska et al., 2014 [25], who present a Random Parameter Bartlett-Lewis Instantaneous Pulse model. Using an instantaneous pulse shape allows us more variability in rainfall intensity over short intervals, and also provides third order theoretical statistics.

Including a wide range of statistics in the fitting process may provide more accurate estimation of parameters, and may help to reproduce the summary statistics. We see all refinements are made with respect to whether we can derive their theoretical expectations for the moments, because we need them for fitting in the GMM. For instance if we used a gamma distribution for the duration of a rain cell, rather than an exponential distribution, then we would not be able to calculate the second order statistics of the BL model. In this case, GMM is not available.

Our focus in Chapter 2 hence is not on model refinements, but rather on a new fitting technique that does not require explicit theritical expressions for the moments.

2. Spatial-Temporal rainfall models

We have two sources of spatial-temporal rainfall data. The first consists of multi-station rain-gauge data. The other comprises radar data that are available from discrete points in space and time.

Some researchers focused on networks of rain-gauge data using different rainfall models. For example Cowpertwait, 2002 [11] fitted the Neyman-Scott rectangular pulse spatial-temporal model to rain-gauge data obtained from 9 sites in Arno Basin, Italy.

Various authors, Cowpertwait, 2006 [10], Burton et al.,2008, 2010 [6, 5], Fower et al. 2002, 2010 [17, 18], Mehrotra & Sharma, 2007 [31] among others, have used different spatial-temporal models such as Poisson clustered based models, multi-site Markov chains, multivariate autoregressive and generalized linear regression approaches, semi-Markov chain models, and non-homogeneous Hidden Markov Models etc. Lovejoy & Schertzer [27, 26], Gupta & Waymire [20, 21] and Seed et al. [42] use multifractal and cascade process models. Similarly Beven and Hall, 2014 (Chapter 7) [4] and Fowler et al., 2007 [16] discuss General Circulation Models that consider downscaling methods for different climatic variables to study spatial-temporal rainfall processes.

For radar data, there are fewer models to be used. Willems, 2001 [49] used both network of rain-guage and radar images for rainfall processes.

Poisson cluster processes can be used on both a network of raingauges and radar images. We further extend the Cox-Isham-Northrop model as well focused on the radar data.

The Poisson cluster rainfall models generate a continuous rainfall process, which can easily be digitized in both time and space. Particularly, these models are useful to obtain upscaling rainfall, where General Circulation Models are used to down scaling. The clustered rainfall models have storm-cell structure. The storm-cell rainfall models may provide the localized rainfall as rain cell occurrences. The rain cells are clustered to the storms in space and time having random intensities that may also represent variability in localized rainfall in space. The storm-cell spatial-temporal models may also capture some of the intense localized patches of rainfall that are not uncommon in observed rainfall processes.

3. Fitting rainfall models using GMM.

Because it has an intractable likelihood function, in the past the BL model has been fitted using the Generalized Method of Moments (GMM). Wheater et al, 2005 [47] and Jesus & Chandler, 2011 [23] present details for GMM fitting rainfall models to observed rainfall processes. We note that other simulation-based model fitting approaches are available, in particular the Simulated Method of Moments (SMM) of McFadden [30] and Pakes and Pollard [36], but have not yet been implemented in rainfall model fittings. Our focus remains on the ABC fitting, because the advantage of ABC over SMM is that it gives access to all the advantages of Bayesian modelling.

1.3.2 Contribution

1. ABC for rainfall models applicable to both temporal and spatial-temporal models

We identified that there is a need to implement a new fitting method that is not only free from likelihood-based methods, but also free from requiring theoretical expectations for moments. Using a wide range of statistics in model fitting procedure may provide a better fit. Either we need to derive a wide range of expectations including higher order moments and use GMM or implement another method that has no prerequisite of theoretical expectations.

GMM fitting matches theoretical and observed moments of the rainfall process and thus is restricted to moments for which we have analytic expressions. On the other hand ABC fitting compares the observed process to simulations and hence places no restrictions on the statistics used for comparison. Our research focused on ABC using Markov Chain Monte Carlo for which we need only data (i.e. observed processes) and model suitable simulations of the observed process. Moreover, this means that ABC can be used for models for which GMM fitting is not available. Initially we aimed to implement ABC to the simplest form of the Bartlett-Lewis model called the rectangular pulse model. In order to successfully implement ABC, we reparameterised the model, and showed that ABC can be used to fit the Bartlett-Lewis rainfall model to real data.

2. Develop two new models: ECST and LNCST models

We extended ABC fitting to a spatial-temporal rainfall model. After successfully using ABC fitting to temporal and spatial-temporal rainfall models, we are at the stage where we are not concerned whether or not our model has theoretical expectations for the moments. We then developed two spatial-temporal rainfall models that provide better representations of the observed rainfall processes. These models may be used in conjunction with urban flood models to evaluate flood risk.

3. Starting values for ABC-MCMC: using the Simulated Method of Moments

ABC fitting compares the observed process to simulations, and thus places no restriction on the statistics used for comparison. The penalty we pay for this increased flexibility is an increase in computational time. Starting points become most important in both numerical optimization of the objective function for GMM and estimating posteriors from the ABC-MCMC algorithm.

For example, in GMM various writers use the Nelder Mead method to identify a global optimal region and then apply a gradient base method to estimate parameter by minimizing the objective function. Similarly, the ABC-MCMC algorithm needs chain burn-in time. We estimate posteriors for parameters removing burn-in time, because we expect the chain should converge to a stationary distribution. Starting points may determine how large burn-in time is needed for the chain to converge at stationary state. If we supply a good starting point then we may have a very short burn-in time. Having this in mind we use the Simulated Method of Moments (SMM). The SMM is the simulation-based model fitting approach as an alternative to GMM. Applying SMM gave us better starting points for chains. This leads to the chain burn-in time being very short, even to the extent that we may not need any burn-in time. This is a novel idea in ABC-MCMC fitting, which works well for the rainfall models we study.

1.4 Thesis Summary

As discussed in § 1.1 two major objectives for the research were (1) to develop a new methodology/technique when likelihood-based methods and Generalized Method of Moments are not suitable for fitting stochastic rainfall models to real data; (2) to develop new spatial-temporal rainfall models which can

give better representations of the observed rainfall processes.

Chapter 2 has two aims: first we describe the new technique of fitting the Bartlett-Lewis rainfall model using Approximate Bayesian Computation and then we compare the results of the fitting with the results from Generalized Method of Moments fitting.

The Bartlett-Lewis (BL) rainfall model is a stochastic model for the rainfall at a single point in space, constructed using a cluster point process. The cluster process is constructed by taking a primary/parent process, called the storm arrival process in our context, and then attaching to each storm point a finite secondary/daughter point process, called a cell arrival process. To each cell arrival point we then attach a rain cell, with an associated rainfall duration and intensity. The total rainfall at time t is then the sum of the intensities from all cells active at that time.

Following Rodriguez-Iturbe et al. 1987 [39], we suppose that the storm arrival process is a Poisson process, and that the cell arrival processes are independent Poisson processes, truncated after an exponentially distributed time (the storm duration). Rain cells are all i.i.d., with independent exponentially distributed duration and intensity.

Because it has an intractable likelihood function, in the past the BL model has been fitted using the GMM. The purpose of this chapter is to show that ABC can also be used to fit this model, and moreover that it gives a better fit than GMM. GMM fitting matches theoretical and observed moments of the process, and thus is restricted to moments for which we have analytic expressions. ABC fitting compares the observed process to simulations, and thus places no restrictions on the statistics used to compare them. The penalty we pay for this increased flexibility is an increase in computational time.

The ABC methodology supposes that we have an observation D from some model $f(\cdot|\boldsymbol{\theta})$, depending on parameters $\boldsymbol{\theta}$, and that we are able to simulate from f. Let π be the prior distribution for $\boldsymbol{\theta}$ and $S = S(D)$ a vector of summary statistics for D; then ABC generates samples from $f(\boldsymbol{\theta}|d(S(D^*), S(D)) < \epsilon)$, where $D^* \sim f(\cdot|\boldsymbol{\theta})$, $\boldsymbol{\theta} \sim \pi$, and d is some distance function. If S is a sufficient statistic, then as $\epsilon \to 0$ this will converge to the posterior $f(\boldsymbol{\theta}|D)$.

The choice of good summary statistics is important to the success of ABC fitting. To fit the BL model we used rainfall aggregated over six-minute and hourly intervals, and then compared the mean, standard deviation, autocorrelation at lags 1 and 2, probability of no rain, mean length of wet and dry periods, standard deviation of wet and dry periods, and the total number of wet and dry periods. We note that for GMM fitting we can only use the first five of these statistics, because we do not have analytic expressions for

the others. Using a simulation study we demonstrate that ABC fitting can give less biased and less variable estimates than GMM. We also give an application to rainfall data from Bass River, Victoria, July 2010. Again we see that the ABC fit is better than the GMM fit.

An important advantage of ABC fitting over GMM fitting is that we can use summaries of the data that capture useful information, whether or not we have an expression for their expectation. Moreover, this means that ABC can be used for models for which GMM fitting is not available. For example, if we used a gamma distribution for the duration of a rain cell, rather than an exponential distribution, then we would not be able to calculate the second order statistics of the model, making GMM fitting impossible. However ABC fitting would proceed as before, with the addition of a single parameter. This opens up the possibility of fitting more realistic stochastic rainfall models. We extend the ABC fitting to a spatial-temporal model in Chapter 3.

In **Chapter 3**, we study the fit of a stochastic spatial-temporal model to high-resolution rainfall radar data for a single rainfall event. The Cox-Isham-Northrop (C-I-N) rainfall model is used to model the 'interior' of a rainfall event. The C-I-N model is stationary and is constructed using a cluster point process. The cluster process is constructed by taking a primary process, called the storm arrival process, and then attaching to each storm center a finite secondary point process, called a cell process. To each cell center we then attach a rain cell, with an associated area, duration and intensity. The storm and cell centers all share a common velocity. The total rainfall intensity at point (x, y) and time t is then the sum of the intensity at (x, y) of all cells active at time t. Because it has an intractible likelihood function, the C-I-N model has been fitted using the Generalized Method of Moments.

This chapter has three aims: the first is to show that Approximate Bayesian Computation can be used to fit a Bayesian version the C-I-N model.

The second aim is to extend the C-I-N model to obtain better modeling of the 'interior' of a rainfall event. There are many ways in which the C-I-N model can be extended. If we do so, however, the GMM is no longer suitable for estimation, as it becomes too difficult to obtain analytic expressions for the moments. Fortunately this does not apply to ABC, which can be applied much as before. For the example we do not even have to modify the set of summary statistics. We generalize the C-I-N model by considering the following modifications:

- Randomised cell eccentricity.
- Rainfall intensity that decreases continuously from the centre to the edge of each cell, rather than acting as a step function.

- Heavy-tailed distributions for cell intensity and size.
- Correlated cell intensity and area.

We propose two new models. In the first model, we considered the first two extensions and compare with existing the C-I-N model. This proposed model does a better job for matching the observed process with the model and reproducing the summary statistics. In the second model, we applied all four extensions with the C-I-N model; this shows better representation of the extreme values of rainfall and a negative correlation between cell intensity and area.

Our third aim to obtain a better way of providing starting the ABC algorithm. The Simulated Method of Moments is a variant of the Generalised Method of Moments that uses Monte Carlo estimates of moments, rather than analytic expressions (McFadden 1989, Pakes and Pollard 1989). Thus, like ABC, using SMM we have much more freedom in the choice of moments used to fit the model to the data. When applying ABC, we found it advantageous to 'jump-start' the algorithm by choosing the initial parameter selection θ_0 using a SMM fit, using the same summary statistics S that we chose for the ABC fitting. If θ_0 has very small posterior probability, then ABC-MCMC requires a prohibitively large burn-in period. We found that using SMM for θ_0 requires much less computation time.

In **Chapter 4**, we extend the number of parameters to be estimated in the ABC-MCMC process; only velocity considered a fixed component. Following Wheater et al., 2005 [47] the velocity of the event, the eccentricity and orientation of cells are all estimated in an ad hoc manner using spatial autocovariance functions, and then fixed. We applied this approach in Chapter three. We maximize the benefit of ABC fitting to estimate the parameters.

We also apply the ABC fitting to different rainfall events obtained from different radar located at Melbourne, Australia and Wardon Hill, UK. The ABC fitting gives consistent parameter estimation for the spatial-temporal stochastic rainfall models .

In **Chapter 5**, we present conclution and future work. In previous Chapters, we used ABC to fit a stochastic temporal rainfall model to high-resolution rainfall rain-gauge data, and stochastic spatial-temporal rainfall models to the radar data for rainfall events. We then showed that ABC readily adapts to more general, and thus more realistic, variants of the model. The Simulated Method of Moments was used to initialize the ABC fit.

For future work we recommend in the short term investigating further modifications to the models, and in the long term integrating these models with runoff-runon models to manage flood risk at urban drainage systems.

Chapter 2

Fitting the Bartlett-Lewis rainfall model using Approximate Bayesian Computation

2.1 Introduction

There are numberous of studies of stochastic rainfall models. We consider a stochastic rainfall model for a single point in space. Point process rainfall models are focused on two type of Poisson cluster processes: the Bartlett-Lewis process and the Neyman-Scott process.

Both the Bartlett-Lewis process and the Neyman-Scott process include two components; primary and secondary processes. The primary process is known as the parent process or, in our context, the storm arrival process. With each parent there is associated a secondary process called the daughter or cell arrival process.

The storm arrival process does not contribute to the rainfall amount. It is the cell arrival process, associated with pulses of random durations and random rainfall intensities, that produces rainfall. So, the total rainfall at time t is the sum of intensities from all cells active at that time, see Figure

2.2.

We study the Bartlett-Lewis rainfall process along with two different estimation approaches: Generalized Method of Moments and Approximate Bayesian Computation techniques. The reason for studying these approaches is that they are both useful if the likelihoods are either unavailable or not in a nice form for theoretical expressions.

The Generalized Method of Moments uses theoretical moments instead of likelihood functions, whereas the Approximate Bayesian Computation replaces those moments with simulated data. Both techniques are suitable for complex and well-defined models. Although there is no direct comparison between them, we apply point estimation in both approaches to do so.

Each approach has its own advantages. For ABC, we can include any summary statistics that we wish. This attribute is missing from GMM, which requires theoretical expression for the moments. GMM needs less computational time, whereas ABC takes much longer.

We try to establish answers to the two following questions. Is ABC suitable for point cluster process models? Does it have better performance than GMM?

Because our primary goal is to compare GMM and ABC fitting, we restrict ourselves to a simple BL model, namely the rectangular pulse model introduced by Rodriguez-Iturbe et al., 1987 [39]. Some more recent refinements can be found in Cowpertwait et al., 2007 and Kaczmarska et al., 2011 [9, 24].

2.2 Bartlett-Lewis Rectangular Pulse Model

Rodriguez-Iturbe et al., 1987 [39] introduced this model based on Poisson cluster processes. Rectangular pulse models are both convenient mathematically and applicable to discrete rainfall time series (Northrop & Stone, 2005 Cowpertwait et. al., 2007 [34, 9]). The models can simulate continuous rainfall time series; they then offer a suitable approximation to discrete rainfall time series that makes possible aggregation over any time intervals like 6 minute, hourly or daily (Cowpertwait et al., 2007, Gyasi-Agyei & Willgoose, 1997 [9, 22]).

The Bartlett-Lewis rainfall model is a cluster-based model, in which rain events have cluster centres known as storm origins. The rain cells known as clusters are associated with their cluster centres. Each rain cell consists of a pulse with a random duration and a random intensity. The intensity is constant throughout a cell's lifetime.

Assume that a rainfall event is a Poisson cluster process. Here an event means whole rainfall process. So first, storms originate as the Poisson process at rate λ per unit time. Here λ is constant for a homogeneous Poisson process, because we assume that storms arrive as constant rate. (Note that the storm process could be inhomogeneous, in which case λ would be a function of time.) Each storm origin generates a number of rain cells. The numbers are known as the cluster size and cluster members are represented by rain cells. Second, the rain cells occur as another Poisson process at rate β per unit time. The cell process is stopped after a random time called storm duration.

The rain cells are associated with the storm origins. This process starts at storm arrival times $T_1,\ T_2,\ \ldots,\ T_n$ and continues with storm durations $D_1, D_2,\ \ldots,\ D_n$. Moreover, the cells are allocated according to interarrival time over the interval between the storm origins and the storm termination points (Cox & Isham, 1980 [12]) see Figure 2.1a. Like the parent process (storm process), the rain cells arrival process is homogeneous in time as β is constant. Each rain cell produces rainfall as random depths during its lifetime and it then terminates. Storm may continue after the cell termination point and there may be no rain in the middle of the storm (Rodriguez-Iturbe et. al., 1987 [39]).

We suppose that the storm duration, cell duration and cell intensity follow exponential distributions with rates γ, η and mean μ_x respectively. The cell intensity is also considered to be constant during a cell's lifetime. Durations and intensities of the cells are mutually independent.

The cell arrival times are $T_i + S_1^i, T_i + S_2^i, T_i + S_3^i, , \ldots, T_i + S_k^i$ for storm i occuring after time T_i before the point $T_i + D_i$. Cells have random durations $L_1^i, L_2^i, L_3^i, , \ldots, L_k^i$ and random intensities $X_1^i, X_2^i, X_3^i, , \ldots, X_k^i$. The overall intensity $Y(t)$ of rainfall at time t is the sum of all intensities from active rain cells:

$$Y(t) = \sum_i \sum_j \mathbb{1}_{T_i+S_j^i<t\leq T_i+S_j^i+L_j^i}\ X_j^i \quad , \text{ where } \mathbb{1} \text{ is one if a cell is active at } t, \text{ otherwise zero.} \tag{2.1}$$

2.2.1 Moments

Rain cells have constant intensities and are i.i.d. as X throughout their lifetimes. Let $X_s(u)$ be the random intensity of a cell originating at time s

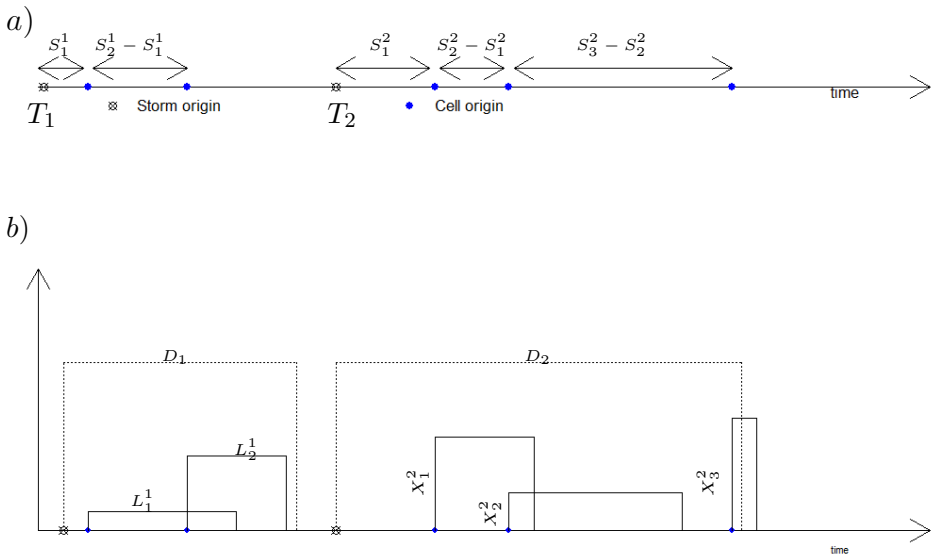

Figure 2.1: Constituent parts of a Bartlett-Lewis process: a) Storm process and cell processes b) Storm durations, cell durations, and cell intensities

measured at time $s + u$. Then

$$X_s(u) \sim X \; \mathbb{1}_{(L>u)}; \tag{2.2}$$

where L, exponentially distributed with parameter η, denotes a cell duration.

Then the total intensity at time t, the sum of the intensities of all cells born before time t and surviving until that time is given by

$$Y(t) = \int_{u=0}^{\infty} X_{t-u}(u)\, dN(t-u). \tag{2.3}$$

where $N(\cdot)$ counts the occurrences of cell origins in the Bartlett-Lewis process and

$$dN(s) = \begin{cases} 1 & \text{if there is a cell origin at } s; \\ 0 & \text{Otherwise.} \end{cases}$$

The intensity of $N(\cdot)$ of the Bartlett-Lewis process of cell occurrences is $\lambda\mu_c$, where $\mu_c = \frac{\beta}{\gamma}$ is the mean number of offspring (cells) per storm (Rodriguez-Iturbe et al. 1987 [39]). Hence, from equation (2.3), the expectation of $Y(t)$ for the Bartlett-Lewis process is found to be

$$
\begin{aligned}
E[Y(t)] &= \int_{u=0}^{\infty} E\{X_{t-u}(u)\}\ E\{dN(t-u)\} \\
&= \int_{u=0}^{\infty} E\{Xe^{-\eta u}\}\ \lambda\mu_c\ du \\
&= \lambda\mu_c\mu_x\frac{1}{\eta},\ \text{where } \mu_x = E[X].
\end{aligned}
$$

$Y(t)$ inherits stationarity from the storm arrival process. The auto-covariance at lag τ is given by

$$
c_Y(\tau) = \int_{u=0}^{\infty}\int_{v=0}^{\infty} E\{X_{t-u}(u)\ X_{t+\tau-v}(v)\}\ \text{cov}\{dN(t-u), dN(t+\tau-v)\}. \tag{2.4}
$$

(see, for example Cox & Miller, 1965 [14] § 9.5 and Rodriguez-Iturbe et. al. 1987 [39] eq. 3.2). We need to evaluate the covariance cov{ $dN(t), dN(t+\tau)$ } first. Cox & Isham, 1980 [12], page 33 described the covariance of a stationary point process as follows:

For $\tau > 0$,

$$
\begin{aligned}
&\text{cov}\{N(t,t+\delta_1), N(t+\tau,t+\tau+\delta_2)\} \\
&\quad = E\{N(t,t+\delta_1)\}E\{N(t+\tau,t+\tau+\delta_2)|N(t,t+\delta_1)\} \\
&\qquad - E\{N(t,t+\delta_1)\}E\{N(t+\tau,t+\tau+\delta_2) \\
&\quad = Pr\{N(t,t+\delta_1)=1\}Pr\{N(t+\tau,t+\tau+\delta_2)=1|N(t,t+\delta_1)=1\} \\
&\qquad - Pr\{N(t,t+\delta_1)=1\}Pr\{N(t+\tau,t+\tau+\delta_2)=1\} + O(\delta_1\delta_2)
\end{aligned}
$$

for $\delta_1, \delta_2 > 0$ small; let $h(\tau) = \text{Pr}\{\ N(t+\tau,t+\tau+\delta_2)=1|N(t,t+\delta_1)=1\}$.

$$
\text{cov}\{N(t,t+\delta_1), N(t+\tau,t+\tau+\delta_2)\} = \lambda\mu_c\ h(\tau)\delta_1\delta_2 - \lambda^2\mu_c^2\delta_1\delta_2;
$$

since the intensity of cell process is $\lambda\mu_c$.

Therefore, for $\tau \geq 0$

$$
\text{cov}\{dN(t), dN(t+\tau)\} = \lambda\mu_c\{\delta(\tau) + h(\tau) - \lambda\mu_c\}dtd\tau.
$$

where δ is the Dirac delta function defined by

$$\int_{-\infty}^{x} \delta(\tau)d\tau = \begin{cases} 0 & \text{if } x < 0, \\ 1 & \text{if } x \geq 0. \end{cases}$$

Cox & Isham, 1980 [12], pages 77 & 78 presented the conditional intensity function $h(\cdot)$ for Poisson cluster processes. Two cells arriving at time t and $t+\tau$ in the Bartlett-Lewis process has two possibilities. They may come from separate storms. In this case the rate of cell arrival is $\lambda\mu_c$. The other possibility is that they may come from the same storm. Cell arrival rate within storm duration is β and storm survival probability $e^{-\gamma\tau}$. Recall that storm durations follow an exponential distribution with rate γ. The probability that both cells belong to the same storm is $\beta e^{-\gamma\tau}$. The conditional intensity is thus $h(\tau) = \lambda\mu_c + \beta e^{-\gamma|\tau|}$. Therefore,

$$\text{cov}\{dN(t), dN(t+\tau)\} = \lambda\mu_c\{\delta(\tau) + \beta e^{-\gamma|\tau|}\}dtd\tau. \tag{2.5}$$

From equation (2.4) and (2.5), we then get

$$\begin{aligned} c_Y(\tau) &= \int_{u=0}^{\infty}\int_{v=0}^{\infty} E\{X_{t-u}(u)\ X_{t+\tau-v}(v)\}\ \lambda\mu_c\{\delta(\tau+u-v) + \beta e^{-\gamma|\tau+u-v|}\}dudv. \\ &= \lambda\frac{1}{\eta}\mu_c\{E[X^2] + \beta\gamma(\gamma^2-\eta^2)^{-1}\mu_x^2\}\ e^{-\eta\tau} - \lambda\beta\mu_c(\gamma^2-\eta^2)^{-1}\mu_x^2\ e^{-\gamma\tau}. \end{aligned}$$

And the variance of the stationary quantity $Y(t)$

$$\text{var}\big(Y(t)\big) = \lambda\frac{1}{\eta}\mu_c\{E[X^2] + \beta(\gamma+\eta)^{-1}\mu_x^2\}. \tag{2.6}$$

For details see Rodriguez-Iturbe et al. 1987 [39].

2.2.2 The Time Aggregation Process

Rainfall data is usually available in the form of time aggregation. We therefore consider the accumulated rainfall over a fixed time interval. Let $Y_i^{(h)}$ be the rainfall intensity for *i-th* interval. The intervals have length h. The

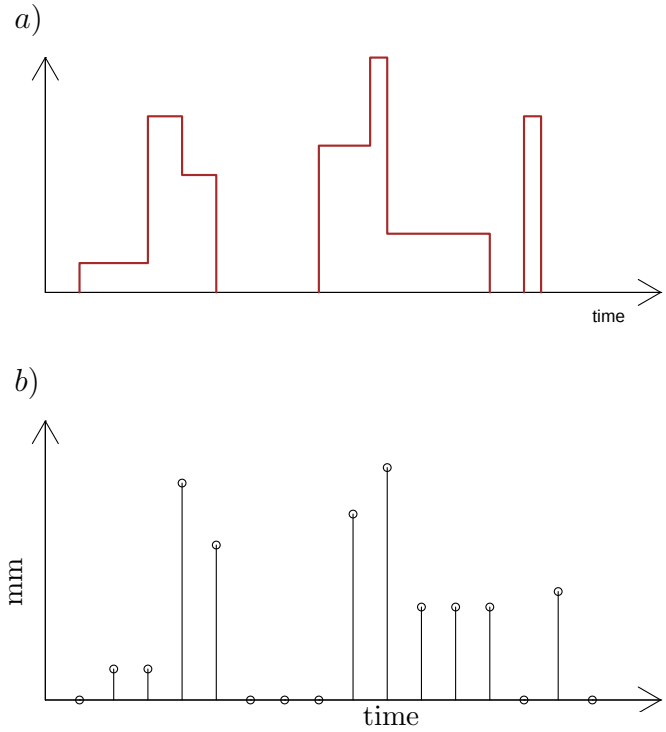

Figure 2.2: a) Total intensity at time t. b) An observed data per h time length.

aggregated process is defined by

$$Y_i^h = \int_{(i-1)h}^{ih} Y(t)\ dt.$$

The first and second order-moments can be obtained by

$$\begin{aligned} E\{Y_i^h\} &= hE\{Y(t)\} \\ &= h\lambda\mu_c\mu_x\eta^{-1}, \text{ where } \mu_c = \beta\ \gamma^{-1}. \end{aligned} \tag{2.7}$$

$$\begin{aligned}\mathrm{Var}\{Y_i^h\} &= 2\int_0^h (h-\tau)c_Y(\tau)d\tau, \\ &= 2h\lambda\mu_c\frac{1}{\eta^2}\big\{E(X^2)+\beta\mu_x^2\frac{1}{\gamma}\big\} + 2\lambda\mu_c\mu_x^2\beta(1-e^{-\gamma h})\gamma^{-2}(\gamma^2-\eta^2)^{-1} \\ &\quad - 2\lambda\mu_c\frac{1}{\eta^3}\big[E(X^2)+\beta\gamma\mu_x^2(\gamma^2-\eta^2)^{-1}\big](1-e^{-\eta h}). \qquad (2.8)\end{aligned}$$

And

$$\begin{aligned}\mathrm{Cov}\{Y_i^h, Y_{i+k}^h\} &= \int_{-h}^{h}(h-|\tau|)c_Y(kh+|\tau|)d\tau, \quad k=1,2,... \\ &= \lambda\mu_c\frac{1}{\eta^3}\{E(X^2)+\beta\gamma\mu_x^2(\gamma^2-\eta^2)^{-1}\}(1-e^{-\eta h})^2e^{-\eta(k-1)h} \\ &\quad - \lambda\mu_c\mu_x^2\beta(1-e^{-\gamma h})^2e^{-\gamma(k-1)h}\gamma^{-2}(\gamma^2-\eta^2)^{-1}. \qquad (2.9)\end{aligned}$$

Let ω_h be the probability of zero rainfall throughout $[0,h]$. (Rodriguez-Iturbe et al., 1987 [39], eq. 4.10) gives the following expression for ω_h :

$$\omega_h = \exp\{-\lambda(h+\mu_T)+\lambda G^*(0,0)[(\gamma+\beta e^{-(\beta+\gamma)h}(\beta+\gamma)^{-1}]\}. \qquad (2.10)$$

where μ_T and $G^*(.,.)$ are defined and calculated in Rodriguez-Iturbe et al., 1987 [41] as

$$\mu_T \simeq \gamma^{-1}\{1+\gamma(\beta+\gamma)\eta^{-2}-\frac{1}{4}\gamma(\beta+\gamma)(\beta+4\gamma)\eta^{-3}+\frac{1}{72}\gamma(\beta+\gamma)(4\beta^2+27\gamma\beta+72\gamma^2)\eta^{-4}\}$$

and

$$G^*(0,0) \simeq \gamma^{-1}\big[1-(\beta+\gamma)\eta^{-1}+(\frac{3}{2}\beta\gamma+\gamma^2+\frac{1}{2}\beta^2)\eta^{-2}\big].$$

2.2.3 Generalized Method of Moments

Although likelihood based techniques have been attempted to fit BL process models, it is neither feasible nor desirable because of the model's complex structure. Furthermore, the intensity is recorded as cumulative rather than instantaneous. The model fitting therefore should carry out using likelihood-free techniques.GMM and ABC are strong candidates because they are likelihood free. This is the first time someone has implemented ABC for the BL model. We will discuss ABC in detail in § 2.3. Presently BL process models

are usually fitted using GMM. Using ABC is new.

The Generalized Method of Moments estimation requires the number of conditions in the objective function to be greater than or equal to the number of model parameters. It is precisely desired because we want some time-aggregated summaries to include in fitting. This results that they are more than the number of model parameters. The GMM is often used in econometric literature. We follow the method presented by Wheater et al, 2005 and Jesus & Chandler, 2011 [47, 23].

Let $\mathbf{V} = (V_1, ..., V_k)'$ be a vector of summary statistics computed from data. The corresponding expected values of $\mathbf{V}$ under the model is denoted by a vector $\tau(\boldsymbol{\theta}) = (\tau_1(\boldsymbol{\theta}), ..., \tau_k(\boldsymbol{\theta}))'$. Estimation of the unknown parameter vector $\boldsymbol{\theta}$ is obtained by

$$\begin{aligned} \hat{\boldsymbol{\theta}} = & \quad \text{argmin}_{\boldsymbol{\theta}}\ G(\boldsymbol{\theta}; \mathbf{V}) \\ = & \quad \text{argmin}_{\boldsymbol{\theta}}\ (\mathbf{V} - \tau(\boldsymbol{\theta}))'\ \mathbf{W}\ (\mathbf{V} - \tau(\boldsymbol{\theta})). \end{aligned}$$

where $\mathbf{W}$ is a positive definite weighting matrix. We will assume $\mathbf{W}$ to be a diagonal matrix. Note that the optimal weights are in fact obtained by taking W equal to the inverse of the covariance matrix, and the diagonal elements of the covariance matrix are the variances. So our weight matrix is an approximation to the optimal choice, where we put all the covariances equal to zero before taking the inverse. In practice the covariance matrix is often very close to singular, so that its inverse is unstable. Therefore, the objective function $G(\boldsymbol{\theta}; \mathbf{T})$ can be written as

$$G(\boldsymbol{\theta}; \mathbf{V}) = \sum_{i=1}^{k} \omega_i [V_i - \tau_i(\boldsymbol{\theta})]^2. \tag{2.11}$$

In theory, the optimal weights ω_i are equal to $\frac{1}{Var(V_i)}$.
To estimate $\text{Var}(V_i)$, first, we may partition the given time series data. If it is possible to estimate summary statistics from partitioned data separately, then for $m > 1$, the fitting properties $\mathbf{V}^{(1)}, ..., \mathbf{V}^{(m)}$ can be calculated for each partitioned dataset. Then $\mathbf{V} = \frac{1}{m} \sum_{i=1}^{m} \mathbf{V}^{(i)}$.

$$\text{Hence,} \quad \widehat{Var}(\mathbf{V}) = \frac{1}{m(m-1)} \sum_{i=1}^{m} (\mathbf{V}^{(i)} - \mathbf{V})(\mathbf{V}^{(i)} - \mathbf{V})'. \tag{2.12}$$

The objective function must be solved by numerically. Note that the required minimization procedure can be complicated. So need to take care because local minima often present. Therefore, the starting values are vital; reason for that gradient based algorithm can fail to reach global minima if starting points are not close enough to promising regions of the parameters Wheater et. al., 200 [47]. So, various writers first used the Nelder-Mead simplex algorithm. Because Nelder-Mead method is more robust and good for identifying promising regions for the parameter space. We tried several different starting points to obtain where the global minima may lie by using the Nelder-Mead simplex algorithm. Once the promising region is identified, then we use Newton-type method, which is a gradient based algorithm. The gradient method is more powerful when having good starting points (Kaczmarska et. al., 2011 [24]).

2.3 Approximate Bayesian Computation

The fundamental difference between Bayesian statistics and frequentist techniques lies in how the parameters θ are conceived (Turner & Zandt, 2012 [45]). In the Bayesian context, parameters are treated as random quantities along with the data. Inferences about parameters are based on the probability distributions of the parameters after some data are observed (Lunn et. al., 2012 [28]).

ABC was introduced by Pritchard e. al., 1999 [38]. The ABC algorithm, which uses summary statistics, as defined in algorithm 1. In this algorithm, S refers to statistics that are expected to be sufficient, but in many cases they are not. d is a metric function and $\epsilon > 0$ is a tolerance level.

Algorithm 1 ABC using summary statistics

for i=1 to N **do**
  repeat
    Generate θ^* from the prior distribution $\pi(\cdot)$
    Simulate data D^* from the likelihood $f(\cdot|\theta^*)$
  until $d(S(D^*), S(D)) \leq \epsilon$
  Set $\theta_i = \theta^*$.
end for

The ABC methodology supposes that we have observations D from some model $f(\cdot|\theta)$ that depends on parameters θ, and that we are able to simulate from f. Let π be the prior distribution for θ and $S = S(D)$ a vector of sum-

mary statistics for D; then ABC generates samples from $f(\theta|d(S(D^*), S(D)) < \epsilon)$, where $D^* \sim f(\cdot|\theta^*)$, θ^* is a proposal for θ distributed according to π, and d is some distance function. If S is a sufficient statistic, then as $\epsilon \to 0$ this will converge to the posterior $f(\theta|D)$.

2.3.1 ABC Markov Chain Monte Carlo

Markov Chain Monte Carlo (MCMC) can be easily embedded within ABC algorithms. ABC was extended to incorporate Markov Chain Monte Carlo (MCMC) by Marjoram et al. 2003 [29], or alternatively Sequential Monte Carlo (SMC) (Sisson et al. 2007, Sisson et al., 2009 and Beaumont et at., 2009 [43, 44, 2]). We will use the ABC-MCMC methodology of Marjoram et al. 2003 [29]. Wegmann et al., 2009 [46] provide some practical advice on implementing ABC-MCMC, and give a proof of the central result in Marjoram et al., 2003 [29].

In this approach, we supply a prior distribution (π) and parameter values are proposed by a proposal distribution q. It then compares summary statistics (S) of simulated and observed data applying a distance function (d).

The algorithm 2 is known as ABC-MCMC without likelihoods. If the proposal distribution is symmetric, α will depend only on the prior.

Algorithm 2 ABC MCMC without likelihood

for $i = 1$ to N **do**
  Given current state $\boldsymbol{\theta}_i$, propose a new state $\boldsymbol{\theta}^*$ using a transition kernel $q(\boldsymbol{\theta}^*|\boldsymbol{\theta}_i)$
  Put $\alpha = \min\left(1, \frac{\pi(\boldsymbol{\theta}^*)q(\boldsymbol{\theta}_i|\boldsymbol{\theta}^*)}{\pi(\boldsymbol{\theta}_i)q(\boldsymbol{\theta}^*|\boldsymbol{\theta}_i)}\right)$.
  if $U(0,1) < \alpha$, **then**
    simulate data $D^* \sim f(\cdot|\boldsymbol{\theta}^*)$
    if $d(S(D^*), S(D)) \leq \epsilon$, **then**
      set $\boldsymbol{\theta}_{i+1} = \boldsymbol{\theta}^*$
    else
      set $\boldsymbol{\theta}_{i+1} = \boldsymbol{\theta}_i$
    end if
  else
    set $\boldsymbol{\theta}_{i+1} = \boldsymbol{\theta}_i$
  end if
end for

Note that MCMC rejection comes before the ABC comparison of simulated and observed data, so as to avoid the unnecessary simulation; this saves computational time. Further, the proposal is accepted only if the proposed θ^* satisfies both conditions.

Note that ABC-MCMC has a higher acceptance rate than ABC, but it introduces correlation into the sample. ABC-MCMC is more efficient than ABC. To properly compare the two, we need to look at the effective sample size we obtain for a fixed simulation effort. We rather focus on implementing the ABC technique to cluster rainfall models in this chapter.

2.3.2 ABC-MCMC Linear Regression Adjustment

Beaumont et al., 2002 [3] introduced a post-estimation scheme of ABC output. This technique provides an adjustment of the posterior density by using local linear regression. The explanatory variables are distances of all summary statistics. Suppose θ_i are samples of the posterior distribution estimated by ABC-MCMC, and D^i the simulation. If we assume that the local linear regression consists of the form,

$$\theta_i = \beta_0 + (S(D^i) - S(D))^T \beta_1 + \delta_i, i = 1, 2, ..., m;$$

where β_0 refers intercept, β_1 is a vector of regression coefficients and δ_i are uncorrelated with mean zero and common variance.

We apply weighted local regression to approximate the posterior distribution, then we can correct θ_i to get

$$\theta_i^* = \theta_i - (S(D^i) - S(D))^T \hat{\beta}_1;$$

where $\hat{\beta}_1$ is the estimate.
$\hat{\beta}_0, \hat{\beta}_1 = \text{argmin}_{\beta_0,\beta_1} \sum_{i=1}^{m} \left\{\theta_i - \beta_0 - (S(D^i) - S(D))^T \beta_1\right\}^2 K_\epsilon(||S(D^i) - S(D)||)$.
where $K_\epsilon(x)$ is the Epanechnikov kernel given by

$$K_\epsilon(x) = \begin{cases} (1 - (\frac{x}{\epsilon})^2); & |x| \leq \epsilon, \\ \\ 0 & |x| > \epsilon. \end{cases}$$

ABC allows us to include a range of summary statistics. Including unnecessary statistics will reduce the performance of the ABC estimator, essentially by introducing noise that makes it harder to distinguish between good

and bad simulations. This can be mitigated somewhat using the regression adjustment method. We have shown comparison in Tables 2.2 and 2.3.

2.4 ABC-MCMC for the BL Model

ABC-MCMC suffers from having dependent parameters. The model parameters are highly dependent. We reparameterise the model parameters to reduce the dependency. This leads us to be successful in applying ABC-MCMC to fitting the BL model to rainfall data.

2.4.1 Reparameterization and Prior Distribution

The total intensity at time t has mean $I_T = \lambda \times \gamma^{-1} \times \beta \times \eta^{-1} \times \mu_x$. Different combinations of parameters can lead to the same total intensity. For instance, low storm arrival rate and long storm duration vice versa. Likewise cell parameters may have different configuration. Firstly we reparameterise the model in order to reduce the dependence between the parameters. In addition we use a log transformation to map their domain from $\mathbb{R}_+$ to $\mathbb{R}$, this simplifies the proposal chain.

We chose first three parameters directly relatable to the observed rainfall, the total intensity at time t has mean $I_T = \lambda\gamma^{-1}\beta\eta^{-1}\mu_x$, the percentage of time covered by storms has mean roughly proportional to $\lambda\gamma^{-1}$, and the percentage of a storm covered by rain cells has mean roughly proportional to $\beta\eta^{-1}$. The final two parameters were chosen to be roughly orthogonal to these three, with respect to the posterior. Our new parameters are

$$\begin{aligned}
\theta(1) &= \log(I_T), \\
\theta(2) &= \log(\lambda\gamma^{-1}), \\
\theta(3) &= \log(\lambda\gamma), \\
\theta(4) &= \log(\beta\eta^{-1}), \\
\theta(5) &= \log(\beta\eta).
\end{aligned}$$

These parameters are still dependent, for example a low storm arrival rate and long storm duration can give the same total intensity as a high storm arrival rate and short storm duration. Nonetheless we found that this reparameterisation improved estimation. We also found that I_T is much easier to estimate than μ_x.

Vague normal priors are used for all the $\theta(i)$; that is $\pi(\theta) \sim N(\mathbf{0}, \sigma^2\mathbf{I})$ for σ^2 large. Note that σ^2 may vary between $\theta(1), \theta(2), \ldots \theta(5)$.

2.4.2 Summary Statistics, Distance Metric and Weighting

We discussed some theoretical moments of the BL model in § 2.2.2. GMM fitting requires moments with analytical expressions, and we used mean, standard deviation, auto-correlation of lag 1 and lag 2 and probability of zero rainfall in an interval for 6-minute and hourly aggregation, giving a total of 9 summary statistics. The hourly mean was not included because it does not give any additional information other than just aggregation of rainfall amount of 6-minute data. For our ABC-MCMC fitting, in addition to these summary statistics, we used mean length of wet and dry periods, standard deviation of wet and dry periods and sum of number of wet and dry periods. There are therefore 19 summary statistics for ABC-MCMC fitting.

The distance measure of the summary statistics we used is the weighted Euclidean distance between observed and simulated data summary statistics. Weights are crucial to the success of ABC-MCMC fitting. The weight is estimated using a sample generated from the model. Particularly the way we have chosen weights for summary statistics is that we simulated the data from the model using initial parameter values. For each simulation we take the difference between the observed and simulated summary statistics, and repeat this 10^5 times. We then normalise the distance measure using the reciprocal of the standard deviation of distance values between the observed and simulated summary statistics. The most disperse distance has least weight. Equivalently, the narrower distances between summary statistics has the higher weight. This yields equal importance to all summary statistics.

We could provide larger weights for the statistics that have most information about the parameters. However it is impossible to decide a-priori which has the most information for parameters. We included first all 19 summary statistics in ABC-MCMC fitting. We then experimented using small set of summary statistics. We found that the fitting consisting of all the summary statistics is better. We therefore kept all 19 summary statistics and estimated posterior distribution of the parameters.

2.4.3 Proposal Chain, Acceptance Rate and Effective Sample Size

As discussed in § 2.3.1, the proposal chain is arbitrary. We considered random walk. We have experienced 1.5 to 10 percent acceptance rate for the ABC-MCMC algorithm provides a good approximation of posterior distributions. Although there is low effective sample size, we obtained good posterior distributions. There is an efficiency of 0.003 (effective sample size over number of simulations).

2.5 Simulated Data Study

In this section, we estimate posteriors using the ABC-MCMC algorithm, and point estimates from the GMM. The chosen simulation time is 2 weeks, we used 6-minute and hourly aggregation data for the simulation study.

2.5.1 ABC-MCMC

We consider two types of rainfall events as storm levels. One is that the rainfall process has frequent storm arrivals and short storm durations. The second is that it has few storm arrivals but relatively long storm durations. Each case has 8 combination sets of parameters. Table 2.1 shows the combination of parameters and their respective values.

Parameter values $(\lambda, \gamma^{-1}, \beta, \eta^{-1}, \mu_x)$	λ	γ^{-1}	β	η^{-1}	μ_x
(0.04, 10.00, 1.00, 1.00, 3.00)	+	+	+	+	+
(0.04, 10.00, 0.50, 1.00, 1.50)	+	+	-	+	-
(0.04, 05.00, 1.00 ,0.50, 3.00)	+	-	+	-	+
(0.04, 05.00, 0.50, 0.50, 1.50)	+	-	-	-	-
(0.02, 10.00, 1.00, 0.50, 1.50)	-	+	+	-	-
(0.02, 05.00, 0.50 ,1.00, 3.00)	-	-	-	+	+
(0.02, 10.00, 0.50, 0.50, 3.00)	-	+	-	-	+
(0.02, 05.00, 1.00, 1.00, 1.50)	-	-	+	+	-
(0.014, 48.00, 1.00, 1.00, 3.00)	+	+	+	+	+
(0.014, 48.00, 0.50, 1.00, 1.50)	+	+	-	+	-
(0.014, 24.00, 1.00, 0.50, 3.00)	+	-	+	-	+
(0.014, 24.00, 0.50, 0.50, 1.50)	+	-	-	-	-
(0.007, 48.00, 1.00, 0.50, 1.50)	-	+	+	-	-
(0.007, 24.00, 0.50, 1.00, 3.00)	-	-	-	+	+
(0.007, 48.00, 0.50, 0.50, 3.00)	-	+	-	-	+
(0.007, 24.00, 1.00, 1.00, 1.50)	-	-	+	+	-

Table 2.1: Experimental design of parameter values. + represents high value and − refer to low value.

As discussed in § 2.4.2, we used 19 summary statistics and a weighted Euclidean distance function. We would like to have tolerance level ϵ as small as possible. We call θ_0 the true value, and it is what we intend to estimate.

Selecting ϵ is a difficult process. Theoretically we want ϵ to be small. However in practice it is more challenging, because with too small a chain could get stuck in low probability parameter space. On the other hand, large ϵ can distort posterior approximation. We first ran a short chain with about 10K iterations with large ϵ. We then investigated chain mixing, acceptance rate and distance of summary statistics etc. We gradually reduced ϵ making sure chain does not get stuck. Once we found reasonable ϵ, we ran a long chain of 100K iterations. We exploited Parallel Programming using the programming language called "Julia". We started a chain as the same initial value i.e. true value but on different computer cores. This gives a different random walk on each core. For instance, we used a PC with 8 cores. We ran one chain in each core (just used 7 cores). There were the 7 distinct chains running in the same time having different random paths. We then collected all chains together.

Figure 2.3 indicates that the posterior distribution of log parameters as discussed in § 2.4.1 converges to the stationary distribution.

The simulation time is 2 weeks. Threshold is $\epsilon = 2.5$ and acceptance rate is 3%. There is no need the burn-in time because we start from the true values. Note that to fairly compare methods, the true values where used as stating points for both GMM and ABC-MCMC methods.

We have transformed those log parameters to the original model parameters using exponentials as follows:

$$\begin{aligned}
\lambda &= \exp\Big(\frac{\theta(2)+\theta(3)}{2}\Big),\\
\gamma^{-1} &= \exp\Big(\frac{\theta(2)-\theta(3)}{2}\Big),\\
\beta &= \exp\Big(\frac{\theta(4)+\theta(5)}{2}\Big),\\
\eta^{-1} &= \exp\Big(\frac{\theta(4)-\theta(5)}{2}\Big),\\
\mu_x &= \exp\Big(\theta(1)-\theta(2)-\theta(4)\Big).
\end{aligned}$$

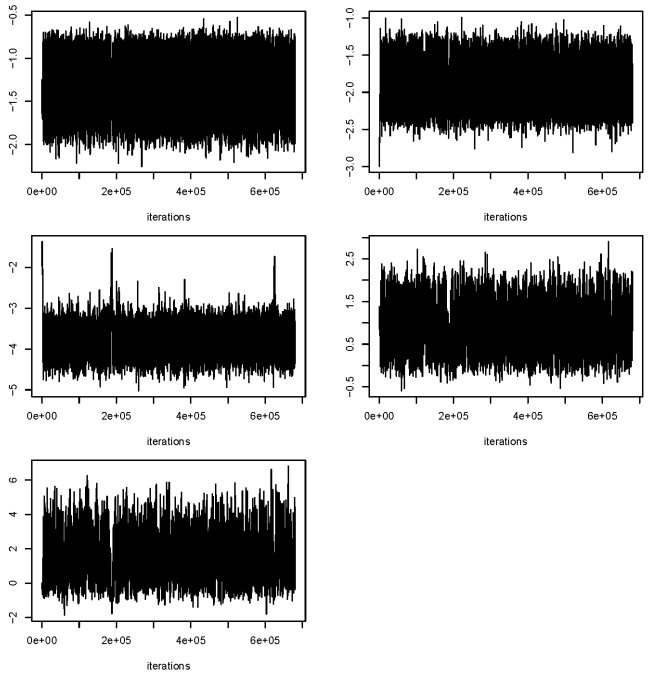

Figure 2.3: Chains for $\theta(1)$-top left, $\theta(2)$)-top right, $\theta(3)$- middle left, $\theta(4)$-middle right, $\theta(5)$- bottom; simulation length = 2 weeks.

The below graphs in Figure 2.4 (before linear adjustment) and 2.5 (after linear adjustment) show the posterior densities of the parameters. We can see that applying the local linear adjustment on the post-estimation process as discussed in § 2.3.2 improves the posteriors because the posterior densities are tighter and the variances of the posteriors are reduced. We also used the weight based on summary distances to estimate the posterior mean shown in Figure 2.5 .

Figure 2.6 shows the joint distributions of the posteriors. We can see there is still some relation between parameters as expected. Lower panel plots are of pairs of posteriors, where the intensity values are the counts of samples in the posterior distributions within a particular area. Lines (red) are the true values of respective the true parameters. The figure is produced using "IDPmisc" package in R.

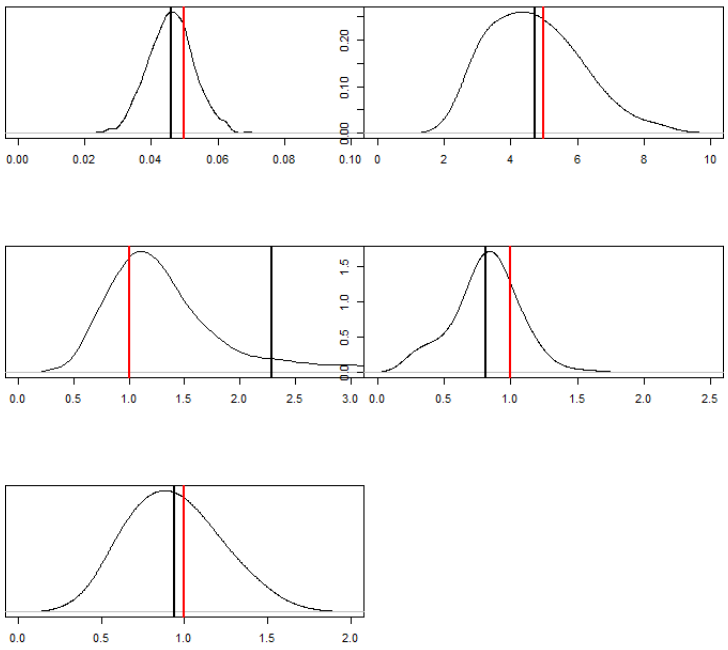

Figure 2.4: Posterior densities of the storm rate (λ) (top left), storm duration (γ^{-1}) (top right), cell rate (β) (middle left), cell duration (η^{-1}) (middle right)and cell intensity(μ_x) (bottom). Red lines are true values and black lines are posterior means.

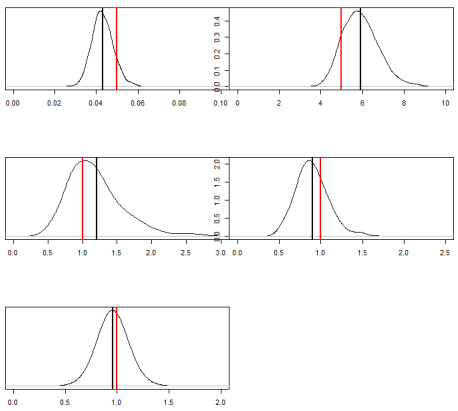

Figure 2.5: Posterior densities of parameters after linear adjustment. Storm rate (λ) (top left), storm duration (γ^{-1})- (top right), cell rate (β) (middle left), cell duration (η^{-1}) (middle right)and cell intensity (μ_x) (bottom). Red lines are true values and black lines are weighted posterior means.

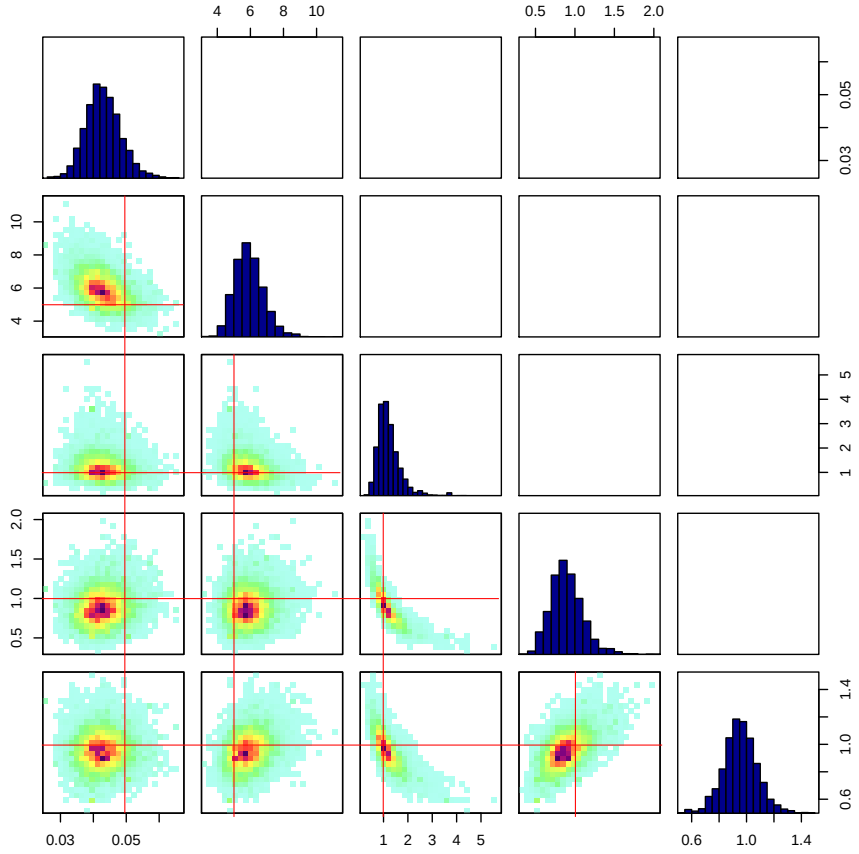

Figure 2.6: From top, diagonal plots are respectively posterior distribution of $\lambda, \gamma^{-1}, \beta, \eta^{-1}$ and μ_x . The true values are (0.05, 5.0, 1.0, 1.0, 1.0). Lower panel plots are pair of posteriors, where intensity values are the count of samples in the posterior distribution sets within a particular area. Lines (red) are the true values of respective parameters.

2.5.2 Comparison

We have estimated the parameters from 16 different combinations of both cases shown as Table 2.1. For comparison study, we used the simulated data. First, we simulated the data using the model with known parameter values. We then considered the simulated data as the observed data. Second, we estimated parameter values using both GMM and ABC-MCMC techniques. As we know GMM gives point estimates. We also calculated posterior means

and medians from posterior distributions as outcomes of the ABC-MCMC algorithm. We repeated the process 100 times. True values, bias, mean squared error and 95% confident intervals of GMM estimation and posterior mean and median are shown in Tables 2.2 and 2.3. The simulation study shows that the posterior means are better estimates than the posterior medians, because they have smaller bias than the posterior medians and also have narrow in confidence interval for the parameters.

Figure 2.7 compares bias of parameter estimation. As we discussed above we simulated the data from given parameter values. We then used the simulated data to estimate parameters using both ABC and GMM. We repeat this 25 times for Figure 2.7. Points are the difference of estimated and true values. X-axis values are number of repetition using the same parameter value. Left figures are estimation from GMM likewise right figures are that from ABC-MCMC. Black lines are zero-bias and blue lines are mean difference. This graphs clearly indicate the ABC-MCMC is better estimation than GMM in simulation study because their mean bias difference is close to zero-bias . The same result is obtained from Table 2.2 and 2.3. Because ABC-MCMC mean square errors are smaller than that of GMM and has small 95% confident interval. There is not clear preferance between posterior means and medians.

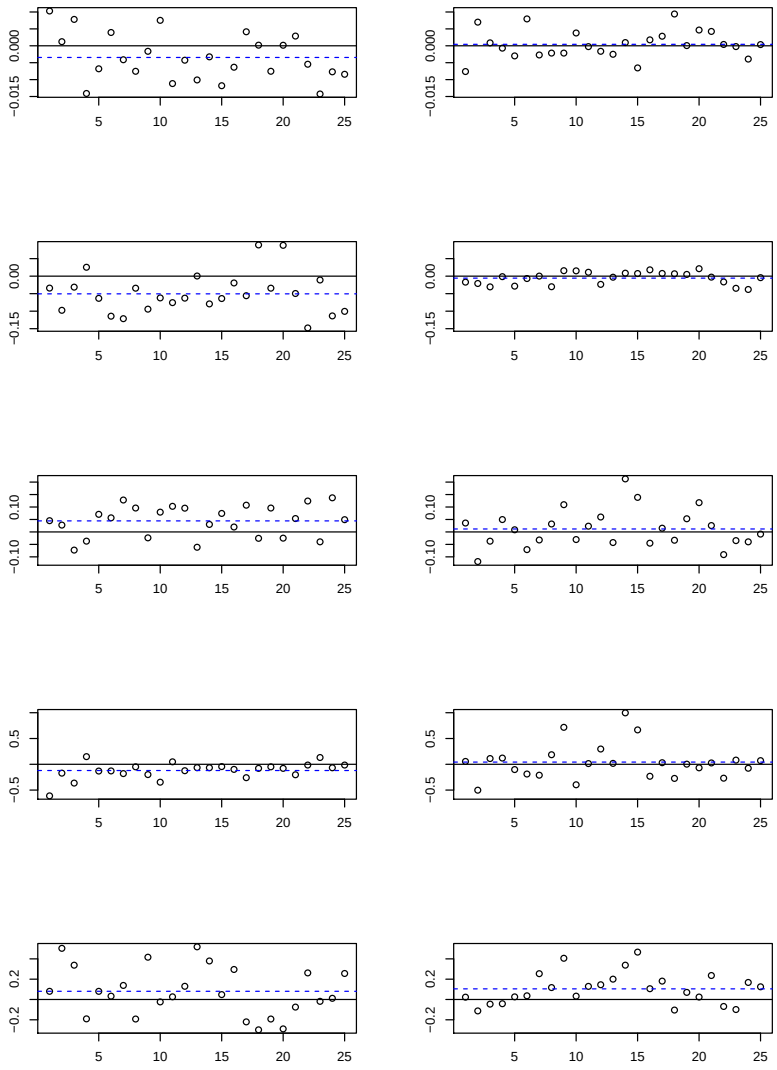

Figure 2.7: From Top to Bottom, plots of average bias of parameters $\lambda, \gamma, \beta, \eta$ and μ_x respectively. The parameter true values are (0.04, 0.20, 0.50, 2.00, 1.50). Points are difference of estimated and true values. X-axis values are number of repetition using the same parameter value. Left figures are estimates from GMM, right figures are those from ABC-MCMC. Lines (black) are zero-bias and dotted lines (blue) are mean difference.

.

	Parameters		Mean squared error				Bias				95%CI		
Set I		True value	GMM	ABC (Posterior mean)	ABC Linear (Posterior mean)	ABC (Posterior median)	GMM	ABC (Posterior mean)	ABC Linear (Posterior mean)	ABC (Posterior median)	GMM	ABC (Posterior mean)	ABC Linear (Posterior mean)
1	λ	0.040	0.0002	**0.0000**	**0.0000**	**0.0000**	0.0071	0.0008	0.0015	**0.0007**	(0.0419, 0.0523)	(0.0392, 0.0424)	(0.0391, 0.0439)
	γ	0.100	0.0003	**0.0001**	**0.0001**	**0.0001**	0.0039	-0.0012	-0.0028	**-0.0005**	(0.0974, 0.1104)	(**0.0947, 0.1029**)	(0.0929, 0.1015)
	β	1.000	0.0740	0.0040	0.0050	**0.0037**	-0.1778	0.0112	**-0.0029**	0.0052	(0.7399, 1.0449)	(0.9864, 1.036)	(0.9688, 1.0253)
	η	1.000	0.0059	0.0054	0.0092	**0.0053**	0.0203	**0.0188**	0.0302	0.0221	(0.9906, 1.0499)	(0.9903, 1.0472)	(0.9937, 1.0667)
	μ_x	3.000	0.3270	**0.0221**	0.0458	0.0240	-0.3662	0.0385	**0.0198**	0.0328	(2.4581, 3.0959)	(**2.9810, 3.0959**)	(2.9345, 3.1050)
2	λ	0.040	0.0001	**0.0000**	0.0001	**0.0000**	0.0029	0.0023	**0.0011**	0.0022	(0.0386, 0.0471)	(0.0405, 0.0441)	(0.0376, 0.0445)
	γ	0.100	0.0002	**0.0001**	0.0005	**0.0001**	**-0.0002**	0.0033	-0.0012	0.0037	(0.0938, 0.1058)	(**0.0992, 0.1074**)	(0.0895, 0.1082)
	β	0.500	0.0027	**0.0025**	0.0146	0.0028	**0.0147**	-0.0155	-0.0638	-0.0171	(0.4948, 0.5346)	(**0.4653, 0.5037**)	(0.3912, 0.4775)
	η	1.000	0.0078	**0.0039**	0.0420	**0.0039**	0.0351	-0.0298	-0.0868	**-0.0177**	(1.0026, 1.0676)	(0.9482, 0.9922)	(0.8319, 0.9946)
	μ_x	1.500	0.0195	0.0045	0.0065	**0.0044**	**-0.0016**	0.0090	0.0331	0.0093	(1.4425, 1.5543)	(1.4823, 1.5356)	(1.5009, 1.5654)
3	λ	0.040	**0.0000**	**0.0000**	**0.0000**	**0.0000**	-0.0006	0.0003	**0.0002**	0.0003	(0.0377, 0.0410)	(0.0391, 0.0415)	(**0.0391, 0.0413**)
	γ	0.200	0.0015	**0.0005**	0.0007	**0.0005**	-0.0058	**0.0025**	0.0052	0.0031	(0.1788, 0.2096)	(0.1936, 0.2113)	(0.1952, 0.2152)
	β	1.000	0.0272	0.0070	0.0107	**0.0058**	0.0427	0.0434	0.0479	**0.0272**	(0.9789, 1.1064)	(1.0147, 1.0719)	(1.0112, 1.0845)
	η	2.000	**0.0221**	0.0629	0.0680	0.0667	**-0.0743**	0.0763	0.0814	0.0947	(1.8742, 1.9771)	(**1.9807, 2.1719**)	(1.9823, 2.1805)
	μ_x	3.000	0.2976	0.0383	0.0600	**0.0342**	-0.1406	0.0232	0.0587	**0.0078**	(2.6485, 3.0703)	(2.9455, 3.1010)	(2.9636, 3.1539)
4	λ	0.040	0.0001	**0.0000**	**0.0000**	**0.0000**	-0.0035	0.0004	-0.0003	**0.0001**	(0.0338, 0.0393)	(0.0388, 0.0421)	(0.0380, 0.0413)
	γ	0.200	0.0058	**0.0003**	0.0005	**0.0003**	-0.0505	-0.0056	-0.0102	**-0.0038**	(0.1266, 0.1924)	(0.1873, 0.2014)	(0.1819, 0.1976)
	β	0.500	0.0057	0.0057	0.0066	**0.0054**	0.0443	0.0119	**0.0049**	0.0079	(0.5020, 0.5689)	(0.4821, 0.5416)	(0.4726, 0.5372)
	η	2.000	**0.0389**	0.1133	0.1282	0.1147	-0.1208	**0.0430**	0.0825	0.0642	(1.8169, 1.9942)	(1.9094, 2.1765)	(1.9432, 2.2219)
	μ_x	1.500	0.0627	0.0339	0.0277	**0.0273**	**0.0807**	0.1046	0.0903	0.0854	(**1.4858, 1.6755**)	(1.5439, 1.6652)	(1.5343, 1.6463)
5	λ	0.020	**0.0000**	**0.0000**	**0.0000**	**0.0000**	0.0006	0.0005	**0.0000**	0.0004	(0.0197, 0.0216)	(0.0194, 0.0215)	(**0.0192, 0.0209**)
	γ	0.100	0.0005	**0.0001**	**0.0001**	**0.0001**	0.0116	0.0016	**0.0006**	0.0026	(0.1034, 0.1197)	(0.0972, 0.1060)	(**0.0972, 0.1040**)
	β	1.000	0.0501	0.0092	0.0102	**0.0086**	0.0851	0.0066	**-0.0002**	0.0047	(1.0023, 1.1679)	(0.9684, 1.0448)	(0.9594, 1.0402)
	η	2.000	**0.0057**	0.0285	0.0523	0.0271	0.0166	-0.0151	0.0233	**-0.0007**	(**1.9872, 2.0460**)	(1.9176, 2.0522)	(1.9323, 2.1143)
	μ_x	1.500	0.0427	**0.0101**	0.0200	0.0103	**-0.0025**	0.0195	0.0364	0.0106	(1.4149, 1.5801)	(**1.4801, 1.5588**)	(1.4817, 1.5911)
6	λ	0.020	**0.0000**	**0.0000**	**0.0000**	**0.0000**	0.0012	0.0028	**0.0010**	0.0022	(0.0188, 0.0236)	(0.0212, 0.0244)	(**0.0198, 0.0221**)
	γ	0.200	**0.0008**	0.0018	0.0012	0.0019	0.0013	**0.0007**	-0.0093	0.0066	(**0.1903, 0.2123**)	(0.1839, 0.2174)	(0.1772, 0.2042)
	β	0.500	**0.0046**	0.0237	0.0200	0.0197	0.0488	0.0133	0.0092	**-0.0042**	(0.5028, 0.5657)	(0.4520, 0.5747)	(0.4528, 0.5657)
	η	1.000	**0.0195**	0.0210	0.0207	0.0209	0.0432	-0.0505	**-0.0193**	-0.0287	(**0.9900, 1.0963**)	(0.8952, 1.0038)	(0.9237, 1.0377)
	μ_x	3.000	0.3436	0.0628	0.0632	**0.0607**	0.1030	0.0352	0.0375	**0.0141**	(2.8721, 3.3338)	(2.9359, 3.1345)	(2.9381, 3.1370)
7	λ	0.020	**0.0000**	**0.0000**	**0.0000**	**0.0000**	-0.0013	0.0002	-0.0001	**0.0000**	(0.0168, 0.0206)	(0.0195, 0.0209)	(**0.0192, 0.0206**)
	γ	0.100	0.0007	**0.0001**	**0.0001**	**0.0001**	0.0072	**0.0009**	0.0010	0.0022 7	(0.0970, 0.1174)	(**0.0962, 0.1055**)	(0.0961, 0.1058)
	β	0.500	0.0167	0.0052	**0.0046**	0.0051	-0.0441	0.0116	0.0195	**0.0076**	(0.4073, 0.5045)	(0.4832, 0.5401)	(**0.4928, 0.5456**)
	η	2.000	**0.0519**	0.1060	0.0892	0.1115	0.0172	-0.0099	0.0682	**0.0081**	(**1.9263, 2.1081**)	(1.8599, 2.1204)	(1.9493, 2.1870)
	μ_x	3.000	0.2201	0.0826	**0.0561**	0.0744	0.1223	0.0709	0.0421	**0.0394**	(2.9411, 3.3035)	(2.9595, 3.1823)	(**2.9469, 3.1373**)
8	λ	0.020	0.0001	**0.0000**	**0.0000**	**0.0000**	0.0049	0.0009	0.0009	**0.0008**	(0.0214, 0.0283)	(**0.0202, 0.0217**)	(0.0200, 0.0218)
	γ	0.200	0.0028	0.0007	**0.0006**	0.0007	-0.0137	0.0053	**0.0009**	0.0080	(0.1658, 0.2068)	(0.1951, 0.2154)	(**0.1910, 0.2108**)
	β	1.000	0.0723	0.0655	**0.0213**	0.0283	0.2191	0.0779	**0.0116**	0.0241	(1.1568, 1.2814)	(0.9804, 1.1754)	(**0.9522, 1.0698**)
	η	1.000	0.0181	0.0057	0.0070	**0.0045**	0.0695	-0.0426	-0.0331	**-0.0275**	(1.0234, 1.1156)	(0.9324, 0.9823)	(0.9354, 0.9983)
	μ_x	1.500	0.0677	0.0158	**0.0090**	0.0151	-0.1836	-0.0239	**-0.0114**	-0.0284	(1.2426, 1.3902)	(1.4268, 1.5255)	(**1.4410, 1.5272**)

Table 2.2: Experiment of parameter estimation. Bias, mean squared errror and 95% CI for parameters.

	Parameters		Mean squared error				Bias				95%CI		
Set II		True value	GMM	ABC (Posterior mean)	ABC Linear (Posterior mean)	ABC (Posterior median)	GMM	ABC (Posterior mean)	ABC Linear (Posterior mean)	ABC (Posterior median)	GMM	ABC (Posterior mean)	ABC Linear (Posterior mean)
9	λ	0.014	0.0001	**0.0000**	**0.0000**	**0.0000**	0.0061	0.0002	-0.0002	**0.0000**	(0.0138,0.0224)	(0.0132, 0.0151)	(**0.0128,0.0147**)
	γ	0.021	0.0003	**0.0000**	**0.0000**	**0.0000**	0.0143	0.0004	**0.0001**	0.0006	(0.0211,0.0391)	(**0.0203, 0.0221**)	(0.0199,0.0219)
	β	1.000	0.0107	**0.0000**	0.0035	0.0031	-0.0128	**-0.0002**	0.0049	0.0006	(0.9462,1.0282)	(**0.9775, 1.0221**)	(0.9812,1.0285)
	η	1.000	0.0090	0.0036	**0.0020**	0.0034	-0.0348	-0.0267	**-0.0185**	-0.0244	(**0.9298,1.0006**)	(0.9518, 0.9947)	(0.9652, 0.9977)
	μ_x	3.000	0.3940	0.0188	**0.0151**	0.0190	-0.2242	**-0.0010**	0.0076	-0.0085	(2.5413,3.0104)	(2.9442, 3.0538)	(**2.9586, 3.0567**)
10	λ	0.014	**0.0000**	**0.0000**	**0.0000**	**0.0000**	0.0029	**-0.0001**	-0.0002	-0.0002	(0.0143, 0.0160)	(0.0131, 0.0148)	(**0.0130, 0.0146**)
	γ	0.021	0.0001	**0.0000**	**0.0000**	**0.0000**	-0.0013	-0.0003	**-0.0001**	**-0.0001**	(0.0165,0.0226)	(**0.0194, 0.0215**)	(0.0195, 0.0219)
	β	0.500	0.0170	0.0022	**0.0014**	0.0023	-0.0995	-0.0055	**-0.0027**	-0.0064	(0.3669,0.4342)	(0.4757, 0.5134)	(**0.4822, 0.5121**)
	η	1.000	0.0200	0.0044	**0.0034**	0.0040	0.1192	-0.0212	**-0.0034**	-0.0173	(1.0888, 1.1496)	(0.9536, 1.0039)	(**0.9726, 1.0205**)
	μ_x	1.500	0.0656	0.0061	**0.0033**	0.0065	0.0520	0.0080	0.0067	**0.0059**	(1.4517, 1.6524)	(1.4770, 1.5391)	(**1.4833,1.5302**)
11	λ	0.014	**0.0000**	**0.0000**	**0.0000**	**0.0000**	0.0009	0.0004	**0.0003**	**0.0003**	(0.0137, 0.0161)	(0.0137, 0.0150)	(0.0137, 0.0149)
	γ	0.042	0.0004	**0.0000**	**0.0000**	**0.0000**	0.0039	0.0009	**0.0007**	0.0014	(0.0377, 0.0535)	(0.0411, 0.0441)	(0.0407, 0.0440)
	β	1.000	0.0167	**0.0025**	0.0047	**0.0025**	**-0.0120**	0.0147	0.0242	0.0121	(0.9365, 1.0396)	(**0.9956, 1.0338**)	(0.9981, 1.0498)
	η	2.000	0.0247	0.0221	0.0292	**0.0215**	0.0457	**0.0021**	0.0266	0.0096	(1.9856, 2.1058)	(1.9426, 2.0615)	(1.9576, 2.0956)
	μ_x	3.000	0.3348	0.0173	**0.0119**	0.0168	0.2494	0.0588	0.0464	**0.0428**	(3.0405, 3.4583)	(3.0118, 3.1058)	(3.0060, 3.0868)
12	λ	0.014	**0.0000**	**0.0000**	**0.0000**	**0.0000**	0.0013	**-0.0003**	-0.0004	**-0.0003**	(0.0145, 0.0162)	(0.0132, 0.0143)	(0.0130, 0.0141)
	γ	0.042	0.0003	**0.0000**	**0.0000**	**0.0000**	0.0100	-0.0005	-0.0003	**-0.0001**	(0.0458, 0.0577)	(0.0396, 0.0427)	(0.0397, 0.0430)
	β	0.500	0.0153	0.0027	0.0034	**0.0025**	-0.0263	0.0128	0.0220	**0.0114**	(0.4253, 0.5221)	(0.4927, 0.5328)	(0.5003, 0.5437)
	η	2.000	0.0398	**0.0361**	0.0399	0.0369	**-0.0261**	0.0408	0.0910	0.0568	(1.8948, 2.0530)	(1.9665, 2.1150)	(2.0198, 2.1621)
	μ_x	1.500	0.1715	0.0133	0.0162	**0.0117**	0.2978	0.0582	0.0535	**0.0491**	(1.6826, 1.9129)	(1.5184, 1.5980)	(1.5072, 1.5998)
13	λ	0.007	**0.0000**	**0.0000**	**0.0000**	**0.0000**	0.0021	0.0004	**0.0003**	**0.0003**	(0.0080, 0.0103)	(0.0068, 0.0080)	(**0.0068, 0.0078**)
	γ	0.021	0.0003	**0.0000**	**0.0000**	**0.0000**	0.0074	-0.0007	-0.0006	**-0.0002**	(0.0224, 0.0340)	(**0.0190, 0.0213**)	(0.0190, 0.0214)
	β	1.000	0.0227	0.0035	**0.0031**	0.0036	0.0269	-0.0101	**-0.0089**	-0.0120	(0.9676, 1.0861)	(0.9667, 1.0131)	(**0.9689, 1.0132**)
	η	2.000	**0.0178**	0.0372	0.0293	0.0387	0.0350	**0.0055**	0.0233	0.0164	(**1.9834, 2.0865**)	(1.9283, 2.0827)	(1.9554, 2.0911)
	μ_x	1.500	0.0697	0.0125	**0.0101**	0.0112	0.1567	0.0585	0.0498	**0.0496**	(1.5716, 1.7417)	(1.5202, 1.5967)	(1.5150, 1.5847)
14	λ	0.007	**0.0000**	**0.0000**	**0.0000**	0.0001	0.0007	0.0002	0.0002	**0.0001**	(0.0061, 0.0092)	(0.0068, 0.0076)	(0.0069, 0.0076)
	γ	0.042	0.0001	**0.0000**	**0.0000**	**0.0000**	0.0052	-0.0013	-0.0007	**-0.0004**	(0.0437, 0.050)	(0.0379, 0.0427)	(0.0384, 0.0435)
	β	0.500	0.0086	0.0069	0.0076	**0.0068**	-0.0495	**-0.0011**	0.0034	-0.0054	(0.4192, 0.4818)	(0.4655, 0.5322)	(0.4685, 0.5384)
	η	1.000	0.0359	0.0131	0.0331	**0.0116**	**0.0163**	-0.0371	0.0169	-0.0191	(0.9408, 1.0918)	(0.9196, 1.0061)	(0.9444, 1.0894)
	μ_x	3.000	0.2042	0.0358	0.0531	**0.0343**	0.2709	-0.0172	-0.0095	-0.0418	(3.1262, 3.4156)	(2.9074, 3.0581)	(2.8984, 3.0826)
15	λ	0.007	**0.0000**	**0.0000**	**0.0000**	**0.0000**	-0.0007	0.0006	**0.0005**	**0.0005**	(0.0055, 0.0071)	(0.0071, 0.0081)	(**0.0070, 0.0080**)
	γ	0.021	0.0002	**0.0000**	**0.0000**	**0.0000**	-0.0006	**0.0004**	0.0008	0.0009	(0.0151, 0.0253)	(0.0200, 0.0225)	(0.02037, 0.0228)
	β	0.500	0.0094	0.0041	**0.0014**	0.0043	0.0143	-0.0157	**-0.0025**	-0.0181	(0.476, 0.5527)	(0.4594, 0.5091)	(**0.4824, 0.5124**)
	η	2.000	**0.0173**	0.0431	0.0309	0.0440	0.0832	-0.0265	0.0392	**-0.0125**	(2.0425, 2.1240)	(1.8911, 2.0559)	(**1.9691, 2.1092**)
	μ_x	3.000	0.2992	**0.0428**	0.0404	0.0406	0.2814	0.0289	0.0064	**0.0017**	(3.0937, 3.4691)	(2.9470, 3.1108)	(2.9243, 3.0885)
16	λ	0.007	**0.0000**	**0.0000**	**0.0000**	**0.0000**	-0.0014	**0.0004**	**0.0004**	**0.0004**	(**0.0069, 0.0079**)	(0.0042, 0.0070)	(0.0069, 0.0079)
	γ	0.042	0.0004	**0.0000**	**0.0000**	**0.0000**	0.0051	0.0018	**0.0015**	0.0026	(0.0412, 0.0452)	(0.0395, 0.0541)	(**0.0415, 0.0455**)
	β	1.000	0.0488	0.0104	**0.0096**	0.0102	-0.1256	0.0057	0.0035	**0.0031**	(**0.9635, 1.0426**)	(0.80162, 0.9471)	(0.9650, 1.0464)
	η	1.000	0.0516	0.0116	**0.0091**	0.0115	-0.0292	**-0.0003**	0.0053	0.0110	(**0.9665, 1.0442**)	(0.8807, 1.0609)	(0.9566, 1.0427)
	μ_x	1.500	0.1193	0.0090	0.0085	**0.0079**	0.0781	0.0378	0.0333	**0.0268**	(1.4982, 1.5685)	(1.4435, 1.7127)	(1.5031, 1.5725)

Table 2.3: Experiment of parameter estimation. Bias, mean squared errror and 95% CI for parameters.

2.6 Application to Real Data

2.6.1 Data

We obtained the rain gauge data from the Bureau of Meteorology, Australia. The data is from one station (tipping bucket) point data for a month. It is every 6-minute time resolution in July 2010. The rainfall amount resolution is 0.2 mm. Any rainfall less than 0.2 was considered as no-rainfall. The time series data plot is shown in Figure 2.8. The location of the rainfall station is Bass River, Victoria as displayed in Figure 2.9.

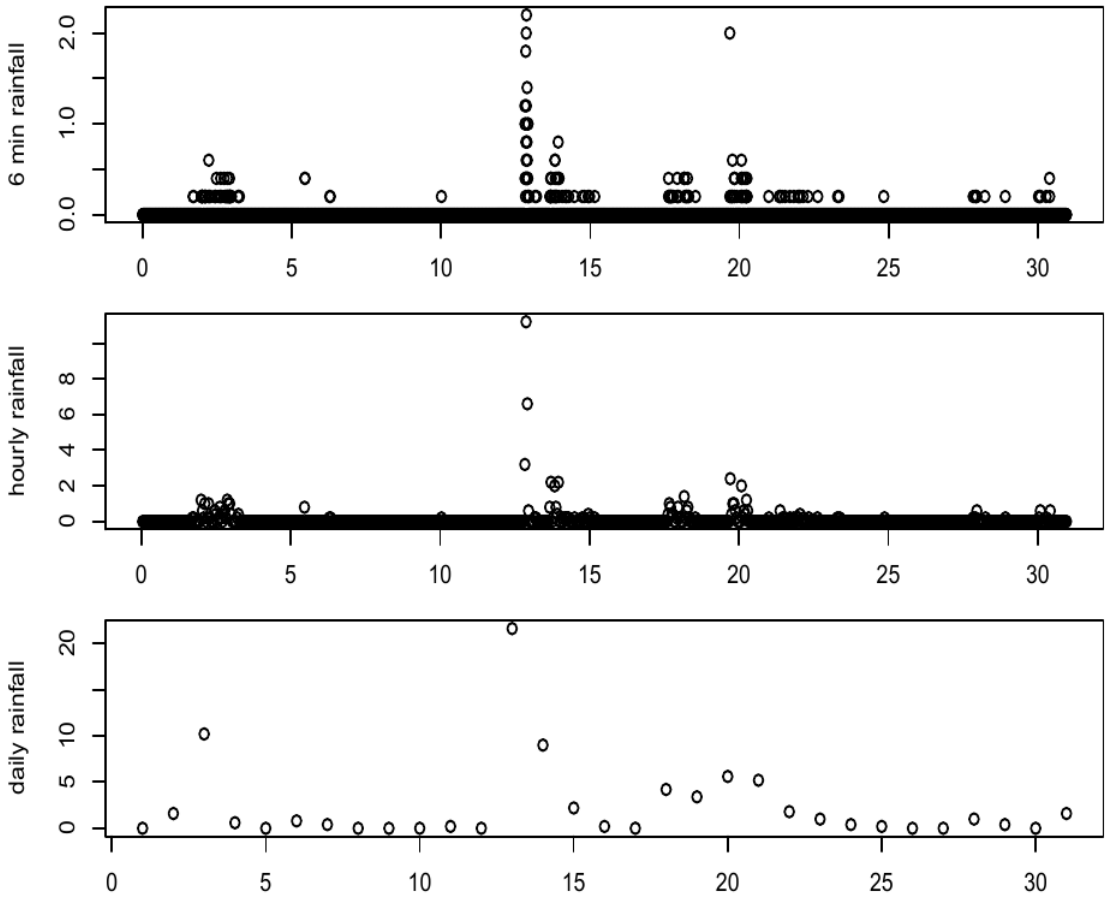

Figure 2.8: Rainfall measurements from Bass River, Victoria, July, 2010. The x-axis is measured in days and the y-axis in mm. Data obtained from the Australian Bureau of Meteorology.

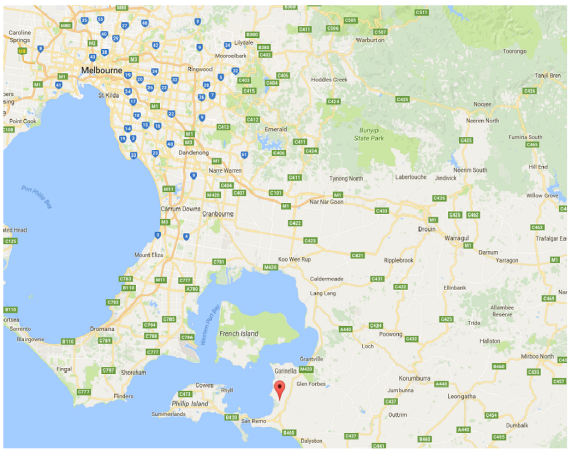

Figure 2.9: Rain gauge data station (Bass River, Melbourne).

2.6.2 Real Data: Fitting the BL Model using ABC

As in section 2.4.1, we chose five parameters $\log(I_T)$, $\log(\lambda \times \gamma^{-1})$, $\log(\lambda\gamma)$, $\log(\beta \times \eta^{-1})$, and $\log(\beta\eta)$ for the model.
The prior distribution of these parameters is normal with mean zero and σ^2 variance. Various choices for the prior standard deviation were considered. We selected 3.0 because this choice could be seen to have no appreciable effect on the bulk of the posterior, while providing mild regularisation to keep the posterior tails in check. We chose steps of proposal chain via $N(\mathbf{0}, 0.2^2\mathbf{I})$. Note that each parameter can have any distribution. Moreover, it can have the same mean but different variance.

2.6.3 Posterior Distribution

The trace-plots in Figure 2.10 show that the posterior distribution converges to a stationary distribution. It is clear that the parameter values oscillate in the parameter space. We can see that there is effective mixing. Plots in Figure 2.11 show the posterior density of log-parameters. The vertical lines are the posterior means of respective parameters. Posterior density functions for log-parameters are good as expected. Figure 2.12 shows the

marginal posterior density in the diagonal and pairwise posterior density in sub-diagonal panels, where the color intensity values reflect the count of samples in the posterior distribution sets within a particular area. We can see correlation between some parameters as expected. These diagnostic plots clearly indicate that the ABC-MCMC algorithm outcomes produce good posteriors for the parameters of the Bartlett-Lewis rainfall model.

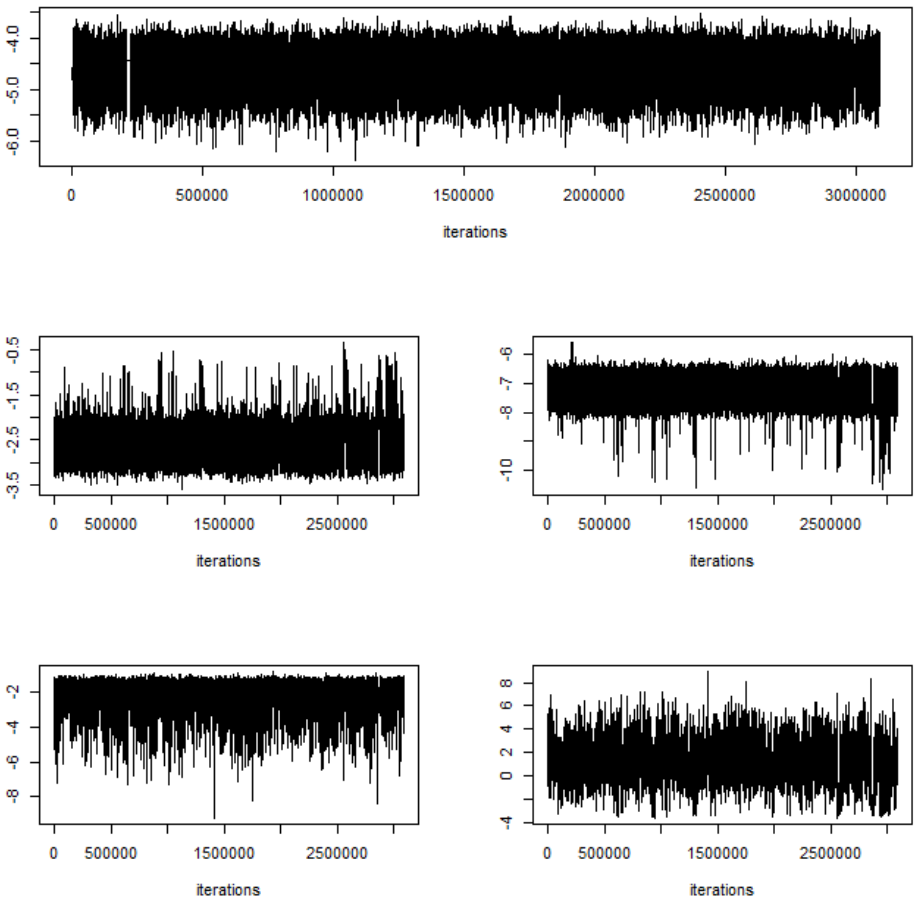

Figure 2.10: Chain values of $\theta(1)$-top , $\theta(2)$- middle left, $\theta(3)$- middle right, $\theta(4)$-bottom left, $\theta(5)$- bottom right.

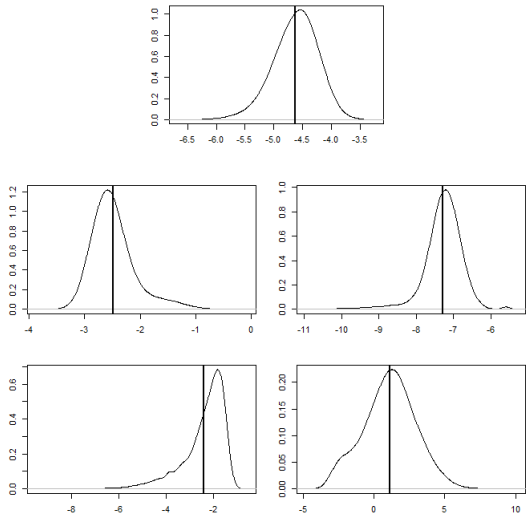

Figure 2.11: Posterior density of $\theta(1)$-top , $\theta(2)$- middle left, $\theta(3)$- middle right, $\theta(4)$-bottom left, $\theta(5)$- bottom right. Vertical lines are the posterior means.

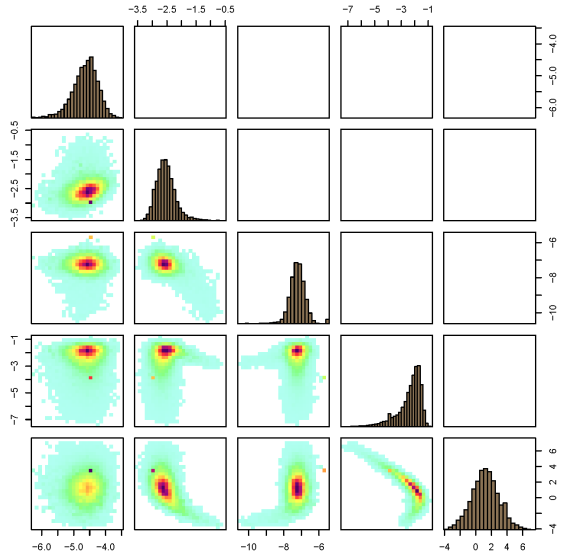

Figure 2.12: Diagonals are the posterior distributions for $\theta(i)$, $i = 1, 2, ..., 5$. Lower panel plots are pairs of posteriors, where the intensity values reflect the count of samples in the posterior distribution sets within a particular area. Blue dotted curves are priors.

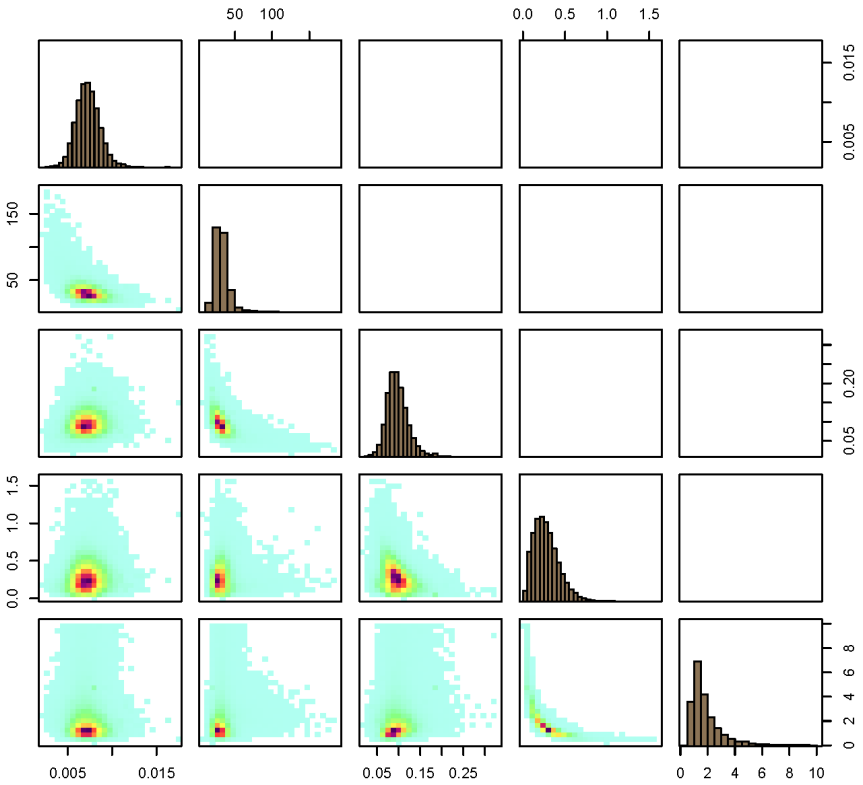

Figure 2.13: Posterior distributions for $\lambda, \gamma^{-1}, \beta, \eta^{-1}$ and μ_x, from the BL model fitted to the Bass River data

2.6.4 Fitting the BL Model using GMM

As in section 2.2.3, we optimised the objective function at equation (2.11) using Nelder-Mead and quasi-Newton algorithms implemented in R. Figure 2.14 shows that the theoretical and empirical moments matched closely. The estimated parameter values are $\lambda = 0.0950, \gamma = 0.3709, \beta = 0.1911, \eta = 0.7091$, and $\mu_x = 1.3957$. In these graphs, we used the estimated parameter values to find theoretical summary statistics for different time. Moreover we show theoretical and observed summary statistics at 6-minute, hourly and every hour up to 6-hour time aggregation.

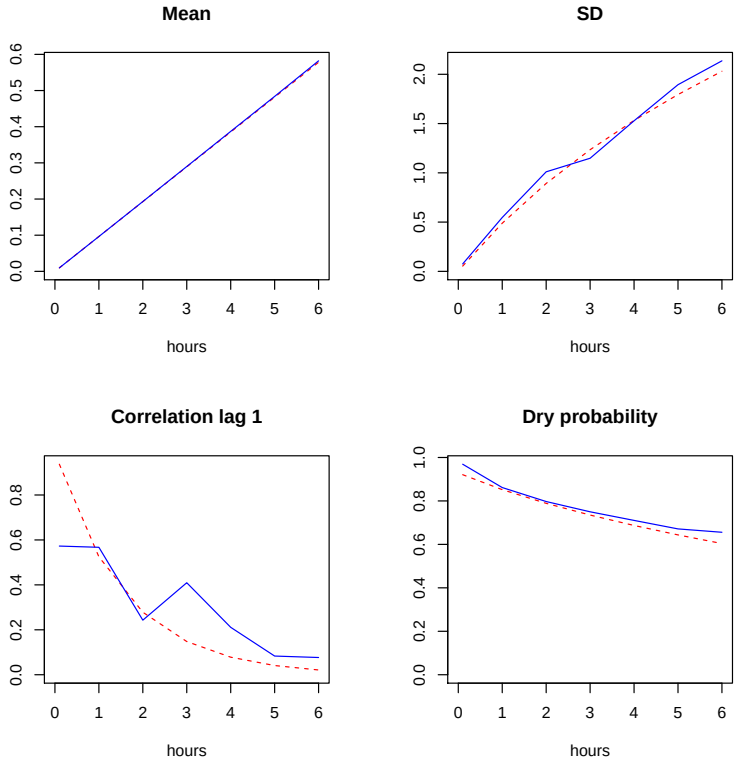

Figure 2.14: Lines (red) are theoretical summary statistics and doted lines (blue) are real data summary statistics.

2.6.5 Parameter Estimation Values

Table 2.4 presents estimated parameter values from both GMM and ABC-MCMC. The ABC and GMM estimates for λ and γ^{-1} roughly similar, and if we take the mean storm coverage i.e. storm rate multiplied by mean duration $(\lambda\gamma^{-1})$, we obtain an even closer match, with 0.226 using ABC posterior means and 0.256 for the GMM fit. The estimates for cell parameters β, η^{-1}, and μ_x are quite different, however if we take the mean storm intensity i.e. $(\beta\eta^{-1}\mu_x)$, we have fairly similar 0.054 using the ABC posterior means and 0.038. Formally, storm coverage and storm intensity are essentially directly observable quantities, making their means easier to estimate.

Parameters (per hour)	GMM	ABC-MCMC (Posterior mean)	95 % credible interval (ABC-MCMC)	ABC-MCMC (Posterior median)
λ	0.0095	0.0071	(0.005, 0.010)	0.007
γ^{-1}	26.9615	32.354	(18.570 , 56.380)	30.728
β	0.0191	0.097	(0.056, 0.156)	0.095
η^{-1}	14.1024	0.279	(0.057, 0.634)	0.256
μ_x	0.1396	1.994	(0.699, 6.450)	1.531

Table 2.4: Parameter estimates for the BL model fitted to the Bass River data. All estimated parameter values are per six minutes except μ_x, which is mm per six minutes.

2.6.6 Comparison between Simulated and Observed Statistics

In this section, we compare the model fitted using ABC and GMM. We use simulation to generate 95% preditive intervals for summary statistics.

In Figure 2.15, we calculate 95% predictive intervals for summary statistics at different levels of temporal aggregations using simulation. For this, we use 3000 samples from the posteriors selecting every 1000th iterations. We can see that almost all observed summary statistics are within the 95% predictive intervals. Only autocorrelation lag 1 and lag 2 for 6-minute and hourly and standard deviation of wet periods for 6-minute are outside of 95% predictive interval. Standard deviation for 5 and 6 hours aggregation crossed the upper bound, but it is completely within the predictive interval when we use posterior means (see Figures 2.16).

For Figures 2.16 and 2.17, we use posteriors means and medians respectively. The summary statistics are calculated using rainfall aggregated over internals of 0.1, 1, 2 , 3 ,4 ,5, and 6 hours, and are obtained from 100 independent simulations. Using different posterior points seems better to estimate 95% predictive interval for the summary statistics.

Similarly for Figure 2.18, we use the GMM estimates to to compute the predictive intervals. We first generate 100 independent simulations, then estimate 95% predictive intervals for various summary statistics. The figure shows that some observed summary statistics are within the 95% predictive intervals. We see that the GMM fitted model only gives a good correspondence between the fitted model and the data for those summary statistics used in the GMM fit. However the ABC fitted model gives a good correspondence for all the summary statistics considered. Therefore the extra summary

statistics such as the number of wet/dry periods, has supported ABC to distinguish cell parameters β, η^{-1}, and μ_x more successfully than GMM.

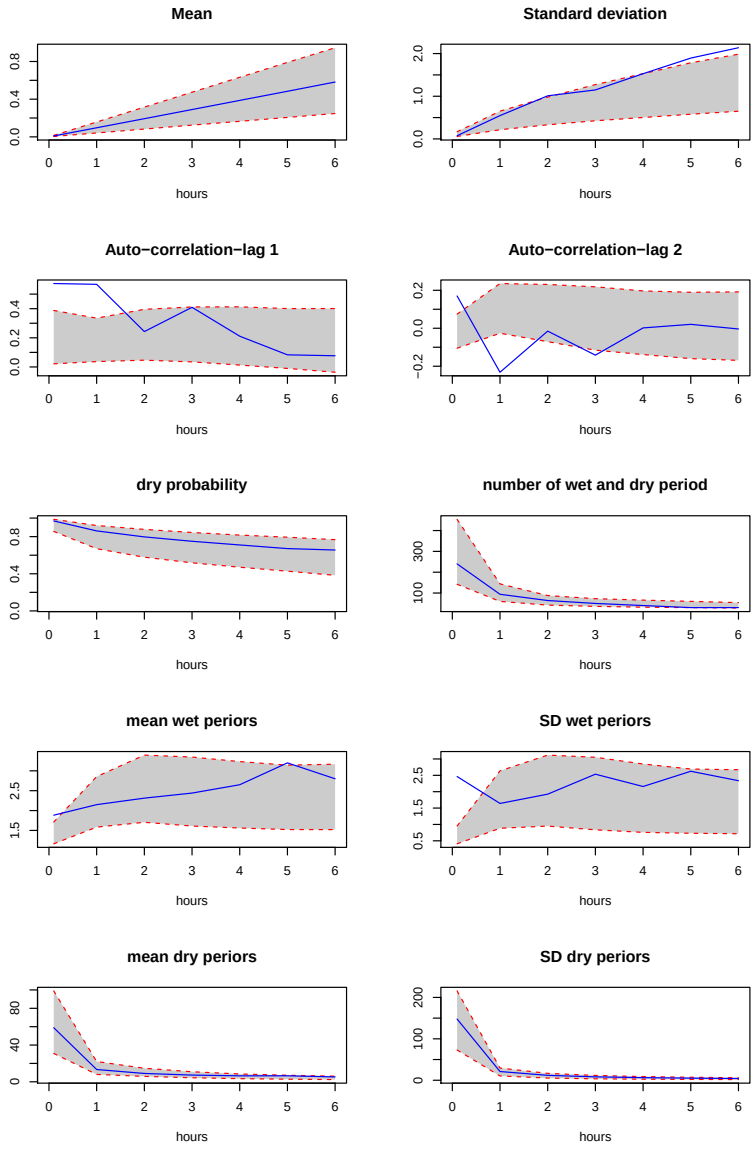

Figure 2.15: 95% predictive intervals for various summary statistics from ABC-MCMC estimates. For each plot, the summary statistics are calculated using rainfall aggregated over intervals of 0.1, 1, 2, 3, 4, 5, 6 hours, and are calculated from 3000 independent simulations using the same number of posterior points. The solid blue lines give the observed summary statistics.

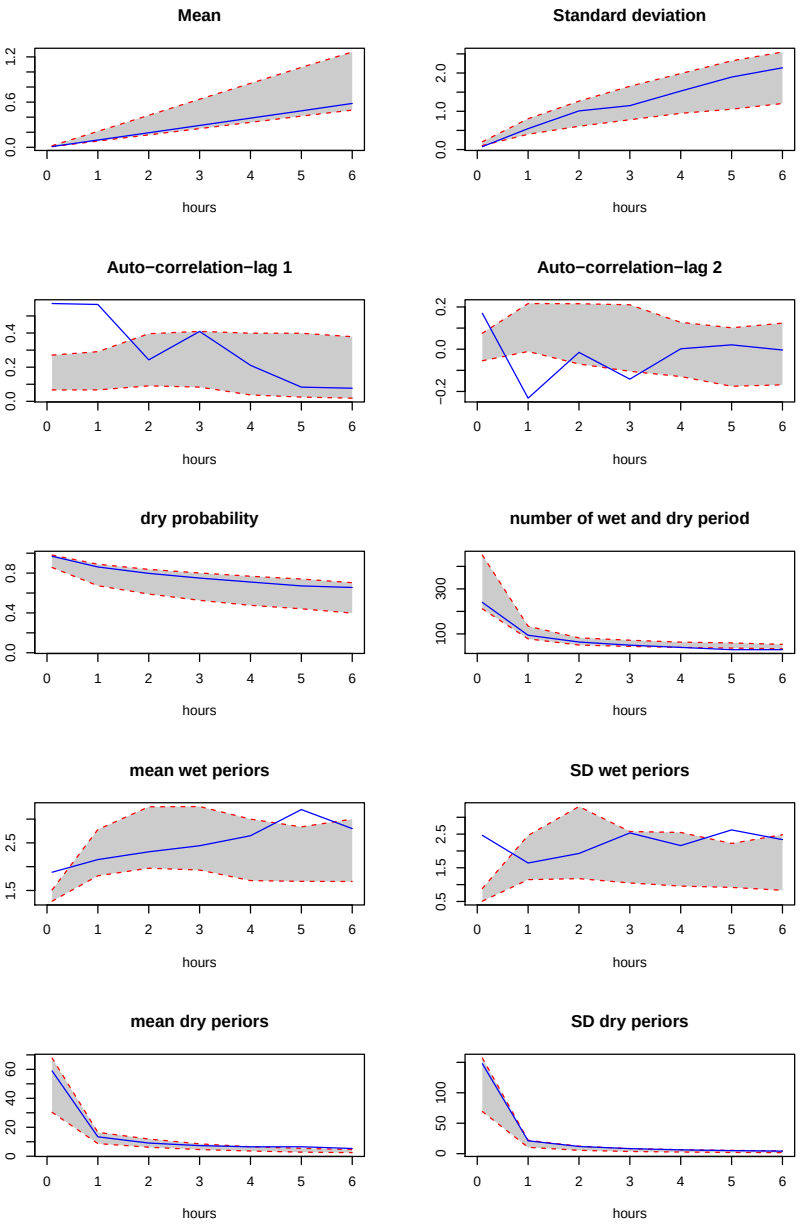

Figure 2.16: 95% predictive intervals for summary statistics from posterior means. For each plot, the summary statistics are calculated using rainfall aggregated over intervals of 0.1, 1, 2, 3, 4, 5, 6 hours, and are calculated from 100 independent simulations used posterior means. The solid blue lines give the observed summary statistics.

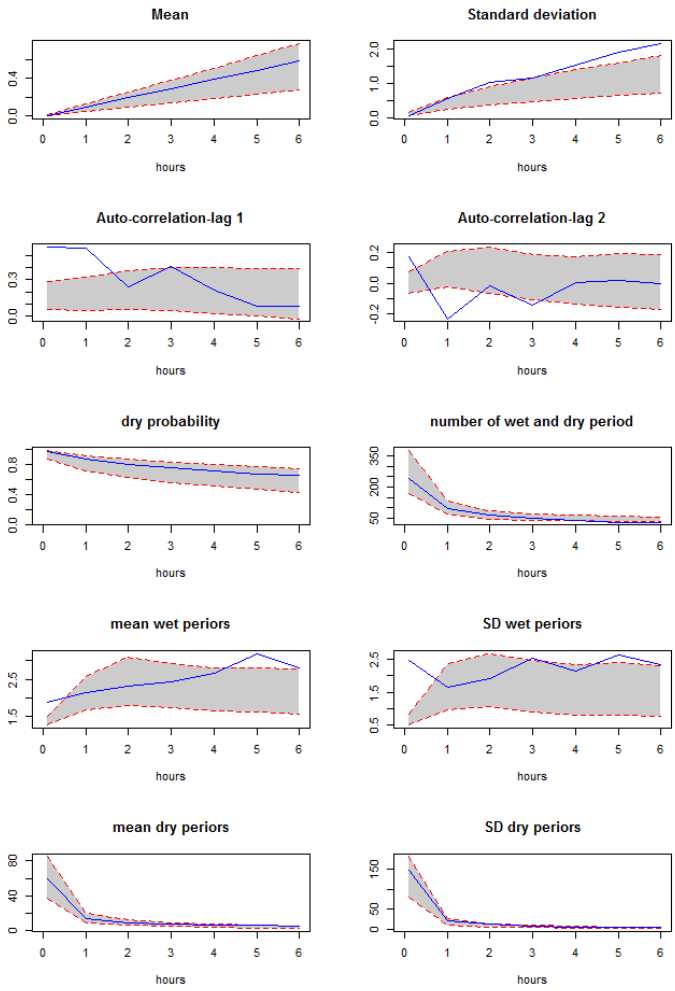

Figure 2.17: 95% predictive intervals for summary statistics from posterior medians. For each plot, the summary statistics are calculated using rainfall aggregated over intervals of 0.1, 1, 2, 3, 4, 5, 6 hours, and are calculated from 100 independent simulations. The solid blue lines give the observed summary statistics

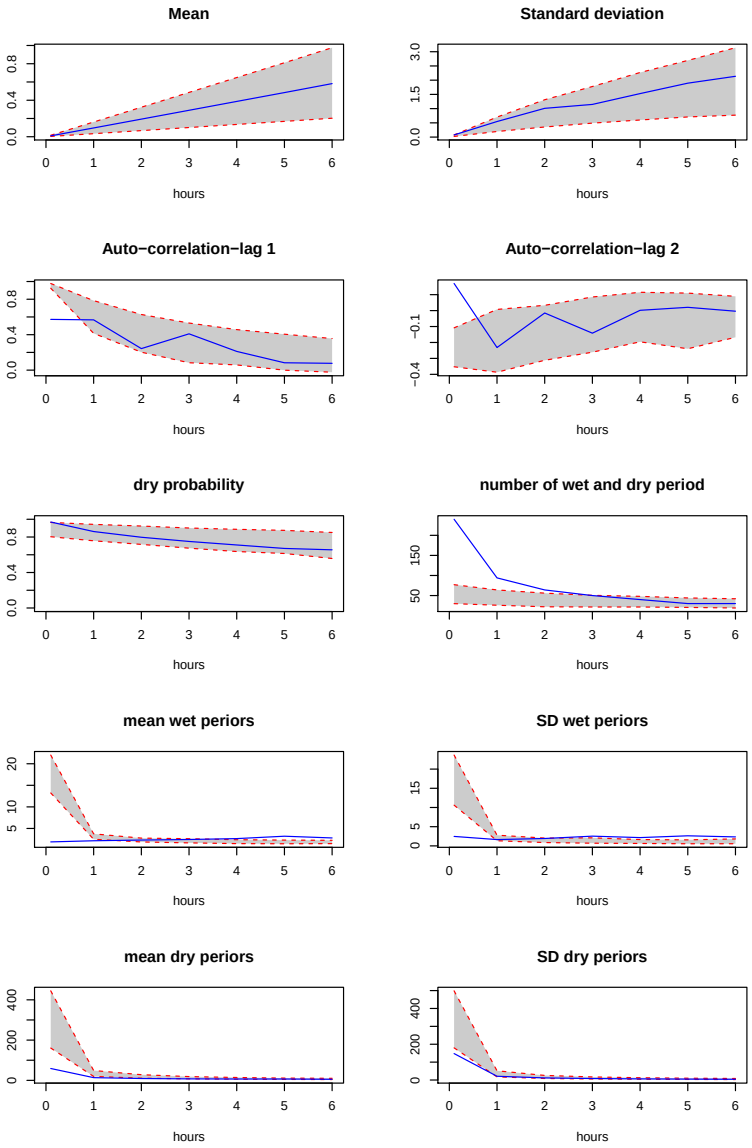

Figure 2.18: 95% predictive intervals for summary statistics from the GMM estimates. For each plot, the summary statistics are calculated using rainfall aggregated over intervals of 0.1, 1, 2, 3, 4, 5, 6 hours, and are calculated from 100 independent simulations. The solid blue lines give the observed summary statistics

2.6.7 Improvement of Parameter Estimation

Figure 2.13 shows correlation between cell duration and intensity. We set the lower bound for cell duration. We assume that cell duration is at least one minute. Once η is restricted, we adjust the priors and proposals. We set priors for $\log(\beta\eta^{-1})$ and $\log(\beta\eta)$ are zero if the cell duration is less than one minute. Similarly we modify the proposal steps for these two parameters.

Because the temporal resolution of our data was six minutes, there is clearly little information available on rain cell durations less than this. We chose a lower bound of one minute for cell durations, because values less than this would be largely unreliable, and because we found it helped with the model fitting generally. Note that even without this bound there is very little posterior mass assigned to cell durations less than one minute, so the bound is only mildly informative.

We used a truncated normal prior distribution for $\theta(4)$ and $\theta(5)$. The rest remain the same as before. From the posteriors obtained in Section 2.6.2 we know that our bounds on $\theta(4)$ and $\theta(5)$ are only mildly informative, but they none-the-less helped improve the overall model fitting in this section.

There is a good mixing (see Figure 2.19). Figure 2.20 shows the posterior distribution in diagonal and posterior pair for the parameters $\phi(i)$. Figure 2.21 shows that the correlation between cell parameters is reduced from what is shown in 2.13.

This sums up there is some improvement in the estimation once we restrict the origin parameter cell duration. We see that there is very little pairwise correlation between the parameters in the posterior. Figure 2.21 gives posteriors for the original parameters $\lambda, \gamma^{-1}, \beta, \eta^{-1}$ and μ_x.

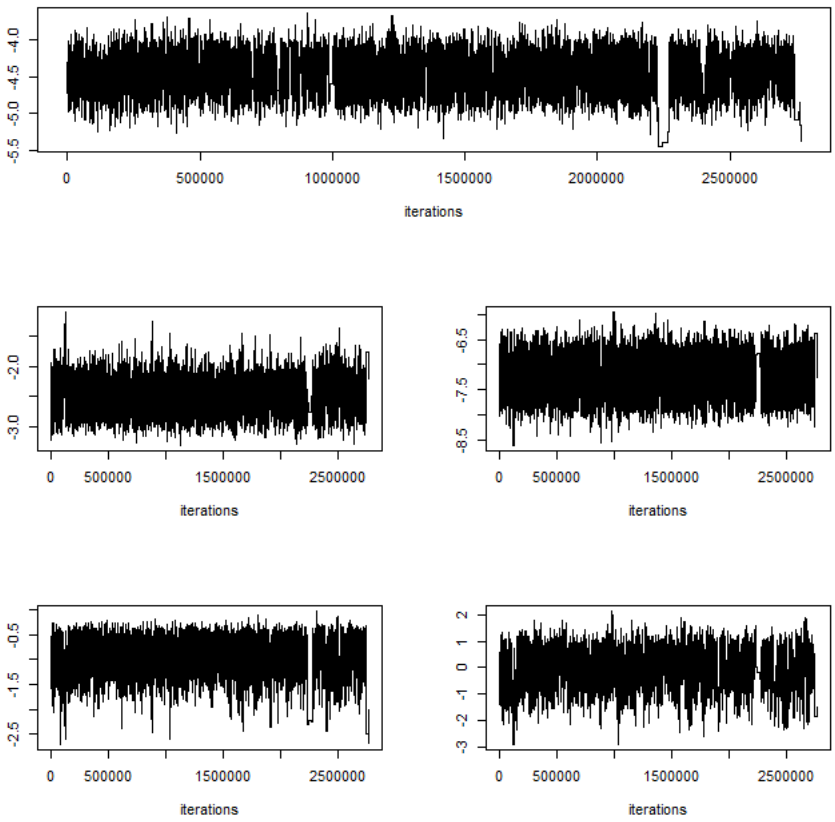

Figure 2.19: Chains for $\theta(1)$-top, $\theta(2)$-middle left, $\theta(3)$-middle right, $\theta(4)$-bottom left, $\theta(5)$-bottom right.

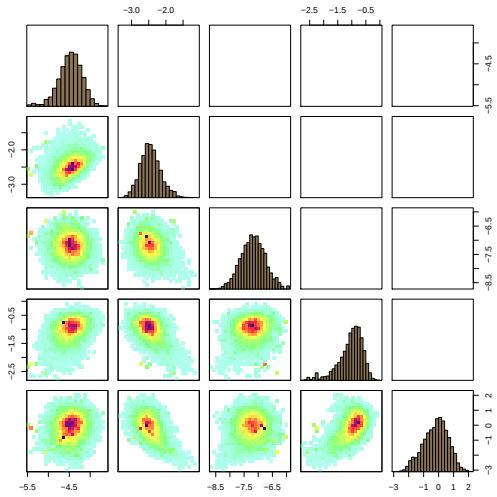

Figure 2.20: Diagonals are posterior distributions for $\theta(i)$, $i = 1, 2, ..., 5$. Lower panel plots are pair of posteriors, where intensity values are the count of samples in the posterior distribution sets within a particular area.

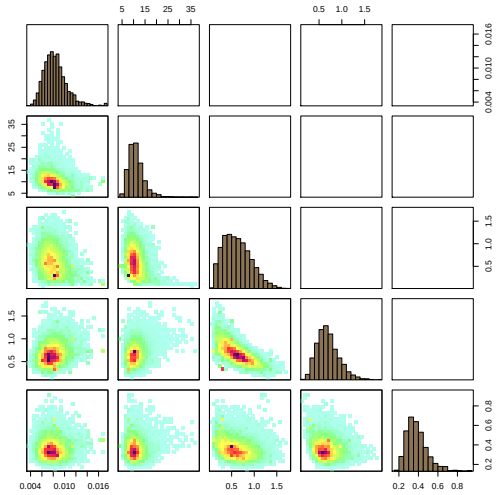

Figure 2.21: Diagonals are posterior distributions. From top, they are respectively $\lambda, \gamma^{-1}, \beta, \eta^{-1}$ and μ_x. Lower panel plots are pair of posteriors, where intensity values are the count of samples in the posterior distribution sets within a particular area.

2.7 Discussion

Using both a simulation study and real data, we have seen that ABC-MCMC gives better fits than GMM of the Bartlett-Lewis rainfall model. An important advantage of ABC fitting over GMM fitting is that we can use summaries of the data that capture useful information, whether or not we have an expression for their expectation. Moreover, this means that ABC can be used for models for which GMM fitting is not available. For example, if we used a gamma distribution for the duration of a rain cell, rather than an exponential distribution, then we would not be able to calculate the second order statistics of the $\{Y_i^h\}$, making GMM fitting impossible. However ABC fitting would proceed as before, with the addition of a single parameter. This opens up the possibility of fitting much more realistic stochastic rainfall models.

Finally we note that unlike GMM, ABC fitting provides credible intervals and not just point estimates.

Chapter 3

Fitting Spatial-Temporal Rainfall Models using Approximate Bayesian Computation

3.1 Introduction

We studied a stochastic model for rainfall processes at a single point in space in Chapter 2. We considered the Bartlett-Lewis (BL) rainfall model, because our primary goal was to compare two likelihood-free fitting techniques: GMM and ABC. We found ABC fitting has advantages over GMM. In this Chapter we extend the study to spatial-temporal rainfall processes.

One way of modelling rainfall processes in a space-time is via a stochastic mechanistic approach. Stochastic models based on Poisson cluster processes are used to model rainfall processes. The cluster process is constructed by taking a primary process, called the storm arrival process, and then attaching to each storm centre a finite secondary point process, called a cell process. The Cox-Isham-Northorp (C-I-N) model is a spatial-temporal stochastic model for a rainfall event, constructed using a cluster point process. In this Chapter we fit the C-I-N model and two new spatial-temporal rainfall

models to high-resolution rainfall radar data for a single rainfall event.

There are many ways in which the Cox-Isham-Northorp spatial-temporal model can be generalized. We present two new spatial-temporal rainfall models with the following modifications:

- Randomized cell eccentricity[1].
- Rainfall intensity that increases continuously from the edge to the centre of each cell, rather than acting as a step function.
- Heavy-tailed distributions for cell intensity and size.
- Correlated cell intensity and area.

3.2 Spatial-Temporal Rainfall Model

We study spatial-temporal rainfall models that are stationary and are used to model the interior of a rainfall event. We assume that we have observations of the rainfall in some finite space-time window $A \times [0, T]$, where T is chosen so that the leading and trailing edges of the rainfall event are not observed and $A \in \mathbb{R}^2$. Remember that to model an actual event we need a separate model for the duration and extent of the event. For example see the approach of Wheater et al., 2005 (§9.3) [47].

The building blocks of Poisson cluster-based spatial-temporal rainfall models are:

- The temporal process of rainfall at a single point in space introduced by Rodriguez-Irurbe et al., 1987 [39].
- The spatial-temporal process of rainfall introduced by Cox & Isham, 1988 [13].
- The Cox-Isham spatial-temporal model for rainfall generalized by Northrop, 1998 [32].

[1]Eccentricity (e) indicates how much the cell shape deviates from being circular. Eccentricity of an ellipse equals $\sqrt{1 - \frac{b^2}{a^2}}$, where a and b are semi-major and semi-minor axes of the ellipse.

3.3 Cox-Isham (C-I) spatial-temporal rainfall model

The Cox-Isham (C-I) spatial-temporal rainfall model has the same temporal structure as the Bartlett-Lewis rectangular pulse model. The model was introduced by Cox & Isham, 1988 [13].

The C-I spatial-temporal rainfall model, based on cluster processes is as follows:

- Storms arrive as a homogeneous Poisson process in $\mathbb{R}^2$ and time.
- The storm centres move with velocity $\mathbf{v} = (v_x, v_y)$.
- Each storm is attached to a finite rain cell process. Each cell centre has the same spatial location as the storm centre, and moves with the same velocity .
- The cell arrival process terminates after the storm duration, which follows an exponential distribution.
- Each cell has a random duration, a random intensity, and a random area having circular shape in space.
- The total rainfall intensity at a point in space-time is the sum of intensities from all cells active at that point.

3.4 Cox-Isham-Northop (C-I-N) Spatial-Temporal Rainfall Model

The Cox-Isham-Northop (C-I-N) model is an extension of the C-I model, due to Northrop 1998 [32]. It is a spatial-temporal stochastic model for the interior of a single rainfall event, constructed using a cluster point process. The cluster process is constructed by taking a primary process, called the storm arrival process in our context, and then attaching to each storm center a finite secondary point process, called a cell process. To each cell centre we then attach a rain cell, with an associated area, duration and intensity. The rain cell process is observed, whereas the storm process is unobserved. What that means is a storm generates rain cells, rain cells produce rainfall with a random intensity over their lifetime within the cell area.

The storm and cell centers all share a common velocity. The total rainfall intensity at point(x, y) and time t is then the sum of the intensity at (x, y) of all cells active at time t.

The model description is outlined as follows:

- The arrival process of storm centres is taken to be a Poisson process in $\mathbb{R}^2 \times [0, \infty)$ with homogeneous rate λ. Let $\mathbf{v} = (v_x, v_y)$ be the velocity of the rainfall event, so if a storm center arrives at $(\mathbf{u}, s)$ then at time $s + t$ it will be at $(\mathbf{u} + t\mathbf{v}, s + t)$. Storm durations are random. Recall that storm durations follow an exponential distribution with rate γ.

- While a storm is active it produces cells at a rate β in time, starting with a cell at the moment the storm center begins. The cell process follows a finite homogeneous Poisson process. If the storm arrives at $(\mathbf{u}, s)$ and produces a cell at time $s + t$, the cell will be centered at $\mathbf{u}+t\mathbf{v}+\mathbf{w}$, where $\mathbf{w}$ comes from a bivariate Gaussian distribution with mean $\mathbf{0}$ and covariance

$$\mathbf{\Sigma} = \begin{pmatrix} \sigma_x^2 & \rho\ \sigma_x\sigma_y \\ \rho\ \sigma_x\sigma_y & \sigma_y^2 \end{pmatrix}.$$

  The cell centre then also moves with velocity $\mathbf{v}$.

- Each cell is elliptical with a semi-major axis of random length M_c.

- Each cell deposits rain at a constant intensity X on all points in space covered by its defining ellipse during its duration L.

- Assume that each rain cell is a scaled version of the cell displacement density contours of the storm within which it is born i.e each has the same eccentricity e and orientation Θ, so that e and Θ are fixed given Σ.

- Assume that M_c, L and X are mutually independent between cells as well as independent of Σ.

- Assume that cell clusters belonging to distinct storms are independent.

The total rainfall intensity at spatial location $\mathbf{u}$ and at time t is the sum of intensities from all cells covering at the point $(\mathbf{u}, t)$.

The model is stationary in time and homogeneous in space. The distribution of cell and storm areas and cell intensity are more flexible than the

durations. The cell area may follow a gamma distribution with two parameters, but the cell intensity X is assumed to be exponentially distributed with mean μ_x. The schematic diagram of spatial structure of the C-I-N model is shown in Fugure 3.1.

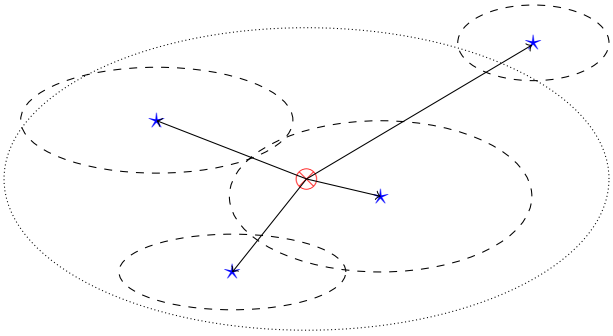

Figure 3.1: Schematic diagram of the spatial structure of the C-I-N model for event interiors. The red point is storm centre at time t in space. Blue start points are cell centres. Lines indicate the cell centres, which are placed from the storm centre. Dotted elliptical area is the storm area. Dashed curves are ellipsoidal cell intensities.

Let cells be elliptical, then the cell, which has semi-major axis (M_c) and semi-minor axis (M_{min_c}), and eccentricity (e), has expected area

$$\begin{aligned} E[CellArea] &= E[\pi M_c \; M_{min_c}] \\ &= \pi E[M_c \; M_{min_c}] \\ &= \pi\sqrt{1-e^2} \; E[M_c^2], \end{aligned}$$

If $M_c \sim \Gamma(\alpha_1, \alpha_2)$ then the mean cell area is given by

$$E[A] = \frac{\pi\sqrt{1-e^2} \; \alpha_1(1+\alpha_1)}{\alpha_2^2}. \tag{3.1}$$

It is assumed that velocity, eccentricity and orientation are common to all storms and cells within the rainfall event.

3.4.1 Mean

We define

$$\mathbb{1}(\mathbf{u}, t\ ;\ \mathbf{u}+\mathbf{u}', t+t') = \begin{cases} 1 & \text{if a cell born at } (\mathbf{u}, t) \text{ covers } (\mathbf{u}+\mathbf{u}') \text{ at } t+t'; \\ 0 & \text{otherwise.} \end{cases}$$

The total intensity at $(\mathbf{u}, t)$ is the sum of intensities of all active cells. It is denoted by $Y(\mathbf{u}, t)$ and given by

$$Y(\mathbf{u}, t) = \int_{\tau=-\infty}^{t} \int_{\mathbf{w}\in\mathbb{R}^2} \mathbb{1}(\mathbf{w}, \tau\ ;\ \mathbf{u}, t) X(\mathbf{w}, \tau)\ dN(\mathbf{w}, \tau).$$

where $X(\mathbf{w}, \tau)$ is the random depth of the cells originating at $(\mathbf{w}, \tau)$ and N counts cell origins.

Suppose μ_c is the mean number of cell per storm. The intensity of cell occurrences, is therefore $\lambda\mu_c$. Let the survivor probability of cells be $\mathcal{F}_L(\cdot)$. The mean of the process is given by

$$\begin{aligned}
\mathbb{E}[Y(\mathbf{u}, t)] &= \int_{\tau=-\infty}^{t} \int_{\mathbf{w}\in\mathbb{R}^2} \mathbb{E}_{X,L,A}[\mathbb{1}(\mathbf{w}, \tau\ ;\ \mathbf{u}, t) X(\mathbf{w}, \tau) dN(\mathbf{w}, \tau)] \\
&= \int_{\tau=-\infty}^{t} \int_{\mathbf{w}\in\mathbb{R}^2} \mathbb{E}_{X,L,A}[\mathbb{1}(\mathbf{w}, \tau\ ;\ \mathbf{u}, t) X(\mathbf{w}, \tau)]\ \ [dN(\mathbf{w}, \tau)] \\
&= \int_{\tau=-\infty}^{t} \int_{\mathbf{w}\in\mathbb{R}^2} \mathbb{E}_{X,L,A}[\mathbb{1}(\mathbf{w}, \tau\ ;\ \mathbf{u}, t) X(\mathbf{w}, \tau)\ ] \lambda\mu_c\ d\mathbf{w}\ d\tau, \\
&\qquad \text{since } N, X,\ L \text{ and } A \text{ are independent,} \\
&= \lambda\mu_c \int_{\tau=-\infty}^{t} \int_{\mathbf{w}\in\mathbb{R}^2} \mathbb{E}_{X,L,A}[\mathbb{1}(\mathbf{w}, \tau\ ;\ \mathbf{u}, t) X(\mathbf{w}, \tau)\ ]\ d\mathbf{w}\ d\tau \\
&= \lambda\mu_c\ \mathbb{E}(A) \int_{\tau=-\infty}^{t} \mathbb{E}[X]\ \mathcal{F}_L(t-\tau)\ d\tau \\
&\qquad \text{where } \mathbb{E}(A) \text{ is expected cell area,} \\
&= \lambda\mu_c\ \mathbb{E}(A)\mathbb{E}[X] \int_{\tau=-\infty}^{t} \mathcal{F}_L(t-\tau)\ d\tau \\
&= \lambda\mu_c\ \mathbb{E}(A)\mathbb{E}[X]\mathbb{E}[L].
\end{aligned} \tag{3.2}$$

We assume that the cell duration is exponentially distributed with parameter η, $\mathbb{E}[X] = \mu_x$ and $\mathbb{E}(A) = \mu_A$. Then

$$\mathbb{E}[Y(\mathbf{u}, t)] = \lambda\ \gamma^{-1}\ \beta\ \eta^{-1}\mu_x\ \mu_A.$$

The semi-major axis of a cell follows a gamma distribution with parameters α_1 and α_2. The expected cell area was given in equation (3.1) and then

$$\mathbb{E}[Y(\mathbf{u}, t)] = \pi\lambda\ \gamma^{-1}\ \beta\ \eta^{-1}\mu_x\ \sqrt{1-e^2}\ \alpha_1(1+\alpha_1)\ \alpha_2^{-2}.$$

3.4.2 Covariance

Suppose that cells are circular with radius R. We suppose two cells originate at $(\mathbf{w_1}, \tau_1)$ and $(\mathbf{w_2}, \tau_2)$. The covariance between two points in space and time is given by

$$\begin{aligned}\operatorname{cov}\{\mathbf{Y}(\mathbf{0}, 0), \mathbf{Y}(\mathbf{u}, t))\} = \int_{\tau_1=-\infty}^{0} \int_{\mathbf{w_1}\in\mathbb{R}^2} \int_{\tau_2=-\infty}^{t} \int_{\mathbf{w_2}\in\mathbb{R}^2} \\ \times\ \mathbb{E}[\mathbb{1}(\mathbf{w_1}, \tau_1\ ;\ \mathbf{0}, 0)X(\mathbf{w_1}, \tau_1)\mathbb{1}(\mathbf{w_2}, \tau_2\ ;\ \mathbf{u}, t)X(\mathbf{w_2}, \tau_2)] \\ \times\ \operatorname{cov}[dN(\mathbf{w_1}, \tau_1), dN(\mathbf{w_2}, \tau_2)]. \qquad (3.3)\end{aligned}$$

(see Cox & Miller, 1965, §9.6 [14] and Cox and Isham, 1988, equation (9) [13].)

Before we evaluate covariance function, we first obtain the covariance density $\operatorname{cov}[dN(\mathbf{w_1}, \tau_1), dN(\mathbf{w_2}, \tau_2)]$. The point process N as before is the cluster process for cell centres.

There are three possible contributions to $\operatorname{cov}[dN(\mathbf{w_1}, \tau_1), dN(\mathbf{w_2}, \tau_2)]$. The first contribution is from within cells. The second contribution is from distinct cells belonging to the same storm. The third contribution is from distinct cells belonging to distinct storms. However this third contribution is zero because the cells from distinct storms are independently placed. Hence

$\text{cov}[dN(\mathbf{w_1}, \tau_1), dN(\mathbf{w_2}, \tau_2)]$ is the sum of two terms.

The first term (contribution within cells) of $\text{cov}[dN(\mathbf{w_1}, \tau_1), dN(\mathbf{w_2}, \tau_2)]$ is

$$\lambda \mu_c \delta(\mathbf{w_1} - \mathbf{w_2}) \times \delta(\tau_1 - \tau_2) d\mathbf{w_1} d\mathbf{w_2} d\tau_1 d\tau_2. \tag{3.4}$$

The second term (contribution from 'between' distinct raincells from the same storm) of $\text{cov}[dN(\mathbf{w_1}, \tau_1), dN(\mathbf{w_2}, \tau_2)]$ is derived as follows. We suppose a storm has two cells originated at $(\mathbf{w_1}, \tau_1)$ and $(\mathbf{w_2}, \tau_2)$ with the storm centred at $(\mathbf{w}, \tau_0)$. Cell arrivals occur at rate β and the storm duration follows an exponential distribution with mean γ^{-1} , so the probability is $\beta e^{-\gamma|\tau_2 - \tau_1|}$ the same as for the BL process in time (see chapter 2 §2.2.1). Suppose the cells are displaced according to bivariate normal distribution in space. Then the second term equals

$$\lambda \mu_c \beta e^{-\gamma|\tau_2 - \tau_1|} \int_{\mathbf{w} \in \mathbb{R}^2} E_\Sigma \Big\{ \Big[\frac{1}{2\pi |\Sigma|^{\frac{1}{2}}} \, e^{\left\{ -\frac{1}{2} \left((\mathbf{w_1} - \mathbf{w})^T \Sigma^{-1} (\mathbf{w_1} - \mathbf{w}) \right) \right\}} \Big] \Big[\frac{1}{2\pi |\Sigma|^{\frac{1}{2}}} \, e^{\left\{ -\frac{1}{2} \left((\mathbf{w_2} - \mathbf{w})^T \Sigma^{-1} (\mathbf{w_2} - \mathbf{w}) \right) \right\}} \Big] \Big\} d\mathbf{w}. \tag{3.5}$$

By integrating (see detail in Northrop(1998) [32]), we get

$$\lambda \mu_c \beta e^{-\gamma|\tau_2 - \tau_1|} \mathbb{E}_\Sigma \Big[\frac{1}{4\pi |\Sigma|^{\frac{1}{2}}} \, e^{\left\{ -\frac{1}{4} \left((\mathbf{w_1} - \mathbf{w_2})^T \Sigma^{-1} (\mathbf{w_1} - \mathbf{w_2}) \right) \right\}} \Big]. \tag{3.6}$$

Since the $\text{cov}[dN(\mathbf{w_1}, \tau_1), dN(\mathbf{w_2}, \tau_2)]$ has two terms, the covariance function (3.3) is the sum of two parts. Assume that rain cell depths X are iid random variables. Likewise a cell duration L is also independent of R and $\mathbf{v}$. The first part, from (3.3) and (3.4), is

$$I = \lambda \, \mu_c \mathbb{E}[X^2] \int_{\tau=-\infty}^{0} \int_{\mathbf{w} \in \mathbb{R}^2} \mathcal{F}_L(t - \tau) \times \mathbb{E}[\mathbb{1}(||(\mathbf{0} - \mathbf{w}) - \mathbf{v}(0 - \tau)|| \leq R) \mathbb{1}(||(\mathbf{u} - \mathbf{w}) - \mathbf{v}(t - \tau)|| \leq R] d\mathbf{w} d\tau. \tag{3.7}$$

Let R_1 and R_2 be radii of two distinct cells, born within the same storm

and centred at $(\mathbf{w_1}, \tau_1)$ and $(\mathbf{w_2}, \tau_2)$. The second part, from (3.3) and (3.6), is

$$\begin{aligned} II = \lambda\ \mu_c \mathbb{E}[X]^2 \int_{\tau_1=-\infty}^{0} \int_{\tau_2=-\infty}^{t} \int_{\mathbf{w_1},\mathbf{w_2}\in\mathbb{R}^2} & \mathcal{F}_L(0-\tau_1)\mathcal{F}_L(t-\tau_2)\beta\ e^{-\gamma|\tau_2-\tau_1|} \\ & \times \mathbb{E}[\mathbb{1}(||(\mathbf{0}-\mathbf{w_1}) - \mathbf{v}(0-\tau_1)|| \leq R_1)\mathbb{1}(||(\mathbf{u}-\mathbf{w_2}) - \mathbf{v}(t-\tau_2)|| \leq R_2] \\ & \times \mathbb{E}_\Sigma\Big[\frac{1}{4\pi|\Sigma|^{\frac{1}{2}}}\ e^{\left\{-\frac{1}{4}\left((\mathbf{w_1}-\mathbf{w_2})^T\Sigma^{-1}(\mathbf{w_1}-\mathbf{w_2})\right)\right\}}\Big] d\mathbf{w_2} d\mathbf{w_1} d\tau_2 d\tau_1. \end{aligned} \tag{3.8}$$

We start by evaluating (I). Recall we are assuming to begin with the circular cell. Let $C(d)$ the area of overlaps of two unit circles with centres distance d apart, then

$$\begin{aligned} C(d) =& \begin{cases} 2\ \cos^{-1}(\frac{d}{2}) - \frac{1}{2}d\sqrt{4-d^2}, & 0 \leq d \leq 2; \\ 0, & d \geq 2. \end{cases} \\ \approx& (\pi - k\ d)^+, \quad \text{for } 0 < k \leq \frac{\pi}{2};\ \text{where } (\cdot)^+ = \max(\cdot, 0). \end{aligned}$$

We know that the raincell duration follows an exponential distribution with parameter η. The survivor probability $\mathcal{F}_L(t-\tau) = e^{-(t-\tau)\eta}$.
The first term becomes

$$\begin{aligned} I =& \lambda\ \mu_c \mathbb{E}[X^2] \int_{\tau=-\infty}^{0} \mathcal{F}_L(t-\tau)\mathbb{E}[R^2 C(||\mathbf{u}-\mathbf{v}t||/R)]d\tau \\ =& \lambda\mu_c\ \mathbb{E}[X^2]\ \frac{e^{-t\eta}}{\eta}\ \mathbb{E}[(\pi R^2 - kR||\mathbf{u}-\mathbf{v}t||)^+]. \end{aligned} \tag{3.9}$$

If $R \sim \exp(s)$ and $||\mathbf{u}-\mathbf{v}t|| = x$ then

$$\begin{aligned}\mathbb{E}[(\pi R^2 - kR||\mathbf{u}-\mathbf{v}t||)^+] &= \int_0^\infty (\pi r^2 - krx)^+ dF \\ &= \int_0^\infty (\pi r^2 - krx)^+ s e^{-sr} dr \\ &= \int_{kx/\pi}^\infty (\pi r^2 - krx) s e^{-sr} dr \\ &= \frac{2\pi}{s^2}\big(\frac{ksx}{2\pi} + 1\big) e^{-skx/\pi};\ \text{for } k > 0.\end{aligned} \tag{3.10}$$

We suppose a storm has two cells with origins at $(\mathbf{w_1}, \tau_1)$ and $(\mathbf{w_2}, \tau_2)$ with the storm centered at $(\mathbf{w}, \tau_0)$. Let R_1 and R_2 be radii of two distinct cells within a storm. The second part (II) of the covariance function in equation (3.3) can be written as

$$\begin{aligned}II =& \lambda\ \mu_c \mathbb{E}[X]^2 \int_{\tau_1=-\infty}^{0} \mathcal{F}_L(0-\tau_1) \int_{\tau_2=-\infty}^{t} \mathcal{F}_L(t-\tau_2)\beta\ e^{-\gamma|\tau_2-\tau_1|} \\ & \int_{\mathbf{w_1},\mathbf{w_2}\in\mathbb{R}^2} \mathbb{E}[\mathbb{1}(||(\mathbf{0}-\mathbf{w_1}) - \mathbf{v}(0-\tau_1)|| \le R_1)\mathbb{1}(||(\mathbf{u}-\mathbf{w_2}) - \mathbf{v}(t-\tau_2)|| \le R_2] \\ & \mathbb{E}_\Sigma\Big[\frac{1}{4\pi|\Sigma|^{\frac{1}{2}}}\ e^{\big\{-\frac{1}{4}\big((\mathbf{w_1}-\mathbf{w_2})^T\Sigma^{-1}(\mathbf{w_1}-\mathbf{w_2})\big)\big\}}\Big] d\mathbf{w_2} d\mathbf{w_1} d\tau_2 d\tau_1.\end{aligned}$$

This can be first estimated for $\mathbf{v} = 0$.

$$\begin{aligned}& \lambda\ \mu_c \mathbb{E}[X]^2 \int_{\tau_1=-\infty}^{0} \mathcal{F}_L(0-\tau_1) \int_{\tau_2=-\infty}^{t} \mathcal{F}_L(t-\tau_2)\beta\ e^{-\gamma|\tau_2-\tau_1|} \\ & \int_{\mathbf{w_1},\mathbf{w_2}\in\mathbb{R}^2} \mathbb{E}[\mathbb{1}(||(\mathbf{0}-\mathbf{w_1})|| \le R_1)\mathbb{1}(||(\mathbf{u}-\mathbf{w_2})|| \le R_2] d\mathbf{w_2} d\mathbf{w_1} d\tau_2 d\tau_1.\end{aligned}$$

The temporal integration gives

$$\int_{\tau_1=-\infty}^{0} \mathcal{F}_L(0-\tau_1) \int_{\tau_2=-\infty}^{t} \mathcal{F}_L(t-\tau_2)\beta\ e^{-\gamma|\tau_2-\tau_1|} d\tau_2 d\tau_1$$
$$= \beta \int_{\tau_1=-\infty}^{0} e^{\eta\tau_1} \int_{\tau_2=-\infty}^{t} e^{(t-\tau_2)\eta}\ e^{-\gamma|\tau_2-\tau_1|} d\tau_2 d\tau_1$$
$$= \beta\Big[\frac{\gamma e^{-\eta t} - \eta e^{-\gamma t}}{\eta(\gamma^2-\eta^2)}\Big]. \tag{3.11}$$

The spatial integration gives

$$\int_{\mathbf{w_1},\mathbf{w_2}\in\mathbb{R}^2} \mathbb{E}[\mathbb{1}(||(\mathbf{0}-\mathbf{w_1}))|| \le R_1)\mathbb{1}(||(\mathbf{u}-\mathbf{w_2}))|| \le R_2] d\mathbf{w_2} d\mathbf{w_1}$$
$$= \int_{|\mathbf{w_1}|\le R_1} \int_{|\mathbf{u}-\mathbf{w_2}|\le R_2} \mathbb{E}_\Sigma\Big[\frac{1}{4\pi|\Sigma|^{\frac{1}{2}}}\ e^{\left\{-\frac{1}{4}\left((\mathbf{w_1}-\mathbf{w_2})^T\Sigma^{-1}(\mathbf{w_1}-\mathbf{w_2})\right)\right\}}\Big] d\mathbf{w_2} d\mathbf{w_1}$$
$$= \frac{1}{4\pi}\ \mathbb{E}_{R_1,R_2,\sigma^2}\Big[\int_{|\mathbf{w_1}|\le R_1} \int_{|\mathbf{u}-\mathbf{w_2}|\le R_2} \frac{1}{\sigma^2}\ e^{\left\{-\frac{1}{4\sigma^2}\left((\mathbf{w_1}-\mathbf{w_2})^T(\mathbf{w_1}-\mathbf{w_2})\right)\right\}}\Big] d\mathbf{w_2} d\mathbf{w_1};$$

where E_{R_1,R_2,σ^2} is expectation over R_1, R_2, σ^2. And suppose $\Sigma = \sigma^2 I$, which gives $|\Sigma| = \sigma^4$.

(3.12)

Therefore the second part of the covariance function for $\mathbf{v} = \mathbf{0}$ and circular cells is

$$\frac{\lambda\mu_c\beta(\gamma e^{-\eta t} - \eta e^{-\gamma t})}{4\pi\eta(\gamma^2-\eta^2)}\ \mathbb{E}_{R_1,R_2,\sigma^2}\Big[\int_{|\mathbf{w_1}|\le R_1} \int_{|\mathbf{u}-\mathbf{w_2}|\le R_2} \frac{1}{\sigma^2}\ e^{\left\{-\frac{1}{4\sigma^2}\left((\mathbf{w_1}-\mathbf{w_2})^T(\mathbf{w_1}-\mathbf{w_2})\right)\right\}}\Big] d\mathbf{w_2} d\mathbf{w_1}. \tag{3.13}$$

$$\text{Let } g(u) = \mathbb{E}_{R_1,R_2,\sigma^2}\Big[\int_{|\mathbf{w_1}|\le R_1} \int_{|\mathbf{u}-\mathbf{w_2}|\le R_2} \frac{1}{\sigma^2}\ e^{\left\{-\frac{1}{4\sigma^2}\left((\mathbf{w_1}-\mathbf{w_2})^T(\mathbf{w_1}-\mathbf{w_2})\right)\right\}}\Big] d\mathbf{w_2} d\mathbf{w_1}. \tag{3.14}$$

Assuming σ^2 has inverse chi-squared distribution, Northrop, 1996 [33] estimated $g(u)$, first expectation over σ^2 and secondly approximate using a

Taylor series expansion of the integrand (see details Northrop, 1996 page 96 [33]).

Thus the covariance for Cox-Isham-Northorp model with circular cells is

$$c(\mathbf{u},t) = \lambda\mu_c\mathbb{E}[X^2]\Big\{\frac{e^{-t\eta}}{u}\mathbb{E}_R\big[R^2\ c(u/R)\big]\ + \frac{\beta(\gamma e^{-\eta t} - \eta e^{-\gamma t})}{4\pi\eta(\gamma^2-\eta^2)}\ g(u)\big]\Big\};$$
$$\text{where } u = |\mathbf{u}| = \sqrt{u_x^2+u_y^2}. \qquad (3.15)$$

We now suppose the cells are elliptical and semi-major axis (M_c). Let $\mathbf{v} = (v_x, v_y)$ be the velocity. Then

$$\mathbb{E}[M_c^2 C(||\mathbf{u}-\mathbf{v}t||/M_c)] = \mathbb{E}[(\pi M_c^2 - kM_c||\mathbf{u}-\mathbf{v}t||)^+]$$

We now consider that distinct elliptical cells have common eccentricity (e) and orientation (Θ). M_{c1} and M_{c2} denote semi-major axises of distinct cells. Put

$$u_x^* = (u_x - v_x t)\cos\Theta + (u_y - v_y t)\sin\Theta.$$
$$u_y^* = \{(u_y - v_y t)\cos\Theta + (u_x - v_x t)\sin\Theta\}/\sqrt{1-e^2}.$$

And let $\delta = \sqrt{(u_x^{*2} + u_y^{*2})}$, then it can be shown that the covariance $c(\mathbf{u},t) = \text{cov}[Y(\mathbf{0},0), Y(\mathbf{u},t)]$ between two points separated by time t unit and $\mathbf{u} = (u_x, u_y)$ in space is given by

$$c(\mathbf{u},t) = \lambda\mu_c\mathbb{E}[X^2]\Big\{\frac{e^{-t\eta}}{\eta}\mathbb{E}_{M_c,\mathbf{V},e,\Theta}\big[M_c^2 C(\delta/M_c)\big]\ + \frac{\beta(\gamma e^{-\eta t} - \eta e^{-\gamma t})}{4\pi\eta(\gamma^2-\eta^2)}\ \mathbb{E}_{\mathbf{V},e,\Theta}\big[g(\delta)\big]\Big\}. \qquad (3.16)$$

(See Northrop, 1998 [32]). Note that the temporal correlation was wrong in Northrop, 1998 [32].

3.4.3 Aggregation of Properties over Space

Radar images give spatial aggregation over pixels. The average rainfall intensity over pixel (i,j), of dimensions l km by l km at time t, is given by:

$$Y_{i,j}^{(l)}(t) = \frac{1}{l^2} \int_{(i-1)l}^{il} \int_{(j-1)l}^{jl} Y(\mathbf{u}, t)\ du_x\ du_y. \tag{3.17}$$

Therefore, the first and second order properties are given by

$$\mathbb{E}[Y_{i,j}^{(l)}(t)] = \mathbb{E}[Y(\mathbf{u}, t)]. \tag{3.18}$$

$$\text{var}[Y_{i,j}^{(l)}(t)] = \frac{1}{l^4} \int_{-l}^{l} \int_{-l}^{l} (l - |u_x|)(l - |u_y|) c(\mathbf{u}, t)\ du_x\ du_y. \tag{3.19}$$

$$\begin{aligned} c^{(l)}(l_x, l_y, t) &= \text{cov}[Y_{i,j}^{(l)}(0), Y_{i+l_x, j+l_y}^{(l)}(t)] \\ &= \frac{1}{l^4} \int_{-l}^{l} \int_{-l}^{l} (l - |u_x|)(l - |u_y|)\ c\Big(u_x + l\ l_x, u_y + l\ l_y, t\Big)\ du_x\ du_y. \end{aligned} \tag{3.20}$$

The autocorrelation function is given by

$$\begin{aligned} \rho^{(l)}(l_x, l_y, t) &= \text{corr}[Y_{i,j}^{(l)}(0), Y_{i+l_x, j+l_y}^{(l)}(t)] \\ &= \frac{c^{(l)}(l_x, l_y, t)}{\text{var}[Y_{i,j}^{(l)}(t)]}. \end{aligned} \tag{3.21}$$

3.5 Ellipsoidal Cell Spatial-Temporal Rainfall Model

We present a more flexible model that offers a better chance of capturing the real form of spatial-temporal rainfall. A visual comparison will be presented in section 3.11.5. We can see that the cell eccentricity varies in the observed process. We therefore assume the eccentricity is a random variable in the new model. It follows a Truncated Normal distribution from zero to one. In our new model, we assume storms have the same eccentricity and orientation. However cells have a random eccentricity, but the same orientation as the storms.

We can also see that the intensity of rainfall is high at the center of observed cells and the intensity reduces with the distance from the centre to the edge of a cell. We assume the intensity of cells is constant over their lifetime but spread in space according to ellipsoid function. Let a and b are

semi-axes of an ellipse. For $|x| \leq |a|$ and $|y| \leq |b|$, the rainfall intensity at (x, y) is given by

$$I_c(x, y) = X\sqrt{1 - \frac{(x - c_1)^2}{a^2} - \frac{(y - c_2)^2}{b^2}}, \tag{3.22}$$

where X is intensity at the ellipse centre (c_1, c_2).

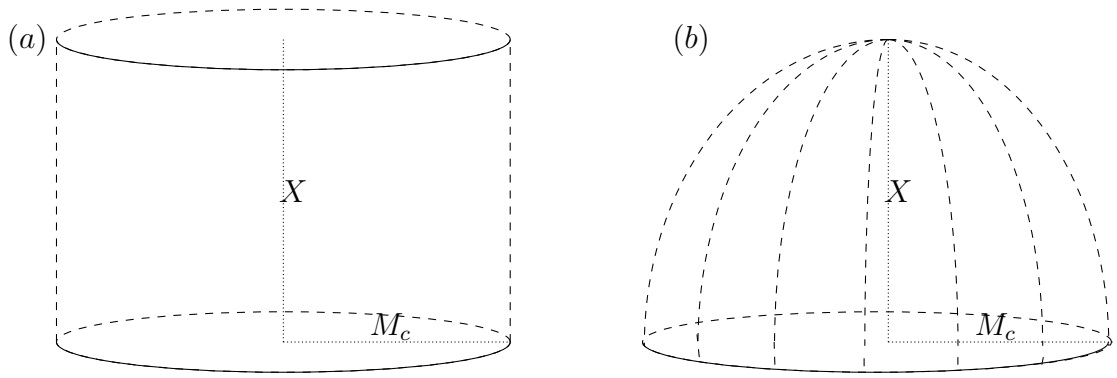

Figure 3.2: Intensity of (a) Elliptic cylindrical cell (b) Ellipsoidal cell. M_c is a major semi-axis of an ellipse.

We propose a new model, which accommodates these two extensions, (1) randomized cell eccentricity and (2) the cell intensity decreases continuously from the centre to the edge. We refer to the model as Ellipsoidal Cell Spatial-Temporal (ECST) Model. Figure 3.2(a) is the intensity of a single cell of the C-I-N model and the intensity of a single cell of the ECST model is shown in Figure 3.2(b).

3.5.1 The ECST Model Description

The Ellipsoidal Cell Spatial-Temporal (ECST) rainfall model is a spatial-temporal stochastic model for rainfall. The ECST model is homogeneous in space and stationary in time and is suitable to model the 'interior' of a rainfall event.

The ECST model is constructed using a cluster point process. The cluster process is constructed by taking a primary process, called the storm arrival process, and then attaching to each storm centre a finite secondary point

process, called a cell process. To each cell centre we then attach a rain cell, with an associated area, duration, and intensity. The storm and cell centres all share a common velocity.

We use a Poisson process for the storm centre arrival process in $\mathbb{R}^2 \times [0, \infty)$ with a homogeneous rate λ. The cell arrival processes are independent Poisson processes at rate β in time truncated after an exponential (γ) amount of time, which we call the storm duration. Let $\mathbf{v} = (v_x, v_y)$ be the velocity of the rainfall event, so if a storm centre arrives at $(\mathbf{u}, s)$ then at time $s + t$ it will be at $(\mathbf{u} + t\mathbf{v}, s + t)$. While a storm is active it produces cells at a rate β in time, starting with a cell at the moment the storm center begins. If the storm arrives at $(\mathbf{u}, s)$ and produces a cell at time $s+t$, the cell will be centered at $\mathbf{u} + t\mathbf{v} + \mathbf{w}$, where $\mathbf{w}$ comes from a Gaussian distribution with mean $\mathbf{0}$ and covariance

$$\mathbf{\Sigma} = \begin{pmatrix} \sigma_x^2 & \rho\ \sigma_x\sigma_y \\ \rho\ \sigma_x\sigma_y & \sigma_y^2 \end{pmatrix}$$

$$= \sigma^2 \begin{pmatrix} \frac{\sigma_x^2}{\sigma^2} & \rho\ \frac{\sigma_x\sigma_y}{\sigma^2} \\ \rho\ \frac{\sigma_x\sigma_y}{\sigma^2} & \frac{\sigma_y^2}{\sigma^2} \end{pmatrix}$$

where σ^2 is variance of cells displacement along the major semi-axis of storm. We suppose that storms have a random size parameterized by σ^2. which has an inverse-gamma distribution, where $\frac{1}{\sigma^2}$ has mean ξ_μ and coefficient of variation ξ_{CV}.

Individual cells have a random duration (L), distributed as $\exp(\eta)$, and a random size. Rain cells are elliptical as storms, with the same orientation Θ, but a random eccentricity e. The eccentricity of an ellipse can be obtained by $\sqrt{1 - \frac{b^2}{a^2}}$, where a and b are semi-major axis and semi-minor axes. If a is close to b, then e close to zero, which means cells are circular. If a is very larger than b, then e close to 1, so cells have banded disc. The randomness gives close match with real data. In observed data, we can see different eccentricity of the cells. Some cells are circular and some are banded shape, and some have between them as different scales, so there is a need to represent this randomness. We therefore assume that cells are elliptical with some random eccentricity. They follow a Truncated Normal distribution from zero to one with mean (μ_e) and variance (σ_e^2), where μ_e is the same as the storm eccentricity.

Individual cells also have a random intensity X at the cell center, which are exponentially distributed with mean μ_x. The rainfall intensity decreases continuously from the centre to the edge of each cell, rather than acting as

a step function. The rainfall intensity at (x, y) is given by

$$I_c(x,y) = X\sqrt{1 - \frac{(x-c_1)^2}{a^2} - \frac{(y-c_2)^2}{b^2}}, \tag{3.23}$$

where X is intensity at the ellipse center (c_1, c_2).

The cell size is given by the semi-major axis (M_c), which is distributed as a $\Gamma(\alpha_1, \alpha_2)$. The displacements, durations, sizes, and intensities of a cell are all independent, and independent of other cells.

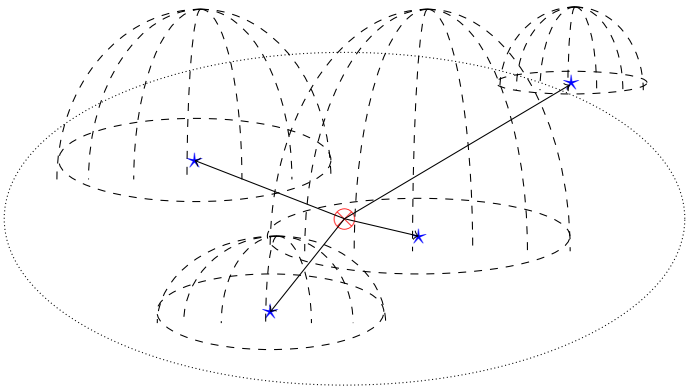

Figure 3.3: ECST cell process in space at time t. The red point is a storm centre at time t in space. Blue start points are cell centres. Lines indicate the cell centres, located relative to the storm centre. Dotted elliptical area is the storm area. Dashed curves are ellipsoidal cell intensities.

We assume that I_c is constant over the cell duration. The intensity of a cell moves with some constant velocity $\mathbf{v}$ while preserving its shape as the top half part of ellipsoid see Figure 3.3.

The expected cell area, which has semi-major axis (M_c), semi-minor axis (M_{min_c}) and average eccentricity (μ_e), is given by

$$\begin{aligned} E[A] &= E[\pi M_c \; M_{min_c}] \\ &= \pi E[M_c \; M_{min_c}] \\ &= \pi\sqrt{1-\mu_e^2} \; E[M_c^2]. \end{aligned}$$

3.5.2 Mean

The total intensity at $(\mathbf{u}, t)$ is the sum of intensities of all active cells.

Suppose N counts the cell centre origins. Suppose μ_c is the mean number of cell per storm. The intensity of cell occurrences, is therefore $\lambda\mu_c$. Let the survivor probability of cells be $\mathcal{F}_L(\cdot)$. The mean of the process is given by

$$\begin{aligned}
\mathbb{E}[Y(\mathbf{u},t)] =& \int_{\tau=-\infty}^{t}\int_{\mathbf{w}\in\mathbb{R}^2} \mathbb{E}_{I_c,L,A}[\mathbb{1}(\mathbf{w},\tau\ ;\ \mathbf{u},t)I_c(\mathbf{u},t)dN(\mathbf{w},\tau)] \\
& \text{where } \mathbb{1} \text{ is an indicator, which is one if the cell is active at } (\mathbf{u},t), \text{otherwise zero} \\
& \text{and } I_c \text{ is the cell intensity at } (\mathbf{u},t), \\
=& \int_{\tau=-\infty}^{t}\int_{\mathbf{w}\in\mathbb{R}^2} \mathbb{E}_{I_c,L,A}[\mathbb{1}(\mathbf{w},\tau\ ;\ \mathbf{u},t)I_c(\mathbf{u},t)]\ \ [dN(\mathbf{w},\tau)]. \\
=& \int_{\tau=-\infty}^{t}\int_{\mathbf{w}\in\mathbb{R}^2} \mathbb{E}_{I_c,L,A}[\mathbb{1}(\mathbf{w},\tau\ ;\ \mathbf{u},t)I_c(\mathbf{u},t)\ ]\lambda\mu_c\ d\mathbf{w}\ d\tau; \\
& \qquad \text{since } N, I_c,\ L \text{ and } A \text{ are independent} \\
=& \lambda\mu_c \int_{\tau=-\infty}^{t}\int_{\mathbf{w}\in\mathbb{R}^2} \mathbb{E}_{I_c,L,A}[\mathbb{1}(\mathbf{w},\tau\ ;\ \mathbf{u},t)I_c(\mathbf{u},t)\ ]\ d\mathbf{w}\ d\tau. \\
=& \lambda\mu_c \int_{\tau=-\infty}^{t} \mathbb{E}[V]\ \mathcal{F}_L(t-\tau)\ d\tau; \text{where V is expected cell volume.} \\
& \text{since } \mathbb{E}(V) = \frac{2}{3}\mathbb{E}[A\times X], \text{ where } A \text{ is cross-section area of a cell,} \\
& \text{and } X \text{ is the cell intensity at the centre.} \\
=& \frac{2}{3}\lambda\mu_c\ \mathbb{E}[A\times X]\int_{\tau=-\infty}^{t} \mathcal{F}_L(t-\tau)\ d\tau; \\
=& \frac{2}{3}\lambda\mu_c\ \mathbb{E}(A)\mathbb{E}[X]\mathbb{E}[L].
\end{aligned}$$

Assume cell duration is exponentially distributed with parameter η. $\mathbb{E}[X] = \mu_x$ and the major-semi axis $M_c \sim \Gamma(\alpha_1, \alpha_2)$ then the mean cells area given μ_e:

$$E[A] = \frac{\pi\sqrt{1-\mu_e^2}\ \alpha_1(1+\alpha_1)}{\alpha_2^2}.$$

Then,

$$\mathbb{E}[Y(\mathbf{u},t)] = \frac{2}{3}\pi\lambda\ \gamma^{-1}\ \beta\ \eta^{-1}\mu_x\ \sqrt{1-\mu_e^2}\ \alpha_1(1+\alpha_1)\alpha_2^{-2}.$$

3.6 Log-Normal Cell Spatial-Temporal Rainfall Model

In the ECST model, to get very high intensity in an arbitrary region we need to have many cells overlapped on the region. An alternative is to allow individual cells to have a cell intensity that follows a heavy tailed distribution. In this section, we consider the second option. So the cell intensity and area, particularly semi-major axis of cells, follow the Log-Normal distribution.

We can also see in an observed process that some small size cells have high intensity. We have an impression that there may be some correlation between cell intensity and size. So the bivariate log-normal distribution for cell intensity and cell semi-major axis can provide an opportunity to study their relationship.

We intend to study through the Log-Normal Cell Spatial-Temporal Model whether there is any correlation between cell intensity and size, and also to investigate whether the LNCST Model can capture localized heavy rainfall.

3.6.1 Model

The Log-Normal Cell Spatial-Temporal (LNCST) model is an extension of the ECST model. The LNCST mode has the same temporal and spatial structure as the ECST model. However, we assume the cell intensity and cell area have a bivariate log-normal distribution.

Briefly, the storm origins have a Poisson process at λ rate in space and time. The cell arrival processes are independent Poisson processes of rate β in time, truncated after storm duration, which is exponentially distributed with γ. The cell has a random duration, a random intensity, a random area, and a random eccentricity. The cell duration follows an exponential distribution (η). We assume that the cell intensity (X) at cell centre and the semi-major axis (M_c) follow a bivariate Log-Normal distribution i.e.

$$\begin{pmatrix} X \\ M_c \end{pmatrix} \sim \log N \left(\begin{pmatrix} \mu_x \\ \mu_{M_c} \end{pmatrix}, \begin{pmatrix} \sigma_X^2 & \rho_{xm_c}\sigma_X\sigma_{M_c} \\ \rho_{xm_c}\sigma_X\sigma_{M_c} & \sigma_{M_c}^2 \end{pmatrix} \right)$$

Storm and cells share the same orientations. The cell intensity reduces continuous from the centre to the edge as the ECST model. The intensity remains constant over the cell duration, and moves with some velocity $\mathbf{v}$. Similarly, the storm and all cells within the storm move with the same velocity $\mathbf{v} = (v_x, v_y)$.

3.7 Empirical Statistics

Radar rainfall data is available at a discrete set of points with pixel (i, j) of l km by l km in space and h length of time, where $i = 1, 2, 3, ..., N_x$ and $j = 1, 2, 3, ..., N_y$. The data array has $N(= N_x \times N_y)$ pixels at time t. Time is also discrete at points $1, 2, 3, ..., T$. The total number of pixels on the data array is $N \times T$. Figure 3.4 shows the data-frame of observed rainfall data.

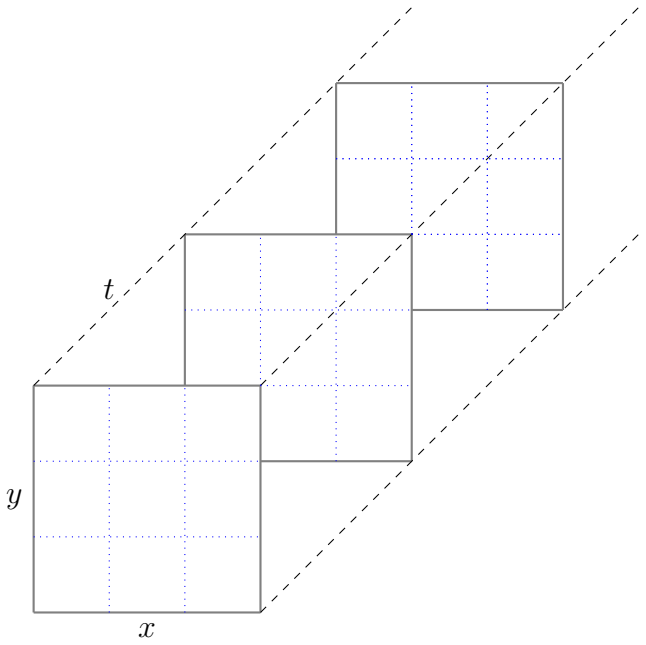

Figure 3.4: Data-frame of observed data set.

$Y_{i,j}^{(l)}(k)$ denotes the rainfall in (i, j)-th $l \times l$ km^2 pixel at discrete time point k. The empirical statistical properties are given by the first two

moments:

$$\bar{y} = \frac{1}{N_x N_y T} \sum_{i=1}^{N_x} \sum_{j=1}^{N_y} \sum_{k=1}^{T} Y_{i,j}^{(l)}(k), \tag{3.24}$$

$$s_y^2 = \frac{1}{N_x N_y T - 1} \sum_{i=1}^{N_x} \sum_{j=1}^{N_y} \sum_{k=1}^{T} [Y_{i,j}^{(l)}(k) - \bar{y}]^2. \tag{3.25}$$

The empirical spatial-temporal covariance function is

$$\widehat{c}(l_x, l_y, l_t) = \frac{1}{(N_x - l_x)(N_y - l_y)(T - l_t) - 1} \sum_{i=1}^{N_x - l_x} \sum_{j=1}^{N_y - l_y} \sum_{k=1}^{T - l_t} [Y_{i,j}^{(l)}(k) - \bar{y}_1][Y_{i+l_x, j+l_y}^{(l)}(k + l_t) - \bar{y}_2]; \tag{3.26}$$

where

$$\bar{y}_1 = \frac{1}{(N_x - l_x)(N_y - l_y)(T - l_t)} \sum_{i=1}^{N_x - l_x} \sum_{j=1}^{N_y - l_y} \sum_{k=1}^{T - l_t} Y_{i,j}^{(l)}(k).$$

$$\bar{y}_2 = \frac{1}{(N_x - l_x)(N_y - l_y)(T - l_t)} \sum_{i=1}^{N_x - l_x} \sum_{j=1}^{N_y - l_y} \sum_{k=1}^{T - l_t} Y_{i+l_x, j+l_y}^{(l)}(k + l_t).$$

Hence, the empirical spatial-temporal correlation is

$$\widehat{\rho}(l_x, l_y, l_t) = \frac{\hat{c}(l_x, l_y, l_t)]}{\sigma_{y_1} \sigma_{y_2}}, \tag{3.27}$$

where

$$\sigma_{y_1}^2 = \frac{1}{(N_x - l_x)(N_y - l_y)(T - l_t) - 1} \sum_{i=1}^{N_x - l_x} \sum_{j=1}^{N_y - l_y} \sum_{k=1}^{T - l_t} [Y_{i,j}^{(l)}(k) - \bar{y}_1]^2,$$

$$\sigma_{y_2}^2 = \frac{1}{(N_x - l_x)(N_y - l_y)(T - l_t) - 1} \sum_{i=1}^{N_x - l_x} \sum_{j=1}^{N_y - l_y} \sum_{k=1}^{T - l_t} [Y_{i+l_x, j+l_y}^{(l)}(k + l_t) - \bar{y}_2]^2.$$

If $Y_{i,j}^{(l)}(k) = 0$, then the (i, j)-th pixel at time point k is dry. The probability that an arbitrary pixel at arbitrary time t is dry, is estimated by

$$\widehat{P}(Y^{(l)}=0)=\frac{1}{N_xN_yT}\sum_{i=1}^{N_x}\sum_{j=1}^{N_y}\sum_{k=1}^{T}\mathbb{1}(Y_{i,j}^{(l)}(k)=0). \tag{3.28}$$

If $Y_{i,j}^{(l)}(k)>0$, then the (i,j)-th pixel at time point k is wet. The dry and wet ratio can be estimated using

$$\frac{\#(Y^{(l)}=0)}{\#(Y^{(l)}>0)}=\frac{\sum_{i=1}^{N_x}\sum_{j=1}^{N_y}\sum_{k=1}^{T}\ \mathbb{1}(Y_{i,j}^{(l)}(k)=0)}{\sum_{i=1}^{N_x}\sum_{j=1}^{N_y}\sum_{k=1}^{T}\ \mathbb{1}(Y_{i,j}^{(l)}(k)>0)}. \tag{3.29}$$

Note that the area of pixel cancels from numerator and denominator.

The other two properties of mean and variance of wet area over time can be easily estimated. Put

$$A_w^k=\sum_{i=1}^{N_x}\sum_{j=1}^{N_y}\mathbb{1}(Y_{i,j}^{(l)}(k)>0)(l\times l),\ k=1,2,3,...,T. \tag{3.30}$$

The mean and variance of wet area over time are estimated by

$$\bar{a}_w=\frac{1}{T}\sum_{k=1}^{T}A_w^k. \tag{3.31}$$

$$\sigma_{a_w}^2=\frac{1}{T-1}\sum_{k=1}^{T}[A_w^k-\bar{a}_w]^2. \tag{3.32}$$

3.8 Radar Data

Following Wheat et al. 2000 [48], the event duration is defined as the time during which the observed process coves the fitting window above some percentage. We focus on the rainfall event, which covers at least 20% of the

event area.

We obtained sample data from the Bureau of Meteorology, Australia. For this study we used radar data collected at Laverton, Melbourne on 24th September 2016 from 12:54 to 16:48 hours. The radar data was calibrated by the Australian Bureau of Meteorology using rain-gauge. The radar coverage is the circular region of 128 km radius. The space is gridded 1×1 km^2 and time resolution is 6-minutes. We restricted ourself to a square study area of size 180×180 km^2 see Figure 3.5. The data matrix is therefore size of $180 \times 180 \times 40$. Each element of the matrix is given some amount (possibly zero) of rain in mm. We consider there is zero rain if a pixel, which has less than 0.01 mm per 6-minutes to avoid radar noise.

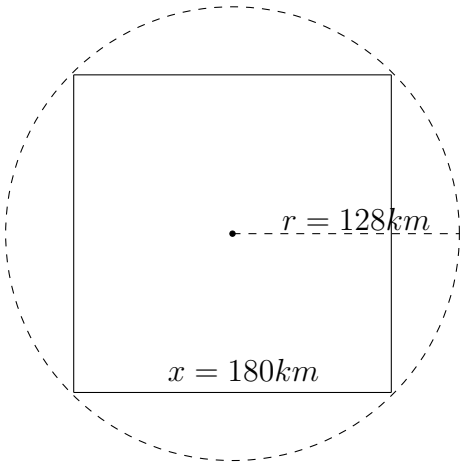

Figure 3.5: Circle is radar coverage and square is study area

3.8.1 Data Exploration

Figure 3.6 shows the maximum value over all pixels for a fixed time. The maximum value is 2.86 mm and minimum value is 1.01 mm. Spatial average rainfall is between 0.04 mm and 0.09 mm (see Figure 3.7). Similarly Figure 3.8 gives percentage spatial coverage over time. The least coverage is 21% and the maximum coverage reaches 56%.

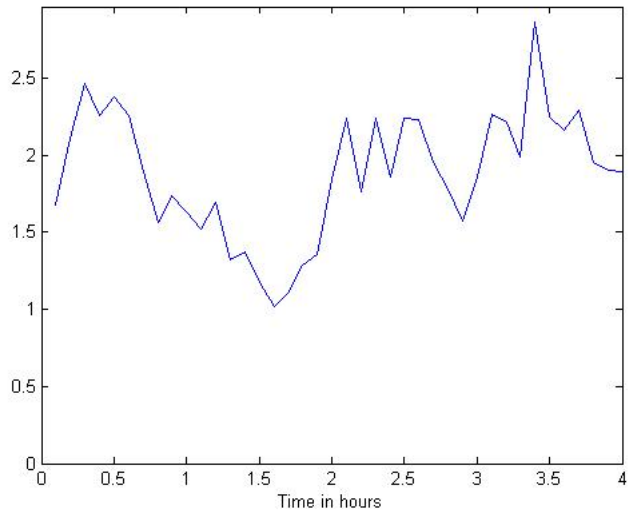

Figure 3.6: Maximum rainfall (mm) on a pixel in space at time t. The rainfall event is rainfall on 24th September 2016 from 12:54 to 16:48 hours in Melbourne.

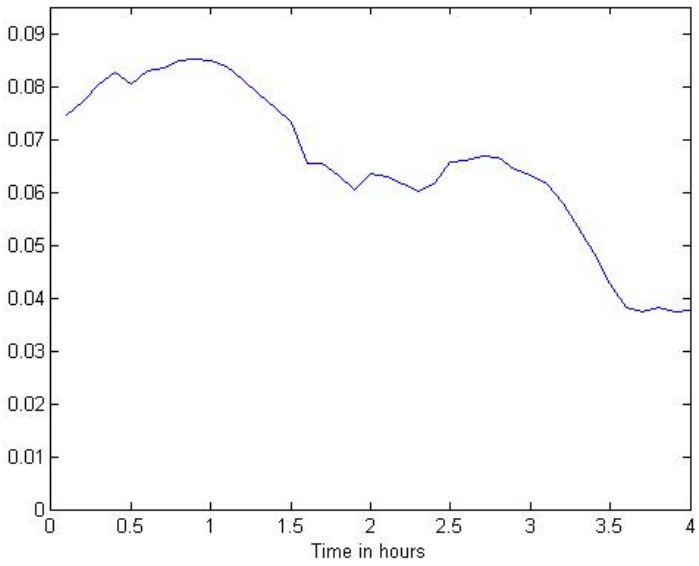

Figure 3.7: Mean rainfall (mm) per pixel in space at time t. The rainfall event is rainfall on 24th September 2016 from 12:54 to 16:48 hours in Melbourne.

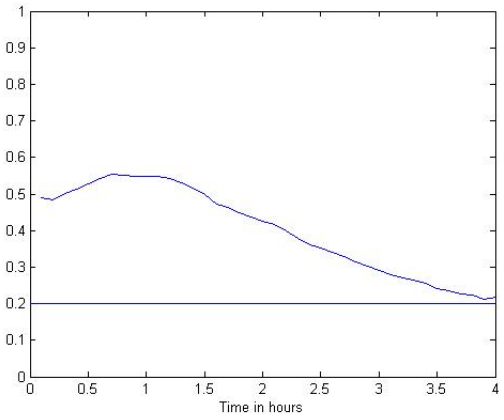

Figure 3.8: Area coverage percentage by rainfall in space at time t. The rainfall event is rainfall on 24th September 2016 from12:54 to 16:48 hours in Melbourne. The horizontal line is 20 % indication line.

3.8.2 Contour Plots

Figures 3.9, 3.10, 3.11, 3.12, and 3.13 show contour plots of the observed rainfall on 24th September from 12:54 to 16:24. Zero rainfall is also white colour.

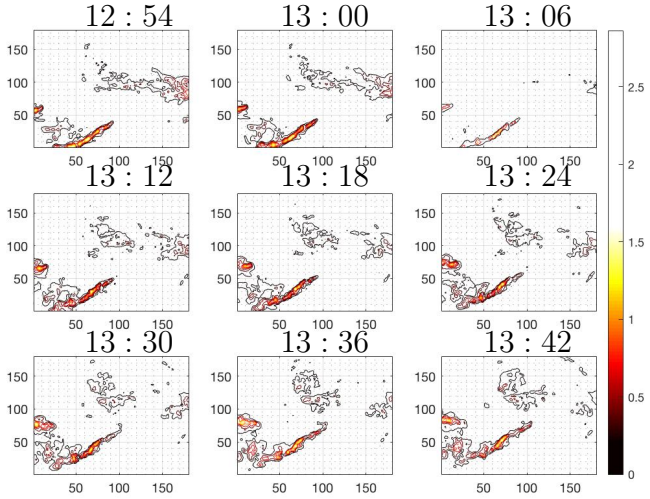

Figure 3.9: Contour plots from observed data. The rainfall is from 12:54 to 13:42 hours on 24th September 2016 in Melbourne. Zero rainfall is also white colour

.

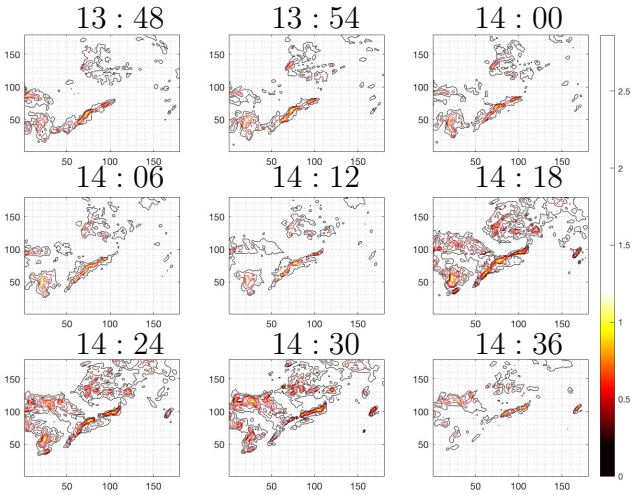

Figure 3.10: Contour plots from observed data. The rainfall is from 13:48 to 14:36 hours on 24th September 2016 in Melbourne. Zero rainfall is also white colour.

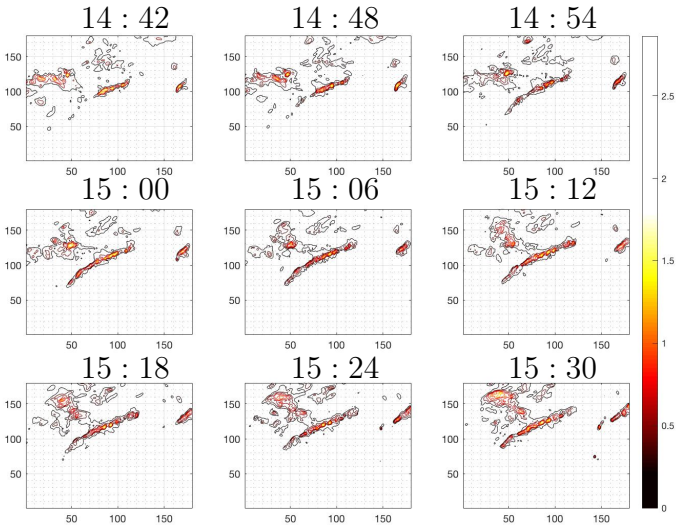

Figure 3.11: Contour plots from observed data. The rainfall is from 14:42 to 15:30 hours on 24th September 2016 in Melbourne. Zero rainfall is also white colour.

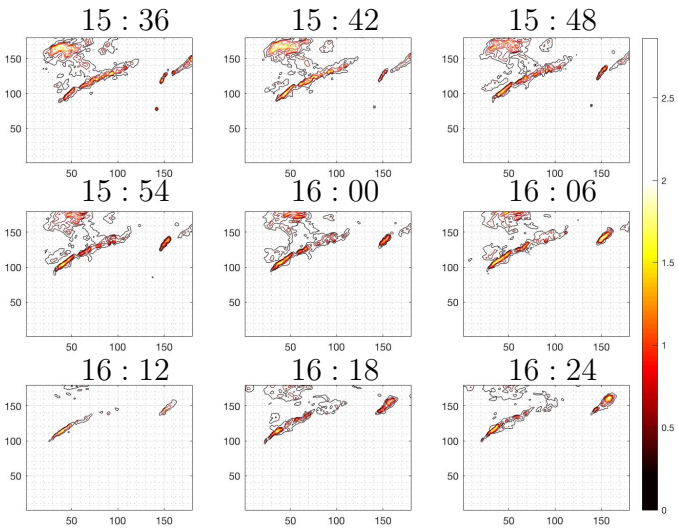

Figure 3.12: Contour plots from observed data. The rainfall is from 15:36 to 16:24 hours on 24th September 2016 in Melbourne. Zero rainfall is white.

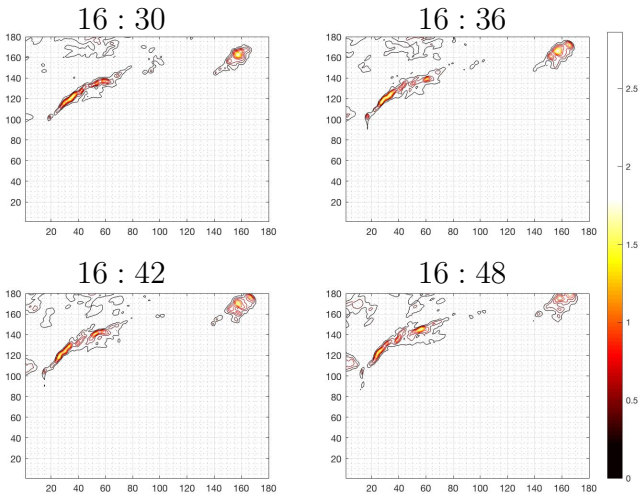

Figure 3.13: Contour plots from observed data. The rainfall is from 16:30 to 16:48 hours on 24th September 2016 in Melbourne. Zero rainfall is white.

3.9 Fitting a Spatial-Temporal Model

The C-I-N and the ECST models have parameters λ, γ, β, e (or μ_e), Θ and random variables cell intensity (X), cell duration (L), cell semi-major axis (M_c), storm semi-major axis (M_s) and the two components of the velocity $\boldsymbol{v} = (v_x, v_y)$. Distributions of these random variables are kept the same in both the C-I-N and ECST models. We assume X and L follow exponential distribution i.e. $X \sim \exp(1/\mu_x)$ and $L \sim \exp(\eta)$. We consider M_c follows gamma distributions i.e. $M_c \sim \Gamma(\alpha_1, \alpha_2)$. The mean cell area μ_A is given by

$$\mu_A = \frac{\pi\sqrt{1-e^2}\ \alpha_1(1+\alpha_1)}{\alpha_2^2}. \tag{3.33}$$

Instead of estimating α_1 and α_2, we estimate μ_A and α_2. Then

$$\alpha_1 = \frac{1}{2}\Big(-1 + \sqrt{1 + \frac{4\mu_A\alpha_2^2}{\pi\sqrt{1-e^2}}}\ \Big).$$

Suppose σ^2 denote the variance of cell displacements in a direction of parallel to the storm semi-major axis. If $\frac{1}{\sigma^2} \sim \text{gamma}(\xi_1, \xi_2)$, then $\xi_m = \xi_1\xi_2$ and $\xi_{cv} = \frac{1}{\sqrt{\xi_1}}$. We estimate the coefficient of variance ξ_{cv} and mean ξ_m.

There therefore are 13 common parameters for the C-I-N model and the ECST model. They are λ, γ, β, e (or μ_e), Θ, μ_A, μ_x, η, α_2, ξ_m , ξ_{cv}, v_x and v_y. We estimate two velocity components and e and Θ using an ad hoc procedure due to Wheat et al. 2000 [48]. The detail is presented in §3.9.1 and 3.9.2. All other parameters are latent variables so we need something more sophisticated to estimate them, namely ABC.

In the past, the C-I-N model fitting has been carried out using GMM. GMM fitting requires moments with analytical expressions. The theoretical expression for the statistics which we want to use for fitting are not available. However ABC supports this case, all we need is that we can easily simulate the process.

3.9.1 Velocity Estimation

We assume that the storm and the cells have the same velocity. Following Wheater et al. 2000 [48], the spatial autocorrelation function $\rho(l_x, l_y, t)$ is applied to estimate the velocity. We estimate ρ using the empirical spatial-

temporal autocorrelation function a discrete set of points in time and space $l_t = 1, 2, 3, ..., T$, $l_x = -n, ..., -3, -2, -1, 0, 1, 2, 3, , ..., n$ and $l_y = -n, ..., -3, -2, -1, 0, 1, 2, 3, ..., n$. Let $(\hat{l}_x, \hat{l}_y, \hat{l}_t)$ be the index of the observed maximum of $\hat{\rho}$. We use 9 pixels centered at $(\hat{l}_x, \hat{l}_y, \hat{l}_t)$ to estimate velocity

$$\hat{v}_x = \frac{\sum_{l_i} \sum_{l_j} l_i \hat{\rho}(l_i, l_j, \hat{l}_t)}{\sum_{l_i} \sum_{l_j} \hat{\rho}(l_i, l_j, \hat{l}_t)};$$

$$\hat{v}_y = \frac{\sum_{l_i} \sum_{l_j} l_j \hat{\rho}(l_i, l_j, \hat{l}_t)}{\sum_{l_i} \sum_{l_j} \hat{\rho}(l_i, l_j, \hat{l}_t)},$$

where $l_i = \hat{l}_x - 1,\ \hat{l}_x,\ \hat{l}_x + 1$ and $l_j = \hat{l}_y - 1,\ \hat{l}_y,\ \hat{l}_y + 1$.

3.9.2 Eccentricity and Orientation Estimation

Assume that the average eccentricity and orientation of cells and storms are the same. We estimate e and Θ using $\hat{\rho}(l_x, l_y, 0)$. We select those pairs (l_x, l_y) for which the spatial correlation is greater than some chosen threshold. We then estimate the covariance-matrix from these pairs, which cover an elliptical region in the (l_x, l_y) plane (see Wheater et al. 2000 [48]). We calculate the first and second largest eigenvalues (λ_1 and λ_2) and corresponding eigenvectors from this covariance- matrix. Then $\hat{e} = \sqrt{1 - \frac{\lambda_2}{\lambda_1}}$ and $\hat{\Theta} = \arctan(\frac{y}{x})$, where y and x are y-coordinate and x-coordinate of the eigenvector corresponding to the largest eigenvalue (λ_1), are the estimation of eccentricity e and orientation Θ respectively.

3.9.3 Summary Statistics

We select the following summary statistics. The first 2 summaries are mean, standard deviation. We use velocity-adjusted spatial-temporal correlation $\rho(l_x + v_x l_t,\ l_y + v_y l_t,\ l_t)$, where $l_x \in \{-1, 0, 1\}$, $l_y \in \{-1, 0, 1\}$ and $l_t \in \{0, 1\}$. We need an integer value for velocity-adjusted correlation functions, so we round off the velocity components to the closest integer. We therefore use 17 correlations of lags $l_x \in \{-1, 0, 1\}$, $l_y \in \{-1, 0, 1\}$ and $l_t \in \{0, 1\}$. $\rho(0, 0, 0)$ is not used because it is just the variance. We also use the probability of an arbitrary pixel being dry at an arbitrary time, and the other 3 summaries, ratio of dry/wet area and mean and standard deviation of wet area over time. We thus include 23 summary statistics for fitting the model.

Table 3.1 shows the values for summary statistics of the observed rainfall process.

Summaries	lags (l_x, l_y, l_t)	Values
Mean (mm per pixel)		0.065
Standard deviation		0.137
Correlation	$(-1,-1,0)$	0.947
$\rho\big(l_x + l_t \times v_x,\ l_y + l_t \times v_y,\ l_t\big)$	$(-1,0,0)$	0.952
	$(-1,1,0)$	0.898
	$(0,-1,0)$	0.963
	$(0,1,0)$	0.963
	$(1,-1,0)$	0.898
	$(1,0,0)$	0.952
	$(1,1,0)$	0.947
	$(-1+v_x,-1+v_y,1)$	0.846
	$(-1+v_x,0+v_y,1)$	0.842
	$(-1+v_x,1+v_y,1)$	0.806
	$(0+v_x,-1+v_y,1)$	0.854
	$(0+v_x,0+v_y,1)$	0.873
	$(0+v_x,1+v_x,1)$	0.855
	$(1+v_x,-1+v_y,1)$	0.821
	$(1+v_x,0+v_y,1)$	0.854
	$(1+v_x,1+v_x,1)$	0.856
$\mathbb{P}(Y^{(l)}=0)$		0.599
Dry wet ratio		0.671
Mean wet area (km^2)		13007
Standard deviation of wet area		3864

Table 3.1: Values of summary statistics. The rainfall event is on 24th September 2016 from 12:54 to 16:48 hours in Melbourne.

3.9.4 ABC-MCMC Algorithm

We repeat the ABC-MCMC algorithm as discussed in §2.3.1 for convenience. We suppose that we have an observation D from some model $f(.|\boldsymbol{\phi})$, and that we are able to simulate from f. Let π be the prior distribution for $\boldsymbol{\phi}$ and $S = S(D)$ a vector of summary statistics for D, then ABC-MCMC generates samples from $f(\boldsymbol{\phi}|d(S(D^*), S(D)) \leq \epsilon)$, where $D^* \sim f(.|\boldsymbol{\phi})$, $\boldsymbol{\phi} \sim \pi$, and d is some distance function. The algorithm is as follows:

Algorithm 3 ABC MCMC

for i=1 to N **do**
  Given current state $\boldsymbol{\phi}_i$, propose a new state $\boldsymbol{\phi}^*$ using proposal density $q(.|\boldsymbol{\phi}_i)$
  Put $\alpha = \min\left(1, \frac{\pi(\boldsymbol{\phi}^*)q(\boldsymbol{\phi}_i|\boldsymbol{\phi}^*)}{\pi(\boldsymbol{\phi}_i)q(\boldsymbol{\phi}^*|\boldsymbol{\phi}_i)}\right)$
  if $U(0,1) < \alpha$, **then**
    simulate data $D^* \sim f(\cdot|\boldsymbol{\phi}^*)$
    if $d(S(D^*), S(D)) \leq \epsilon$, **then**
      set $\boldsymbol{\phi}_{i+1} = \boldsymbol{\phi}^*$
    else
      set $\boldsymbol{\phi}_{i+1} = \boldsymbol{\phi}_i$
    end if
  else
    set $\boldsymbol{\phi}_{i+1} = \boldsymbol{\phi}_i$
  end if
end for

3.9.5 Starting ABC using SMM

There are lots tuning parameters in ABC fitting. Starting points are one most important. McFadden, 1989 and Pakes & Pollard, 1989 [30, 36] presented a Simulated Method of Moments (SMM) as simulation based version of GMM. When applying ABC, we found it advantageous to 'jump-start' the algorithm by choosing the initial parameter selection ϕ_0 using an SMM fit,

For ABC-MCMC, if we can provide good starting points, the burn-in time is short, even we may not need burn-in time for chain mixing. We use SMM, which provides us useful starting points for ABC.

Let $\mathbf{V} = (V_1, ..., V_k)'$ be a vector of summary statistics computed from data. The corresponding expected values of $\mathbf{V}$ under the model is denoted by a vector $\tau^*(\boldsymbol{\phi}) = (\tau_1(\boldsymbol{\phi}), ..., \tau_k(\boldsymbol{\phi}))'$. Estimation of the unknown parameter vector $\boldsymbol{\phi}$ is obtained by

$$\hat{\boldsymbol{\phi}} = \quad \text{argmin}_{\boldsymbol{\phi}} \ (\mathbf{V} - \tau^*(\boldsymbol{\phi}))' \ \mathbf{W} \ (\mathbf{V} - \tau^*(\boldsymbol{\phi})),$$

where $\mathbf{W}$ is a positive finite weighting matrix, which is often taken to be a diagonal matrix, in which case the objective function $G(\boldsymbol{\phi}; \mathbf{V})$ can be written as

$$G(\boldsymbol{\phi}; \mathbf{V}) = \sum_{i=1}^{k} w_i [V_i - \tau_i^*(\boldsymbol{\phi})]^2. \tag{3.34}$$

The optimal weights w_i are equal to $\text{Var}\,(V_i)^{-1}$.

The idea of SMM is that we estimate $\tau^*(\boldsymbol{\phi})$ using the average of a simulated sample. Literally we are minimizing the distance between the observed and simulated expectations. Thus like ABC, using SMM we have much more freedom in the choice of moments used to fit the model to the data. We use a random search to optimise the objective function $\hat{G}(\cdot)$. Note that it is a random function. An alternative approach would be stochastic gradient descent.

The starting point for ABC-MCMC is the parameter value, which minimizes $\hat{G}$. If $\boldsymbol{\phi}_0$ has very small posterior probability, then ABC-MCMC requires a prohibitively large burn-in period or may just freeze. So this provides a good starting points. The other advantage is that it gives us a distribution $S(D^*)$ that we can use to estimate the weights w_i of the distance function.

It is common to use a separate ABC step to estimate $\boldsymbol{\phi}_0$, we found that using SMM instead requires much less computation time.

3.9.6 Process Burn-in Period

Recall the intensity at (x, y, t) is the sum of intensities from all active cells at (x, y, t). Assume the rainfall event to be homogeneous in space and stationary in time. Following Wheat et al. 2000 [48], the event duration is defined as the time during which the observed process coves the fitting window above some percentage. We focus on the rainfall event, which covers at least 20% of the event area. The simulated process therefore should follow the same coverage attribute. So we need to simulate the rainfall process for longer than time period considered. The question that arises is for how long we need to simulate the rainfall process. We take a practical approach. First we fitted spatial-temporal models to real data. The posteriors for the parameters from initial fitting to the event are in Appendix 1 for the C-I-N model. We simulate data from posteriors. We then look at how the simulated processes behave. Figures 3.14 and 3.15 show the simulated data total intensities and coverage during the specified rainfall event.

Figures 3.14 and 3.15 show that after 2 hours the process appears stationary and all simulations achieve 20% coverage threshold. So we simulate the rainfall process 2 hours extra time.

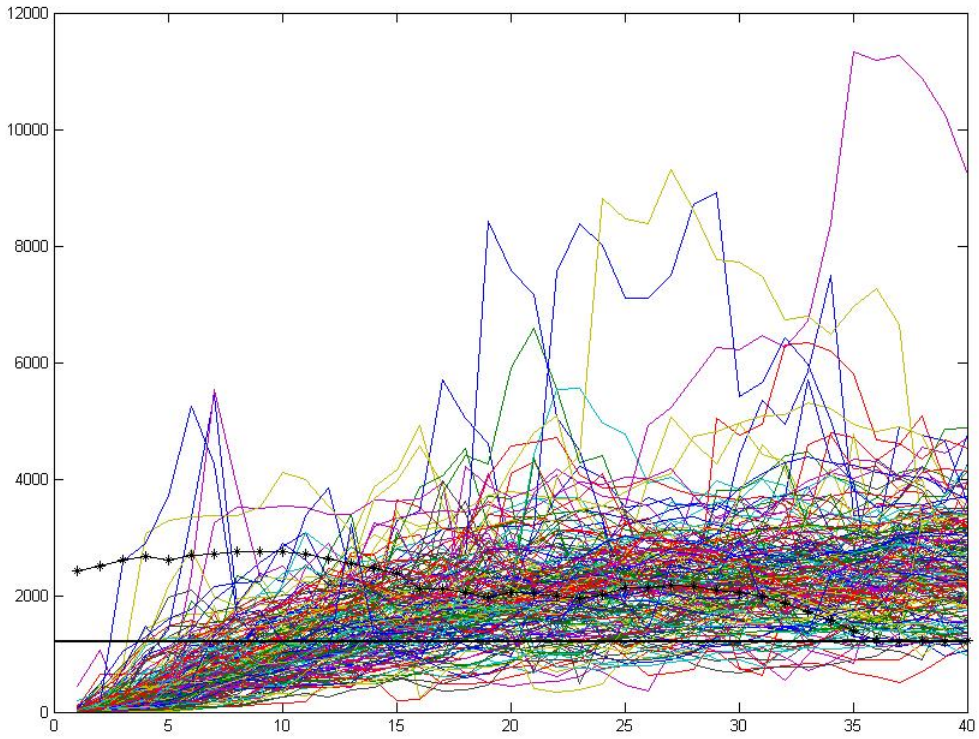

Figure 3.14: Total rainfall from 200 simulated data from the models are colour lines. Starred black line is the total rainfall over the area in time for real data. Black horizontal line is the minimum total rainfall during the rainfall event. X-axis is the time (6-minutes as one time unit). The rainfall event is rainfall on 24th September 201 from12:54 to 16:48 hours in Melbourne.

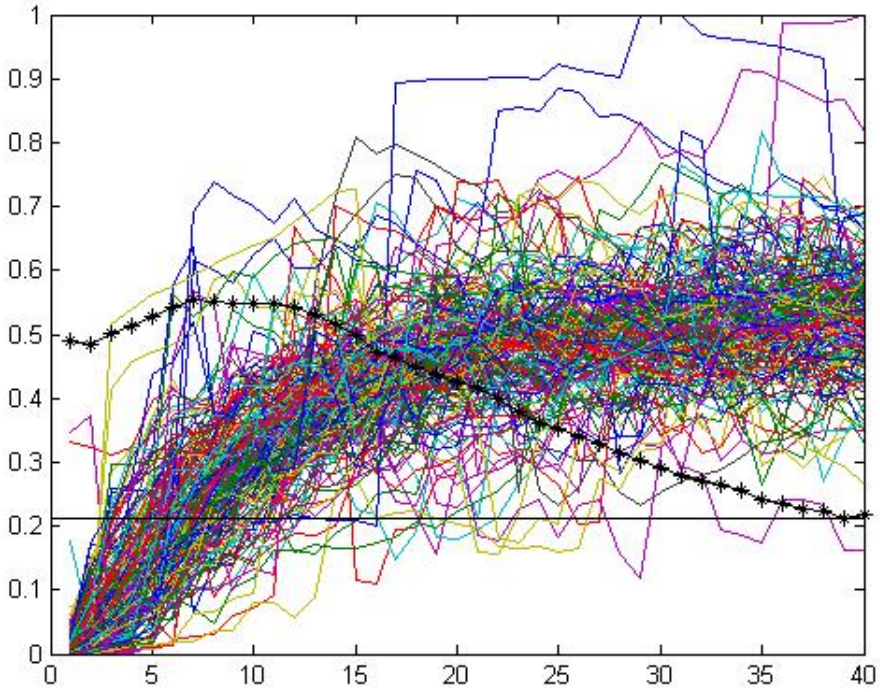

Figure 3.15: Area coverages from 200 simulated data for the models are colour lines. Starred black line is for real data coverage. Black horizontal line is the minimum total rainfall during the rainfall event. X-axis is the time (6-minutes as one time unit). The rainfall event is on 24th September 201 from12:54 to 16:48 hours in Melbourne.

3.10 Fitting the C-I-N Model

We take a two step approach. Using the method discussed § 3.9, first we estimate velocity, eccentricity, and orientation using the empirical spatial autocorrelation function. We then fix them and use the ABC-MCMC to estimate the remaining parameters.

We obtain estimates $e = 0.86$ and $\Theta = 39^o$. We estimate the velocity $\mathbf{v} = (0.10, 29.9)km$ per hour. The Figure 3.16 shows that the highest correlation is at spatial lag(0, 3).

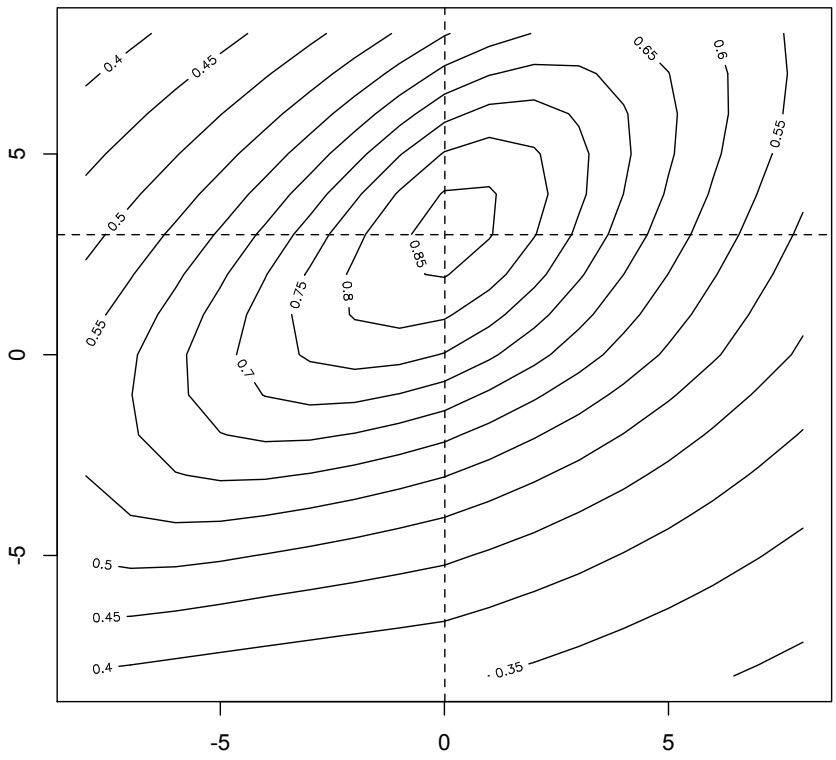

Figure 3.16: Spatial correlation. Dashed vertical line is as estimated $v_x = 0.01$ and dashed horizontal line is $v_y = 2.99$ per 6-minutes. The rainfall event is rainfall on 24th September 2016 from 12:54 to 16:48 hours in Melbourne.

3.10.1 Applying ABC-MCMC to the C-I-N Model

Prior Distribution and Reparameterization

Firstly we reparameterise the model, to reduce the dependence between the parameters. In addition we use a log transformation to map parameter domains from $\mathbb{R}_+$ to $\mathbb{R}$ for the first 9 parameters, which simplifies the choice of the proposal chain too.

The similar way defined in §2.4.1 we combine storm level parameters: storm rate λ and storm mean duration γ^{-1} as $\lambda \times \gamma^{-1}$ and $\lambda \times \gamma$. Similarly rain cells parameters: cell arrival rate β, cell mean duration η^{-1}, cell intensity

μ_x, and cell mean area μ_A are recombined as, $\beta \times \eta^{-1}$ and $\beta \times \eta$, and $\mu_x \times \mu_A$ and $\mu_x \times \mu_A^{-1}$.

In total we have 13 parameters:

$$\begin{aligned}
\phi(1) &= \log(\lambda\gamma^{-1}) \\
\phi(2) &= \log(\lambda\gamma) \\
\phi(3) &= \log(\beta\eta^{-1}) \\
\phi(4) &= \log(\beta\eta) \\
\phi(5) &= \log(\mu_x\mu_A) \\
\phi(6) &= \log(\mu_x\mu_A^{-1}) \\
\phi(7) &= \log(\alpha_2) \\
\phi(8) &= \log(\xi_m) \\
\phi(9) &= \log(\xi_{cv}) \\
\phi(10) &= e \\
\phi(11) &= \Theta \\
\phi(12) &= v_x \\
\phi(13) &= v_y
\end{aligned}$$

The parameters are interdependent, even with this reparameterization. For instance, a rainfall event which has a low storm arrival rate and a long storm duration and another rainfall event, which has a high storm rate and a short storm duration, can produce the same total intensity at $(\mathbf{u}, t)$. Similarly a long storm duration and a low cells arrival rate, and a short storm duration and a high cells arrival rate can generate the same number of cells for a storm. Therefore Poisson cluster stochastic rainfall models are challenging to fit. However our experience is that this reparameterisation improves estimation.

Initially normal priors were used for all the $\phi(i); i = 1, 2, ..., 9$; that is $\pi(\boldsymbol{\phi}(i)) \sim N(\mathbf{0}, \sigma^2\mathbf{I})$ for σ^2 large. However, we found that this produced some extreme posterior points, particularly when we transformed log parameters to original parameters see Figure 1 in Appendix. To avoid these extreme values we choose the following truncations, for $\phi(7)$ truncated normal $(-\infty, \log(3)]$, for $\phi(8)$ truncated normal $(-\infty, \log(6)]$, and for $\phi(9)$ truncated normal $(-\infty, \log(10)]$ with mean zero and variance as before.

Proposal Distribution and Distance Metric

Because of log transformation, we have now parameter domain $\mathbb{R}^9$. This simplifies the proposal chain, because there are no boundaries.

For the proposal chain we just use a random walk with steps distribution as $N(\mathbf{0}, 0.2^2\mathbf{I})$ increments.

For distance measure d, we choose weighted Euclidean distance:

$$d(S(D^*), S(D)) = \Big[\sum_i w_i \ (S^*(i) - S(i))^2 \Big]^{\frac{1}{2}}$$

where $S^*(i)$ and $S(i)$ are respectively the $i\text{-}th$ component of $S(D^*)$ and $S(D)$. The choice of weights is important. We choose w_i inversely proportional to variance of $i\text{-}th$ summary statistics using a sample generated from $f(.|\hat{\boldsymbol{\phi}})$, where $\hat{\boldsymbol{\phi}}$ is a preliminary estimate of $\boldsymbol{\phi}$ (Prangle, 2017 [37]). This balances the importance of S.

Posterior Distribution

Because the parameter region is high dimensional there is a possibility the chain gets stuck on low probability region, so good starting values of the parameter set are crucial. The choice of starting values also determines that how quickly the chain converges to stationary distribution. We apply the SMM to obtain a good starting points. Applying Algorithm 3 we obtain posteriors for $\phi(i), i = 1, ..., 9$.

Clearly we see in Figure 3.17, the chains have converge to stationary distributions. The Markov chains have clearly moved around the parameter space. The effective sample sizes are above 200 in each case. To increase the effective sample sizes, we may run the algorithm for longer.

Figure 3.18 gives posterior densities for all 9 parameters, which look good as we can see nice peak for each density curve. Acceptance rate is 4.1% with a threshold $\epsilon = 10$. Theoretically we want ϵ to be very small. Small ϵ gives better approximation of posteriors, however very small ϵ may lead bad mixing. In practice, we need to choose ϵ such that chains get well mixing and provide a good posterior approximation.

The joint distribution of posteriors is another diagnostic test of whether the estimated parameters are highly correlated. We expect some correlation of them because the original parameters of the model are highly dependent.

In Figure 3.19, the diagonal plots are histograms for parameters $\phi(i), i = 1, 2, 3, ..., 9$. The lower panels are joint distribution for pairs of $\phi(i)$,$i = 1, 2, \ldots, 9$. We see that there is very little pairwise correlation between the parameters in the posterior.

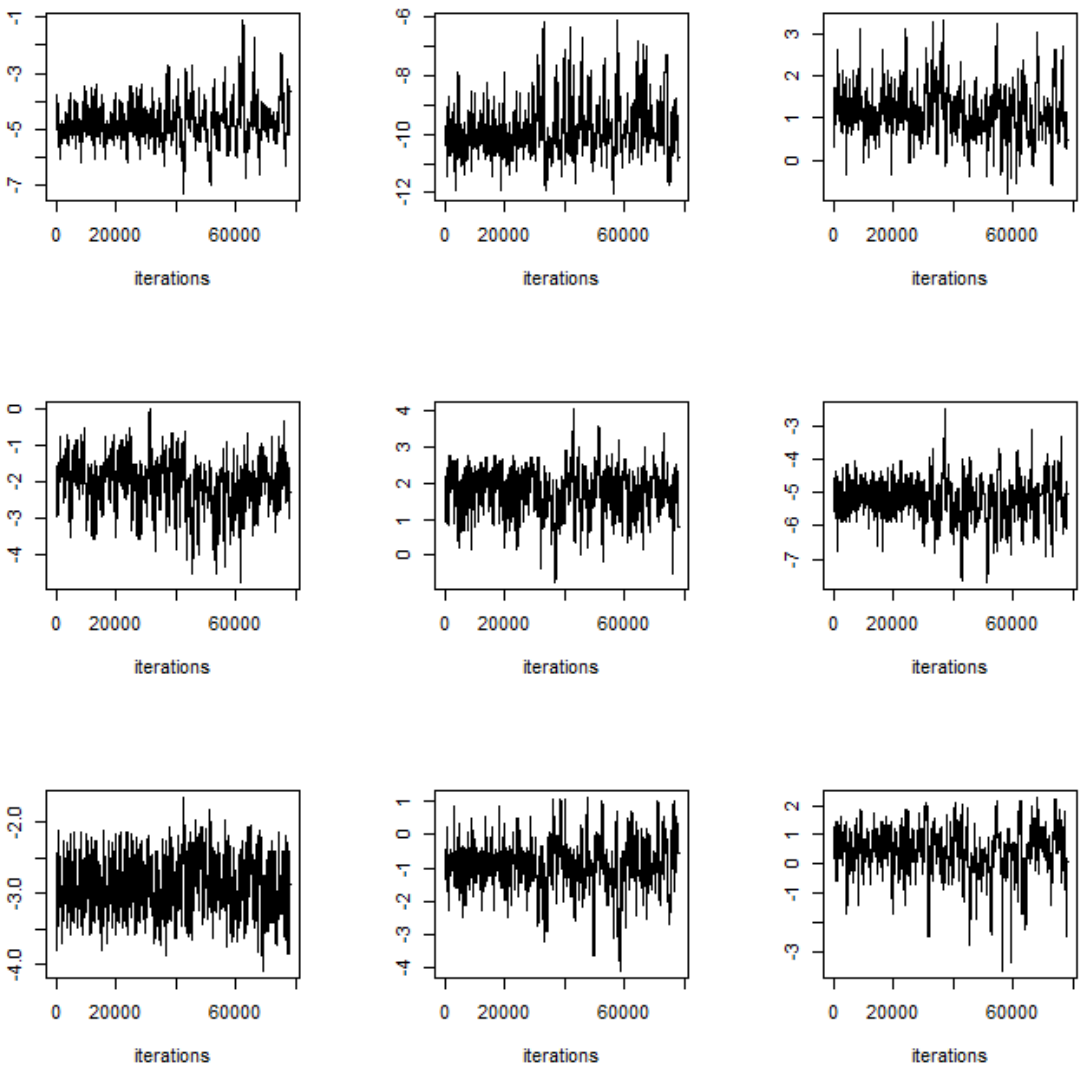

Figure 3.17: Chains for $\phi(i)$,$i = 1, 2, \ldots, 9$ (from top left to right). The rainfall event is on 24th September 2016 from 12:54 to 16:48 hours in Melbourne.

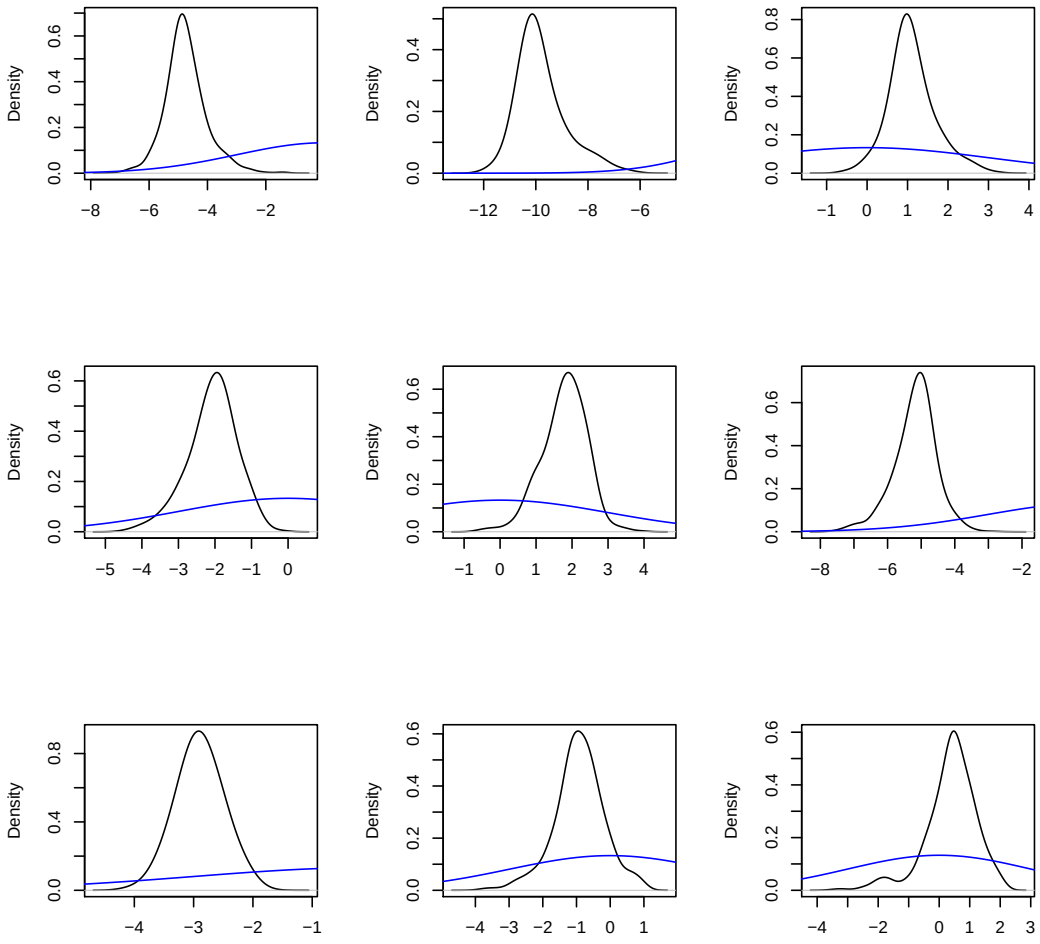

Figure 3.18: Posteriors for $\phi(i)$,$i = 1, 2, \ldots, 9$ (from top left to right). Blue curves are priors. The rainfall event is on 24th September 2016 from 12:54 to 16:48 hours in Melbourne.

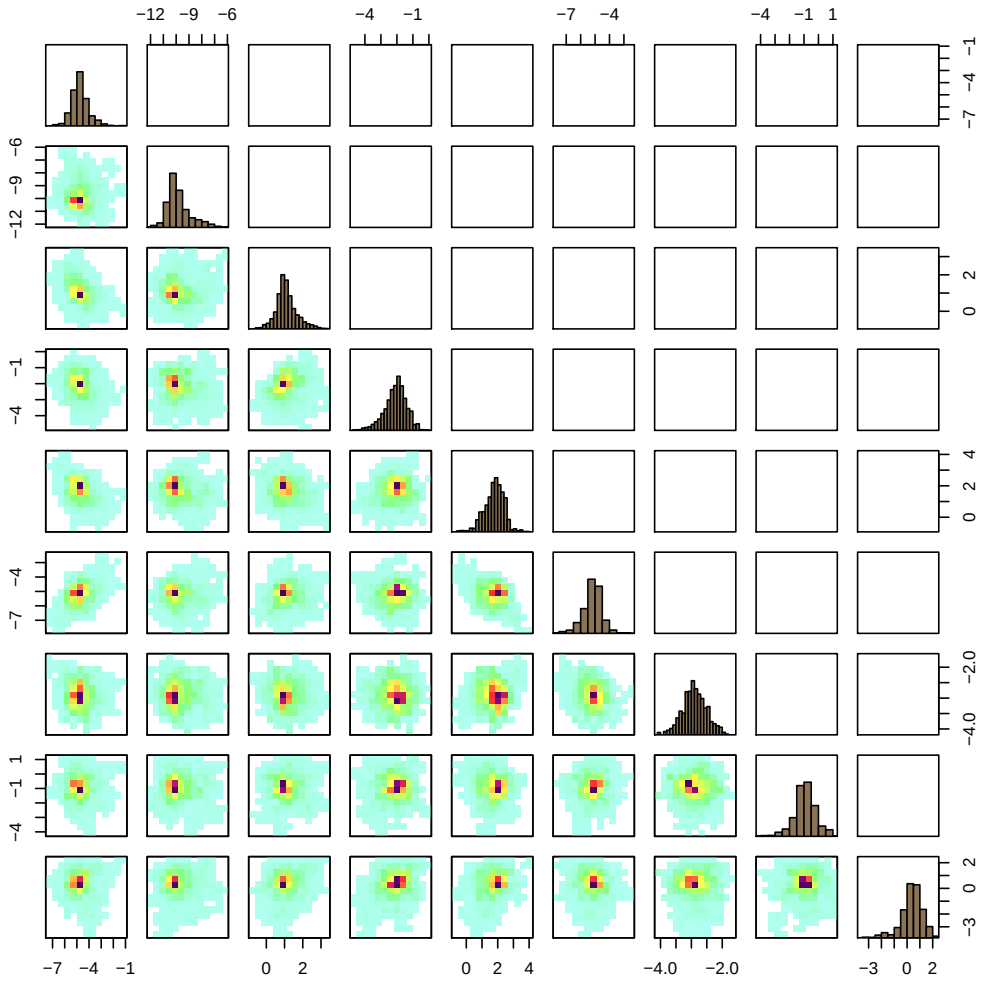

Figure 3.19: Posteriors (diagonals) for $\phi(i)$, $i = 1, 2, \ldots, 9$ and joint posteriors in the lower panel. The rainfall event is on 24th September 2016 from 12:54 to 16:48 hours in Melbourne.

Figure 3.20 shows that posteriors for original parameters, which are obtained from exponentials as follows:

$$
\begin{aligned}
\lambda &= \exp\Big(\frac{\phi(1)+\phi(2)}{2}\Big) \\
\gamma^{-1} &= \exp\Big(\frac{\phi(1)-\phi(2)}{2}\Big) \\
\beta &= \exp\Big(\frac{\phi(3)+\phi(4)}{2}\Big) \\
\eta^{-1} &= \exp\Big(\frac{\phi(3)-\phi(4)}{2}\Big) \\
\mu_x &= \exp\Big(\frac{\phi(5)+\phi(6)}{2}\Big) \\
\mu_A &= \exp\Big(\frac{\phi(5)-\phi(6)}{2}\Big) \\
\alpha_2 &= \exp(\phi(7)) \\
\xi_m &= \exp(\phi(8)) \\
\xi_{cv} &= \exp(\phi(9))
\end{aligned}
$$

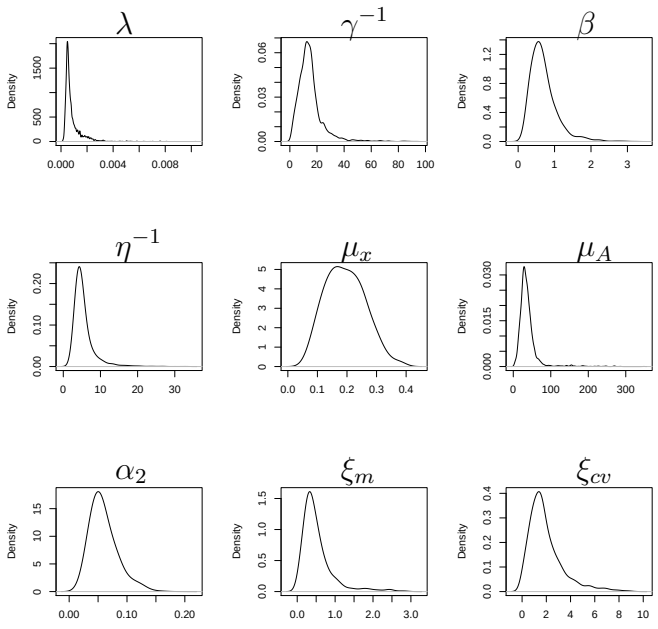

Figure 3.20: Posteriors for parameters λ , $\gamma^{-1}, \beta,\ \eta^{-1}, \mu_x, \mu_A,\ \alpha_2,\ \xi_m,\ \xi_{cv}$. The rainfall event is on 24th September 2016 from 12:54 to 16:48 hours in Melbourne.

Table 3.2 shows posterior means, medians, and 95 % credible intervals. We can see some credible intervals are wide, particularly mean storm duration γ^{-1}, mean cell duration η^{-1}, and mean cell area μ_A. This may be because of the parameters dependency as discussed above. However, the estimates look plausible. For example mean storm duration is greater than mean cell duration.

Parameter	Mean	Median	95 % Credible Interval
λ	0.0008	0.0006	(0.0003, 0.0026)
γ^{-1}	14.816	13.233	(2.9086, 38.585)
β	0.6968	0.6201	(0.2321, 1.7451)
η^{-1}	5.3733	4.6462	(2.6768, 13.180)
μ_x	0.1946	0.1917	(0.0792, 0.3332)
μ_A	37.299	32.677	(11.839, 93.733)
α_2	0.0595	0.0548	(0.0255, 0.1211)
ξ_m	0.5199	0.4006	(0.0738, 1.8749)
ξ_{cv}	1.9438	1.5953	(0.1467, 6.0694)

Table 3.2: Estimated posterior means, medians and credible intervals. Fitted the C-I-N model to the rainfall event on 24th September 2016 from 12:54 to 16:48 hours in Melbourne..

3.10.2 Diagnostics

In this section, we present Monte-Carlo 95% predictive intervals to check model fit. For this we generate data simulated under the model using sampled posteriors, and show how the simulated data looks comparison with observed data.

The outputs of ABC-MCMC Algorithm 3 are ergodic samples from the posteriors for $\phi(i), i = 1, ..., 9$. We have about 100 thousand posterior parameter sets. It is time consuming and unrealistic to simulate data from all of them, so we take a sub-sample of size 500, and for each member of the sub-sample we simulate data from the C-I-N model. The sub-sample is selected using sampling weights assigned using the Epanechnikov kernel as described in Section 2.3.2. Each member of the posterior sample has an associated distance to the observed data, and its sampling weight is $K_\epsilon(\cdot)$, where K_ϵ is given by

$$K_\epsilon(x) = \begin{cases} (1 - (\frac{x}{\epsilon})^2); & |x| \leq \epsilon; \\ \\ 0 & |x| > \epsilon. \end{cases}$$

where ϵ is the threshold distance.

To demonstrate model fit, we present Monte-Carlo predictive 95% intervals in Figures 3.21, 3.22, 3.23, and 3.24. Almost all observed summary statistics are within the intervals.

Figure 3.21 shows the 95% intervals for the mean rainfall, standard deviation of rainfall and dry probability in the first row (a), (b), and (c) respectively for spatial aggregation from 1×1 km^2 to 6×6 km^2 pixels. The mean rainfall, standard deviation of rainfall, and dry probability are in the second row (d), (e), and (f) respectively for temporal aggregation, 6-minute, 12 minute and 18-minute and 24-minute of $1 \times 1km^2$ pixels. The mean, standard deviation, and dry probability are in the last row (g), (h), and (i) respectively for temporal aggregation, 6-minute, 12 minute and 18-minute and 24-minute of $2 \times 2km^2$ pixels.

Figure 3.22 shows the 95% Monte-Carlo predictive intervals for the spatial autocorrelation lags (-1,-1,0), (0,-1,0), and (-1,0,0) in the first row (a), (b), and (c) respectively for spatial aggregation, 1×1 km^2 to 6×6 km^2 pixels. The spatial autocorrelation lags (-1,-1,0), (0,-1,0), and (-1,0,0) are in the second row (d), (e), and (f) respectively for temporal aggregation, 6-minute, 12 minute and 18-minute and 24-minute of $1 \times 1km^2$ pixels. The spatial autocorrelation lags (-1,-1,0), (0,-1,0), and (-1,0,0) are the last row (g), (h), and (i) respectively for temporal aggregation, 6-minute, 12 minute and 18-minute and 24-minute of $2 \times 2km^2$ pixels .

Figures 3.23 shows the 95% Monte-Carlo predictive intervals for the spatial autocorrelation lags $(1 + v_x, 1 + v_y, 1), ((0 + v_x, 1 + v_y, 1)$, and $(1 + v_x, 0 + v_y, 1)$ in the first row (a), (b), and (c) respectively for spatial aggregation, 1×1 km^2 to 6×6 km^2 pixels. The spatial autocorrelation lags $(1+v_x, 1+v_y, 1), ((0+v_x, 1+v_y, 1)$, and $(1+v_x, 0+v_y, 1)$ are in the second row (d), (e), and (f) respectively for temporal aggregation, 6-minute, 12 minute and 18-minute and 24-minute of 1×1 km^2 pixels. The spatial autocorrelation lags $(1 + v_x, 1 + v_y, 1), ((0 + v_x, 1 + v_y, 1)$, and $(1 + v_x, 0 + v_y, 1)$ are in the last row (g), (h), and (i) respectively for temporal aggregation, 6-minute, 12 minute and 18-minute and 24-minute of 2×2 km^2 pixels.

Figure 3.24 shows the 95% Monte-Carlo predictive intervals for the summary statistics: dry/wet area ratio, mean wet area over time, and standard deviation of wet area over time for different spatial aggregation. Plots $(a), (b)$, and (c) are for spatial aggregation $l \times l$ km^2 pixel, $l = 1, 2, 3, 4, 6$. Plots $(d), (e)$, and (f) are for spatial autocorrelations for temporal aggregation of 1×1 km^2 pixel. Plots $(g), (h)$, and (i) are for spatial autocorrelations for temporal aggregation of 2×2 km^2 pixel.

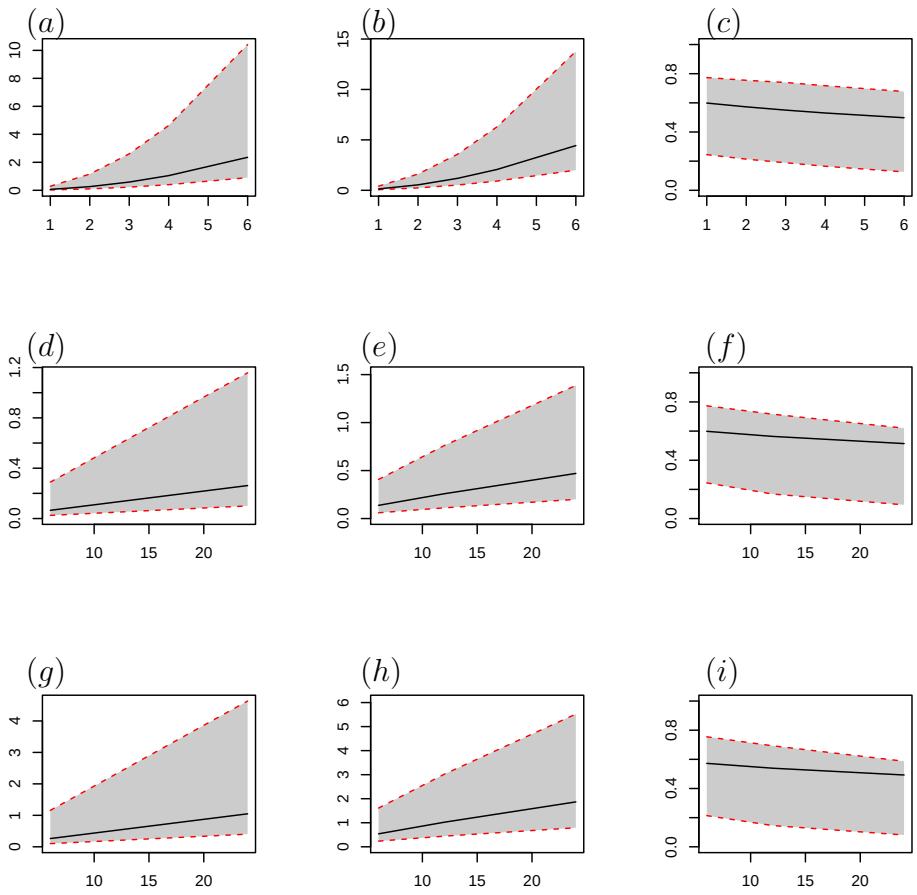

Figure 3.21: 95 % Monte-Carlo predictive intervals. Plots (a), (b), and (c) are of means, standard deviations, and dry probabilities respectively. X-axis is spatial aggregation of $l \times l$ km^2, $l = 1, 2, 3, 4, 6$. Plots (d), (e), and (f) are of means, standard deviations, and dry probabilities against time 6, 12, 18, and 24 minutes for 1×1 km^2 pixels. Plots (g), (h), and (i) are of means, standard deviations, and dry probabilities against time 6, 12, 18, and 24 minutes for 2×2 km^2 pixels. The rainfall event is on 24th September 2016 from 12:54 to 16:48 hours in Melbourne.

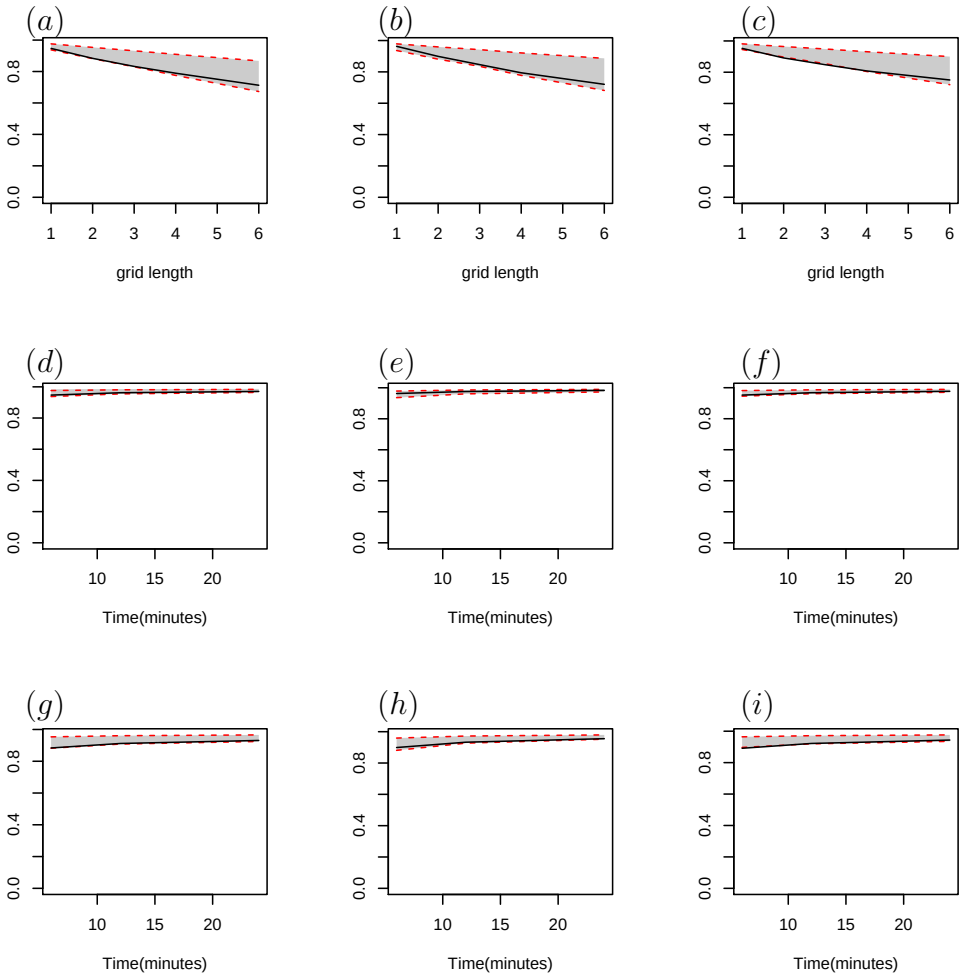

Figure 3.22: 95 % Monte-Carlo predictive intervals. Plots $(a), (b)$, and (c) are $\rho(-1,-1,0))$, $\rho(0,-1,0))$, and $\rho(-1,0,0))$. X-axis is spatial aggregation $l \times l$ km^2 pixel, $l = 1, 2, 3, 4, 6$. Plots $(d), (e)$, and (f) are $\rho(-1,-1,0)$, $\rho(0,-1,0))$, and $\rho(-1,0,0)$. X-axis is temporal aggregation at 6, 12, 18, and 24 minutes for 1×1 km^2 pixels. Plots $(g), (h)$, and (i) are $\rho(-1,-1,0)$, $\rho(0,-1,0))$, and $\rho(-1,0,0)$ for 2×2 km^2 pixels. The rainfall event is on 24th September 2016 from 12:54 to 16:48 hours in Melbourne.

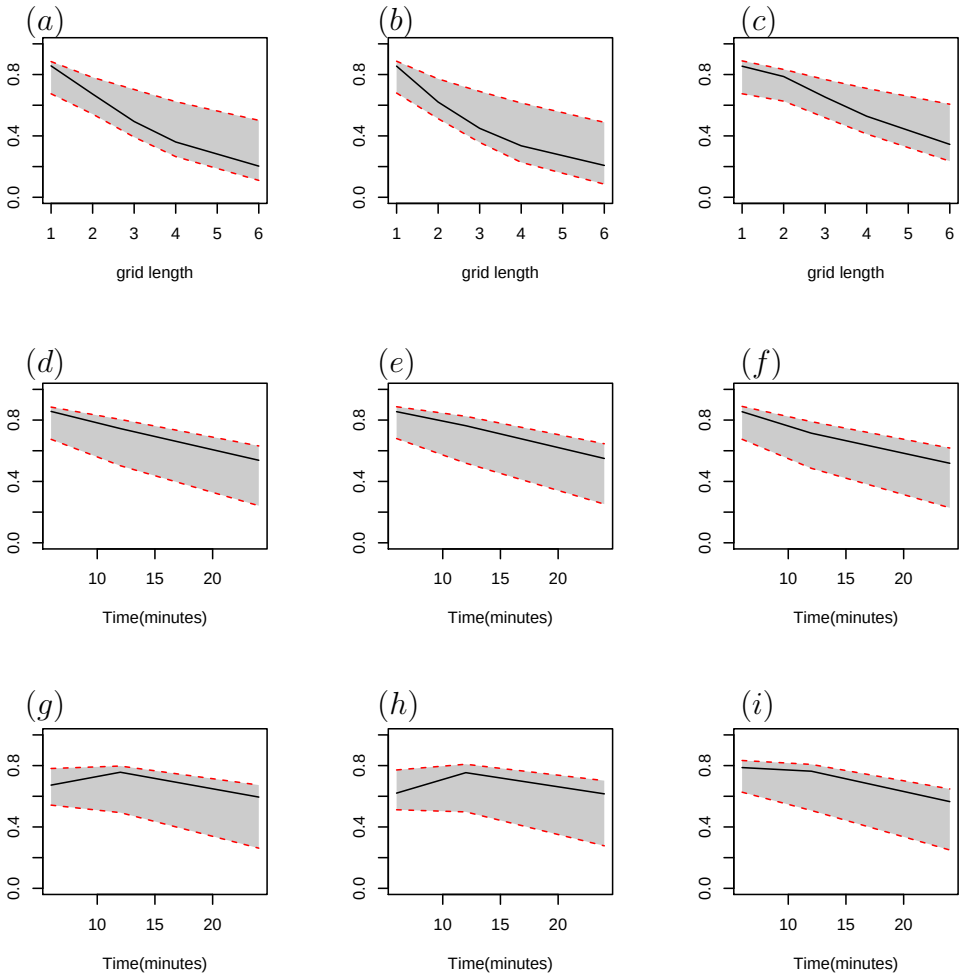

Figure 3.23: 95 % Monte-Carlo predictive intervals. Plots $(a), (b)$, and (c) are $\rho(1 + v_x, 1 + v_y, 1))$, $\rho(0 + v_x, 1 + v_y, 1))$, and $\rho(1 + v_x, 0 + v_y, 1))$. X-axis is spatial aggregation $l \times l$ km^2 pixel, $l = 1, 2, 3, 4, 6$. Plots $(d), (e)$, and (f) are $\rho(1 + v_x, 1 + v_y, 1))$, $\rho(0 + v_x, 1 + v_y, 1))$, and $\rho(1 + v_x, 0 + v_y, 1))$ for 1×1 km^2 pixels. X-axis is temporal aggregation at 6, 12, 18, and 24 minutes. Plots $(g), (h)$, and (i) are $\rho(1 + v_x, 1 + v_y, 1))$, $\rho(0 + v_x, 1 + v_y, 1))$, and $\rho(1 + v_x, 0 + v_y, 1))$. for 2×2 km^2 pixels. The rainfall event is on 24th September 2016 from 12:54 to 16:48 hours in Melbourne.

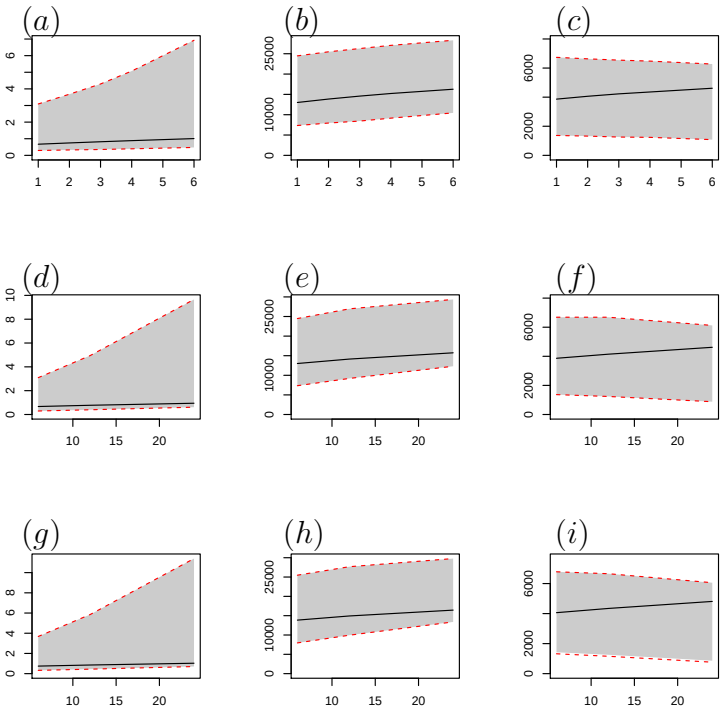

Figure 3.24: 95 % Monte-Carlo predictive intervals. Plots $(a), (b)$, and (c) are dry/wet area ratio, mean wet area, and stand deviation of wet area over time. X-axis is spatial aggregation $l \times l$ km^2 pixel, $l = 1, 2, 3, 4, 6$. Plots $(d), (e)$, and (f) are dry/wet area ratio, mean wet area, and stand deviation of wet area over time. X-axis is temporal aggregation at 6, 12, 18, and 24 minutes for 1×1 km^2 pixels. Plots $(g), (h)$, and (i) are dry/wet area ratio, mean wet area, and stand deviation of wet area over time for 2×2 km^2 pixels. The rainfall event is on 24th September 2016 from 12:54 to 16:48 hours in Melbourne.

3.10.3 Simulation

Figures 3.25, 3.26, 3.27, and 3.28 are contour plots of a simulation. In observed data contour plots Figures 3.9, 3.10, 3.11, and 3.12, we can see high intensity in the centre of rainfall area and it gradually reduces to the edge. This is not seen in the simulation, so this issue is addressed in our new model (ECST model) by defining a intensity spread function in space.

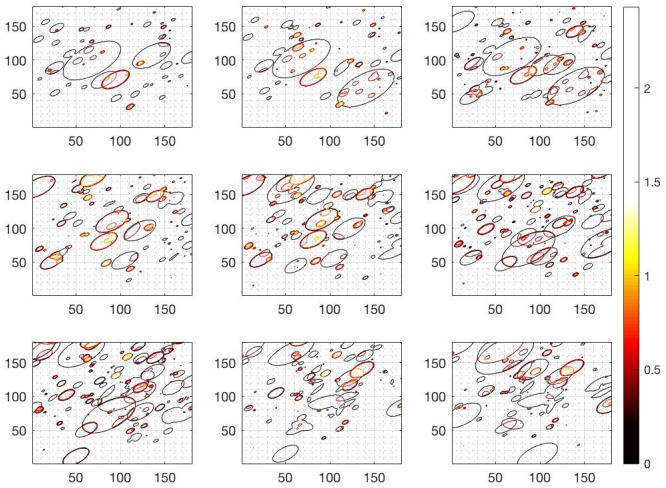

Figure 3.25: Contour plots of simulated data from the C-I-N model using fitted posterior points to the rainfall event. Zero rainfall is white. The time step is 6-minutes.

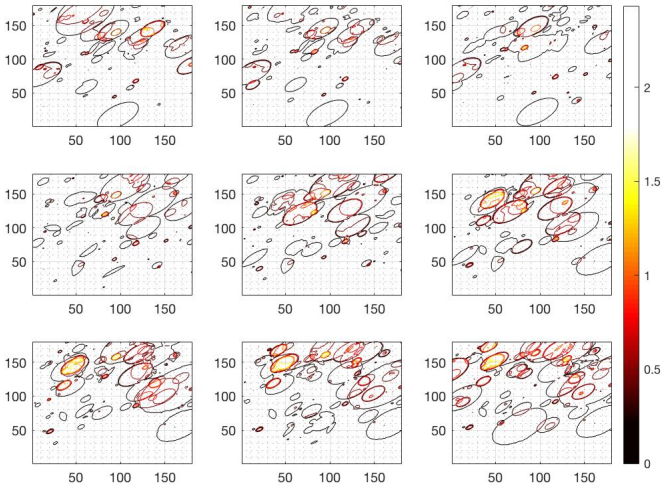

Figure 3.26: Contour plots of simulated data from the C-I-N model using fitted posterior points to the rainfall event. Zero rainfall is white. The time step is 6-minutes.

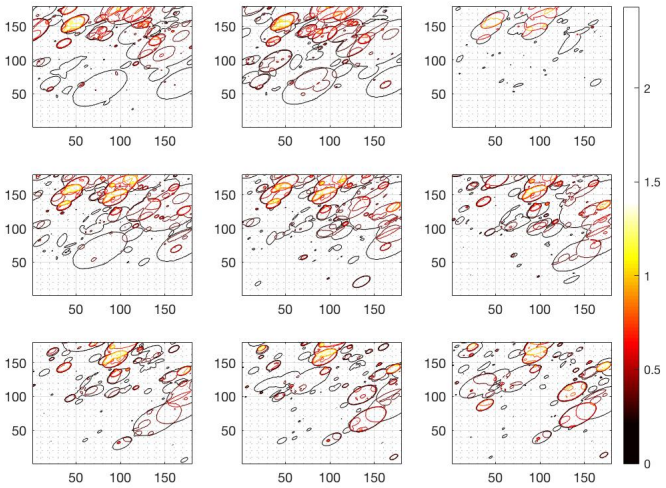

Figure 3.27: Contour plots of simulated data from the C-I-N model using fitted posterior points to the rainfall event. Zero rainfall is white.

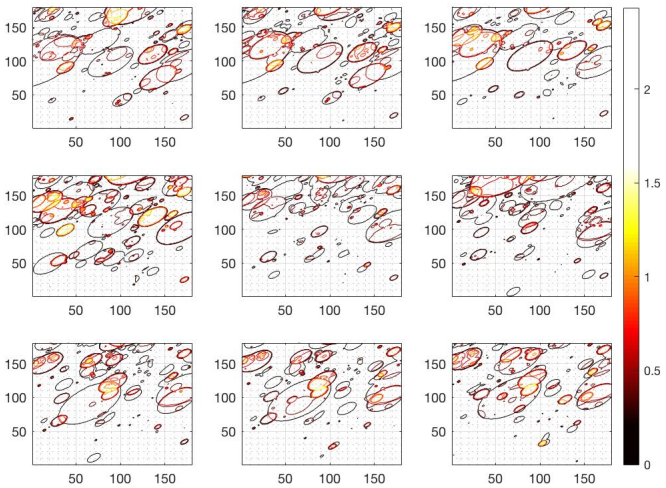

Figure 3.28: Contour plots of simulated data from the C-I-N model using fitted posterior points to the rainfall event. Zero rainfall is white.

3.11 Fitting the ECST Model

3.11.1 Random Eccentricity

We allow eccentricity of cell to be random in the ECST model. We assume that eccentricity of storm and mean eccentricity of cells are the same. We estimate the mean eccentricity of cells using the spatial autocorrelation function, and then use as it a fixed value in ABC fitting like the C-I-N model fitting. The mean eccentricity is fixed, however each rain cell has distinct eccentricity. We assume cell eccentricity follows Truncated Normal distribution from zero to one with mean μ_e and variance σ_e^2.

The variance is estimated using time series of snap shot of radar data. For instance, if we have 4 hours for every 6-minute time steps, then we have spatial data for 40 time points. We then have 40 estimated values for 40 time points using the spatial autocorrelation function. We finally take variance of these estimations. We experience that there is very small variance than what we see in the observed data. This could be we use same cells over time for whole region. Apparently what we see in different part of the study region that cells have distinct shape in terms of eccentricity. We divide the study region into four equal parts, then estimate eccentricity for each part at one time point. Finally we have 4×40 estimation of μ_e, the variance of these estimation is taken as the variance of the eccentricity. One could divide the study reason into 9 parts and repeat the same process, which depends up on how big region is.

We evaluate $\Theta = 39^o$, $\mu_e = 0.86$, and $\sigma_e = 0.2$. Similarly, we estimate the velocity $\mathbf{v} = (0.10, 29.9)km$ per hour as discussed in § 3.9.1. Once again we keep these parameters as fixed as the same way like the C-I-N model fitting.

3.11.2 Applying ABC-MCMC to the ECST model

Prior Distributions and Reparameterisation

Similarly the C-I-N model, we reparameterise the parameters of the ECST model and choose following new parameters: $\lambda \times \gamma^{-1}$, $\lambda \times \gamma$, $\beta \times \eta^{-1}$, $\beta \times \eta$, $\mu_x \times \mu_A$ and $\mu_x \times \mu_A^{-1}$.

Instead of estimating both α_1 and α_2, we estimate α_2 only, because α_1 is

obtained given μ_A, α_2 , and μ_e by

$$\alpha_1 = \frac{1}{2}\Big(-1 + \sqrt{1 + \frac{4\mu_A\alpha_2^2}{\pi\sqrt{1-\mu_e^2}}} \ \Big)$$

We assume that storms are elliptical in space. The cell centres are displaced from storms centres using independently drawn distances from bivariate normal distribution with mean zero and covariance matrix

$$\Sigma = \begin{pmatrix} \sigma_x^2 & \rho\ \sigma_x\sigma_y \\ \rho\ \sigma_x\sigma_y & \sigma_y^2 \end{pmatrix}.$$

We consider that all storm have same ρ, but they have different scale of the major-semi axis lengths. Let's assume σ is standard deviation cells displacement along with the major semi-axis of storm. So the covariance matrix can be written as

$$\Sigma = \sigma^2 \begin{pmatrix} \frac{\sigma_x^2}{\sigma^2} & \rho\ \frac{\sigma_x\sigma_y}{\sigma^2} \\ \rho\ \frac{\sigma_x\sigma_y}{\sigma^2} & \frac{\sigma_y^2}{\sigma^2} \end{pmatrix}.$$

Assume σ^2 is random. Results distinct storm has distinct size, which can be defined using some distribution on σ^2. We therefore assume the precision $\frac{1}{\sigma^2}$ for semi-major axis of storm follows gamma distribution with shape and scale parameters.

As the C-I-N model, we use mean (ξ_m) and coefficient of variance (ξ_{cv}) instead of shape and scale parameters for gamma distribution. If $\frac{1}{\sigma^2} \sim$ gamma(ξ_1, ξ_2), then $\xi_m = \xi_1\xi_2$ and $\xi_{cv} = \frac{1}{\sqrt{\xi_1}}$. Then our eight-th and nine-th parameters are ξ_m and ξ_{cv}. These 9 parameters are chosen after log-transformation, because log-transformation maps parameter domain $\mathbb{R}_+$ to whole line $\mathbb{R}$. Beside these parameters, we have five additional parameters

μ_e, σ_e, Θ, v_x, and v_y. Thus our new 14 parameters are

$$\begin{aligned}
\phi(1) &= \log(\lambda\gamma^{-1}) \\
\phi(2) &= \log(\lambda\gamma) \\
\phi(3) &= \log(\beta\eta^{-1}) \\
\phi(4) &= \log(\beta\eta) \\
\phi(5) &= \log(\mu_x\mu_A) \\
\phi(6) &= \log(\mu_x\mu_A^{-1}) \\
\phi(7) &= \log(\alpha_2) \\
\phi(8) &= \log(\xi_m) \\
\phi(9) &= \log(\xi_{cv}) \\
\phi(10) &= \mu_e \\
\phi(11) &= \Theta \\
\phi(12) &= \sigma_e \\
\phi(13) &= v_x \\
\phi(14) &= v_y
\end{aligned}$$

Initially normal priors were used for all the $\phi(i); i = 1, 2, ..., 9$; that is $\pi(\boldsymbol{\phi}(i)) \sim N(\mathbf{0}, \sigma^2\mathbf{I})$ for σ^2 large. However, we experienced that this produced some extreme posterior points for original parameters see Figure 2 in Appendix . To avoid these extreme values we choose the following truncations, for $\phi(7)$ truncated normal $(-\infty, \log(3)]$, for $\phi(8)$ truncated normal $(-\infty, \log(6)]$, and for $\phi(9)$ truncated normal $(-\infty, \log(10)]$ with mean zero and variance as before.

Proposal Distribution and Summary Measure

We estimate 5 parameters e, Θ, v_x, v_y, and σ_e from given observed data set using the empirical spatial autocorrelation function. We then supply these to the ABC-MCMC step. We estimate nine posteriors for $\phi(i), i = 1, ..., 9$.

As for any MCMC procedure, the proposal chain needs to be chosen so that it mixes well and explores the whole parameter space. We use a random walk with $N(\mathbf{0}, \sigma^2\mathbf{I})$ increments.

For the distance measure d, we choose weighted Euclidean distance:

$$d(S(D^*), S(D)) = \Big[\sum_i w_i \ (S^*(i) - S(i))^2 \Big]^{\frac{1}{2}}$$

where $S^*(i)$ and $S(i)$ are respectively the i-th component of $S(D^*)$ and $S(D)$. The weights w_i are inversely proportional to variance of $i\text{-}th$ summary statistics using a sample generated from $f(.|\hat{\boldsymbol{\phi}})$, where $\hat{\boldsymbol{\phi}}$ is a preliminary estimate of $\boldsymbol{\phi}$ [37]. This gives equal importance to each components of S.

Posterior Distribution

Trace plots are used to verify that the chains are mixing nicely in Figure 3.29. Acceptance rate for proposal is 5%. Figures 3.30 and 3.32 give the estimated posterior densities for $\phi(i)$ and the original (untransformed) parameters. The diagonals are marginal densities and the off-diagonals pairwise densities see in Figure 3.31.

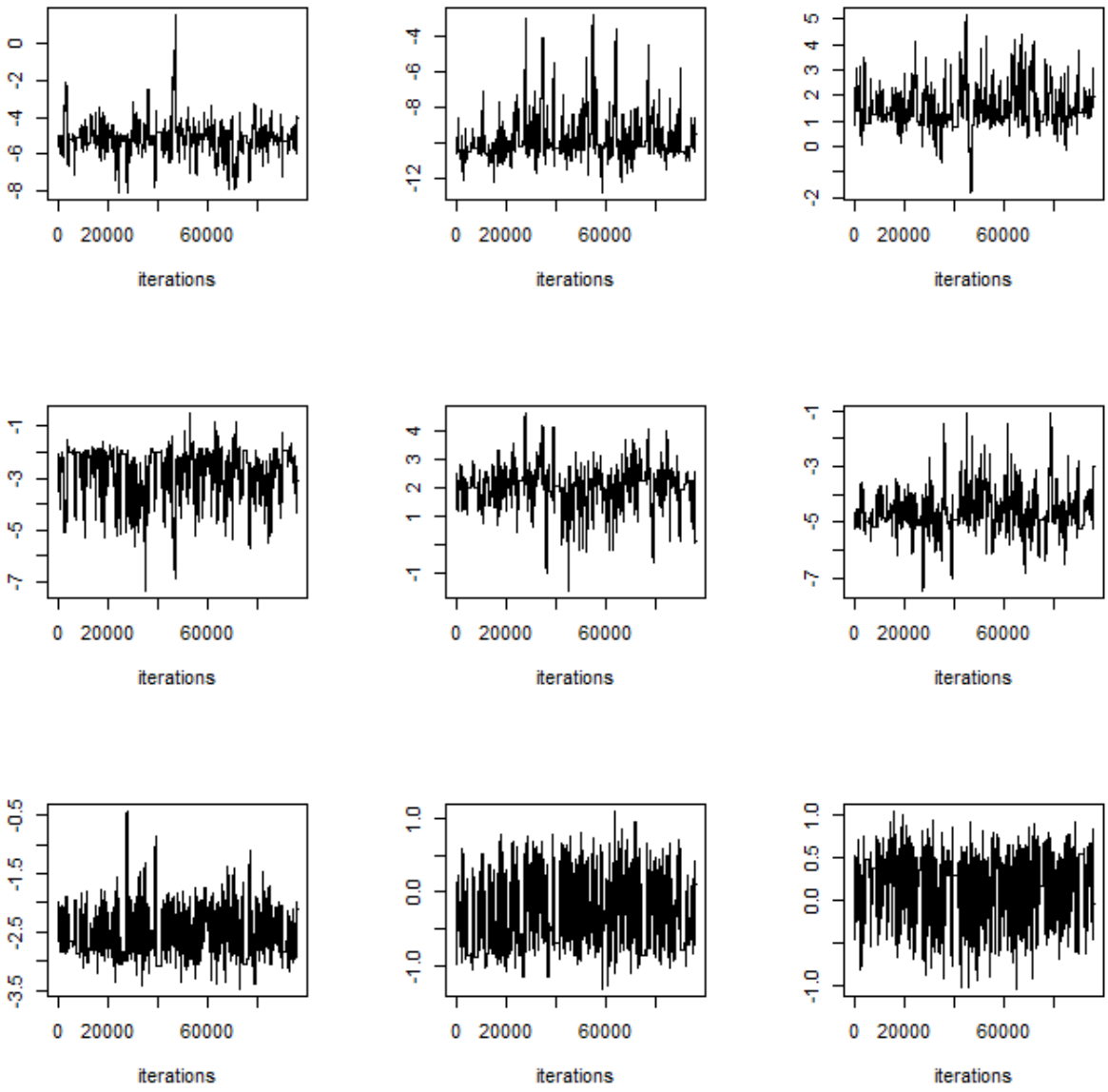

Figure 3.29: Chains for $\phi(i)$,$i = 1, 2, \ldots, 9$ (from top left to right). The rainfall event is rainfall on 24th September 2016 from12:54 to 16:48 hours in Melbourne.

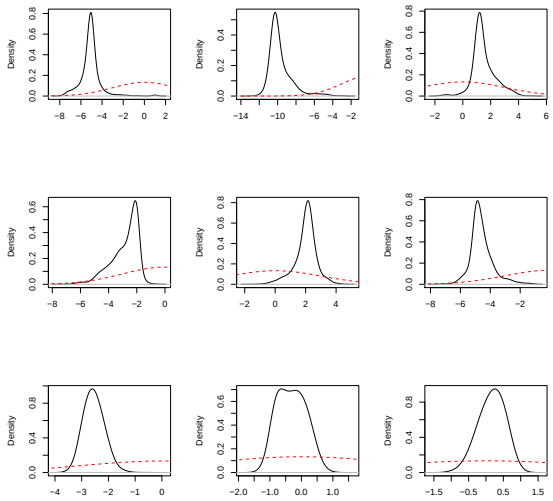

Figure 3.30: Posteriors for $\phi(i)$,$i = 1, 2, \ldots, 9$ (from top left to right). Red dotted curves are priors. The rainfall event is rainfall on 24th September 2016 from 12:54 to 16:48 hours in Melbourne.

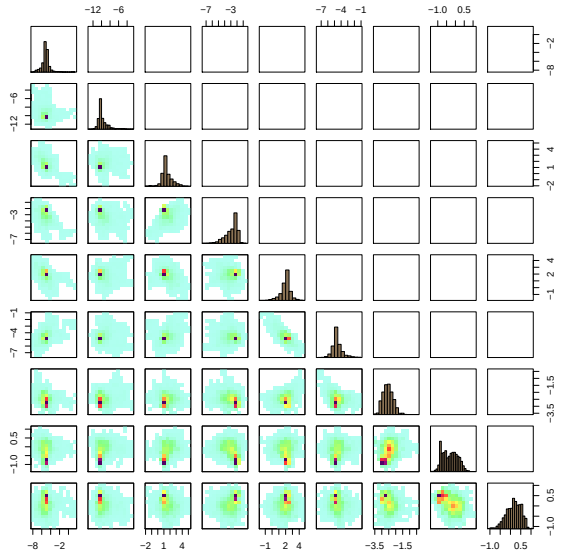

Figure 3.31: Posteriors (diagonals) for $\phi(i)$, $i = 1, 2, \ldots, 9$ and lower panel plots are joint posteriors . The rainfall event is rainfall on 24th September 2016 from 12:54 to 16:48 hours in Melbourne.

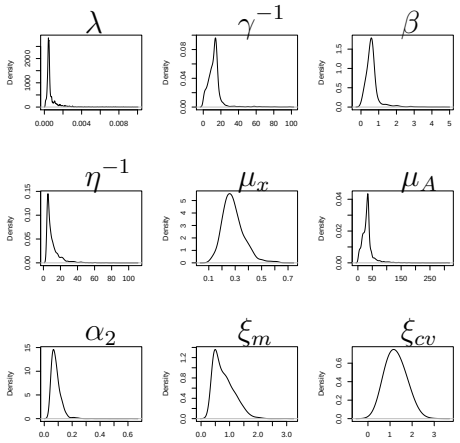

Figure 3.32: Posteriors for parameters $\lambda\ , \gamma^{-1}, \beta,\ \eta^{-1}, \mu_x, \mu_A,\ \alpha_2,\ \xi_m,\ \xi_{cv}$. The rainfall event is rainfall on 24th September 2016 from 12:54 to 16:48 hours in Melbourne.

Table 3.3 shows posterior means, medians and 95 % credible intervals for original parameters $\lambda\ , \gamma^{-1}, \beta,\ \eta^{-1}, \mu_x, \mu_A,\ \alpha_2,\ \xi_m,\ \xi_{cv}$.

Parameters	Mean	Median	95 % Credible Interval
λ	0.0008	0.0005	(0.0002, 0.0036)
γ^{-1}	12.734	12.391	(1.0938, 38.497)
β	0.6166	0.5722	(0.1171, 1.8787)
η^{-1}	10.788	7.6700	(4.0369, 35.960)
μ_x	0.2850	0.2731	(0.1508, 0.4848)
μ_A	33.002	31.541	(4.6533, 92.161)
α_2	0.0840	0.0771	(0.0441, 0.1617)
ξ_m	0.8022	0.7224	(0.3761, 1.6064)
ξ_{cv}	1.2535	1.2105	(0.5601, 2.1132)

Table 3.3: Estimated average values for parameters of the ECST Model and their credible intervals, fitted to the rainfall event on 24th September 2016 from 12:54 to 16:48 hours in Melbourne.

3.11.3 Diagnostics

To demonstrate model fit, we present Monte-Carlo 95% predictive interval for temporal and spatial aggregation summary statistics in this section.

Figures 3.33, 3.34, 3.35, and 3.36 show 95% Monte-Carlo predictive intervals for summaries with different spatial and temporal aggregations. These

Figures show improvement than those in Figures 3.21, 3.22, 3.23, and 3.24 in §3.10.2.

Figures 3.33 shows 95% Monte-Carlo predictive intervals for mean, standard deviation, and dry probability in the plots (a), (b), and (c) respectively for 1×1 km^2 to 6×6 km^2 pixels. Mean, standard deviation, and dry probability are in (d), (e), and (f) respectively for temporal aggregation, 6-minute, 12 minute and 18-minute and 24-minute of $1 \times 1 km^2$ pixels. Similarly mean, standard deviation, and dry probability are in the last row (g), (h), and (i) respectively for temporal aggregation, 6-minute, 12 minute and 18-minute and 24-minute of $2 \times 2 km^2$ pixels.

Figure 3.34, shows 95% Monte-Carlo predictive intervals for spatial autocorrelation at lags (-1,-1,0), (0,-1,0), and (-1,0,0) in (a), (b), and (c) respectively for spatial aggregation 1×1 km^2 to 6×6 km^2 pixels. Spatial autocorrelation at lags (-1,-1,0), (0,-1,0), and (-1,0,0) are in (d), (e), and (f) respectively for temporal aggregation, 6-minute, 12 minute and 18-minute and 24-minute of 1×1 km^2 pixels. Similarly spatial autocorrelation at lags (-1,-1,0), (0,-1,0), and (-1,0,0) are in (g), (h), and (i) respectively for temporal aggregation, 6-minute, 12 minute and 18-minute and 24-minute of $2 \times 2 km^2$ pixels.

Figure 3.35 shows 95% Monte-Carlo predictive intervals for spatial autocorrelation at lags $(1 + v_x, 1 + v_y, 1), ((0 + v_x, 1 + v_y, 1)$, and $(1 + v_x, 0 + v_y, 1)$ in the (a), (b), and (c) respectively for spatial aggregations $l \times l$ pixels. $l = 1, 2, ..., 6$. Spatial autocorrelation at lags $(1 + v_x, 1 + v_y, 1), ((0 + v_x, 1 + v_y, 1)$, and $(1 + v_x, 0 + v_y, 1)$ are in (d), (e), and (f) respectively for temporal aggregation, 6-minute, 12 minute and 18-minute and 24-minute of 1×1 km^2 pixels. Similarly summary statistics- spatial autocorrelation at lags $(1 + v_x, 1 + v_y, 1), ((0 + v_x, 1 + v_y, 1)$, and $(1 + v_x, 0 + v_y, 1)$ are in the last row (g), (h), and (i) respectively for temporal aggregation, 6-minute, 12 minute and 18-minute and 24-minute of 2×2 km^2 pixels.

Figure 3.36 shows 95% Monte-Carlo predictive intervals for dry/wet area ratio, mean wet area, and stand deviation of wet area over time in plots $(a), (b)$, and (c). X-axis is spatial aggregation $l \times l$ km^2 pixel, $l = 1, 2, 3, 4, 6$. Plots $(d), (e)$, and (f) are dry/wet area ratio, mean wet area, and stand deviation of wet area over time for 1×1 km^2 pixels. Plots $(g), (h)$, and (i) are dry/wet area ratio, mean wet area, and stand deviation of wet area over time for 2×2 km^2 pixels.

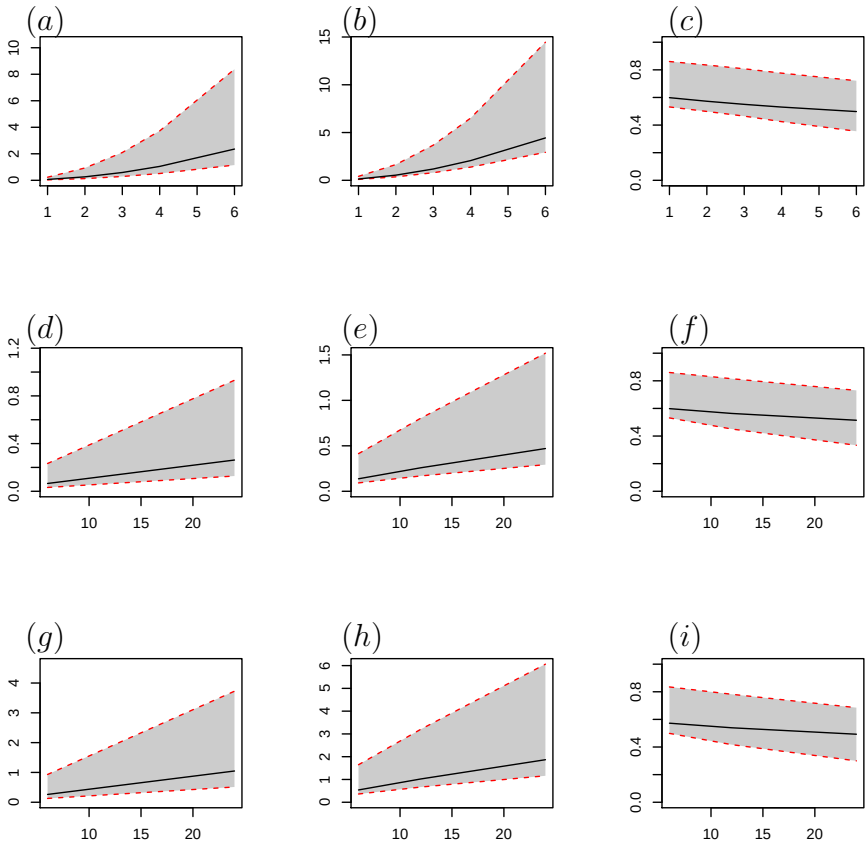

Figure 3.33: 95 % Monte-Carlo predictive intervals. Plots (a), (b), and (c) are of means, standard deviations, and dry probabilities respectively. X-axis is spatial aggregation of $l \times l$ km^2, $l = 1, 2, 3, 4, 6$. Plots (d), (e), and (f) are of means, standard deviations, and dry probabilities against time 6, 12, 18, and 24 minutes for 1×1 km^2 pixel. Plots (g), (h), and (i) are of means, standard deviations, and dry probabilities against time 6, 12, 18, and 24 minutes for 2×2 km^2 pixel. The rainfall event is on 24th September 2016 from 12:54 to 16:48 hours in Melbourne.

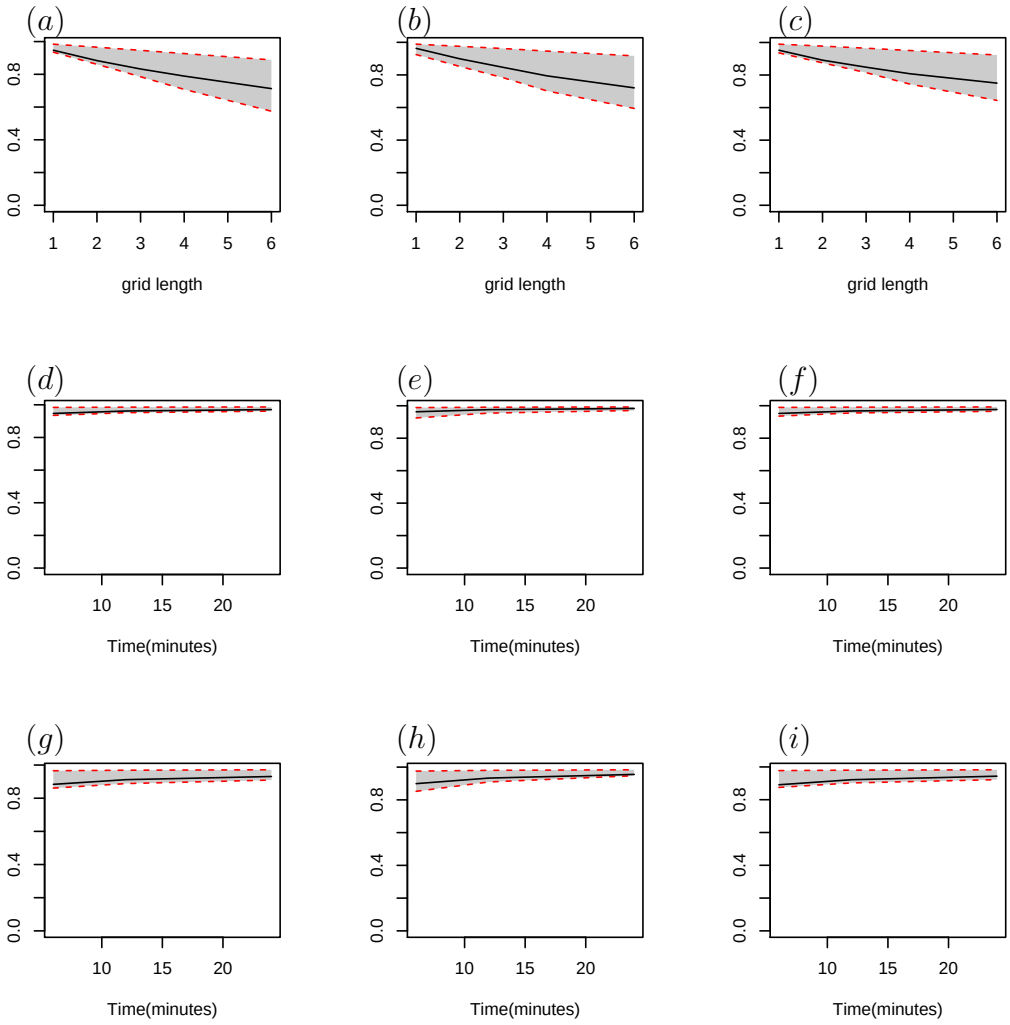

Figure 3.34: 95 % Monte-Carlo predictive intervals. Plots $(a), (b)$, and (c) are $\rho(-1,-1,0))$, $\rho(0,-1,0))$, and $\rho(-1,0,0))$. X-axis is spatial aggregation $l \times l$ km^2 pixel, $l = 1, 2, 3, 4, 6$. Plots $(d), (e)$, and (f) are $\rho(-1,-1,0)$, $\rho(0,-1,0))$, and $\rho(-1,0,0)$. X-axis is temporal aggregation at 6, 12, 18, and 24 minutes for 1×1 km^2 pixel. Plots $(g), (h)$, and (i) are $\rho(-1,-1,0)$, $\rho(0,-1,0))$, and $\rho(-1,0,0)$. X-axis is temporal aggregation at 6, 12, 18, and 24 minutes for 2×2 km^2 pixels.. The rainfall event is on 24th September 2016 from 12:54 to 16:48 hours in Melbourne.

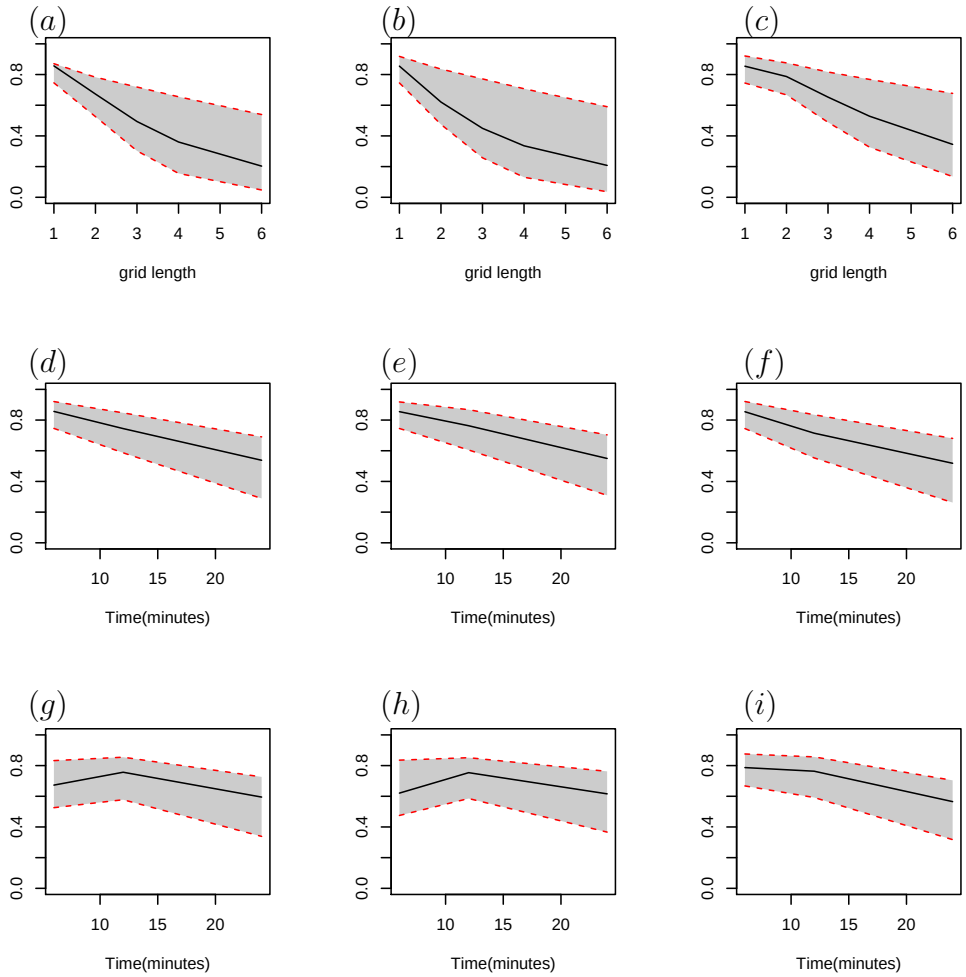

Figure 3.35: 95 % Monte-Carlo predictive intervals. Plots $(a), (b)$, and (c) are $\rho(1 + v_x, 1 + v_y, 1))$, $\rho(0 + v_x, 1 + v_y, 1))$, and $\rho(1 + v_x, 0 + v_y, 1))$. X-axis is spatial aggregation $l \times l$ km^2 pixel, $l = 1, 2, 3, 4, 6$. Plots $(d), (e)$, and (f) are $\rho(1+v_x, 1+v_y, 1))$, $\rho(0+v_x, 1+v_y, 1))$, and $\rho(1+v_x, 0+v_y, 1))$ 1×1 km^2 pixels. . X-axis is temporal aggregation at 6, 12, 18, and 24 minutes. Plots $(g), (h)$, and (i) are $\rho(1+v_x, 1+v_y, 1))$, $\rho(0+v_x, 1+v_y, 1))$, and $\rho(1+v_x, 0+v_y, 1))$ for 2×2 km^2 pixels. The rainfall event is on 24th September 2016 from 12:54 to 16:48 hours in Melbourne.

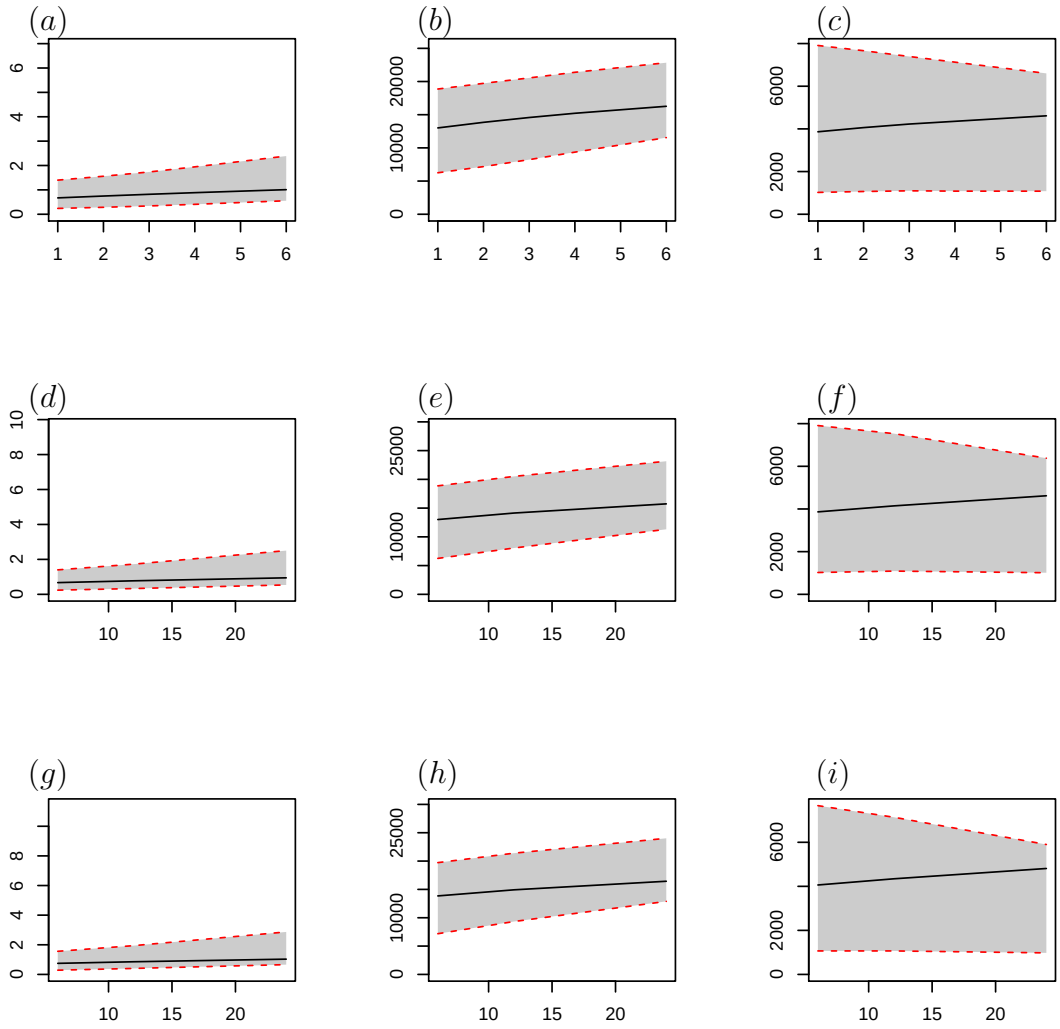

Figure 3.36: 95 % Monte-Carlo predictive intervals. Plots $(a), (b)$, and (c) are dry/wet area ratio, mean wet area, and stand deviation of wet area over time. X-axis is spatial aggregation $l \times l$ km^2 pixel, $l = 1, 2, 3, 4, 6$. Plots $(d), (e)$, and (f) are dry/wet area ratio, mean wet area, and stand deviation of wet area over time for 1×1 km^2 pixels. X-axis is temporal aggregation at 6, 12, 18, and 24 minutes. . Plots $(g), (h)$, and (i) are dry/wet area ratio, mean wet area, and stand deviation of wet area over time. X-axis is temporal aggregation at 6, 12, 18, and 24 minutes for 2×2 km^2 pixels. The rainfall event is on 24th September 2016 from 12:54 to 16:48 hours in Melbourne.

3.11.4 Simulation

We can see contour plots of a simulation from the ECST model in Figures 3.37 3.38, 3.39 & 3.40. These contour plots show better match than contour plots of data generated by the C-I-N model in Figures 3.25, 3.26, 3.27, and 3.28, particularly, higher intensities at centre of the cells.

The ECST mode is generating the rainfall similar to the observed rainfall as having high intensity at centre and rainfall decreases continuously with distance from the centre to the edge.

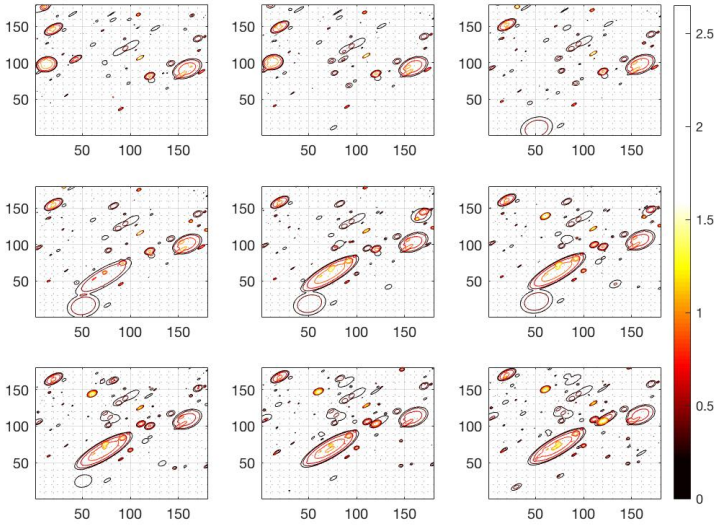

Figure 3.37: Contour plots of simulated data from the ECST model using fitted posterior points to the rainfall event. Zero rainfall is white. The time step is 6-minutes.

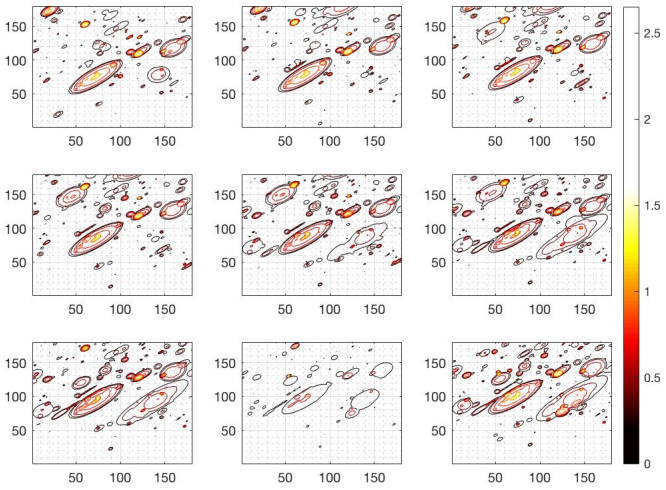

Figure 3.38: Contour plots of simulated data from ECST model using fitted posterior points to the rainfall event. Zero rainfall is white. The time step is 6-minutes.

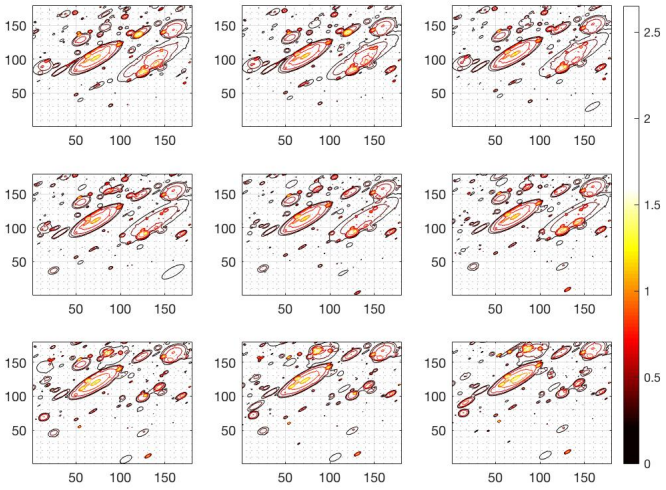

Figure 3.39: Contour plots of simulated data from ECST model using fitted posterior points to the rainfall event. Zero rainfall is white.

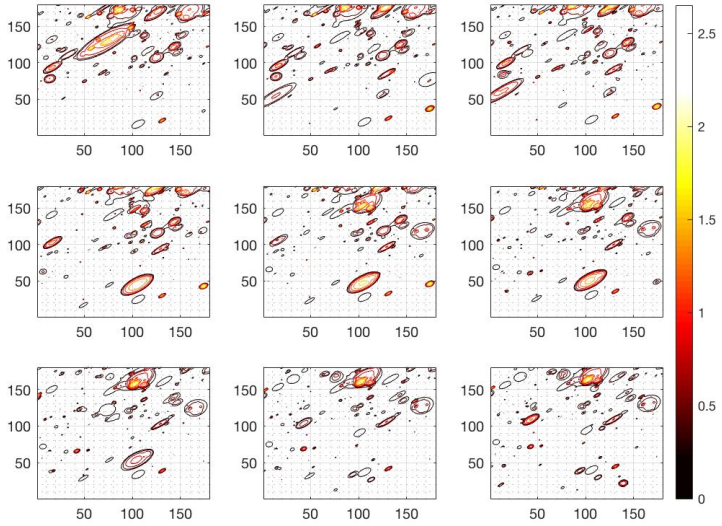

Figure 3.40: Contour plots of simulated data from ECST model using fitted posterior points to the rainfall event.Zero rainfall is white.

3.11.5 Comparison of the C-I-N Model and the ECST Model

In Figure 3.41, plot (b) is a contour plot of simulated data from the C-I-N model and plot (c) is a contour plot of simulated data from the ECST model. Plot (c) seems a better match to observed data in plot (a). As we see in observed data, typically the centre of rain cells has high intensity, which gradually decreases with distance from the centre. The ECST model is doing better job of capturing this behaviour.

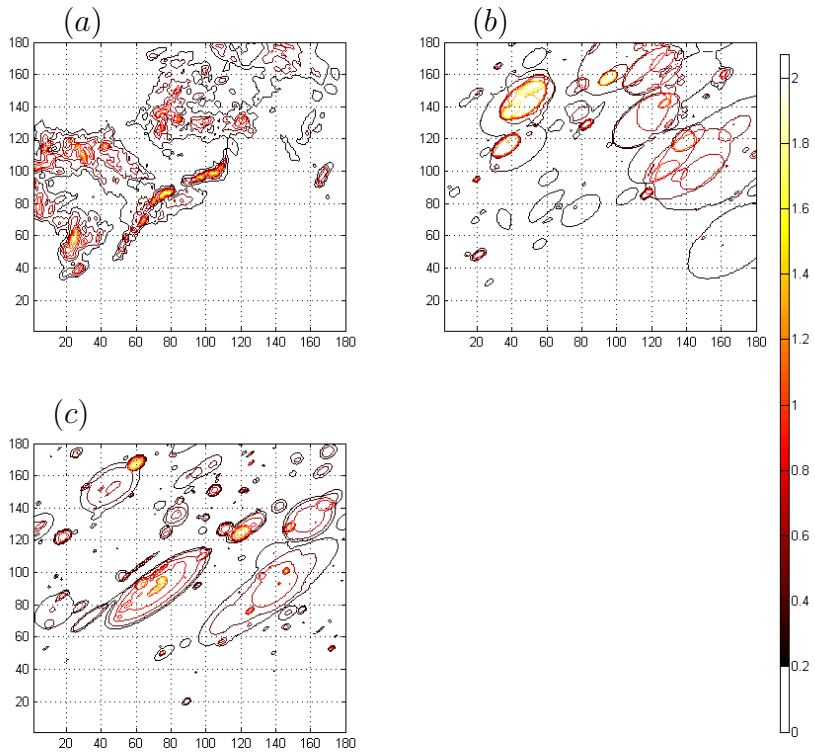

Figure 3.41: Contour plots for a single time-point fitted using ABC. a) Calibrated rainfall radar data, courtesy of the Australian Bureau of Meteorology b) simulated from the C-I-N model fitted using ABC, and c) simulated from the ECST model.

3.11.6 Mean Squared Errors

Mean errors and mean squared errors for simulated data summary statistics from both C-I-N and ECST models are shown in Table 3.4. We can see that the ECST model has less mean error and mean squared error for most of summary statistics. The smaller mean squared error means the ECST model is doing better fitting than the C-I-N model.

Summaries	Observed	Mean Error		Mean Squared Error	
		C-I-N	ECST	C-I-N	ECST
Mean (mm per pixel)	0.065	0.033	0.008	0.006	0.001
Standard deviation	0.137	0.042	0.034	0.009	0.004
Correlation lags:					
$(-1,-1,0)$	0.947	0.012	0.015	0.000	0.000
$(-1,0,0)$	0.952	0.013	0.011	0.000	0.000
$(-1,1,0)$	0.898	0.021	0.014	0.001	0.001
$(0,-1,0)$	0.963	-0.003	-0.006	0.000	0.000
$(0,1,0)$	0.963	-0.003	-0.006	0.000	0.000
$(1,-1,0)$	0.898	0.021	0.014	0.001	0.001
$(1,0,0)$	0.952	0.013	0.011	0.000	0.000
$(1,1,0)$	0.947	0.012	0.015	0.000	0.000
$(-1+v_x,-1+v_y,1)$	0.846	-0.046	-0.013	0.005	0.002
$(-1+v_x,0+v_y,1)$	0.842	-0.043	-0.013	0.005	0.002
$(-1+v_x,1+v_y,1)$	0.806	-0.039	-0.017	0.004	0.002
$(0+v_x,-1+v_y,1)$	0.854	-0.054	-0.025	0.006	0.003
$(0+v_x,0+v_y,1)$	0.873	-0.048	-0.015	0.005	0.002
$(0+v_x,1+v_x,1)$	0.855	-0.057	-0.028	0.006	0.002
$(1+v_x,-1+v_y,1)$	0.821	-0.055	-0.031	0.006	0.003
$(1+v_x,0+v_y,1)$	0.854	-0.058	-0.028	0.006	0.003
$(1+v_x,1+v_x,1)$	0.856	-0.062	-0.029	0.007	0.002
$\mathbb{P}(Y^{(l)}=0)$	0.599	-0.012	0.079	0.017	0.011
Dry wet ratio	0.671	0.168	-0.176	0.048	0.061
Mean wet area (km^2)	13007	387	-2548	17371693	11925866
SD of wet area	3864	-618	-1396	2292835	2980240

Table 3.4: Observed summary statistics, mean error, and mean squared error fitted to the rainfall event on 24th September 2016 from 12:54 to 16:48 hours in Melbourne.

3.11.7 Posterior Predictive Probability

We fitted two models to the same rainfall event as discussed §3.10 and §3.11. We then checked model fits in §3.10.2 and §3.11.3 using 95 % predictive intervals. In this section, we want to compare performance of these models. Particularly we are interested in simulation processes, generated under which model, look similar to the observed process. Gelman et al., 2013 [19] suggest posterior predictive p-values to evaluate the model fit by comparing the observed data to the posterior predictive distribution using simulations. We

follow this approach here.

The posterior predictive p-value is defined as the probability that the generated data could be similar to the observed data, as measured from some distance function d as follows:

$$p = \mathbb{P}(d(S(D^*), S(D)) < c \mid D^*), \quad \text{for some given constant } c > 0.$$

We sample from posteriors using weights with replacement. The weights are calculated using the Epanechnikov kernel function as descussed in §3.10.2. We simulate the data from sampled posterior points. We then calculate summary statistics. Finally, we obtain distance between simulated data summary statistics and corresponding observed summary statistics.

Suppose $S(D^*)$ and $S(D)$ are the simulated data and observed data summarry statistics respectively. The distance for individual summary is defined by

$$d_j(S(D^*), S(D) = \|S_j(D^*) - S_j(D))\|, \text{where } S_j \text{ denote } j\text{-th summary.}$$

We need to rescale the summary distance because some summary distance is very small as correlations and some summary distances are very high like mean wet area over time. The following weight is used as normalizing constants :

$$w_j = \frac{1}{\sqrt{\text{var}(S_j(D^*) - S_j(D))}}$$

The total distance of all summaries is estimated by

$$d(S(D^*), S(D) = \sum w_j \|S_j(D^*) - S_j(D)\|, \text{where } j = 1, 2, 3, ..., k.$$

We estimate posterior predictive p-value using following steps. We first sample ϕ_i from posteriors. We obtain the simulation data using ϕ_i from the model. The distance between the observed and simulation is estimated using distance measure function. We generate N simulations from different posterior samples. Finally we estimate the predictive p-value, which is equivalent to $\frac{1}{N}\#\{i : d(S(D^*), S(D)) < c\}$ for some given constant $c > 0$.

Figures 3.42 and 3.43 show that posterior predictive probability for summary statistics. Predictive probabilities for statistics from the ECST model are higher than that from the C-I-N model. Particularly predictive probabilities for mean, standard deviation (see in Figure 3.42, (a) and (b)), and

9 velocity adjusted spatial autocorrelations ($\rho(l_x + v_x l_t,\ l_y + v_y l_t,\ l_t)$, where $l_x = \{-1, 0, 1\}$, $l_y = \{-1, 0, 1\}$ and $l_t = \{1\}$) see in Figure 3.42 (k) & (l), and Figure 3.43 (a) to (g), are higher for the ECST model than that of the C-I-N model.

Predictive probabilities for dry probability for an arbitrary pixel, dry/wet ratio, and mean wet area over time (in Figure 3.43 (h), (i), and (j)) have no preferable between two models. This is reasonable because both model have the same structure for these properties.

Predictive probabilities for spatial correlations at lag -1 and 1 among x-axis and y-axis, especially $\rho(-1, -1, 0), \rho(0, -1, 0), \rho(0, 1, 0)$, and $\rho(1, 1, 0)$ are better for the C-I-N model see in Figure 3.42 $(c), (f), (g)$, and (j), particulrly, velocity unadjusted spatial autocorrelations statistics. In the C-I-N model, the intensity at centre of ellipse and other area are the same, but the ECST model intensity at one grid to very next grid is different. So correlation velocity unadjusted at lag 1 among x-axis and y-axis for the ECST model may have less than that for the C-I-N model.

Predictive probability of the total distance for summary statistics from the ECST mode is better than that from the C-I-N model in Figure 3.43 (l). Similarly, for most of individual summary, except velocity unadjusted autocorrelations, the ECST model is doing better than the C-I-N model. This concludes that the ECST model has higher probability to produce the data closer to observe data in terms of summary statistics.

Note that Epanechnikov density is chosen to calculate weights using the total distance. The weights provide that the posterior points which produce simulated data closed to observe data, have higher probability than whose simulation has large difference between simulated and observed data summary statistics. We simulate data using the samples 500 posterior points, then estimate summary statistics. So we have 500 sample of each summary, then estimate predictive probability given distance (c). We plot predictive probability against c in Figures 3.42 and 3.43.

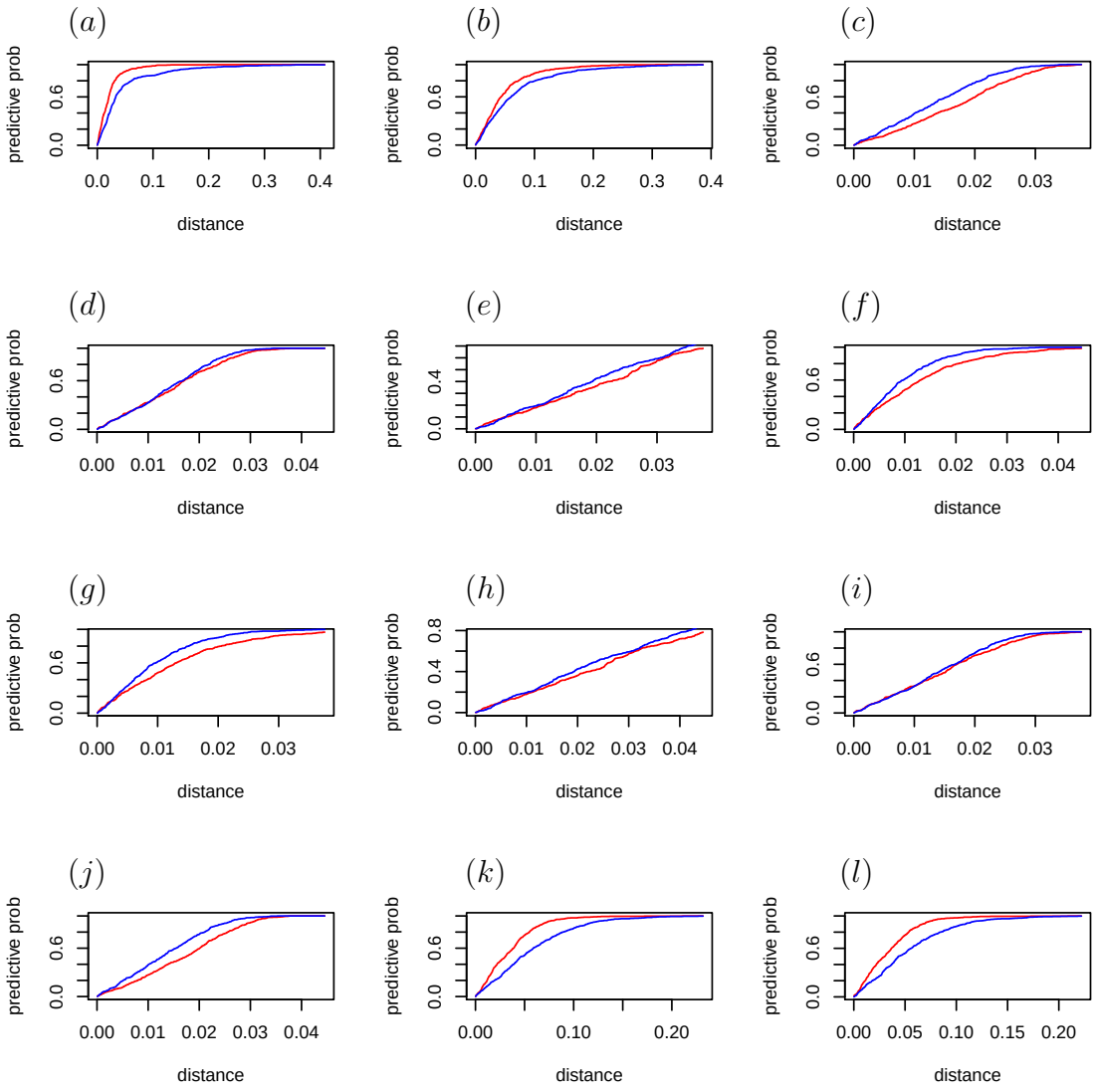

Figure 3.42: Predictive probability for the C-I-N model (blue line) and the ECST model (red line) fitting the rainfall event at 24th September 2016,12:54 to 16:48 in Melbourne. Plots (a) and (b) are for mean and standard deviation summaries. Plots (c) to (j) are spatial correlations $\rho(-1,-1,0), \rho(-1,0,0), \rho(1,1,0), \rho(0,-1,0), \rho(0,1,0), \rho(1,-1,0), \rho(1,0,0)$, and $\rho(1,1,0)$. And plots (k) and (l) are of $\rho(-1+v_x,-1+v_y,1)$, and $\rho(-1+v_x,0+v_y,1)$.

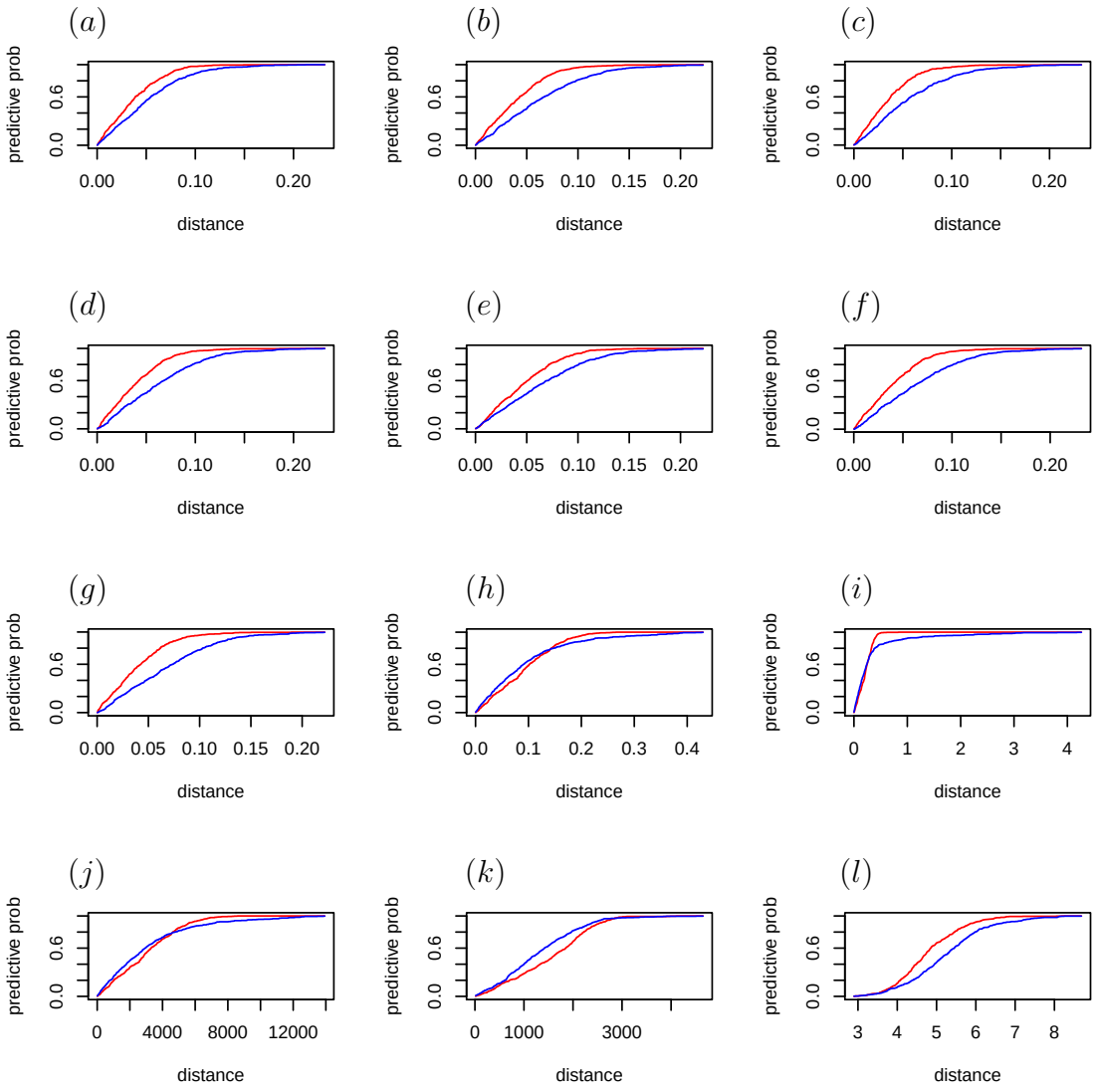

Figure 3.43: Predictive probability for the C-I-N model (blue line) and the ECST model (red line). Plots (a) to (g) are of spatial autocorrelations $\rho(-1+v_x, 1+v_y, 1), \rho(0+v_x, -1+v_y, 1), \rho(0+v_x, 0+v_y, 1), \rho(0+v_x, 1+v_y, 1), \rho(1, +v_x, -1+v_y, 1), \rho(1, +v_x, 0+v_y, 1)$, and $\rho(1, +v_x, 1+v_y, 1)$. Plots (h) and (i) are of dry probability of an arbitrary pixel and dry and wet area ratio. Plots (j) and (k) are of mean wet area over time and standard deviation of wet area over time. And plot (l) is of total distance form all summaries. The rainfall event is on 24th September 2016 from 12:54 to 16:48 hours in Melbourne.

3.12 Fitting the LNCST Model

We take the same approach for fitting the LNCST model to observed data as the ECST model. We first estimate orientation, eccentricity and velocity. We then use these as fixed values in the ABC-MCMC process. In previous section, we already estimated the velocity $\mathbf{v} = (0.10, 29.9)km$ per hour, $\mu_e = 0.86$, $\Theta = 39^o$, and $\sigma_e = 0.2$.

3.12.1 Applying ABC-MCMC to the LNCST Model

3.12.2 Prior Distribution and Reparameterization

The LNCST model has the same structure of storm arrival process and cell arrival and duration as the ECST model. However the cell intensity at cell centre and semi-major axis follow bivariate log-normal distributions i.e.

$$\begin{pmatrix} X \\ M_c \end{pmatrix} \sim \log N \left(\begin{pmatrix} \mu_x \\ \mu_{M_c} \end{pmatrix}, \begin{pmatrix} \sigma_X^2 & \rho_{xm_c}\sigma_X\sigma_{M_c} \\ \rho_{xm_c}\sigma_X\sigma_{M_c} & \sigma_{M_c}^2 \end{pmatrix} \right)$$

We then have five new parameters: mean intensity at centre μ_x & variance σ_X^2, mean semi-major axis μ_{m_c} & variance $\sigma_{m_c}^2$, and correlation between them ρ_{xm_c}.

The correlation ρ_{xm_c} has domain (-1, 1). We take transformation $\log\left(\frac{\rho_{xm_c}+1}{1-\rho_{xm_c}}\right)$, which maps domain (-1, 1) to $\mathbb{R}$.

The LNCST mode has the following 16 parameters:

$$
\begin{aligned}
\psi(1) &= \log(\lambda\gamma^{-1}) \\
\psi(2) &= \log(\lambda\gamma) \\
\psi(3) &= \log(\beta\eta^{-1}) \\
\psi(4) &= \log(\beta\eta) \\
\psi(5) &= \log(\mu_x) \\
\psi(6) &= \log(1/\sigma_X^2) \\
\psi(7) &= \log(\mu_{m_c}) \\
\psi(8) &= \log(1/\sigma_{m_c}^2) \\
\psi(9) &= \log\left(\frac{\rho_{xm_c}+1}{1-\rho_{xm_c}}\right) \\
\psi(10) &= \log(\xi_m) \\
\psi(11) &= \log(\xi_{cv}) \\
\psi(12) &= \mu_e \\
\psi(13) &= \Theta \\
\psi(14) &= \sigma_e \\
\psi(15) &= v_x \\
\psi(16) &= v_y
\end{aligned}
$$

Like before, normal priors are used for all the $\psi(i); i = 1, 2, ..., 9$. μ_e, Θ, σ_e v_x, and v_y are estimated using the spatial autocorrelation function. In the same way for C-I-N and ECST models, we chose the following priors for $\psi(10)$ truncated normal from $(-\infty, \log(6)]$ and for $\psi(11)$ truncated normal from $(-\infty, \log(10)]$.

3.12.3 Proposal Distribution and Distance Measure

We estimate 5 parameters μ_e, σ_e, Θ, v_x, and v_y from given observed data set using the spatial autocorrelation function. We then estimate eleven posterior distributions for first 11 parameters using ABC.

For the proposal chain we just use a random walk with $N(\mathbf{0}, 0.2^2\mathbf{I})$ increments.

For distance measure d, we choose weighted Euclidean distance:

$$d(S(D^*), S(D)) = \Big[\sum_i w_i \ (S^*(i) - S(i))^2 \Big]^{\frac{1}{2}}$$

where $S^*(i)$ and $S(i)$ are respectively the i-th component of $S(D^*)$ and $S(D)$. The weights w_i are inversely proportional to variance of $i\text{-}th$ summary statistics.

3.12.4 Posterior Distribution

We use the SMM to choose the initial parameter selection ψ_0. We can clearly see in the Figure 3.44 that there is a good mixing. Figure 3.45 displays estimated posterior densities of all 11 parameters, which looks good as we can see nice peak on density curves. However the density at Figure 3.45 and histogram at Figure 3.46 show bi-modality for the parameter $\psi(8)$. It is not clear at this point, why this parameter become harder to estimate. Further research is needed. Acceptance rate is around 11% with a threshold $\epsilon = 8$.

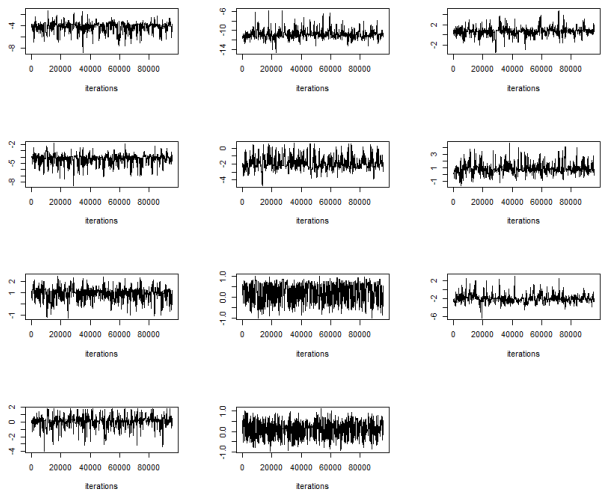

Figure 3.44: Chains for $\psi(i)$,$i = 1, 2, \ldots, 11$ (from top left to right) of the rainfall event on 24th September 2016 from 12:54 to 16:48 hours in Melbourne.

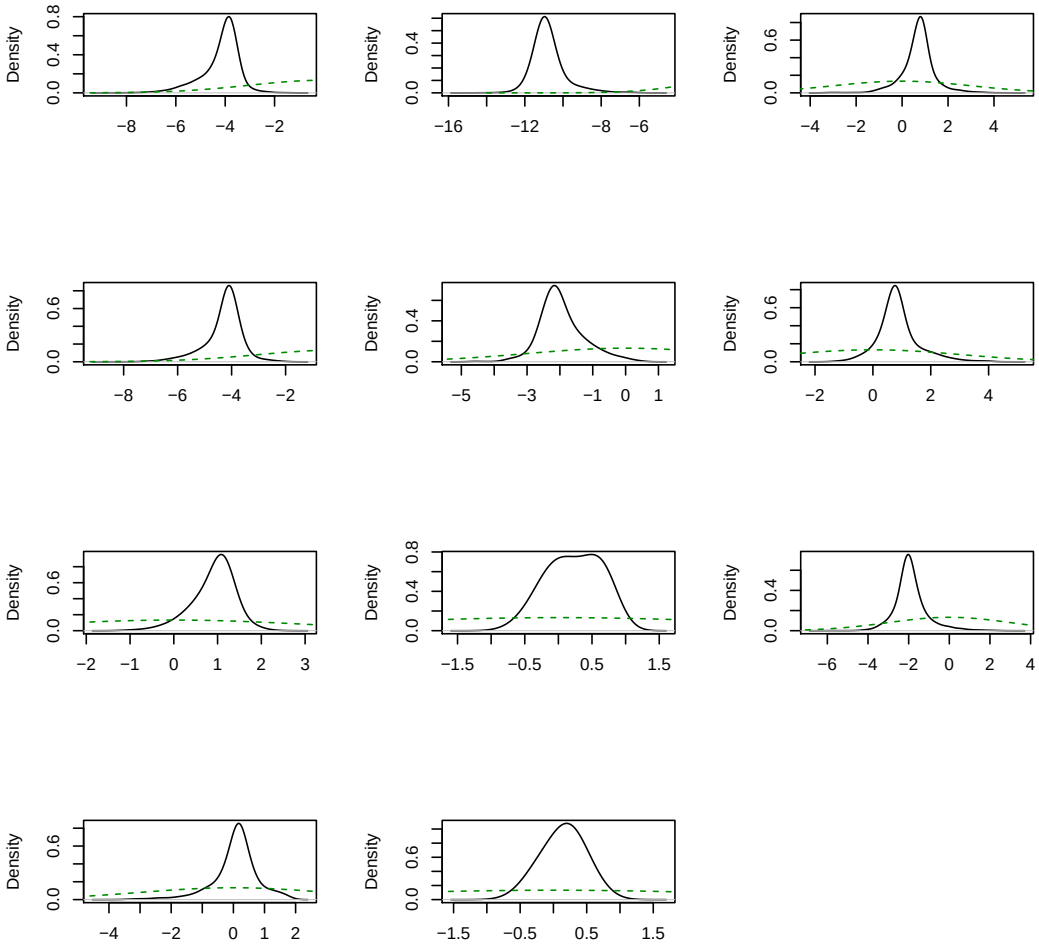

Figure 3.45: Posteriors for $\psi(i)$,$i = 1, 2, \ldots, 11$ (from top left to right) of the rainfall event on 24th September 2016 from 12:54 to 16:48 hours in Melbourne. Green curves are priors.

In Figure 3.46, the diagonal plots are histograms for parameters $\psi(i), i = 1, 2, 3, ..., 11$. The lower panels are pair distribution of horizontal and vertical parameters respectively. The colour label from light green to dark blue indicates the dense population of posterior points of pair distributions. As we expect there is high density of the points in particular region.

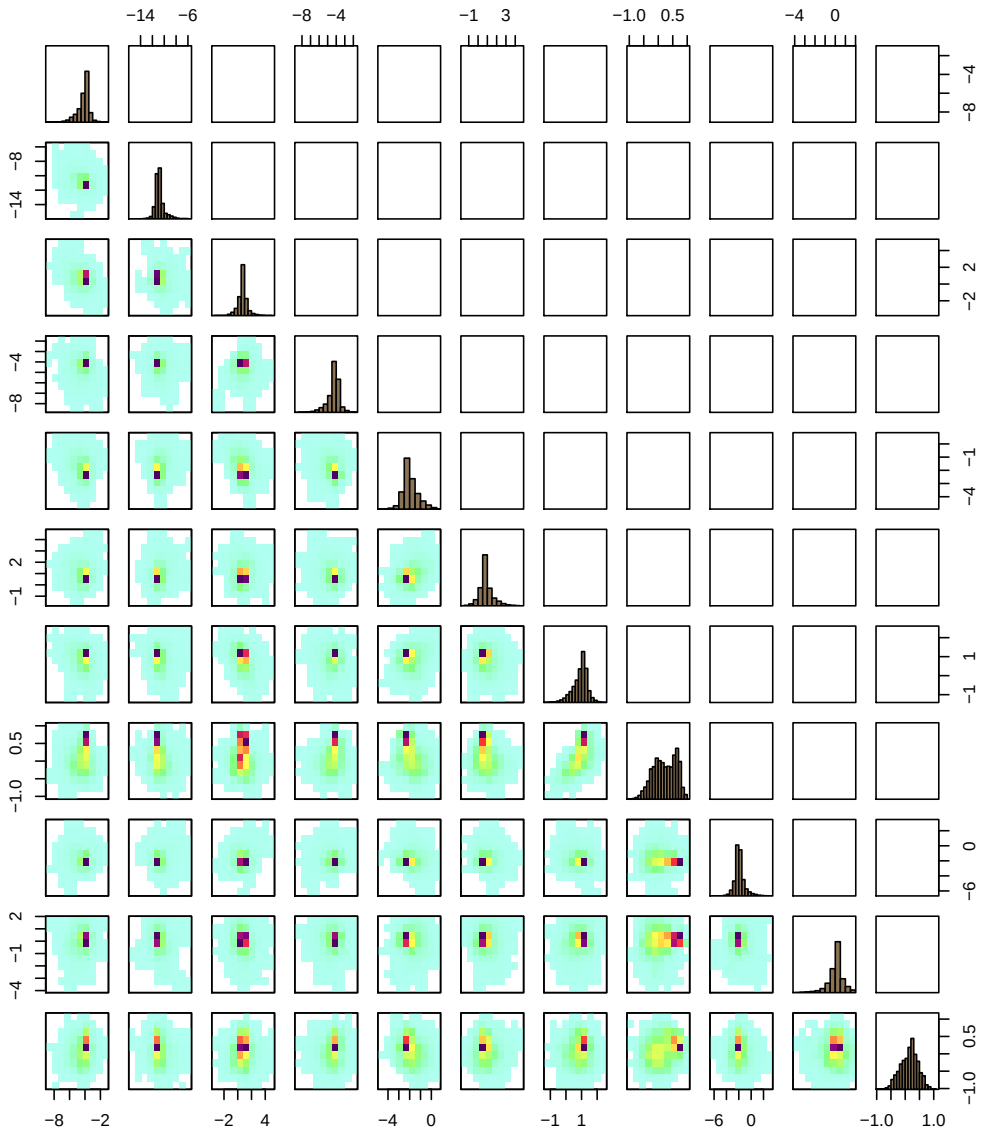

Figure 3.46: Posteriors (diagonals) and joint posteriors for $\psi(i)$, $i = 1, 2, \ldots, 11$ of the rainfall event on 24th September 2016 from 12:54 to 16:48 hours in Melbourne.

Figure 3.47 show that posteriors of original parameters, which are obtained back from exponentials:

$$\begin{aligned}
\lambda &= \exp\Big(\frac{\psi(1)+\psi(2)}{2}\Big) \\
\gamma^{-1} &= \exp\Big(\frac{\psi(1)-\psi(2)}{2}\Big) \\
\beta &= \exp\Big(\frac{\psi(3)+\psi(4)}{2}\Big) \\
\eta^{-1} &= \exp\Big(\frac{\psi(3)-\psi(4)}{2}\Big) \\
\mu_x &= \exp(\psi(5)) \\
\sigma_X^2 &= 1/\exp(\psi(6)) \\
\mu_{m_c} &= \exp(\psi(7)) \\
\sigma_{m_c}^2 &= 1/\exp(\psi(8)) \\
\rho_{xm_c} &= \frac{\exp(\psi(9))-1}{\exp(\psi(9))+1} \\
\xi_m &= \exp(\psi(10)) \\
\xi_{cv} &= \exp(\psi(11))
\end{aligned}$$

Table 3.5 gives posterior means, medians and 95 % credible intervals. We can see some credible intervals are wider than the C-I-N model and the ECST model, particularly mean storm duration γ^{-1}, mean cell duration η^{-1}. Because of this variability, this model may capture extremes for the rainfall events. This will be discussed in details in the §3.13.

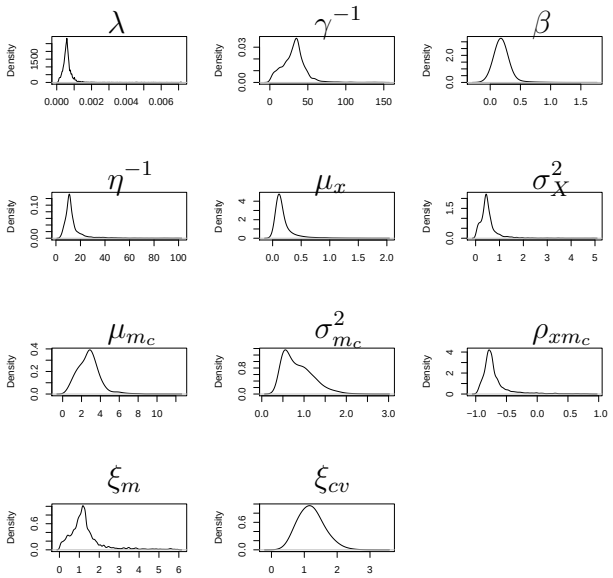

Figure 3.47: Posteriors for parameters $\lambda\,, \gamma^{-1}, \beta,\ \eta^{-1}, \mu_x,\ \sigma_X^2, \mu_{m_c}, \sigma_{m_c}^2, \rho_{xm_c},\ \xi_m,\ \xi_{cv}$ of the rainfall event on 24th September 2016 from 12:54 to 16:48 hours in Melbourne.

Parameters	Mean	Median	95% Credible Interval
λ	0.0006	0.0006	(0.0002, 0.00150
γ^{-1}	31.797	32.462	(4.4944, 64.524)
β	0.1887	0.1801	(0.0457, 0.4429)
η^{-1}	13.883	11.407	(5.6338, 42.133)
μ_x	0.1882	0.1258	(0.0426, 0.7603)
σ_X^2	0.5235	0.4519	(0.0671, 1.5503)
μ_{m_c}	2.7478	2.7523	(0.7829 , 5.6306)
$\sigma_{m_c}^2$	0.8602	0.7859	(0.4335, 1.7103)
ρ_{xm_c}	-0.6906	-0.7564	(-0.9327, 0.0996)
ξ_m	1.3331	1.1647	(0.1671, 4.3280)
ξ_{cv}	1.2102	1.1901	(0.6291, 1.9917)

Table 3.5: Estimated posterior means, medians and credible intervals for parameters. Fitted the ECST model to the rainfall event on 24th September 2016 from 12:54 to 16:48 hours in Melbourne.

3.12.5 Simulation

We can see contour plots of simulated rainfall from the LNCST model in Figures 3.48 3.49, 3.50 & 3.51. The time step is every 6- minute.

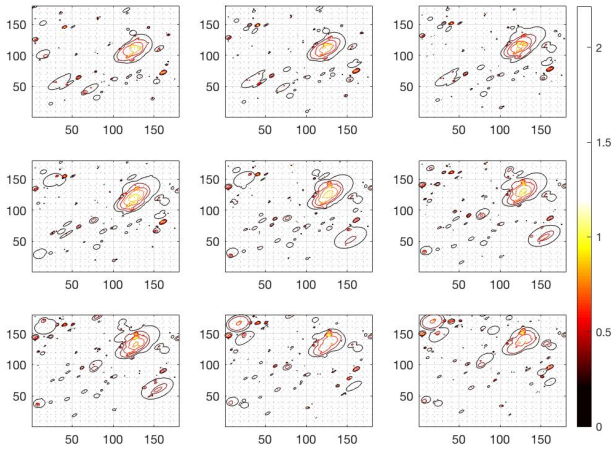

Figure 3.48: Contour plots of simulated data from the LNDST model using fitted posterior points to the rainfall event. Zero rainfall is white. The time step is 6-minutes.

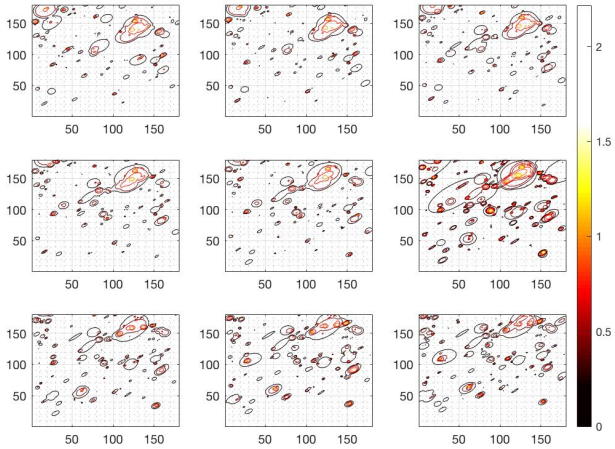

Figure 3.49: Contour plots of simulated data from the LNCST model using fitted posterior points to the rainfall event. Zero rainfall is white. The time step is 6-minutes.

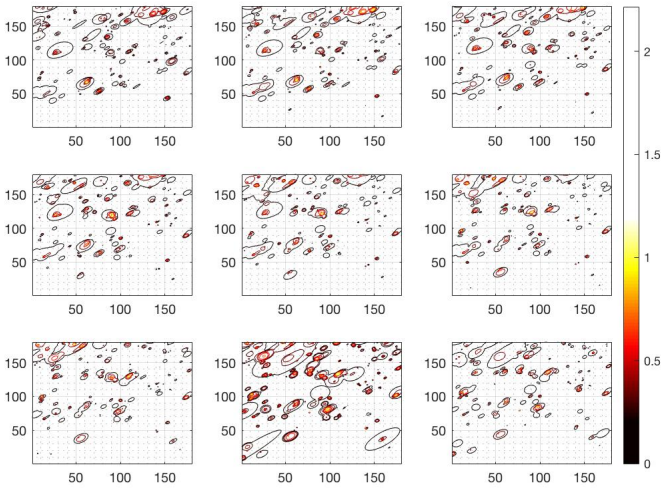

Figure 3.50: Contour plots of simulated data from the LNCST model using fitted posterior points to the rainfall event. Zero rainfall is white. The time step is 6-minutes.

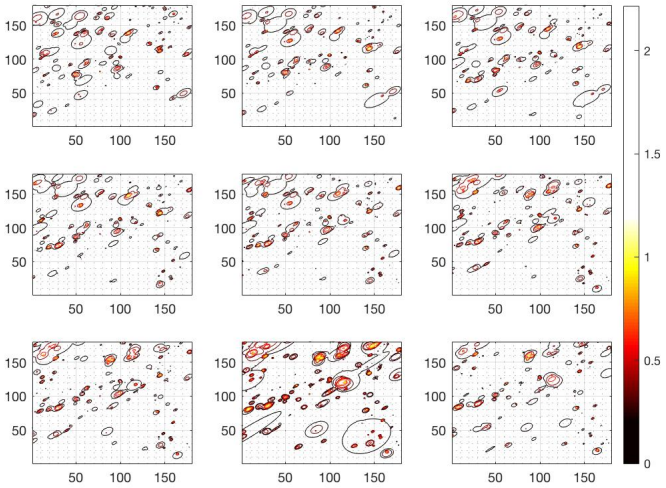

Figure 3.51: Contour plots of simulated data from the LNCST model using fitted posterior points to the rainfall event. Zero rainfall is white.

3.12.6 Diagnostics

To check model fit, we will presents 95% Monte-Carlo predictive intervals for spatial and temporal aggregation summary statistics.

Figures 3.52, 3.53, 3.54 , and 3.55 show 95% Monte-Carlo predictive intervals for summary statistics with different spatial and temporal aggregations.

Figure 3.52 shows the predictive intervals for mean, standard deviation, and dry probability are in the first row (a), (b), and (c) for spatial aggregation, 1×1 km^2 to 6×6 km^2 pixels. Similarly mean, standard deviation, and dry probability are in (d), (e), and (f) for temporal aggregation, 6-minute, 12 minute and 18-minute and 24-minute of $1 \times 1km^2$ pixels. Mean, standard deviation, and dry probability for temporal aggregation, 6-minute, 12 minute and 18-minute and 24-minute of $2 \times 2km^2$ pixels are in (g), (h), and (i) respectively.

Figure 3.53 shows the intervals for spatial autocorrelation for different spatial and temporal aggregations. Spatial autocorrelation at lags (-1,-1,0), (0,-1,0), and (-1,0,0). Spatial autocorrelation lags (-1,-1,0), (0,-1,0), and (-1,0,0) are in w (a), (b), and (c) respectively for spatial aggregation, 1×1 km^2 to 6×6 km^2 pixels. Spatial autocorrelation lags (-1,-1,0), (0,-1,0), and (-1,0,0) are in (d), (e), and (f) respectively for temporal aggregation, 6-minute, 12 minute and 18-minute and 24-minute of $1 \times 1km^2$ pixels. Similarly spatial autocorrelation lags (-1,-1,0), (0,-1,0), and (-1,0,0) are respectively in the last row (g), (h), and (i) respectively for temporal aggregation, 6-minute, 12 minute and 18-minute and 24-minute of $2 \times 2km^2$ pixels.

Figure 3.54 show the intervals for spatial autocorrelation time adjusted lags $(1 + v_x, 1 + v_y, 1), ((0 + v_x, 1 + v_y, 1)$, and $(1 + v_x, 0 + v_y, 1)$ for different spatial and temporal aggregations. Spatial autocorrelation at lags $(1+v_x, 1+v_y, 1), ((0+v_x, 1+v_y, 1)$, and $(1+v_x, 0+v_y, 1)$ are in (a), (b), and (c) respectively for spatial aggregation, 1×1 km^2 to 6×6 km^2 pixels. Spatial autocorrelation lags $(1+v_x, 1+v_y, 1), ((0+v_x, 1+v_y, 1)$, and $(1+v_x, 0+v_y, 1)$ are in the second row (d), (e), and (f) respectively temporal aggregation, 6-minute, 12 minute and 18-minute and 24-minute of 1×1 km^2 pixels. Similarly spatial autocorrelation lags $(1 + v_x, 1 + v_y, 1), ((0 + v_x, 1 + v_y, 1)$, and $(1+v_x, 0+v_y, 1)$ are in the last row (g), (h), and (i) respectively for temporal aggregation, 6-minute, 12 minute and 18-minute and 24-minute of 2×2 km^2 pixels.

Figure 3.55 shows the intervals for dry/wet area ratio, mean wet area over time, and standard deviation of wet area over time for spatial aggregation. Plots $(a), (b)$, and (c) are dry/wet area ratio, mean wet area, and stand deviation of wet area over time. Plots $(d), (e)$, and (f) are dry/wet area ratio, mean wet area, and stand deviation of wet area over time. Similarly

plots $(g), (h)$, and (i) are dry/wet area ratio, mean wet area, and stand deviation of wet area over time at 6, 12, 18, and 24 minute for 2×2 km^2 pixels.

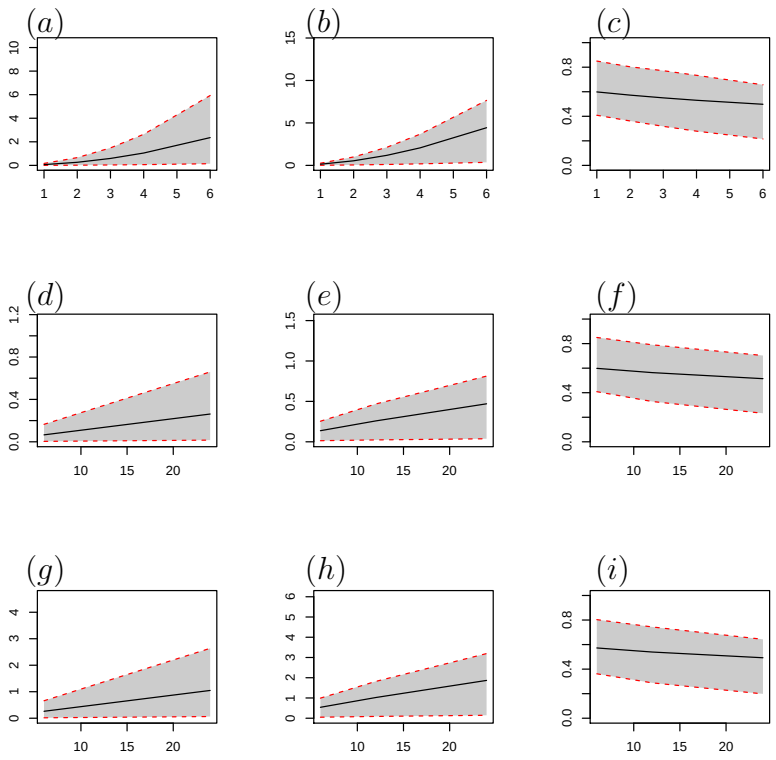

Figure 3.52: 95 % Monte-Carlo predictive intervals for summary statistics. Plots (a), (b), and (c) are of means, standard deviations, and dry probabilities respectively. X-axis is spatial aggregation of $l \times l$ km^2, $l = 1, 2, 3, 4, 6$. Plots (d), (e), and (f) are of means, standard deviations, and dry probabilities against time 6, 12, 18, and 24 minutes for 1×1 km^2 pixels. Plots (g), (h), and (i) are of means, standard deviations, and dry probabilities against time 6, 12, 18, and 24 minutes 2×2 km^2 pixels. The rainfall event is rainfall on 24th September 2016 from 12:54 to 16:48 hours in Melbourne.

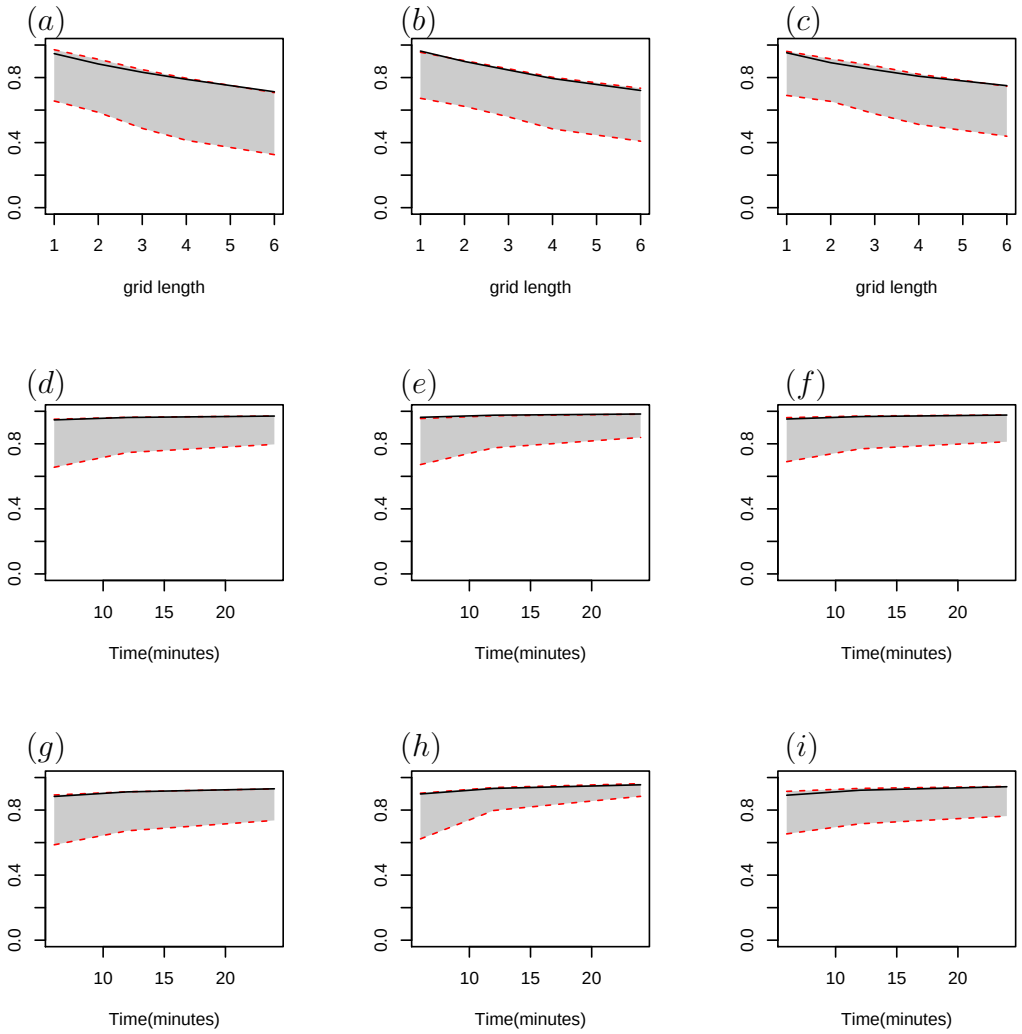

Figure 3.53: 95 % Monte-Carlo predictive intervals for summary statistics. Plots $(a), (b)$, and (c) are $\rho(-1,-1,0))$, $\rho(0,-1,0))$, and $\rho(-1,0,0))$. X-axis is spatial aggregation $l \times l$ km^2 pixel, $l = 1, 2, 3, 4, 6$. Plots $(d), (e)$, and (f) are $\rho(-1,-1,0)$, $\rho(0,-1,0))$, and $\rho(-1,0,0)$. X-axis is temporal aggregation at 6, 12, 18, and 24 minutes for 1×1 km^2 pixel. Plots $(g), (h)$, and (i) are $\rho(-1,-1,0)$, $\rho(0,-1,0))$, and $\rho(-1,0,0)$ 2×2 km^2 pixel. X-axis is temporal aggregation at 6, 12, 18, and 24 minutes. The rainfall event is on 24th September 2016 from 12:54 to 16:48 hours in Melbourne.

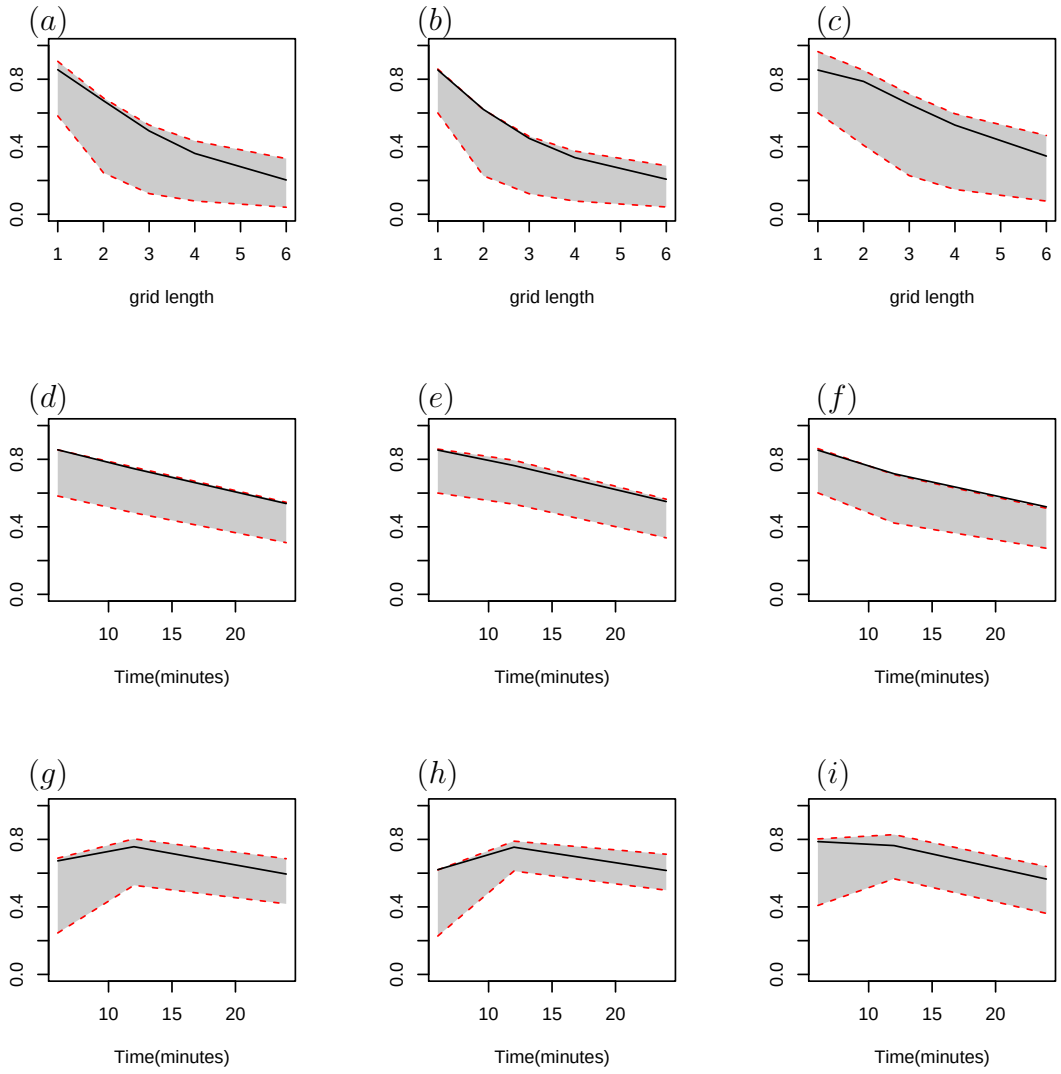

Figure 3.54: 95 % Monte-Carlo predictive intervals. Plots $(a), (b)$, and (c) are $\rho(1 + v_x, 1 + v_y, 1))$, $\rho(0 + v_x, 1 + v_y, 1))$, and $\rho(1 + v_x, 0 + v_y, 1))$. X-axis is spatial aggregation $l \times l$ km^2 pixel, $l = 1, 2, 3, 4, 6$. . Plots $(d), (e)$, and (f) are $\rho(1+v_x, 1+v_y, 1))$, $\rho(0+v_x, 1+v_y, 1))$, and $\rho(1+v_x, 0+v_y, 1))$ 1×1 km^2 pixels. X-axis is temporal aggregation at 6, 12, 18, and 24 minutes. Plots $(g), (h)$, and (i) are $\rho(1+v_x, 1+v_y, 1))$, $\rho(0+v_x, 1+v_y, 1))$, and $\rho(1+v_x, 0+v_y, 1))$ 2×2 km^2 pixels. The rainfall event is on 24th September 2016 from 12:54 to 16:48 hours in Melbourne.

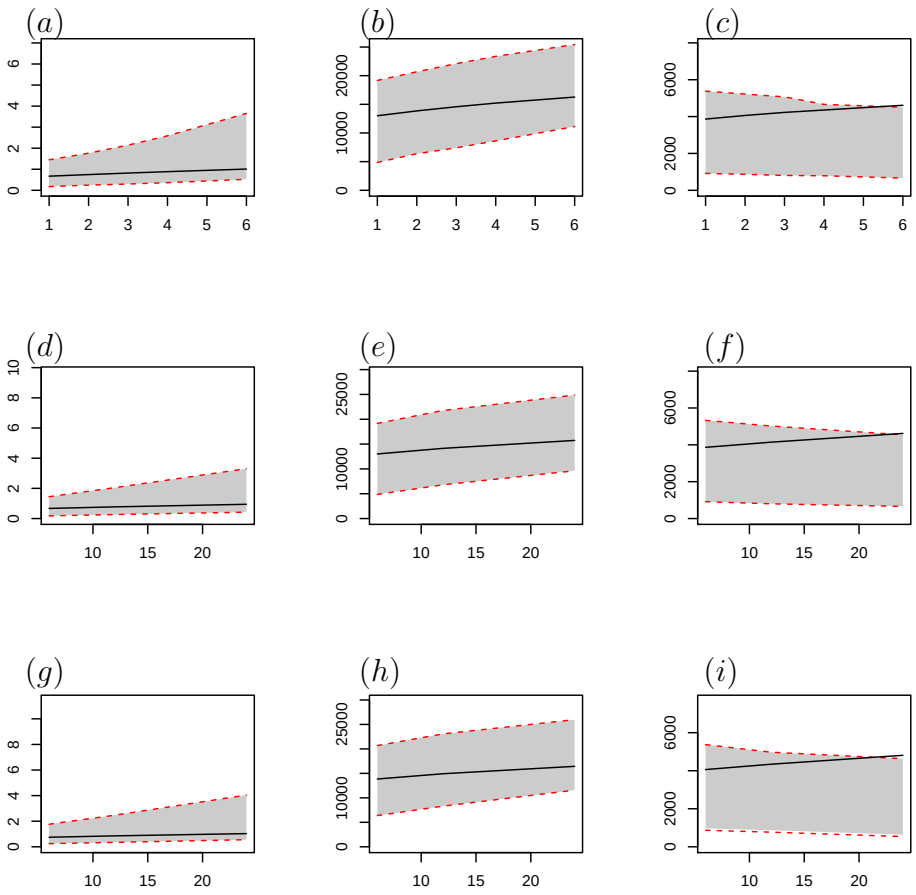

Figure 3.55: 95 % Monte-Carlo predictive intervals. Plots $(a), (b)$, and (c) are dry/wet area ratio, mean wet area, and stand deviation of wet area over time. X-axis is spatial aggregation $l \times l$ km^2 pixel, $l = 1, 2, 3, 4, 6$. Plots $(d), (e)$, and (f) are dry/wet area ratio, mean wet area, and stand deviation of wet area over time for 1×1 km^2 pixels. X-axis is temporal aggregation at 6, 12, 18, and 24 minutes. Plots $(g), (h)$, and (i) are dry/wet area ratio, mean wet area, and stand deviation of wet area over time for 2×2 km^2 pixels. The rainfall event is on 24th September 2016 from 12:54 to 16:48 hours in Melbourne.

The 95% Monte-Carlo predictive intervals for mean, standard deviation and a pixel dry probability of different spatial and temporal aggregations contains corresponding observed statistics in Figure 3.52 look better than that of generated from the C-I-N and ECST models as the intervals are narrow and observed statistics lie central of the intervals. These statistics are well reproduced by the NLCST model than that of other two models.

Figures 3.53 and 3.54 showed that the observed correlations $\rho\big(l_x + l_t \times v_x, l_y + l_t \times v_y,\ l_t\big)$ at $t = 0, 1$ are within the respective intervals. However they are close to the upper boundary, which indicates that model underestimates these statistics, where as the C-I-N model overestimates these as the observed statistics are close to lower boundary in Figures 3.22 and 3.23. The ECST model estimates most of these statistics overall better than that of other models having most of observed statistics are almost central of the intervals see Figures 3.34 and 3.35.

Other three statistics- wet/dry area ratio, mean of wet area and standard deviation of wet area are also well estimated by the ECST and LNCST models than the C-I-N model, because the 95% Monte-Carlo predictive intervals are wide in the Figure 3.24 and that of in Figures 3.36 and 3.55.

In conclusion, this model is not doing better than the ECST model for overall rainfall distribution, however it is doing a better job at fitting extreme rainfall distribution for the rainfall event, which will discuss in next section.

3.13 Extreme rainfall event

We are interested in which model is best fitting the tail distribution of the rainfall event. We follow Coles, 2001 [7] for extreme events analysis for the rainfall process. Let $X_1, X_2, \cdots, X_n$ be a sequence of independent and identically distributed random variables, having the marginal distribution F.

The threshold excesses $Y_1, Y_2, \cdots, Y_k$ are defined as $Y_j = X_j - u$ for $j = 1, 2, \cdots, k$, where u is threshold. If Y_j follows a generalized Pareto distribution with parameter ν and ς, then the mean of excesses of a threshold is given by

$$\mathbb{E}(Y - u_0 | Y > u_0) = \tfrac{\nu}{1-\varsigma},\ \text{provided } \varsigma < 1.$$

We suppose that the generalized Pareto distribution is valid for excesses of the threshold u_0 , then for all $u > u_0$,

$$\mathbb{E}(Y - u | Y > u) = \frac{\nu_{u_0} + \varsigma u}{1 - \varsigma}.$$

The plot of mean of excesses of threshold u against u gives a way of estimating u_0 by choosing u_0 so that $\mathbb{E}(Y - u | Y > u)$ is linear for $u > u_0$. Mean of

excesses is estimated by $\frac{1}{k}\sum_{j=1}^{k}(y_j - u)$, where $u < \max(Y)$ and $y_1, y_2, \cdots, y_k$ are observations those excessed u.

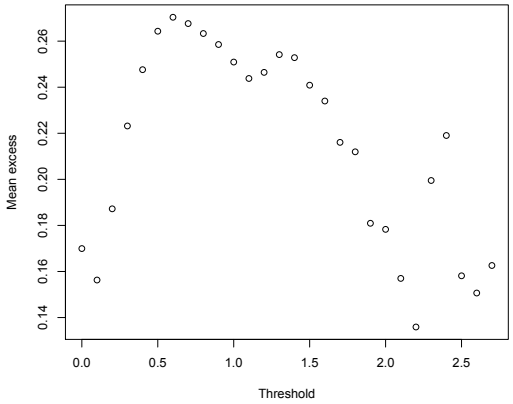

Figure 3.56: Mean residual life plot for the rainfall event on 24th September 2016 from 12:54 to 16:48 hours in Melbourne.

The mean residual life plot Figure 3.56 shows that after $u = 1.4$, there is approximate linearity. This indicates the choice $u_0 = 1.4$ is reasonable.

We are looking at whether the distribution of threshold exceeded values of observed data is the same as that of simulated data. Figures 3.57, 3.58, and 3.59 show quantile-quantile plots for distribution of observed data and simulated data exceeded threshold. The top Figure 3.57 (a) is q-q plot observed excesses per pixel ($1 \times 1 km^2$) against that of simulation from the C-I-N model. Similarly plots (b), and (c), but simulations from the ECST model and the LNCST model respectively. All three plots (a), (b), and (c) have fair fitting the tail distribution, however the plot (c) matches the best. The threshold is $u_0 = 1.4$.

Similarly Figures 3.58, and 3.59 are the same, but spatial aggregation of pixel $2 \times 2 km^2$ and $3 \times 3 km^2$. Thresholds are 6.5 mm per 2×2 km^2 pixel and 11 mm per 3×3 km^2 pixel respectively. These plots also refer the heavy tail rainfall distribution of an event and simulation from the LNCST model is the best of the three.

In conclusion, The LNST model fits the tail distribution better than the other models.

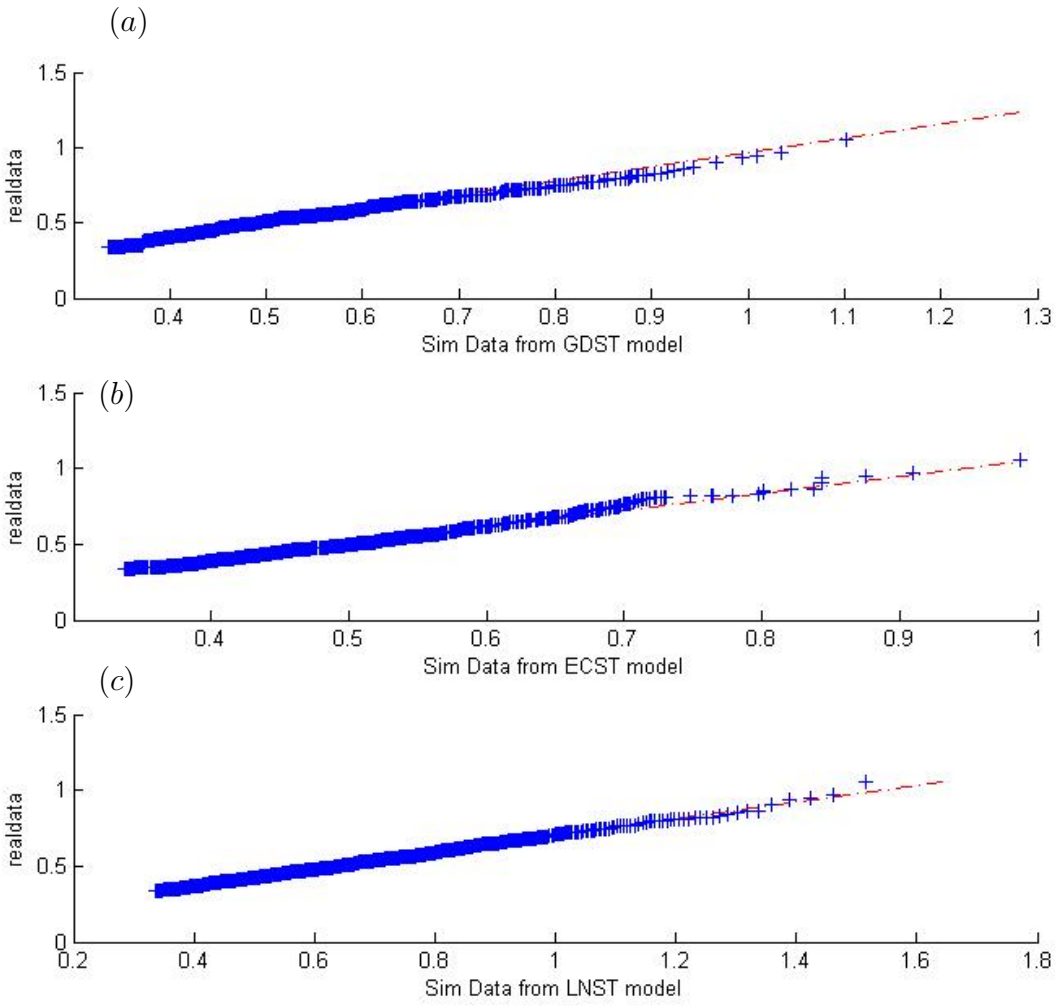

Figure 3.57: Quantile plot for log values exceeded the threshold 1.4 mm per 1 $\times 1$ km^2 pixel . Top plot for simulation data from the C-I-N model against observed data, middle plot for simulated data from the ECST model against observed data and bottom plot for simulated data from the LNCST mode against observed data. The red straight line refers that two sets of the data have the same distribution. Observed data is from the rainfall event on 24th September 2016 from 12:54 to 16:48 hours in Melbourne.

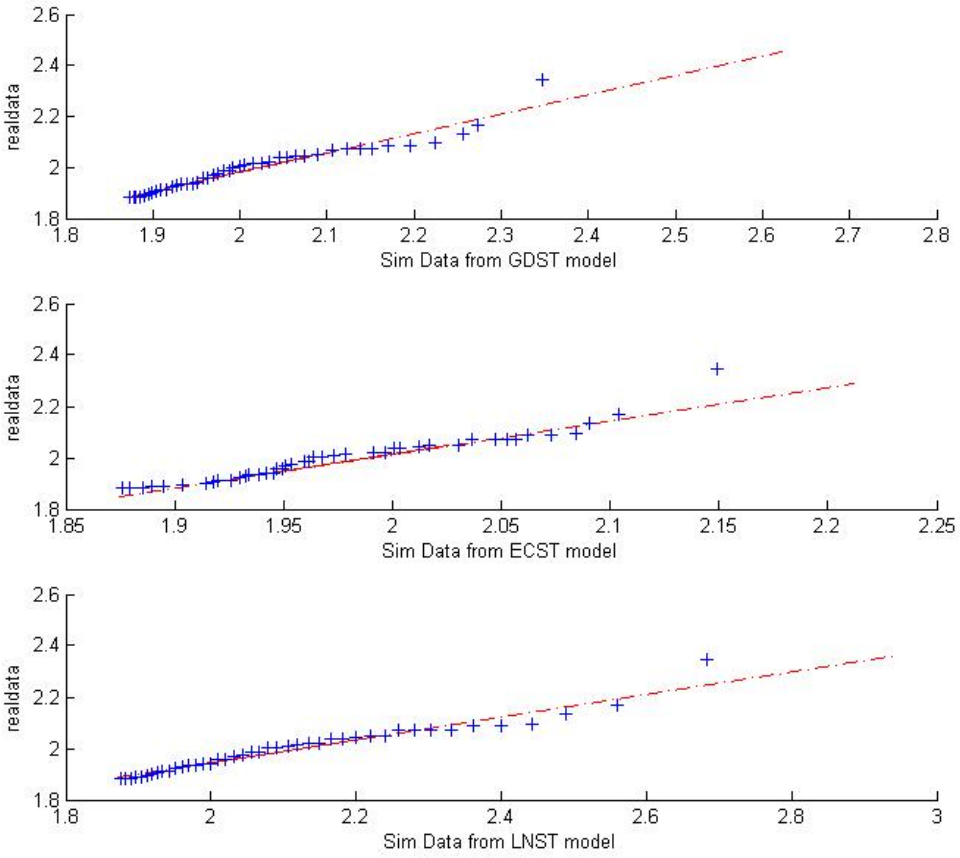

Figure 3.58: Quantile plot for log values exceeded the threshold 6.5 mm per 2 $\times 2\ km^2$ pixel . Top plot for simulation data from the C-I-N model against observed data, middle plot for simulated data from the ECST model against observed data and bottom plot for simulated data from the LNC ST mode against observed data. The red straight line refers that two sets of the data have the same distribution. Observed data is from the rainfall event on 24th September 2016 from 12:54 to 16:48 hours in Melbourne.

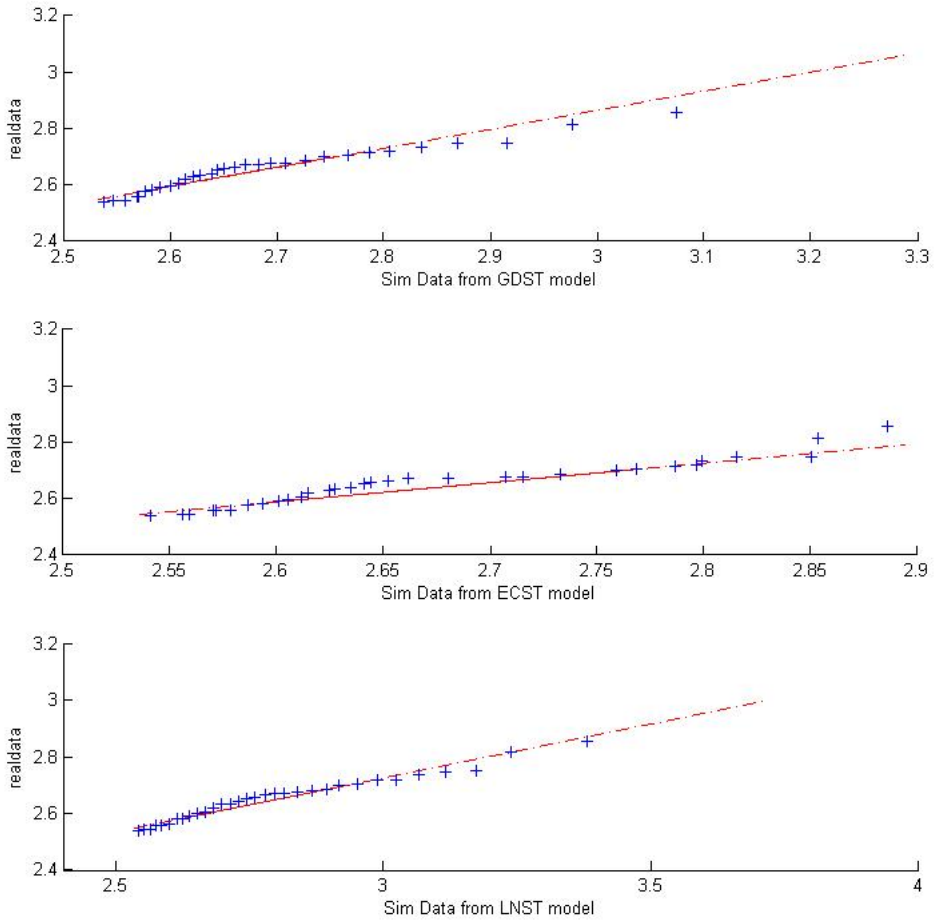

Figure 3.59: Quantile plot for lag values exceeded the threshold 11 mm per 3 $\times 3\ km^2$ pixel . Top plot for simulation data from the C-I-N model against observed data, middle plot for simulated data from the ECST model against observed data and bottom plot for simulated data from the LNCST mode against observed data. The red straight line refers that two sets of the data have the same distribution. Observed data is from the rainfall event on 24th September 2016 from 12:54 to 16:48 hours in Melbourne.

3.14 Discussion

We demonstrated that ABC can be used to fit a Bayesian version the C-I-N model.

We developed a new ECST model, which has a random eccentricity of the elliptical cell and the cell intensity at a point in space is obtained according to a spread function. We allowed the storm orientation and eccentricity both to be random, but the simulated rain-band appeared to be distorted. We want the rainband to be preserved as real data shows. From simulation experience, we keep storm eccentricity and orientation the same for all storms in an event. Similarly orientation is the same for all cells. As we see the observed data typically the centre of rain cells has high intensity, which gradually decreases with distance from the centre. The ECST model is doing better job at capturing this behavior.

Using the posterior distribution of $S(D^*)$ we showed that the modified model gives a better fit. A simulation from the fitted model is given in Figure 3.41, for a single time-point; qualitatively it also shows a better match with the observed process.

From another new NLCST model we obtained the information that there is a negative relationship between cell intensity and area. Posterior mean and posterior median of ρ_{xm} are -0.69 and -0.76 see Table 3.5, which shows that the correlation is moderately large. The 95 % credible interval is $(-0.93, 0.10)$.

We also studied that whether the NLCST model can capture heavy tail distribution of rainfall. For which we used different spatial aggregation to look at whether the observed exceeded rainfall distribution matches to simulated one. Figures 3.57, 3.58, and 3.59 refer that the LNCST model is doing better than the rest.

In this chapter, the eccentricity and orientation are estimated using the empirical spatial autocorrelation function. However the next chapter we will include these parameters in the ABC-MCMC step.

Chapter 4

Applications to Different Radar Data

In this chapter, we select two new rainfall events. One is from Melbourne radar. The other one is from the radar located at Wardon Hill, UK. We are interested in whether the ABC fitting is consistent.

We also extend the number of parameters to be estimated in the ABC-MCMC step, only parameters velocity $\mathbf{v} = (v_x, v_y)$ and σ_e are fixed. All other parameters will be estimated in ABC-MCMC step. Remember that previously eccentricity and orientation of cells were estimated using the spatial autocorrelation function.

4.1 Melbourne Radar Data

We select a different rainfall event than the rainfall event used in Chapter 3. The radar data was collected at Laverton, Melbourne on 24th September 2016. The rainfall data was also calibrated by the Australian Bureau of Meteorology using rain-gauge. The actual rainfall process was the rainfall event on 24th September 2016 for a period of 3 hours from 07:48 to 10:42 hours. As described in the previous Chapter, the radar coverages the circular region of 128 km radius. The space is gridded 1×1 km^2 and time increment is 6-minute. We restricted ourself as a square study area of length 180 km see Figure 3.5. We have 180×180 number of pixels for each time point. There therefore is a matrix of $180 \times 180 \times 30$. Each element of the matrix is

given some amount (possibly zero) of rain in mm.

Figure 4.1 shows that coverage percentage, total intensity, mean intensity, and maximum rainfall at a pixel over time. The plot (a) gives the percentage coverage over time. The least coverage is 33% and the maximum coverage reaches 45%. Total intensity over the whole grid is in the plot (b). Minimum average rainfall per pixel is 0.03 mm and 0.05 mm is maximum average rainfall per pixel, which can be seen in the plot (c). The maximum rainfall 1.2 mm and minimum rainfall 0.37 mm are shown in the plot (d). Table 4.1 shows summary statistics.

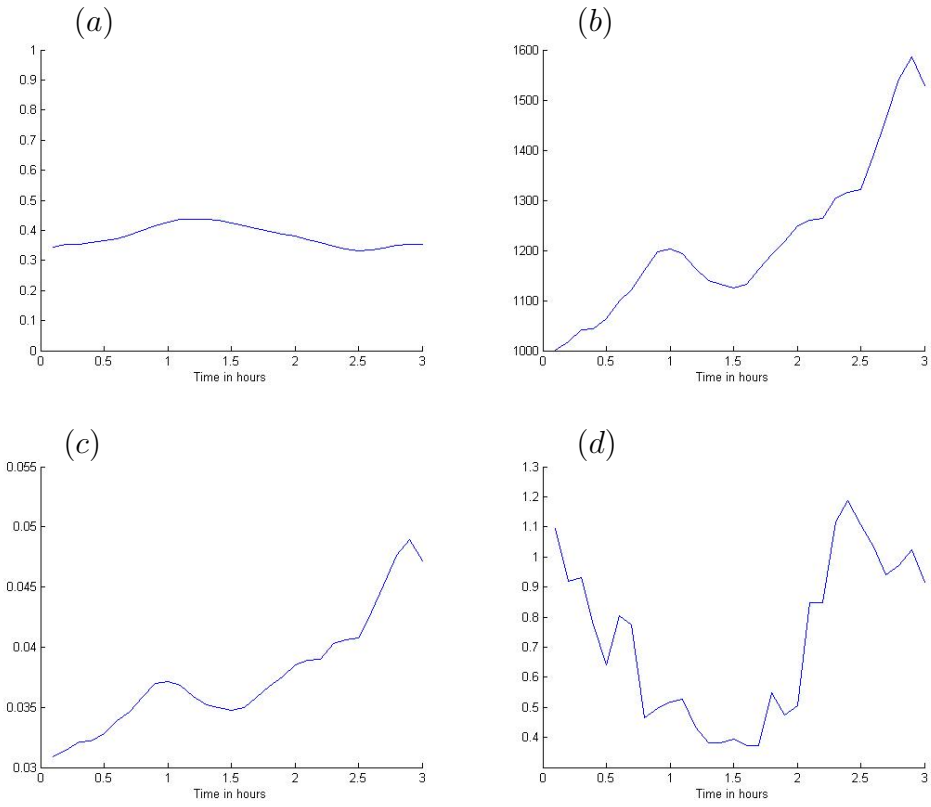

Figure 4.1: Plot (a) shows the study region coverage % over time. Plot (b) gives sum of intensities of all pixels at time t. Mean per pixel at time t is shown in plot (c). maximum intensity in a pixel at time t is displayed in plot (d). The rainfall event is on 24th September 2016 from 07:48 to 10:42 hours in Melbourne.

The velocity $\mathbf{v} = (19.9, 20.0)$ km per hour was estimated using the spatial autocorrelation function. Table 4.1 gives summary statistics of the observed process.

Summaries	lags (l_x, l_y, l_t)	Values
Mean (mm per pixel)		0.038
Standard deviation		0.070
Correlation	$(-1,-1,0)$	0.954
$\rho\big(Y(l_x + l_t \times v_x,\ l_y + l_t \times v_y,\ l_t)\big)$	$(-1,0,0)$	0.978
	$(-1,1,0)$	0.961
	$(0,-1,0)$	0.975
	$(0,1,0)$	0.975
	$(1,-1,0)$	0.961
	$(1,0,0)$	0.978
	$(1,1,0)$	0.954
	$(-1+v_x,-1+v_y,1)$	0.854
	$(-1+v_x,0+v_y,1)$	0.868
	$(-1+v_x,1+v_y,1)$	0.864
	$(0+v_x,-1+v_y,1)$	0.857
	$(0+v_x,0+v_y,1)$	0.869
	$(0+v_x,1+v_x,1)$	0.862
	$(1+v_x,-1+v_y,1)$	0.851
	$(1+v_x,0+v_y,1)$	0.859
	$(1+v_x,1+v_x,1)$	0.849
$\mathbb{P}(Y^{(l)}=0)$		0.585
Dry wet ratio		0.709
Mean wet area (km^2)		13444
Standard deviation of wet area		1286

Table 4.1: Observed summary statistics. The rainfall event is on 24th September 2016 from 07:48 to 10:42 hours in Melbourne.

4.1.1 Fitting the C-I-N Rainfall Model using ABC

The parameters were transformed to reduce dependence and skewness. The new parameters are:

$$\begin{aligned}
\phi(1) &= \log(\lambda\gamma^{-1}) \\
\phi(2) &= \log(\lambda\gamma) \\
\phi(3) &= \log(\beta\eta^{-1}) \\
\phi(4) &= \log(\beta\eta) \\
\phi(5) &= \log(\mu_x\mu_A) \\
\phi(6) &= \log(\mu_x\mu_A^{-1}) \\
\phi(7) &= \log(\alpha_2) \\
\phi(8) &= \log(\xi_m) \\
\phi(9) &= \log(\xi_{cv}) \\
\phi(10) &= \log\big(\frac{e}{1-e}\big) \\
\phi(11) &= \log\big(\frac{\Theta}{\pi-\Theta}\big) \\
\phi(12) &= v_x \\
\phi(13) &= v_y
\end{aligned}$$

Normal priors are used for all the $\phi(i); i = 1, 2, ..., 6, 10, 11$; Recall that there were previously some extreme posterior points, particularly when we transformed log parameters to original parameters (see Figure 1 in Appendix). To avoid these extreme values, we used a truncated normal prior for parameters $\phi(7)$, $\phi(8)$, and $\phi(9)$. The following priors for $\phi(7)$ truncated normal from $(-\infty, \log(3)]$, for $\phi(8)$) truncated normal from $(-\infty, \log(6)]$, and for $\phi(9)$ truncated normal from $(-\infty, \log(10)]$ works well.

For the proposal chain we just use a random walk with $N(\mathbf{0}, 0.2^2\mathbf{I})$ increments.

We have kept the same set of summary statistics S as before and the same distance measure d.

Posterior Distribution

Plots of estimated posteriors for parameter $\phi(i); i = 1, 2, ..., 11$ are given in Figure 4.3. The trace plots for the posteriors are displayed in Figure 4.2. Similarly joint posteriors are shown in Figure 4.4. These diagnostic plots demonstrate the the ABC-MCMC is good for fitting the C-I-N model to the

rainfall event. Plots of posteriors for original parameters (untransformed) are showed in Figure 4.5.

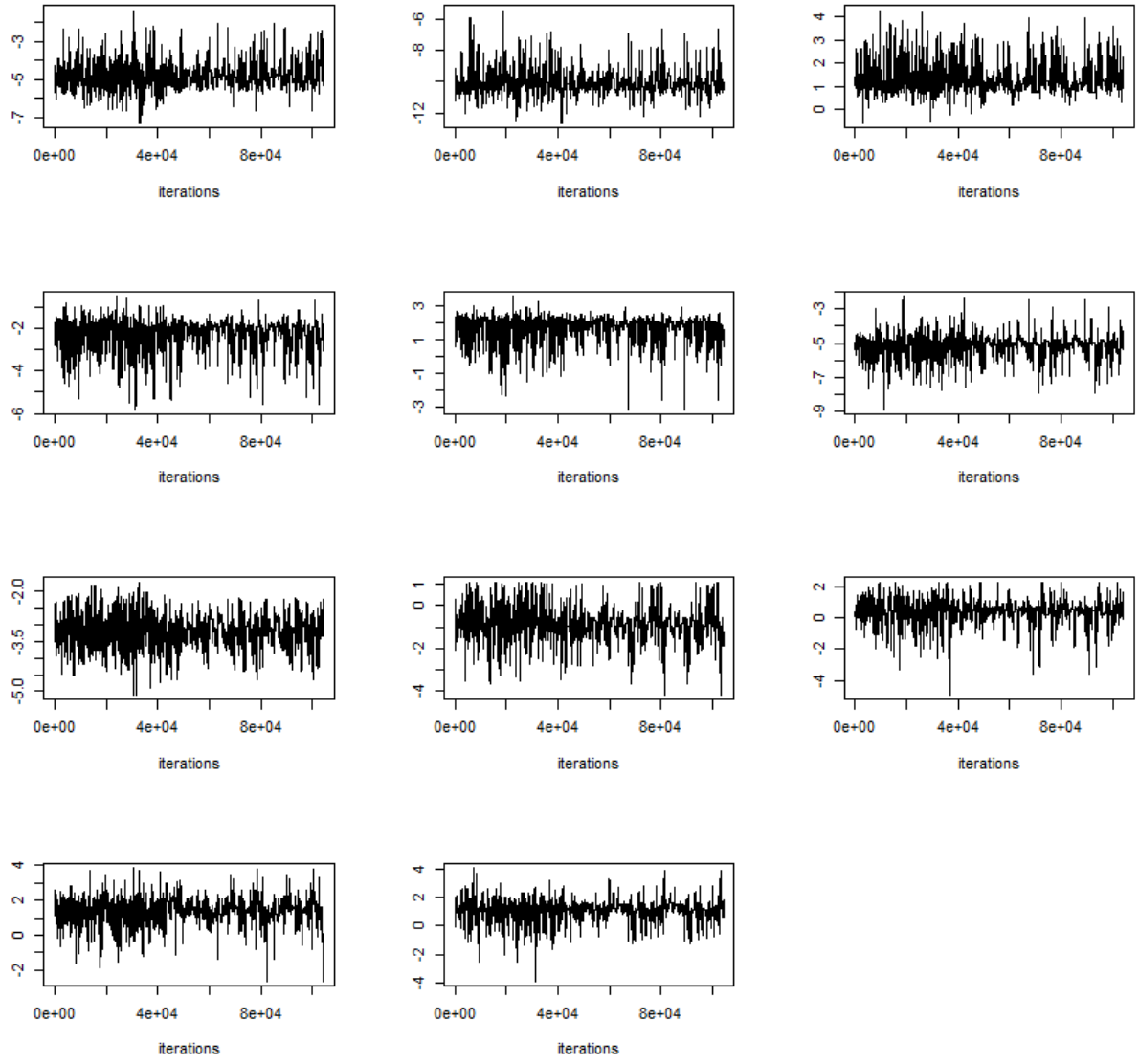

Figure 4.2: Chains for $\phi(i)$,$i = 1, 2, \ldots, 11$ (from top left to right). The rainfall event is on 24th September 2016 from 07:48 to 10:42 hours in Melbourne.

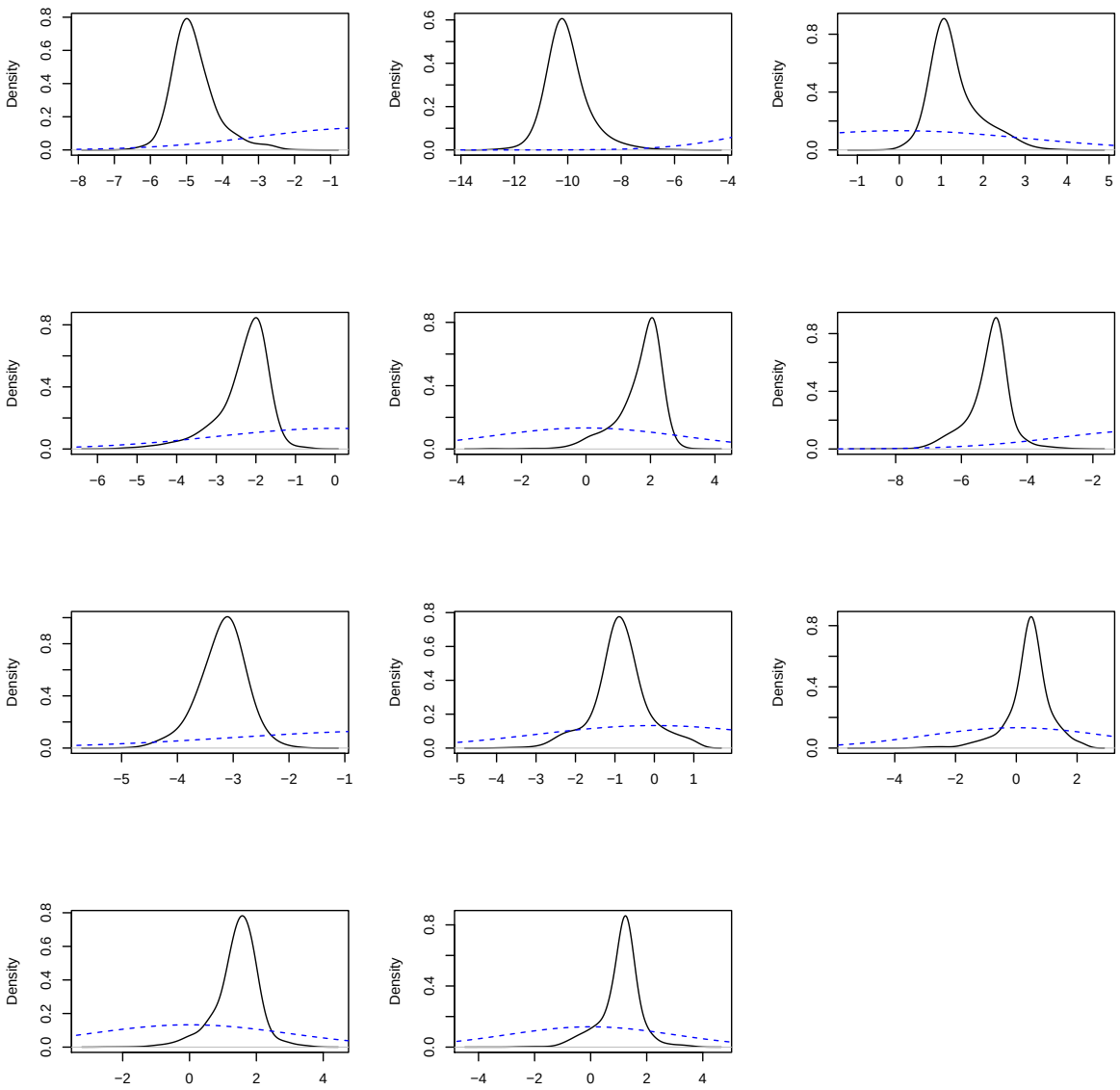

Figure 4.3: Posteriors for $\phi(i)$,$i = 1, 2, \ldots, 11$ (from top left to right). Blue curves are priors. The rainfall event is rainfall on 24th September 2016 from 07:48 to 10:42 hours in Melbourne.

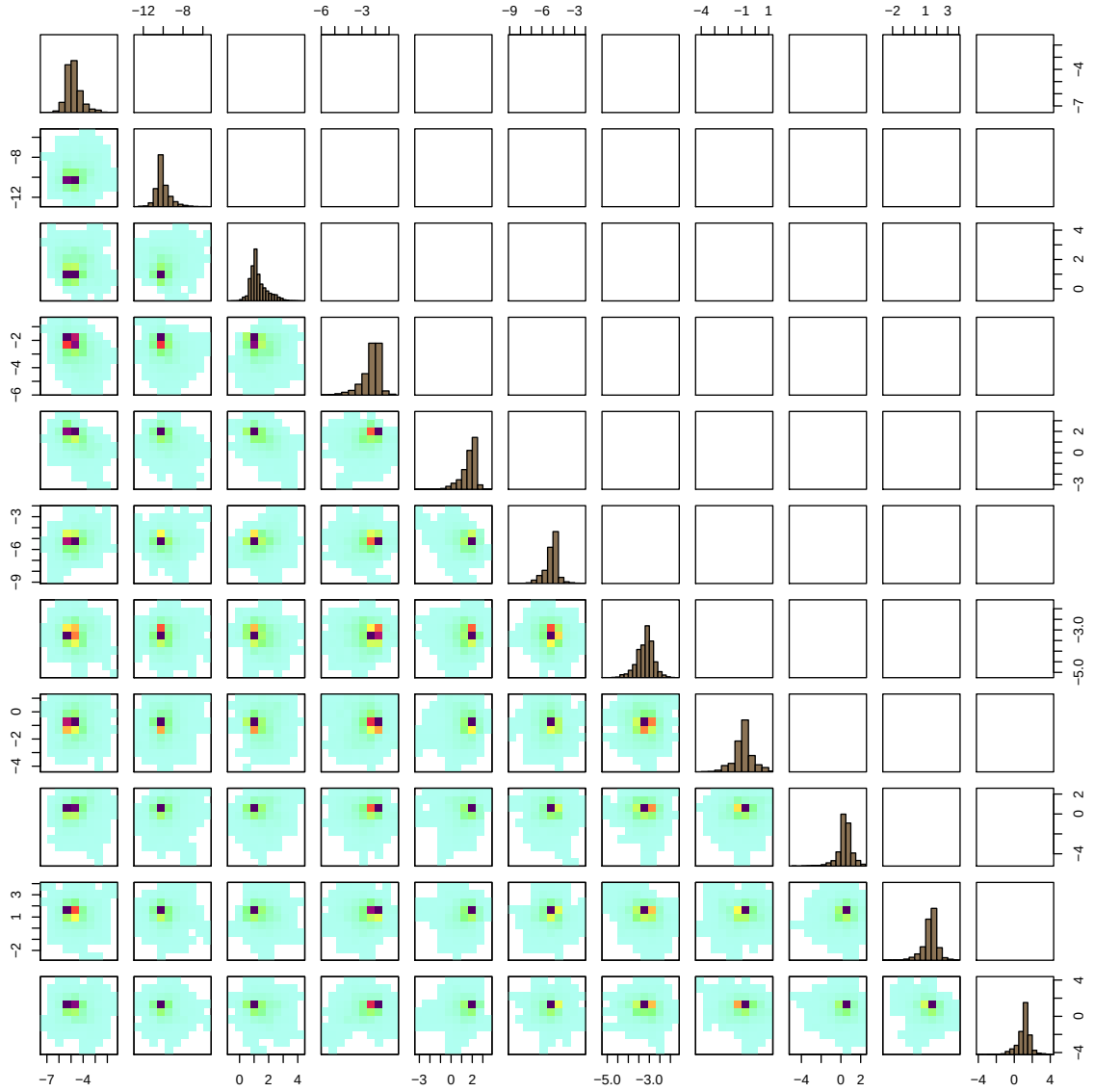

Figure 4.4: Posteriors (diagonals) for $\phi(i)$, $i = 1, 2, \ldots, 9$ and joint posteriors in the lower panel. The rainfall event is rainfall on 24th September 2016 from 07:48 to 10:42 hours in Melbourne.

Figure 4.5 shows that posteriors for original parameters, which are obtained from exponentials as follows:

$$
\begin{aligned}
\lambda &= \exp\left(\frac{\phi(1)+\phi(2)}{2}\right) \\
\gamma^{-1} &= \exp\left(\frac{\phi(1)-\phi(2)}{2}\right) \\
\beta &= \exp\left(\frac{\phi(3)+\phi(4)}{2}\right) \\
\eta^{-1} &= \exp\left(\frac{\phi(3)-\phi(4)}{2}\right) \\
\mu_x &= \exp\left(\frac{\phi(5)+\phi(6)}{2}\right) \\
\mu_A &= \exp\left(\frac{\phi(5)-\phi(6)}{2}\right) \\
\alpha_2 &= \exp(\phi(7)) \\
\xi_m &= \exp(\phi(8)) \\
\xi_{cv} &= \exp(\phi(9)) \\
e &= \frac{\exp(\phi(10))}{\exp(\phi(10))+1} \\
\Theta &= \frac{\pi\,\exp(\phi(11))}{\exp(\phi(11))+1} \\
v_x &= \phi(12) \\
v_y &= \phi(13)
\end{aligned}
$$

Table 4.2 shows posterior means, medians and 95 % credible intervals.

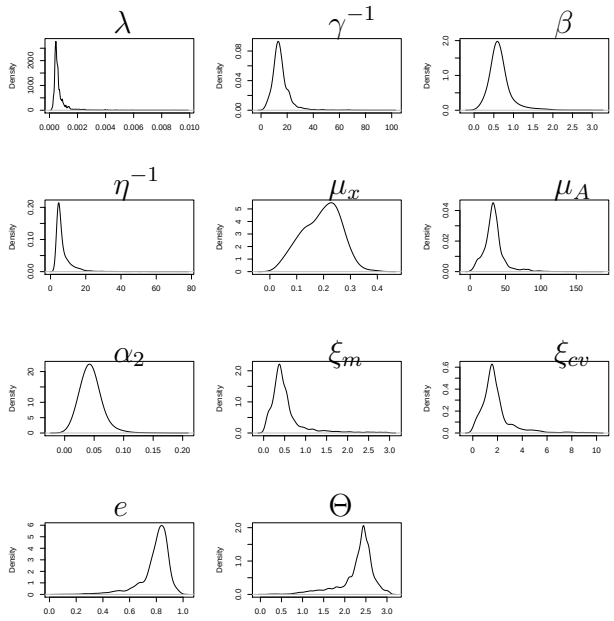

Figure 4.5: Posteriors for parameters λ , γ^{-1}, β, η^{-1}, μ_x, μ_A, α_2, ξ_m, ξ_{cv}, e, and Θ. The rainfall event is rainfall on 24th September 2016 from 07:48 to 10:42 hours in Melbourne.

Parameters	Mean	Median	95% Credible Interval
λ	0.0007	0.0005	(0.0003, 0.0025)
γ^{-1}	15.094	13.975	(5.3099, 33.328)
β	0.6547	0.6105	(0.2431, 1.4569)
η^{-1}	7.1096	5.3596	(3.4542, 19.733)
μ_x	0.1924	0.1990	(0.0547, 0.3074)
μ_A	33.466	32.388	(8.8582, 75.159)
α_2	0.0442	0.0436	(0.0155, 0.0847)
ξ_m	0.5371	0.4136	(0.0916, 2.0332)
ξ_{cv}	1.8795	1.6144	(0.2537, 5.5658)
e	0.7895	0.8194	(0.4628, 0.9287)
Θ	2.2915	2.4134	(1.0920, 2.8660)

Table 4.2: Estimated posterior means, medians and credible intervals for parameters. Fitted the C-I-N model to the rainfall event on 24th September 2016 from 07:48 to 10:42 hours in Melbourne..

4.1.2 Fitting Ellipsoidal Cell Spatial-Temporal Rainfall Model

As before, the velocity $\mathbf{v} = (19.9, 20.0)$ km per hour was estimated using spatial autocorrelation function. For priors we used the $N(0, 3.0^2)$ distribution for $\phi(i)$, for $i = 1, ..., 6, 10, 11$, and for $\phi(7)$ truncated normal from $(-\infty, \log(3)]$, for $\phi(8)$) truncated normal from $(-\infty, \log(6)]$, and for $\phi(9)$ truncated normal from $(-\infty, \log(10)]$. As for any MCMC procedure, the proposal chain needs to be chosen so that it mixes well and explores the whole parameter space. We used a random walk with $N(\mathbf{0}, 0.2^2\mathbf{I})$ increments.

The trace plots for the posteriors are shown in Figure4.6. The Markov chains have moved around the parameter space, though more mixing would be desirable. The results presented required several weeks of simulations, and unfortunately there was not the time to generate more samples.

We have kept the same set of summary statistics S as before and the same distance measure d.

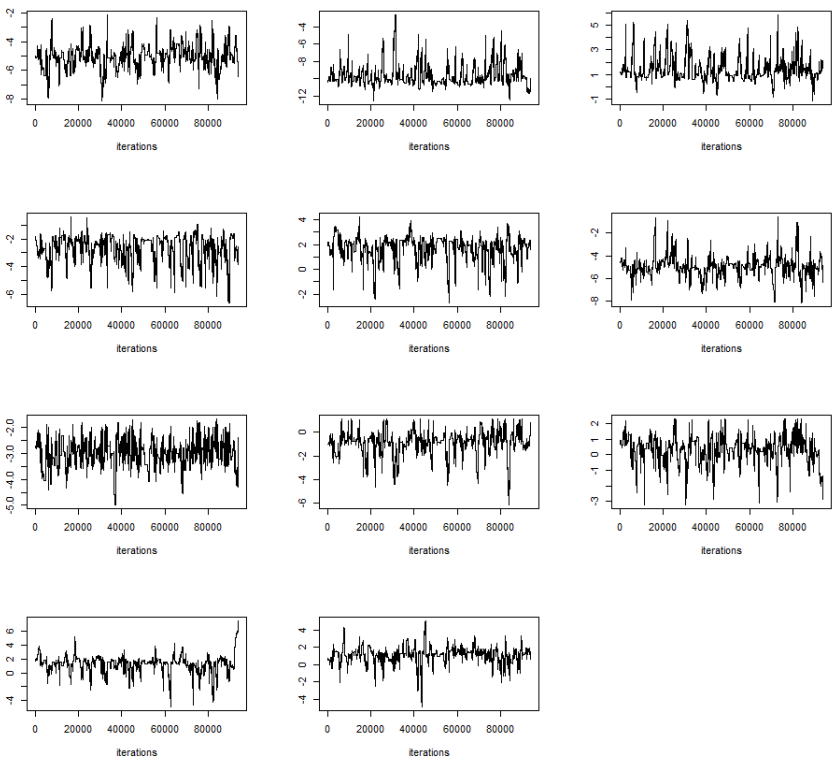

Figure 4.6: Chains for $\phi(i)$,$i = 1, 2, \ldots, 11$ (from top left to right). The rainfall event is on 24th September 2016 from 07:48 to 10:42 hours in Melbourne.

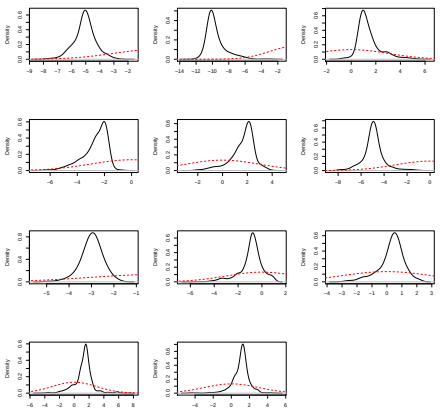

Figure 4.7: Posteriors for $\phi(i)$,$i = 1, 2, \ldots, 11$ (from top left to right). Red dotted curves are priors. The rainfall event is on 24th September 2016 from 07:48 to 10:42 hours in Melbourne.

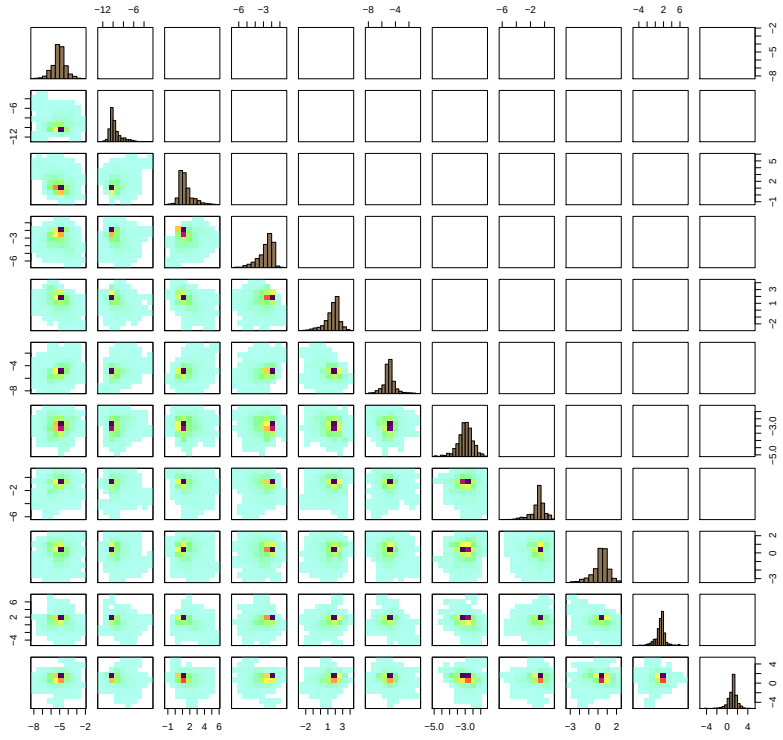

Figure 4.8: Posteriors (diagonals) for $\phi(i)$, $i = 1, 2, \ldots, 11$ and lower panel plots are joint posteriors . The rainfall event is on 24th September 2016 from 07:48 to 10:42 hours in Melbourne..

Figure 4.9 shows that posteriors for original parameters.

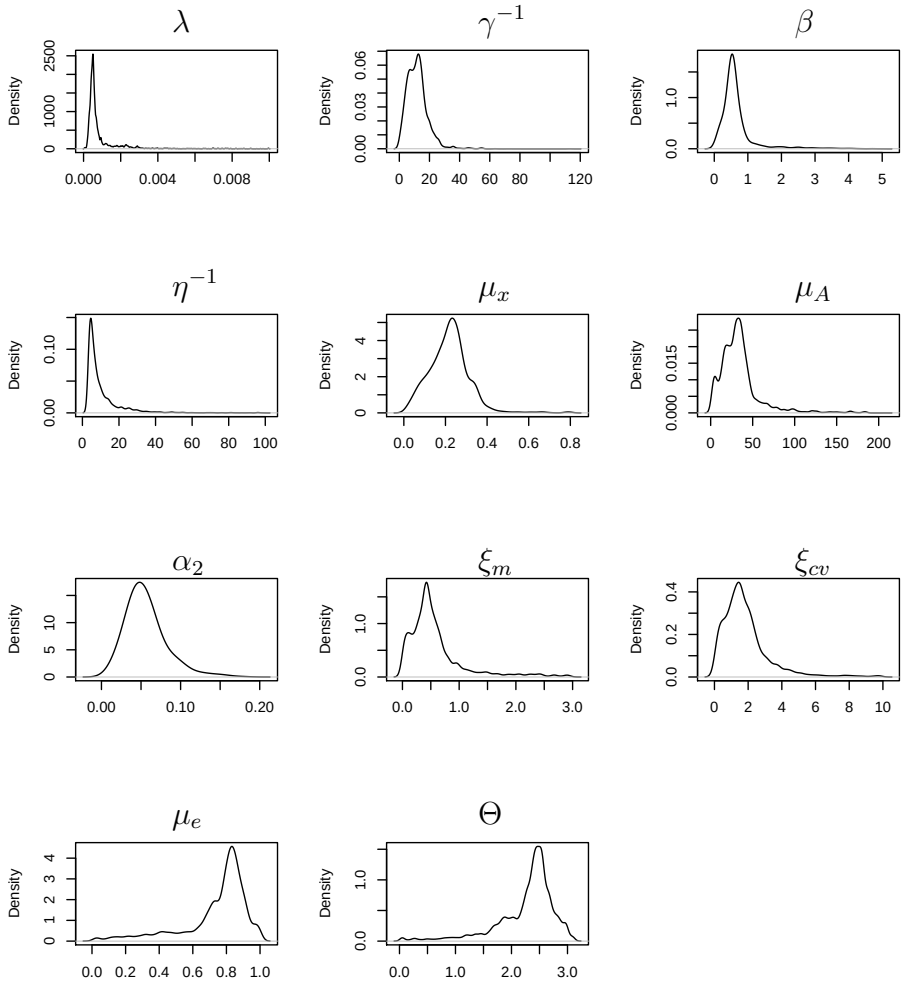

Figure 4.9: Posteriors for parameters λ , $\gamma^{-1}, \beta,\ \eta^{-1}, \mu_x, \mu_A,\ \alpha_2,\ \xi_m,\ \xi_{cv}, \mu_e$, and Θ. The rainfall event is on 24th September 2016 from 07:48 to 10:42 hours in Melbourne.

Parameters	Mean	Median	95% Credible Interval
λ	0.0009	0.0005	(0.0003, 0.0045)
γ^{-1}	11.799	11.391	(1.6150, 26.092)
β	0.6551	0.5515	(0.1136, 2.4732)
η^{-1}	10.395	6.6499	(3.3520, 39.636)
μ_x	0.2177	0.2208	(0.0469, 0.4058)
μ_A	33.872	30.614	(3.297, 100.772)
α_2	0.0560	0.0513	(0.0169, 0.1252)
ξ_m	0.5756	0.4451	(0.0299, 2.2536)
ξ_{cv}	1.8280	1.5295	(0.1619, 5.7586)
μ_e	0.7374	0.8047	(0.1607, 0.9764)
Θ	2.2609	2.4074	(0.7238, 2.9672)

Table 4.3: Estimated posterior means, medians and 95% credible intervals for parameters. Fitted the ECST Model to the rainfall even on 24th September 2016 from 07:48 to 10:42 hours in Melbourne.

4.1.3 Fitting Log-Normal Cell Spatial-Temporal Rainfall Model

Similar to previous fittings, we obtained the velocity $\mathbf{v} = (19.9, 20.0)$ km per hour and then fixed. For the remaining parameters, we estimate posterior distribution for parameters. For priors we used the $N(0, 3.0^2)$ distribution for $\phi(i)$, for $i = 1, ..., 9, 12, 13$, and for $\phi(10))$ truncated normal from $(-\infty, \log(6)]$, and for $\phi(11)$ truncated normal from $(-\infty, \log(10)]$.

For the proposal chain we just use a random walk with $N(\mathbf{0}, 0.2^2\mathbf{I})$ increments.

The same set of summary statistics S are used as before and the same distance measure d.

Figure 4.10 shows the Morkov chains from parameters $\phi(i), i = 1, 2, 3, ..., 13$ and the posterior and prior densities are shown in Figure 4.11. The Markov chains have moved around the parameter space, though more mixing would be desirable. The results presented required several weeks of simulations, and unfortunately there was not the time to generate more samples.

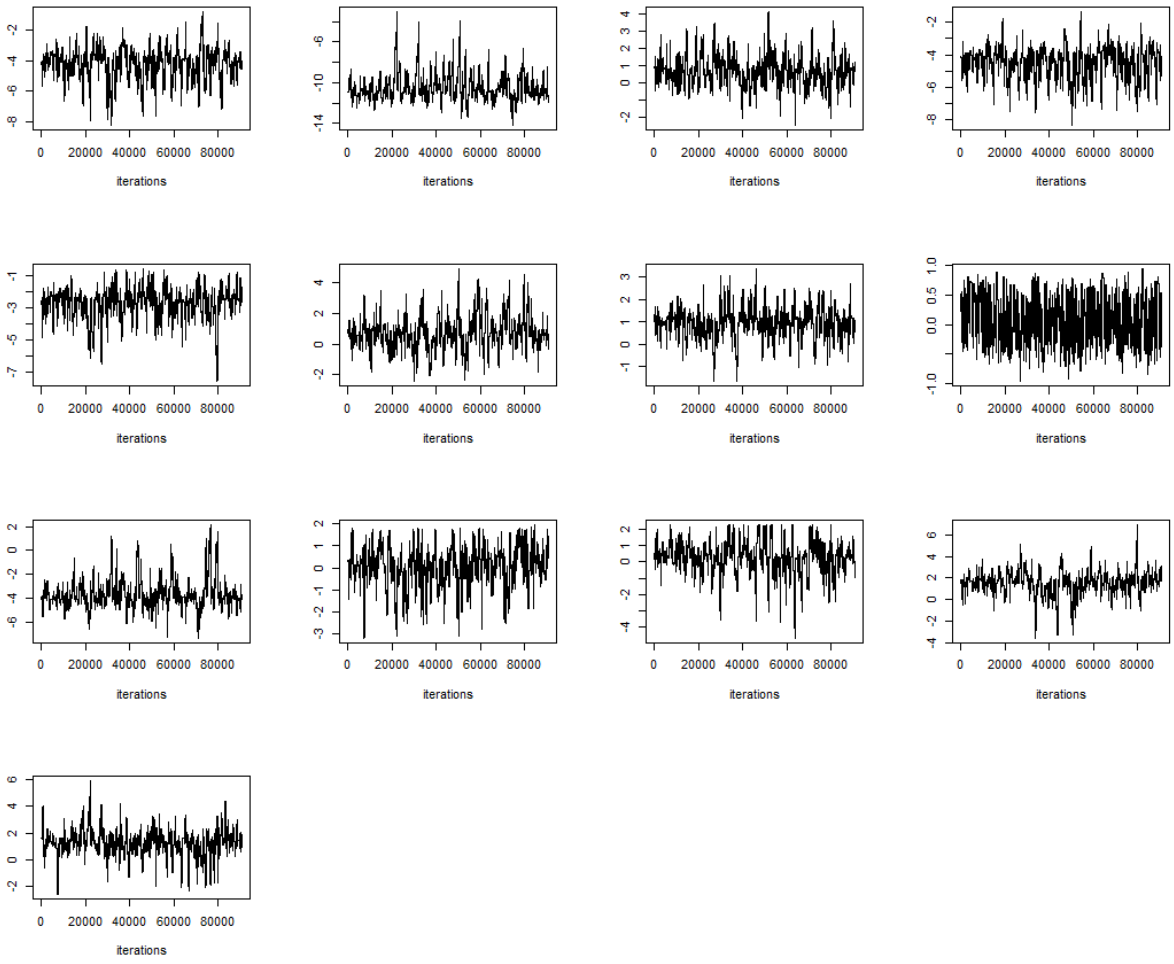

Figure 4.10: Chains for $\psi(i)$,$i = 1, 2, \ldots, 13$ (from top left to right) of the rainfall event on 24th September 2016 from 07:48 to 10:42 hours in Melbourne.

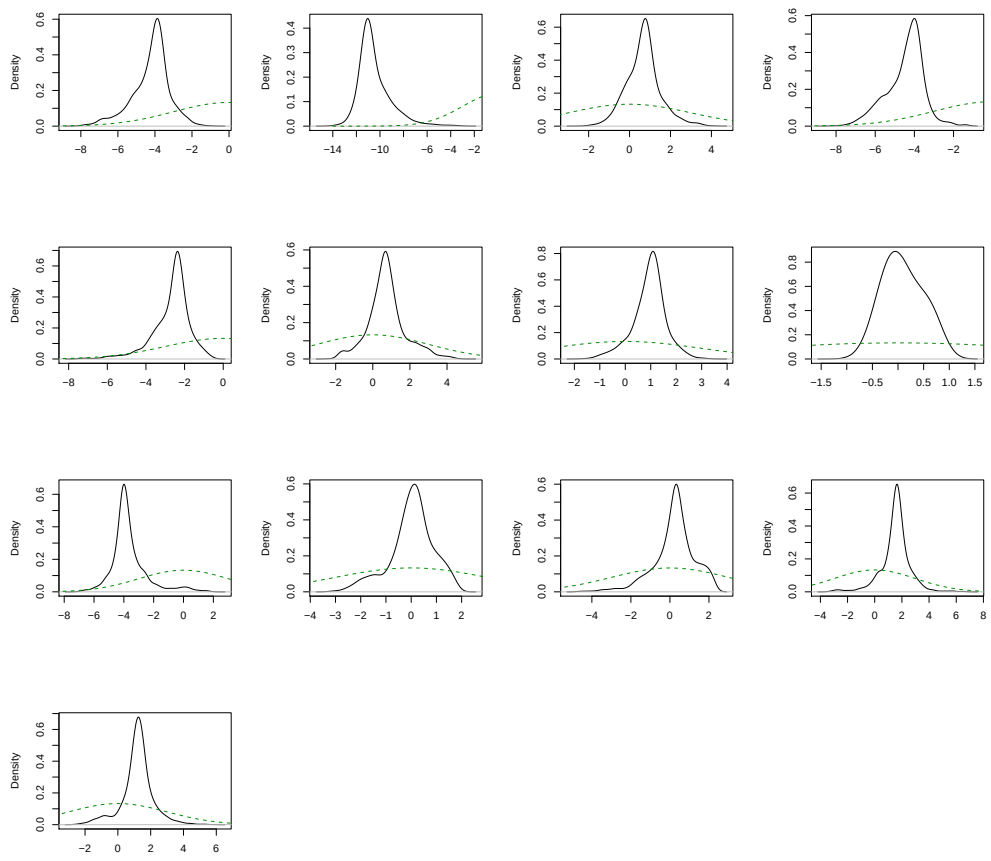

Figure 4.11: Posteriors for $\psi(i)$,$i = 1, 2, \ldots, 13$ (from top left to right) of the rainfall event on 24th September 2016 from 07:48 to 10:42 hours in Melbourne. Green curves are priors.

In Figure 4.12, the diagonal plots are histograms for parameters $\psi(i), i = 1, 2, 3, ..., 13$. The lower panels are pair distribution of horizontal and vertical parameters respectively. The colour label from light green to dark blue gives dense population of posterior points of pair distributions. As we expect there is high density of the points in particular region.

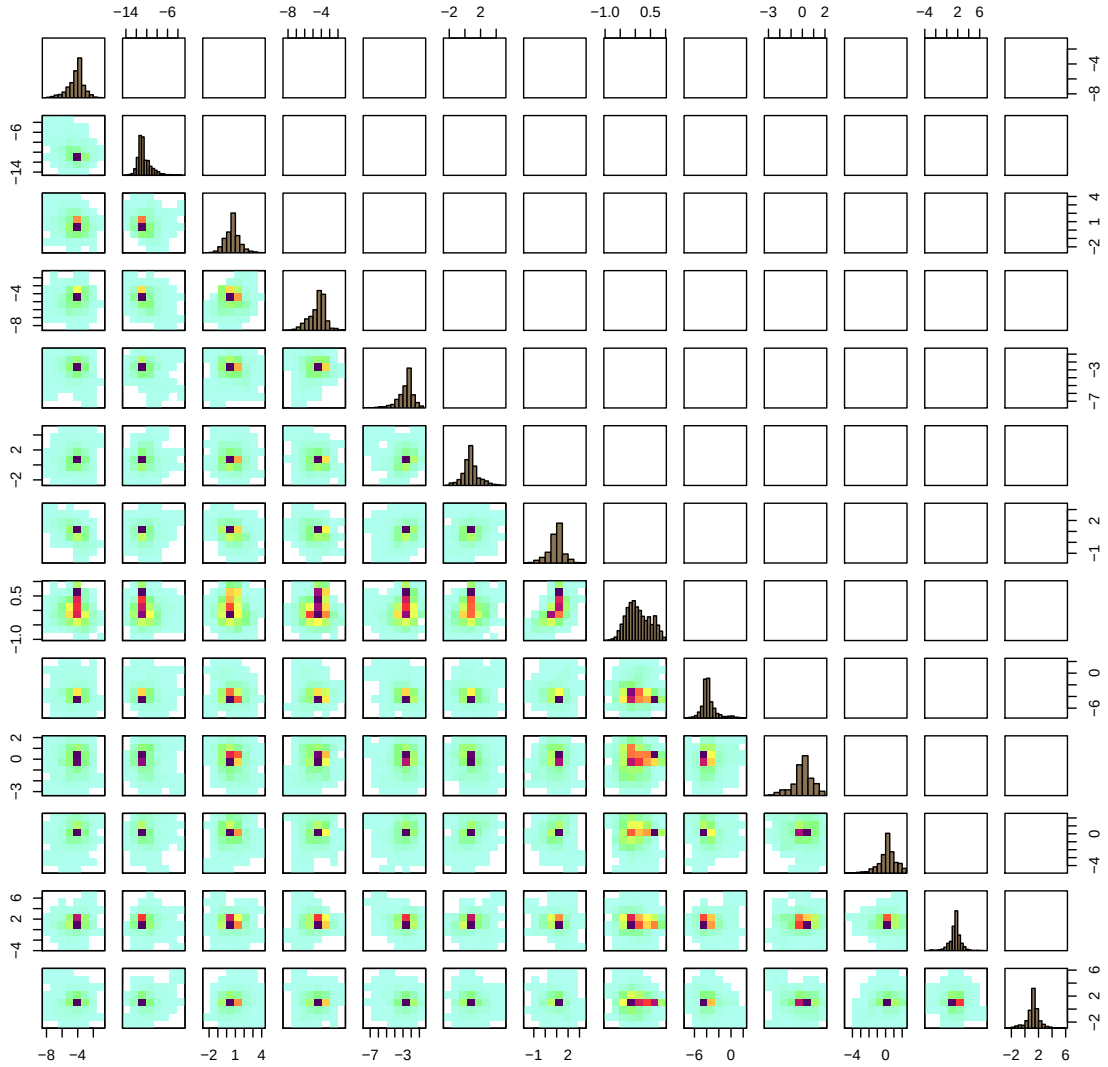

Figure 4.12: Posteriors (diagonals) and joint posteriors for $\psi(i)$, $i = 1, 2, \ldots, 13$ of the rainfall event on 24th September 2016 from 07:48 to 10:42 hours in Melbourne.

Figure 4.13 shows that posteriors of original parameters, which are obtains back from exponentials:

$$
\begin{aligned}
\lambda &= \exp\Big(\frac{\psi(1)+\psi(2)}{2}\Big) \\
\gamma^{-1} &= \exp\Big(\frac{\psi(1)-\psi(2)}{2}\Big) \\
\beta &= \exp\Big(\frac{\psi(3)+\psi(4)}{2}\Big) \\
\eta^{-1} &= \exp\Big(\frac{\psi(3)-\psi(4)}{2}\Big) \\
\mu_x &= \exp(\psi(5)) \\
\sigma_X^2 &= 1/\exp(\psi(6)) \\
\mu_{m_c} &= \exp(\psi(7)) \\
\sigma_{m_c}^2 &= 1/\exp(\psi(8)) \\
\rho_{xm_c} &= \frac{\exp(\psi(9))-1}{\exp(\psi(9))+1} \\
\xi_m &= \exp(\psi(10)) \\
\xi_{cv} &= \exp(\psi(11)) \\
\mu_e &= \frac{\exp(\psi(12))}{\exp(\psi(12))+1} \\
\Theta &= \frac{\pi\,\exp(\psi(13))}{\exp(\psi(13))+1} \\
v_x &= \phi(14) \\
v_y &= \phi(15)
\end{aligned}
$$

Table 4.4 show posterior means, medians and 95 % credible intervals for parameters.

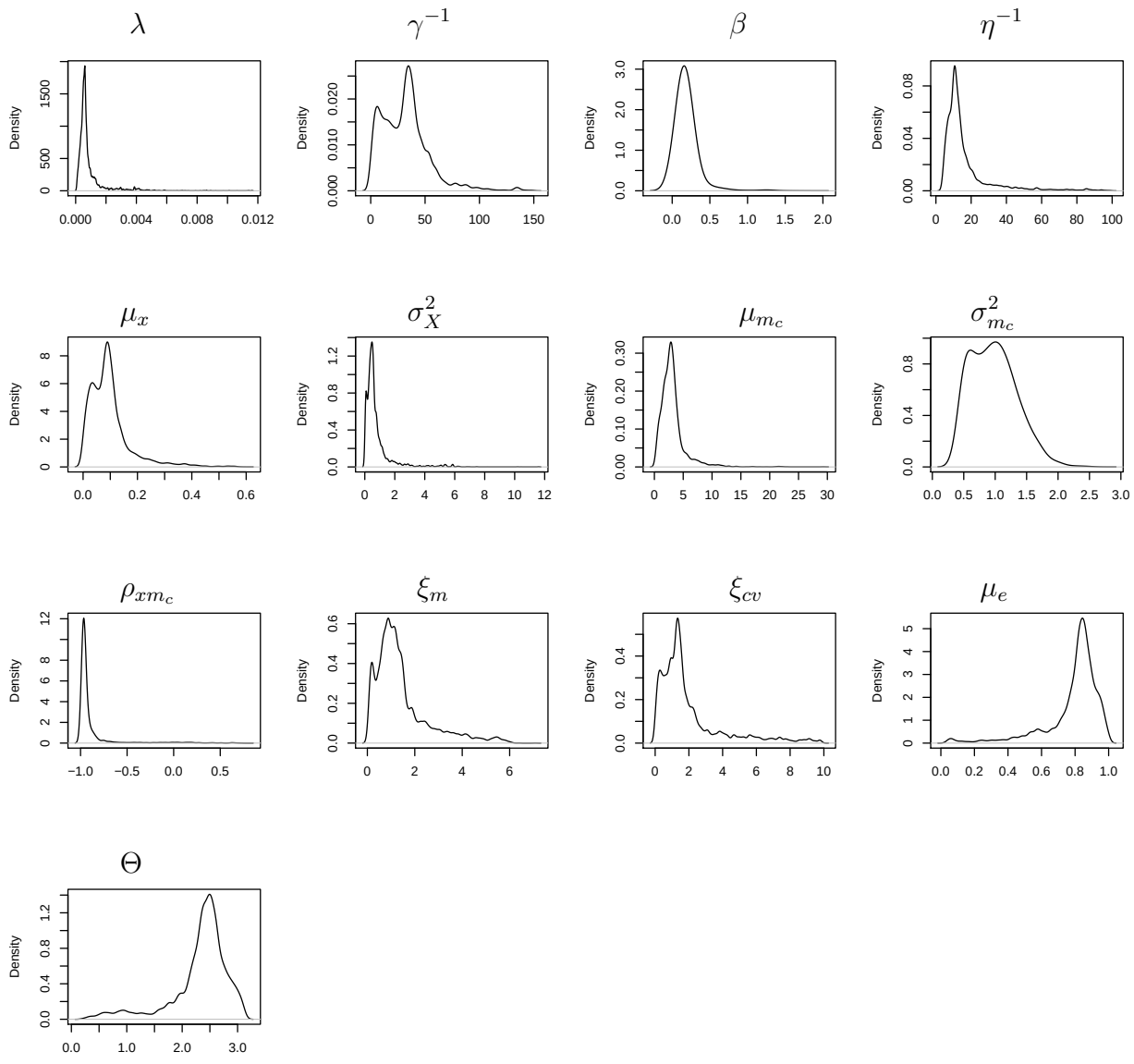

Figure 4.13: Posteriors for parameters λ , γ^{-1}, β, η^{-1}, μ_x, σ_X^2, μ_{m_c}, $\sigma_{m_c}^2$, ρ_{xm_c}, ξ_m, ξ_{cv}, μ_e, and Θ, fitted to the rainfall event on 24th September 2016 from 07:48 to 10:42 hours in Melbourne.

Parameters	Mean	Median	95% Credible Interval
λ	0.0009	0.0006	(0.0002, 0.0040)
γ^{-1}	31.573	31.613	(1.8565, 87.505)
β	0.1843	0.1664	(0.0309, 0.5627)
η^{-1}	16.399	11.803	(4.8640, 64.736)
μ_x	0.0961	0.0844	(0.0053, 0.3242)
σ_X^2	0.7611	0.5041	(0.0432, 4.1003)
μ_{m_c}	3.1159	2.7745	(0.5412, 8.8749)
$\sigma_{m_c}^2$	0.9755	0.9570	(0.4447, 1.7389)
ρ_{xm_c}	-0.8905	-0.9600	(-0.9931 0.0365)
ξ_m	1.4122	1.0970	(0.1255, 4.7924)
ξ_{cv}	1.9754	1.3653	(0.0966, 8.0061)
μ_e	0.7872	0.8323	(0.2581, 0.9718)
Θ	2.3177	2.4343	(0.7071, 3.0203)

Table 4.4: Estimated posterior means, medians and their credible Intervals for parameters. Fitted the LNCST mode to the rainfall event on 24th September 2016 from 07:48 to 10:42 hours in Melbourne.

4.2 Wardon Hill Radar Data

In this section, we applied ABC-MCMC to fit the ECST model to a different radar data, recorded at Wardon Hill, UK. The rainfall event is on 7th July 2004 of a period of 4 hours from 19:00 to 22:55 hours.

We obtained the rainfall data from the Met Office, UK. The Wardon Hill radar coverages a circular region of 100 km radius. The space is gridded 2×2 km^2 and time increment is 5-minutes. We restricted ourselves as a square study area of length 140 km each side see Figure 4.14. We therefore have 70×70 array of 2×2 km^2 pixels. The data is an $70 \times 70 \times n$ array, where n is the number of time partitions. We use a 4-hours rainfall event in this chapter, therefore n is 48. Each element of the matrix is given some amount (possibly zero) of rain in mm. We consider there is zero rain if a pixel, which has less than 0.02 mm in per 5-minute to avoid radar noise.

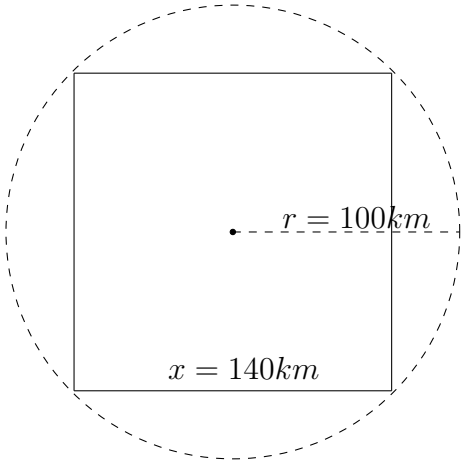

Figure 4.14: Circle is radar coverage and square is study area

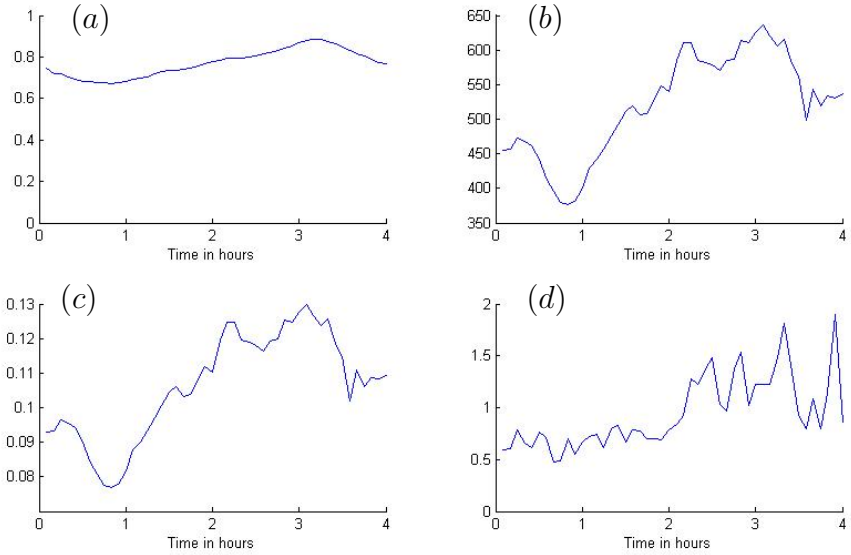

Figure 4.15: Plot (a) shows the study region coverage proportion over time. Plot (b) gives sum of intensities of all pixels at time t. Mean per pixel at time t is shown in plot (c). maximum intensity in a pixel at time t is displayed in plot (d). The rainfall event is on 7th July 2004 from 19:00 to 22:55 hours in Wardon Hill, UK.

The velocity $\mathbf{v} = (-24.48, -0.49)km$ per hour was estimated using spatial autocorrelation function. Table 4.5 gives summary statistics of the observed process.

Summaries	lags (l_x, l_y, l_t)	Values
Mean (mm per pixel)		0.106
Standard deviation		0.111
Correlation	$(-1,-1,0)$	0.795
$\rho\big(Y(l_x + l_t \times v_x,\ l_y + l_t \times v_y,\ l_t)\big)$	$(-1,0,0)$	0.895
	$(-1,1,0)$	0.835
	$(0,-1,0)$	0.864
	$(0,1,0)$	0.864
	$(1,-1,0)$	0.835
	$(1,0,0)$	0.895
	$(1,1,0)$	0.795
	$(-1+v_x,-1+v_y,1)$	0.612
	$(-1+v_x,0+v_y,1)$	0.650
	$(-1+v_x,1+v_y,1)$	0.625
	$(0+v_x,-1+v_y,1)$	0.695
	$(0+v_x,0+v_y,1)$	0.733
	$(0+v_x,1+v_x,1)$	0.677
	$(1+v_x,-1+v_y,1)$	0.785
	$(1+v_x,0+v_y,1)$	0.812
	$(1+v_x,1+v_x,1)$	0.714
$\mathbb{P}(Y^{(l)}=0)$		0.230
Dry wet ratio		3.349
Mean wet area (km^2)		15093
Standard deviation of wet area		1307

Table 4.5: Observed Summary statistics. The rainfall event is on 7th July 2004 from 19:00 to 22:55 hours in Wardon Hill, UK.

4.2.1 Fitting the ECST Model

As before we estimate the velocity using spatial autocorrelation function. For remaining parameters, we use the ABC to estimate their posteriors. For priors we used the $N(0, 3.0^2)$ distribution for $\phi(i)$, for $i = 1, ..., 6, 10, 11$, and for $\phi(7)$ truncated normal from $(-\infty, \log(3)]$, for $\phi(8))$ truncated normal from $(-\infty, \log(6)]$, and for $\phi(9)$ truncated normal from $(-\infty, \log(10)]$

For the proposal chain, we used a random walk with $N(\mathbf{0}, 0.2^2\mathbf{I})$ increments.

We have kept the same set of summary statistics S as before, and the distance measure d.

Trace plots are displayed in Figure 4.16. The Markov chains have moved around the parameter space, though more mixing would be desirable. The results presented required several weeks of simulations, and unfortunately there was not the time to generate more samples. In Figure 4.17 we plot marginal densities and pairwise densities.

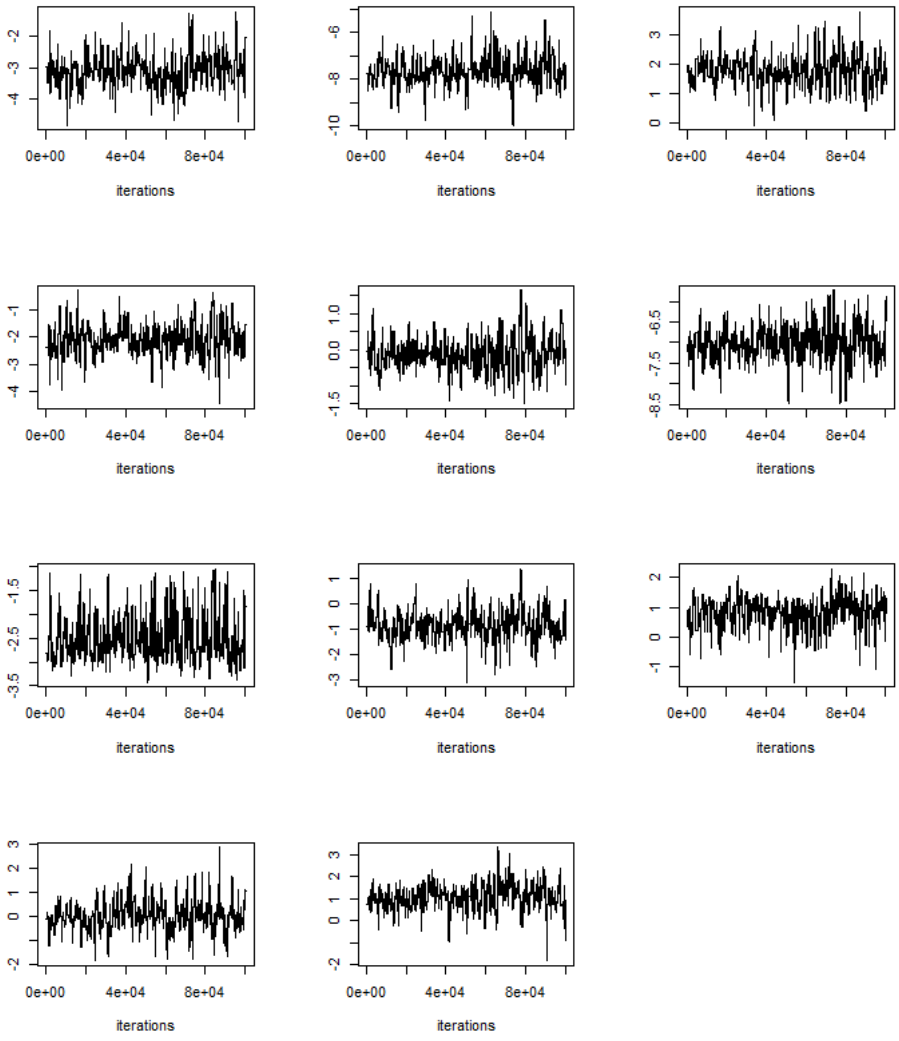

Figure 4.16: Chains for $\phi(i)$,$i = 1, 2, \ldots, 11$ (from top left to right). The rainfall event is on 7th July 2004 from 19:00 to 22:55 hours in Wardon Hill, UK.

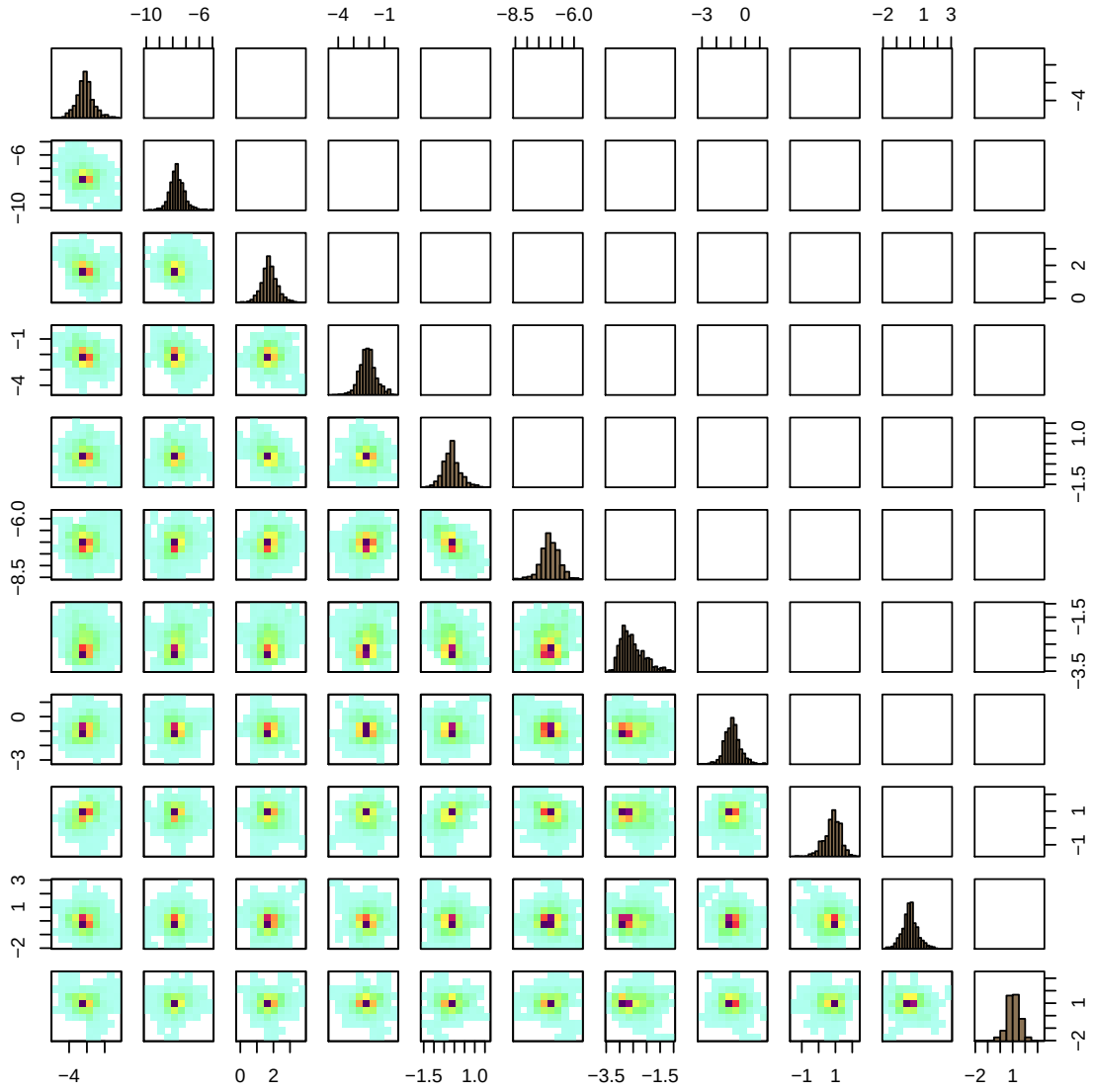

Figure 4.17: Posteriors (diagonals) for $\phi(i)$, $i = 1, 2, \ldots, 11$ and lower panel plots are joint posteriors . The rainfall event is on 7th July 2004 from 19:00 to 22:55 hours in Wardon Hill, UK.

Figure 4.18 shows that posteriors for original parameters λ , $\gamma^{-1}, \beta,\ \eta^{-1},$ $\mu_x,\ \mu_A,\ \alpha_2,\ \xi_m,\ \xi_{cv}, \mu_e,$ and Θ.

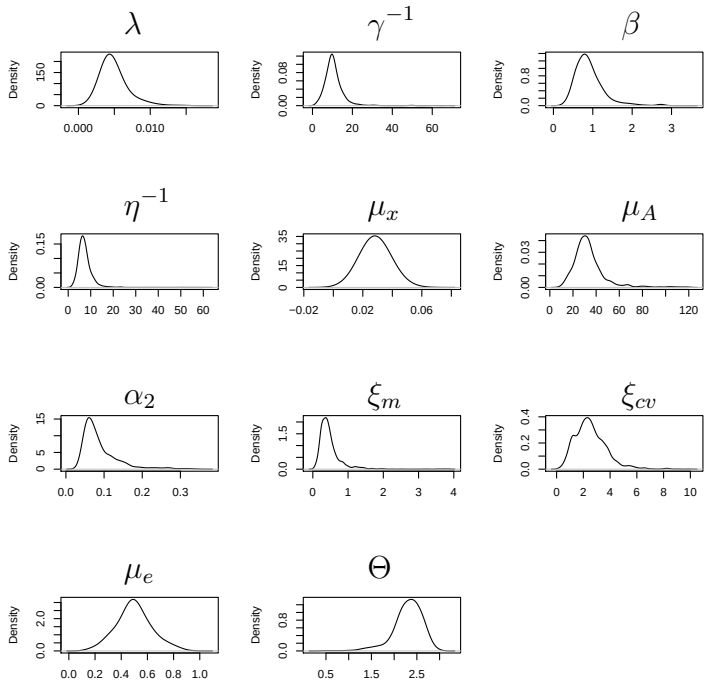

Figure 4.18: Posteriors for parameters λ , γ^{-1}, β, η^{-1}, μ_x, μ_A, α_2, ξ_m, ξ_{cv}, μ_e, and Θ. The rainfall event is on 7th July 2004 from 19:00 to 22:55 hours in Wardon Hill, UK.

Parameters	Mean	Median	95% Credible Interval
λ	0.0049	0.0045	(0.0022, 0.0098)
γ^{-1}	10.698	9.9569	(3.9474, 21.956)
β	0.9116	0.8373	(0.4015, 1.9076)
η^{-1}	7.3179	6.8431	(3.0657, 14.271)
μ_x	0.0285	0.0280	(0.0195, 0.0411)
μ_A	33.774	31.364	(14.789, 77.411)
α_2	0.0893	0.0733	(0.0423, 0.2415)
ξ_m	0.4895	0.4039	(0.1444, 1.4112)
ξ_{cv}	2.5485	2.3898	(0.7550, 5.4446)
μ_e	0.4982	0.4954	(0.2418, 0.7895)
Θ	2.2984	2.3428	(1.4445, 2.7913)

Table 4.6: Estimated posterior means, medians and credible intervals. for parameters. Fitted the ECST Model to the rainfall event is on 7th July 2004 from 19:00 to 22:55 hours in Wardon Hill, UK.

4.3 Parameter estimation comparison

In this section, we compare parameter estimation for three distinct rainfall events. We selected three rainfall events to fit spatial temporal rainfall models. Event 1 was the rainfall at Melbourne on 24th September 2016 from 12:54 to 16:48 hours. The fitting spatial-temporal models to this event was discussed in the Chapter 3. Event 2 was the rainfall on the same day from 7:48 to 10:42 at Melbourne. The details were discussed in §4.1. The rainfall on 7th July 2004 from 19:00 to 22:55 hours at Wardon Hill, UK was selected as event 3, which was discussed in §4.2.

Tables 4.7 and 4.9 present posterior medians and 95% credible intervals for parameters. The estimated values from the C-I-N and the LNST models fitted to event 1 and event 2 looks similar, which shows that the ABC fitting is consistent. We fitted the ECST model to these events as well.

We also fitted the ECST model to one additional rainfall event at Wardon Hill, UK. Table 4.8 presents posterior medians and 95% credible intervals for parameters. Estimates are similar, however λ and μ_x are quite different in event 3 than the rest. If we take their product $(\lambda \times \mu_x)$ we will get the similar values. Using posterior medians, we have the product 0.00014 for event 1, 0.00011 for event 2, and 0.00013 for event 3.

Parameters	Event 1 (Post. median)	Event 2 (Post. median)	Event 1 (CI)	Event 2 (CI)
λ	0.0006	0.0005	(0.0003, 0.0026)	(0.0003, 0.0025)
γ^{-1}	13.233	13.975	(2.9086, 38.585)	(5.3099, 33.328)
β	0.6201	0.6105	(0.2321, 1.7451)	(0.2431, 1.4569)
η^{-1}	4.6462	5.3596	(2.6768, 13.180)	(3.4542, 19.733)
μ_x	0.1917	0.1990	(0.0792, 0.3332)	(0.0547, 0.3074)
μ_A	32.677	32.388	(11.839, 93.733)	(8.8582, 75.159)
α_2	0.0548	0.0436	(0.0255, 0.1211)	(0.0155, 0.0847)
ξ_m	0.4006	0.4136	(0.0738, 1.8749)	(0.0916, 2.0332)
ξ_{cv}	1.5953	1.6144	(0.1467, 6.0694)	(0.2537, 5.5658)
e		0.8194		(0.4628, 0.9287)
Θ		2.4134		(1.0920, 2.8660)

Table 4.7: Posterior medians and credible intervals estimated from fitting the C-I-N model to two rainfall events in Melbourne using ABC.

	Event 1 (Post. median)	Event 2 (Post. median)	Event 3 (Post. median)	Event 1 (CI)	Event 2 (CI)	Event 3 (CI)
λ	0.0005	0.0005	0.0045	(0.0002, 0.0036)	(0.0003, 0.0045)	(0.0022, 0.0098)
γ^{-1}	12.391	11.391	9.9569	(1.0938, 38.497)	(1.6150, 26.092)	(3.9474, 21.956)
β	0.5722	0.5515	0.8373	(0.1171, 1.8787)	(0.1136, 2.4732)	(0.4015, 1.9076)
η^{-1}	7.6700	6.6499	6.8431	(4.0369, 35.960)	(3.3520, 39.636)	(3.0657, 14.271)
μ_x	0.2731	0.2208	0.0280	(0.1508, 0.4848)	(0.0469, 0.4058)	(0.0195, 0.0411)
μ_A	31.541	30.614	31.364	(4.6533, 92.161)	(3.297, 100.772)	(14.789, 77.411)
α_2	0.0771	0.0513	0.0733	(0.0441, 0.1617)	(0.0169, 0.1252)	(0.0423, 0.2415)
ξ_m	0.7224	0.4451	0.4039	(0.3761, 1.6064)	(0.0299, 2.2536)	(0.1444, 1.4112)
ξ_{cv}	1.2105	1.5295	2.3898	(0.5601, 2.1132)	(0.1619, 5.7586)	(0.7550, 5.4446)
μ_e		0.8047	0.4954		(0.1607, 0.9764	(0.2418, 0.7895)
Θ		2.4074	2.3428		(0.7238, 2.9672	(1.4445, 2.7913)

Table 4.8: Posterior medians and credible intervals estimated from fitting the ECST model to three rainfall events using ABC. Event 1 and event 2 were in Melbourne and the event 3 was in Wardon Hill, UK.

Parameters	Event 1 (Post. median)	Event 2 (Post. median)	Event 1 (CI)	Event 2 (CI)
λ	0.0006	0.0006	(0.0002, 0.0015)	(0.0002, 0.0040)
γ^{-1}	32.462	31.613	(4.4944, 64.524)	(1.8565, 87.505)
β	0.1801	0.1664	(0.0457, 0.4429)	(0.0309, 0.5627)
η^{-1}	11.407	11.803	(5.6338, 42.133)	(4.8640, 64.736)
μ_x	0.1258	0.0844	(0.0426, 0.7603)	(0.0053, 0.3242)
σ_X^2	0.4519	0.5041	(0.0671, 1.5503)	(0.0432, 4.1003)
μ_{m_c}	2.7523	2.7745	(0.7829, 5.6306)	(0.5412, 8.8749)
$\sigma_{m_c}^2$	0.7859	0.9570	(0.4335, 1.7103)	(0.4447, 1.7389)
ρ_{xm_c}	-0.7564	-0.9600	(-0.9327, 0.0996)	(-0.9931 0.0365)
ξ_m	1.1647	1.0970	(0.1671, 4.3280)	(0.1255, 4.7924)
ξ_{cv}	1.1901	1.3653	(0.6291, 1.9917)	(0.0966, 8.0061)
μ_e		0.8323		(0.2581, 0.9718)
Θ		2.4343		(0.7071, 3.0203)

Table 4.9: Posterior medians and credible intervals estimated from fitting the LNST model to two rainfall events in Melbourne using ABC.

4.4 Discussion

We considered two new rainfall events in this chapter to demonstrate that the ABC-MCMC procedure gives consistent results for different events. We also used the ABC-MCMC algorithm to estimate all model parameters except cell eccentricity variance and the velocity. Recall that eccentricity and orientation were estimated using an ad-hoc method in Chapter 3.

The different events selected are obtained from two different radars. All three rainfall events move in different directions: event 1 moves with velocity v = (0.10, 29.9) km per hour, event 2 travels with velocity v = (19.9,20.0) km per hour and for event 3, the velocity v = (-24.48, -0.49) km per hour. The mean rainfall per pixel are also quite different, with values of 0.065, 0.038 and 0.026 for events 1, 2 and 3 respectively.

Using the ad-hoc method of Chapter 3, the eccentricity and orientation for event 2 were estimated to be 0.84 and 2.24, which are within the 95 % credible intervals given in Table 4.2. Similarly the eccentricity and orientation for event 3 were 0.75 and 2.45, and both are within the 95 % credible intervals seen in Table 4.6. This shows that we do not need to estimate eccentricity and orientation separately, but can estimate these parameters from the ABC-MCMC procedure.

We presented all parameter estimates in Tables 4.7, 4.8 and 4.9 from three models fitted to three different events. The results show that ABC-MCMC readily adapts to more general, and thus more realistic, variants of the model.

Chapter 5

Conclusion and Future Work

5.1 Conclusion

Using both a simulation study and real data, we have seen that the ABC-MCMC gives better fits than GMM, for fitting a Bartlett-Lewis rainfall model. From the modelling perspective, an important advantage of ABC fitting over GMM fitting is that we can use summaries of the data that capture useful information, whether or not we have an expression for their expectation. Moreover, this means that ABC can be used for models for which GMM fitting is not available. For example, if we used a gamma distribution for the duration of a rain cell, rather than an exponential distribution, then we would not be able to calculate the second order statistics of the B-L rainfal model, making GMM fitting impossible. However ABC fitting would proceed as before, with the addition of a single parameter.

We included a wide range of statistics to fit rainfall models to spatial-temporal data. This allowed us to develop more realistic stochastic rainfall models. We proposed two new spatial-temporal rainfall models, which clearly showed a better fit than the C-I-N model to the observed rainfall process.

With the advantage of flexibility in choice of summary statistics there is the disadvantage of an increase in computational time. To reduce the computational time we proposed a novel method to initiate the ABC procedure. The Simulated Method of Moments is utilised to initialize the ABC. This method reduces the computational time by finding a feasible starting point, reducing the need for a burn in, and providing a set of weights for the distance measure.

The models we studied are easy to simulate, but very difficult to obtain analyse theoretically. We established that ABC is readily applicable to the estimation of temporal and spatial-temporal rainfall models based on cluster processes. We were able to fit the models using scientifically relevant summary statistics, because ABC does not require their corresponding likelihoods. This approach also opens the opportunity of fitting much more realistic stochastic rainfall models. This is significant because simulations of realistic rainfall model are important to study climatic variables in hydrological processes.

5.2 Future work

Bivariate log-normal distribution for cell intensity and cell major semi-axis was an opportunity to study relationships between them using the Log-Normal Cell Spatial-Temporal model. However this model produced more spoty rain cells than expected. In future, we could consider whether cell major semi-axis follows the gamma distribution. We also expect some cells with extreme intensity. Cell intensity therefore may follow heavy tail distributions which may give better representation of extreme rainfall.

Spatial-temporal rainfall models discussed in this thesis are stationary in time and homogeneous in space. Rainfall processes, however, are unlikely to be always stationary in time and homogeneous in space. We have found that there are rare rainfall events which spread out evenly over the whole study region. We experienced that most rainfall events are concentrated in some parts of the region. If we consider that the rainfall process is an inhomogeneous process, this may give better representation of the rainfall process. However, the process becomes more complex. We could consider storm arrival processes as inhomogeneous in space, which can lead to more storms arriving in some parts of the region, and rain cells are clustered with the storms. Theoretical expectations for the moments can be difficult to derive, but the ABC-MCMC provides an alternative method to fit these models without deriving their expectations.

In recent years, there has been increasing interest in stochastic modelling of flood risk and water resource management. Stochastic models for precipitation have been applied to provide an assessment of the impact of future change in hydrological processes. The spatial distribution of rainfall and its development over time are essential to hydrological applications. Our models may be used in conjunction with urban flood models to determine and assess the flood risks, as we require simulated process input to flood models, partic-

ularly where the observed data is not available. A research on integrating our spatial-temporal rainfall models into urban flood models is recommended.

Bibliography

[1] M.C. Acreman. A simple sotchastic model of hourly rainfall for farnborrough, england. *Hydrological Sciences*, 35:119–148, 1990.

[2] Mark A Beaumont, Jean-Marie Cornuet, Jean-Michel Marin, and Christian P Robert. Adaptive approximate bayesian computation. *Biometrika*, 96(4):983–990, 2009.

[3] Mark A Beaumont, Wenyang Zhang, and David J Balding. Approximate bayesian computation in population genetics. *Genetics*, 162(4):2025–2035, 2002.

[4] Hall Jim Beven Keith et al. *Applied uncertainty analysis for flood risk management*. World Scientific, 2014.

[5] A Burton, HJ Fowler, CG Kilsby, and PE O'Connell. A stochastic model for the spatial-temporal simulation of nonhomogeneous rainfall occurrence and amounts. *Water Resources Research*, 46(11), 2010.

[6] A Burton, CG Kilsby, HJ Fowler, PSP Cowpertwait, and PE O'Connell. Rainsim: A spatial–temporal stochastic rainfall modelling system. *Environmental Modelling & Software*, 23(12):1356–1369, 2008.

[7] Stuart Coles. *An Introduction to Statistical Modeling of Extreme Values*. Springer: London, 2001.

[8] Paul Cowpertwait. A generalized point process model for rainfall. *Proc. Roy. Soc. London*, 447:23–37, 1994.

[9] Paul Cowpertwait, Valerie Isham, and Christian Onof. Point process models of rainfall: developments for fine-scale structure. *Proc. Roy. Soc. London*, 463:2569–2587, 2007.

[10] Paul SP Cowpertwait. A spatial–temporal point process model of rainfall for the thames catchment, uk. *Journal of Hydrology*, 330(3-4):586–595, 2006.

[11] PSP Cowpertwait, CG Kilsby, and PE O'Connell. A space-time neyman-scott model of rainfall: Empirical analysis of extremes. *Water Resources Research*, 38(8), 2002.

[12] D. R. Cox and V. Isham. *Point processes*. London:Chapman & Hall, 1980.

[13] D. R. Cox and V. Isham. A Simple Spatial-Temporal Model of Rainfall. *Proceedings of the Royal Society A: Mathematical, Physical and Engineering Sciences*, 415(1849):317–328, 1988.

[14] David Roxbee Cox and Hilton David Miller. *The theory of stochastic processes*. Lomdon:Chapman & Hall, 1965.

[15] Dara Entekhabi, I. Rodriguez-Iturbe, D. R. Cox, and Peter S. Eagleson. Probabilistic representation of the temporal rainfall process by a modified neyman-scott rectangular pulses model: Parameter estimation and validation. *Water Resources research*, 25:295–302, 1989.

[16] Hayley J Fowler, Stephen Blenkinsop, and Claudia Tebaldi. Linking climate change modelling to impacts studies: recent advances in downscaling techniques for hydrological modelling. *International journal of climatology*, 27(12):1547–1578, 2007.

[17] HJ Fowler, CG Kilsby, and PE OConnell. A stochastic rainfall model for the assessment of regional water resource systems under changed climatic condition. *Hydrology and Earth System Sciences*, 4(2):263–281, 2000.

[18] HJ Fowler, CG Kilsby, PE O'connell, and A Burton. A weather-type conditioned multi-site stochastic rainfall model for the generation of scenarios of climatic variability and change. *Journal of Hydrology*, 308(1-4):50–66, 2005.

[19] Andrew Gelman, Hal S Stern, John B Carlin, David B Dunson, Aki Vehtari, and Donald B Rubin. *Bayesian data analysis*. Chapman and Hall/CRC, 2013.

[20] Vijay K Gupta and Ed Waymire. Multiscaling properties of spatial rainfall and river flow distributions. *Journal of Geophysical Research: Atmospheres*, 95(D3):1999–2009, 1990.

[21] Vijay K Gupta and Edward C Waymire. A statistical analysis of mesoscale rainfall as a random cascade. *Journal of Applied Meteorology*, 32(2):251–267, 1993.

[22] Yeboah Gyasi-Agyei and Garry R. Willgoose. A hybrid model for point rainfall modelling. *Water Resources research*, 30:1699–1706, 1997.

[23] J. Jesus and R. E. Chandler. Estimating functions and the generalized method of moments. (September):871–885, 2011.

[24] Jo Kaczmarska. Further development of bartlett–lewis models for fine-resolution rainfall. *Research Rep*, 312, 2011.

[25] Jo Kaczmarska, Valerie Isham, and Christian Onof. Point process models for fine-resolution rainfall. *Hydrological Sciences Journal*, 59(11):1972–1991, 2014.

[26] Shaun Lovejoy and Daniel Schertzer. Multifractals, universality classes and satellite and radar measurements of cloud and rain fields. *Journal of Geophysical Research: Atmospheres*, 95(D3):2021–2034, 1990.

[27] So Lovejoy and D Schertzer. Generalized scale invariance in the atmosphere and fractal models of rain. *Water Resources Research*, 21(8):1233–1250, 1985.

[28] David Lunn, Chris Jackson, Nicky Best, Andrew Thomas, and David Spiegelhalter. *The BUGS book: A practical introduction to Bayesian analysis*. CRC press, 2012.

[29] Paul Marjoram, John Molitor, Vincent Plagnol, and Simon Tavaré. Markov chain monte carlo without likelihoods. *Proceedings of the National Academy of Sciences*, 100(26):15324–15328, 2003.

[30] Daniel McFadden. A method of simulated moments for estimation of discrete response models without numerical integration. *Econometrica*, 57:995–1026, 1989.

[31] R Mehrotra and Ashish Sharma. A semi-parametric model for stochastic generation of multi-site daily rainfall exhibiting low-frequency variability. *Journal of Hydrology*, 335(1-2):180–193, 2007.

[32] Paul Northrop. A clustered spatial-temporal model of rainfall. *The Royal Sciety*, 454(1975):1875–1888, 1998.

[33] Paul Northrop. Modelling and statistical analysis of spatial-temporal rainfall fields., Ph. D. thesis, University of London, 1996.

[34] Paul J. Northrop and Tom M. Stone. Some process for rainfall: further develepoment. Department of Statistical Science, University College London. 2005.

[35] Christian Onof and Howard S. Wheater. Improved fitting of the Bartlett-Lewis Rectangular Pulse Model for hourly rainfall. *Hydrological Sciences Journal*, 39(6):663–680, 1994.

[36] Ariel Pakes and David Pollard. Simulation and the asymptotics of optimization estimators. *Econometrica*, 57:1027–1057, 1989.

[37] Dennis Prangle. Adapting the abc distance function. *Bayesian Analysis*, 12(1):289–309, 2017.

[38] Jonathan K Pritchard, Mark T Seielstad, Anna Perez-Lezaun, and Marcus W Feldman. Population growth of human y chromosomes: a study of y chromosome microsatellites. *Molecular biology and evolution*, 16(12):1791–1798, 1999.

[39] I. Rodriguez-Iturbe, D. R. Cox, and V. Isham. Some models for rainfall based on stochastic point processe. *Proc. Roy. Soc. London*, 410:269–288, 1987.

[40] I. Rodriguez-Iturbe, D. R. Cox, and V. Isham. A point process model for rainfall: further developments. *Proc. Roy. Soc. London*, 417:283–298, 1988.

[41] I. Rodriguez-Iturbe, B. Febres de Power, and J. B. & Valés. Rectangular pulses point process models for rainfall: Analysis of empirical data. *Journal of Geophysical Research*, 92:9645–9656, 1987.

[42] Alan W Seed, R Srikanthan, and Merab Menabde. A space and time model for design storm rainfall. *Journal of Geophysical Research: Atmospheres*, 104(D24):31623–31630, 1999.

[43] Scott A Sisson, Yanan Fan, and Mark M Tanaka. Sequential monte carlo without likelihoods. *Proceedings of the National Academy of Sciences*, 104(6):1760–1765, 2007.

[44] Scott A Sisson, Yanan Fan, and Mark M Tanaka. Sequential monte carlo without likelihoods. *Proceedings of the National Academy of Sciences*, 106:16889, 2009.

[45] Brandon M Turner and Trisha Van Zandt. A tutorial on approximate bayesian computation. *Journal of Mathematical Psychology*, 56(2):69–85, 2012.

[46] Daniel Wegmann, Christoph Leuenberger, and Laurent Excoffier. Efficient approximate bayesian computation coupled with markov chain monte carlo without likelihood. *Genetics*, 182(4):1207–1218, 2009.

[47] H. S. Wheater, R. E. Chandler, C. J. Onof, V. S. Isham, E. Bellone, C. Yang, D. Lekkas, G. Lourmas, and M. L. Segond. Spatial-temporal rainfall modelling for flood risk estimation. *Stochastic Environmental Research and Risk Assessment*, 19(6):403–416, 2005.

[48] H. S. Wheater, C Isham, V. S.and Onof, RE Chandler, PJ Northrop, P Guiblin, SM Bate, DR Cox, and D Koutsoyiannis. *Generation of spatially consistent rainfall data*. Department of Statistical Science, University College London. Report to MAFF, 2000.

[49] Patrick Willems. Stochastic description of the rainfall input errors in lumped hydrological models. *Stochastic environmental research and risk assessment*, 15(2):132–152, 2001.

Appendix

This page is intentionally left blank.

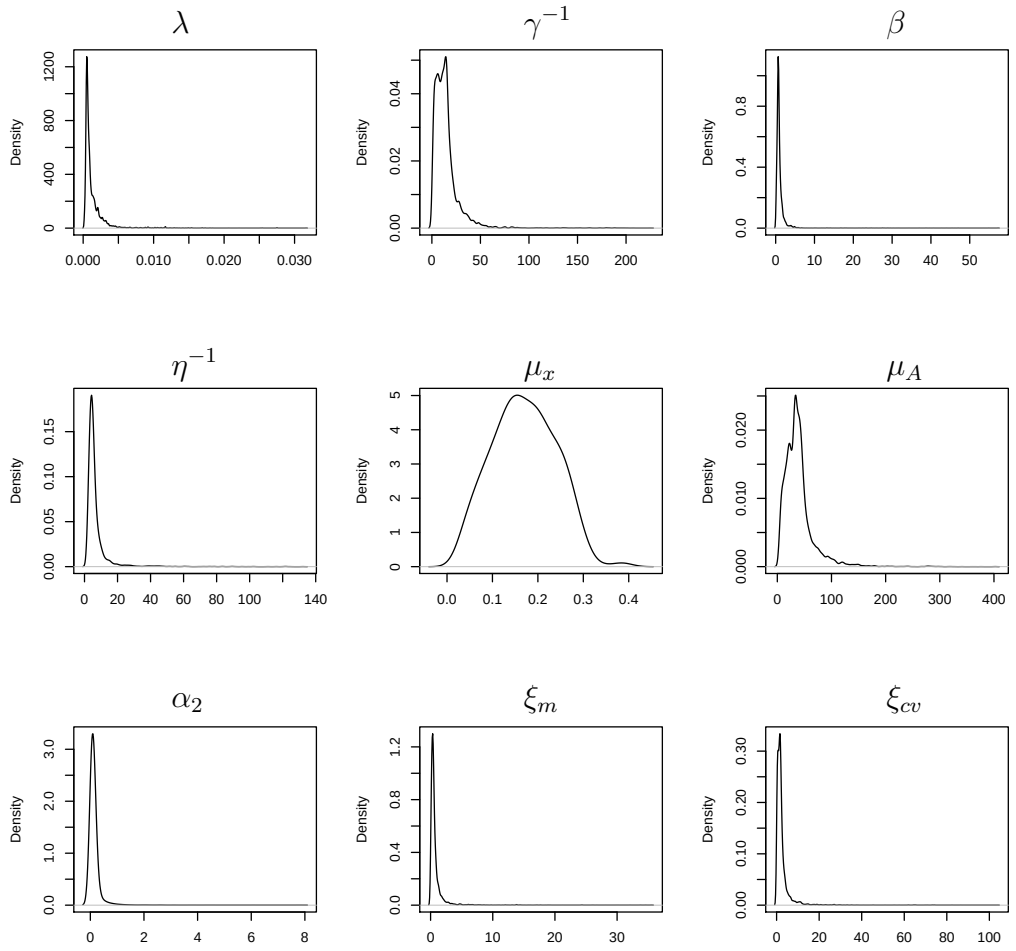

Figure 1: Posteriors for parameters λ , $\gamma^{-1}, \beta,\ \eta^{-1}, \mu_x, \mu_A,\ \alpha_2,\ \xi_m,\ \xi_{cv}$. The posteriors are for C-I-N model parameters. The rainfall event is rainfall on 24th September 2016 from 07:48 to 10:42 hours in Melbourne.

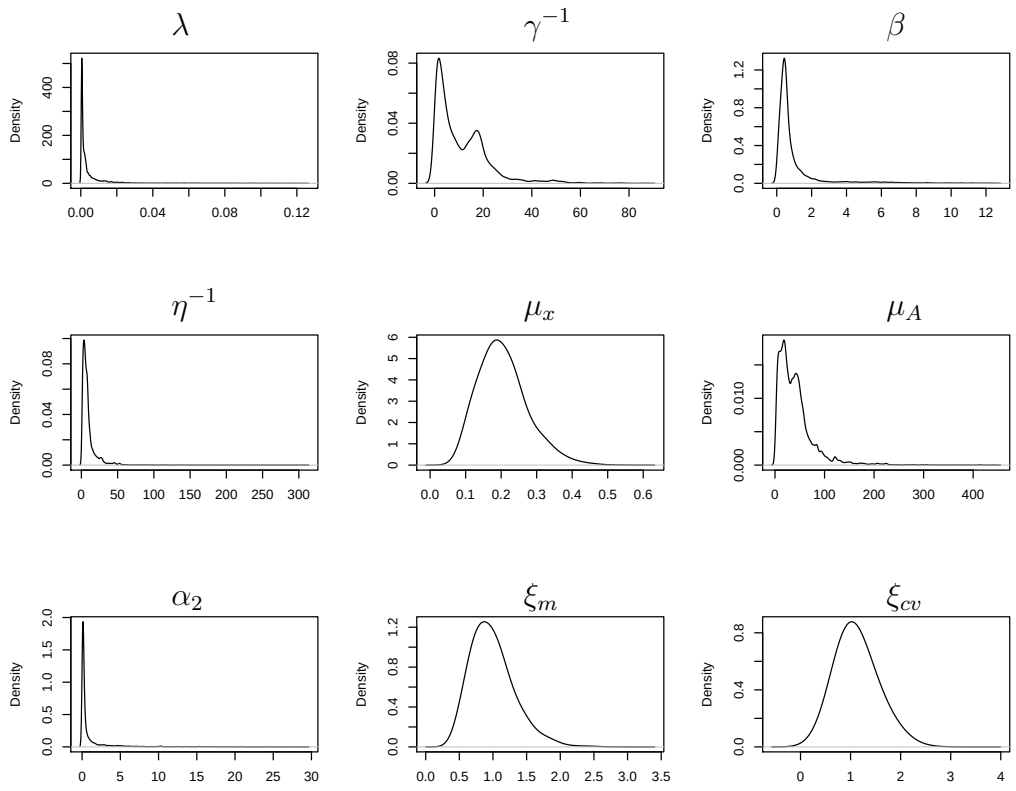

Figure 2: Posteriors for parameters λ , $\gamma^{-1}, \beta,\ \eta^{-1}, \mu_x, \mu_A,\ \alpha_2,\ \xi_m,\ \xi_{cv}$.The posteriors are for ECST model parameters. The rainfall event is rainfall on 24th September 2016 from 07:48 to 10:42 hours in Melbourne.